



## BOJCAS: Bolted joints in composite aircraft structures

Michael A. McCartney

### Publication date

01-01-2003

### Licence

This work is made available under the [CC BY-NC-SA 1.0](#) licence and should only be used in accordance with that licence. For more information on the specific terms, consult the repository record for this item.

### Document Version

1

### Citation for this work (HarvardUL)

McCartney, M.A. (2003) 'BOJCAS: Bolted joints in composite aircraft structures', available: <https://hdl.handle.net/10344/5049> [accessed 22 Feb 2023].

This work was downloaded from the University of Limerick research repository.

For more information on this work, the University of Limerick research repository or to report an issue, you can contact the repository administrators at [ir@ul.ie](mailto:ir@ul.ie). If you feel that this work breaches copyright, please provide details and we will remove access to the work immediately while we investigate your claim.

# FINAL TECHNICAL REPORT

**CONTRACT N° :** G4RD-CT-1999-00036  
**PROJECT N° :**  
**ACRONYM :** BOJCAS  
**TITLE :** Bolted Joints in Composite Aircraft Structures

**PROJECT CO-ORDINATOR :** University of Limerick

**PARTNERS :**

University of Limerick	(ULIM)
Airbus UK Limited	(AUK)
Airbus Deutschland GmbH	(AD)
SAAB AB	(SAAB)
Centro Italiano Ricerche Aerospaziali S.C.p.A.	(CIRA)
QinetiQ	(QinetiQ)
The Swedish Defence Research Agency	(FOI)
Stichting Nationaal Lucht-en Ruimtevaartlaboratorium	(NLR)
Institute of Structures and Advanced Materials	(ISTRAM)
Kungl Tekniska Högskolan	(KTH)
Stehlin-Merazzi Research S.A.	(SMR)

**REPORTING PERIOD : FROM** 01/Feb/2000 **TO** 31/May/2003

**PROJECT START DATE :** 01/Feb/2000 **DURATION :** 40 Months

**Date of issue of this report :** 31/July/2003



Project funded by the European Community  
under the 'Competitive and Sustainable Growth'  
Programme (1998-2002)

## Note on Partner Names

Since the start of the project, four partners have undergone a change of name (some more than once). **Since these new names have now been recognised in amendments to the contract, they are used in this report.** For reference, the table below shows the old and new names and abbreviations:

Original Name	Old Abbreviation	New Name	New Abbreviation
British Aerospace (Operations) Limited	BAe	Airbus UK	AUK
DaimlerChrysler Aerospace Airbus GmbH	DA	Airbus Deutschland	AD
The Aeronautical Research Institute of Sweden	FFA	Aeronautics Division, Swedish Defence Research Agency (FOI)	FOI
Defence Evaluation and Research Agency	DERA	QinetiQ	QinetiQ

The only **exception** to the use of the new names is in the naming of the benchmark structures. The names “**BAe benchmark structures**” and “**DA benchmark structures**” are retained.

# 1. Table of Contents

	Note on Partner Names	2
1	Table of Contents	3
2	Executive Publishable Summary	4
3	Objectives of the Project	5
4	Scientific and Technical Description of the Results	9
	4.1 Workpackage 1 Design Requirements	9
	4.2 Workpackage 2 Global Design Methods	18
	4.2.1 Task 2.1 Design of Benchmark Structures	18
	4.2.2 Task 2.2 Benchmark Modelling w/ existing Global Design Methods	29
	4.2.3 Task 2.3 Development of Global Design Methods	44
	4.2.4 Task 2.4 Industrial Assessment of Global Design Methods	60
	4.3 Workpackage 3 Benchmark Structure Fabrication and Test	71
	4.4 Workpackage 4 Detailed Design Methods	91
	4.4.1 Task 4.1 Three-dimensional Stress Analysis	91
	4.4.2 Task 4.2 Damage Modelling and Failure Criteria	115
	4.4.3 Task 4.3 Coupled Global-Local Methods	131
	4.4.4 Task 4.4 Parameter Studies	147
	4.5 Workpackage 5 Specimen Structure Fabrication and Test	172
	4.6 Workpackage 6 Design Methodology	194
	4.6.1 Task 6.1 Assessment of Detailed Design Methods	194
	4.6.2 Task 6.2 Design Guidelines	195
	4.7 Workpackage 7 Network Management	196
	4.7.1 Task 7.1 Management	196
	4.7.2 Task 7.2 Exploitation	196
5	List of Deliverables	198
6	Comparison of initially planned activities and work actually accomplished	216
7	Management and Co-ordination Aspects	219
	7.1 Performance of the Consortium	219
	7.2 Contacts for Follow-up	220
	7.3 Publications	222
8	Results and Conclusions	226
9	Acknowledgements	229
10	References	230

## 1.1 List of Tables

Table 5:	List of Deliverables	198
Table 7.1:	Manpower and Progress Follow-up Tables	232
Table 7.2	Budget Follow-up tables	242



## **Executive Publishable Summary**

The objective of BOJCAS was to develop advanced design methods for bolted joints in composite aircraft structures. This is a critical technology supporting the introduction of composites into the primary structure of large commercial aircraft. Design methods in existence before BOJCAS dated from the 70s/80s, were largely empirical, and tended to be overly reliant on testing. The methods developed in BOJCAS incorporate recent developments in computational mechanics and are more adaptable to new materials, and configurations. This gives them the potential to significantly reduce testing, and hence time/cost of development, as well as aircraft weight with consequent increase in efficiency. This should also help to ensure continued safety.

The project was divided into two strands directed towards two major goals: global design methods for preliminary design, and detailed design methods for final design of critical joints. Each strand contained major testing and analysis components. At the global level, a series of benchmark structures representative of primary, multi-fastener joint configurations, were defined and tested. The structures addressed key issues such as composite-to-metal joints (for potential composite wings), bolted repairs, and joint optimisation. Global design techniques were developed based on two-dimensional finite element methods, and validated on the benchmarks. At the detailed level, an extensive programme of specimen tests supported the development of detailed design methods, based on three-dimensional finite element techniques. These account for non-uniform through-thickness stress distributions, which are particularly important for primary joints with thick laminates. Progressive damage models and new fatigue-based failure criteria were developed, and automated model-building tools were created. Bridging the two strands were methods to automatically couple global and detailed methods. Tests were extensively instrumented and detailed fractographic failure analysis was performed. The tests and analyses formed the basis for design guidelines on key issues.

The main results were:

- Global design methods, for preliminary design of complex, multi-fastener joints
- Detailed design methods for final design of critical joints
- Methods to couple global and detailed design methods
- Design guidelines for primary composite bolted joints based on analyses and tests
- Basic research information on the behaviour of composite bolted joints

# 1 Objectives of the Project

As stated in the Executive Summary, the principal objective of BOJCAS was to develop advanced design methods for bolted joints in composite aircraft structures. The methods were to be based on the finite element method, and three particular approaches were to be addressed:

- Global methods, for preliminary design of complex, multi-fastener joints
- Detailed methods for final design of critical joints
- Methods to couple global and detailed methods

To support these developments, an extensive series of experiments was to be performed. The experiments provided data for validation of the models, but also provided much basic research information that will be useful for years to come. Many novel instrumentation techniques were also used, and comparison with modelling helped to evaluate these techniques for their potential future use in this and other areas.

The original work programme structure is shown in Figs. 3.1 and 3.2.

As can be seen, BOJCAS was divided into seven workpackages as follows:

1. Design Requirements
2. Global Design Methods
3. Benchmark Structure Fabrication and Test
4. Detailed Design Methods
5. Specimen Structure Fabrication and Test
6. Design Methodology
7. Network Management

The work was broadly divided into two strands: WP 1, 2, and 3 at the global level, and WP 4 and 5 at the detailed or local level. The link between the two levels was to be provided by the global-local methods. Additionally results from the detailed level were to feed upwards to help improve the global methods.

In WP 1, design requirements were to be determined for key aircraft joint configurations, and benchmark structures representative of these configurations were to be defined.

In Task 2.1, the benchmark structures were to be designed with existing in-house industry tools, and detailed drawings produced. Predictions of load distributions and failure loads/modes were also to be made with existing tools to act as a baseline for comparison with the methods developed in BOJCAS.

Global modelling of the benchmark structures was initially to take place using existing methods to provide baseline results (Task 2.2). Then at the end of Month 12, interim results from Tasks 4.1, 4.2 and 4.3 were to feed into Task 2.3 to allow for the first phase of development of an improved global methodology. The second development phase for

the global methods was to begin at the end of Month 21, when predictions on the benchmark structures were to be available from the global methods (Task 2.2, 2.3) and the global-local methods (Task 4.3), the specimen testing (WP 5) and benchmark testing (WP 3) was to be complete, and results were to be available from the detailed analyses in Tasks 4.1 and 4.2.

In Task 2.4, the industry was to implement the global methods developed in Task 2.3 into their own codes of choice, validate them against the benchmark test results, and provide an assessment of the various global methods in a unified report produced by the three industry partners.

In WP 5 the primary purpose of the specimen test programme was to support the detailed modelling methods in WP 4, but they also supported generic themes running through the project at all levels (e.g. composite-to-metal joints, bolted repairs).

The activities in WP 4 were divided into three initial tasks. Task 4.1 was devoted to full three-dimensional finite element analysis of multi-fastener joints. Pre-processors for generation of such models were also to be developed. Task 4.2 involved the development of progressive damage models, and fatigue failure criteria. Both these tasks were to be validated against specimen tests. In Task 4.3 the global-local methods were to be developed and tested on the benchmark structures.

In Task 4.4, the techniques developed in Tasks 4.1, 4.2 and 4.3 were to be further validated against test results in BOJCAS and the literature, and their abilities to predict the effects of parameter changes (e.g. w/d, e/d, etc.) assessed.

In WP 6, the detailed design tools developed were to be assessed, and design guidelines generated from the analyses and tests were to be documented.

In WP 7, to aid in exploitation of the results, a CD-ROM or DVD disk was to be produced with electronic copies of all the reports. A web site was also to be produced, and the Technology Implementation Plan (TIP) was to be developed.

Broadly speaking, this structure was followed in the programme. Delays in several tasks meant that results did not feed in at the original time envisaged, but nevertheless eventually, all the aspects of the programme were covered, including the links between the global and local levels.

A detailed assessment of the deviations from the original work plan is deferred until Section 6.



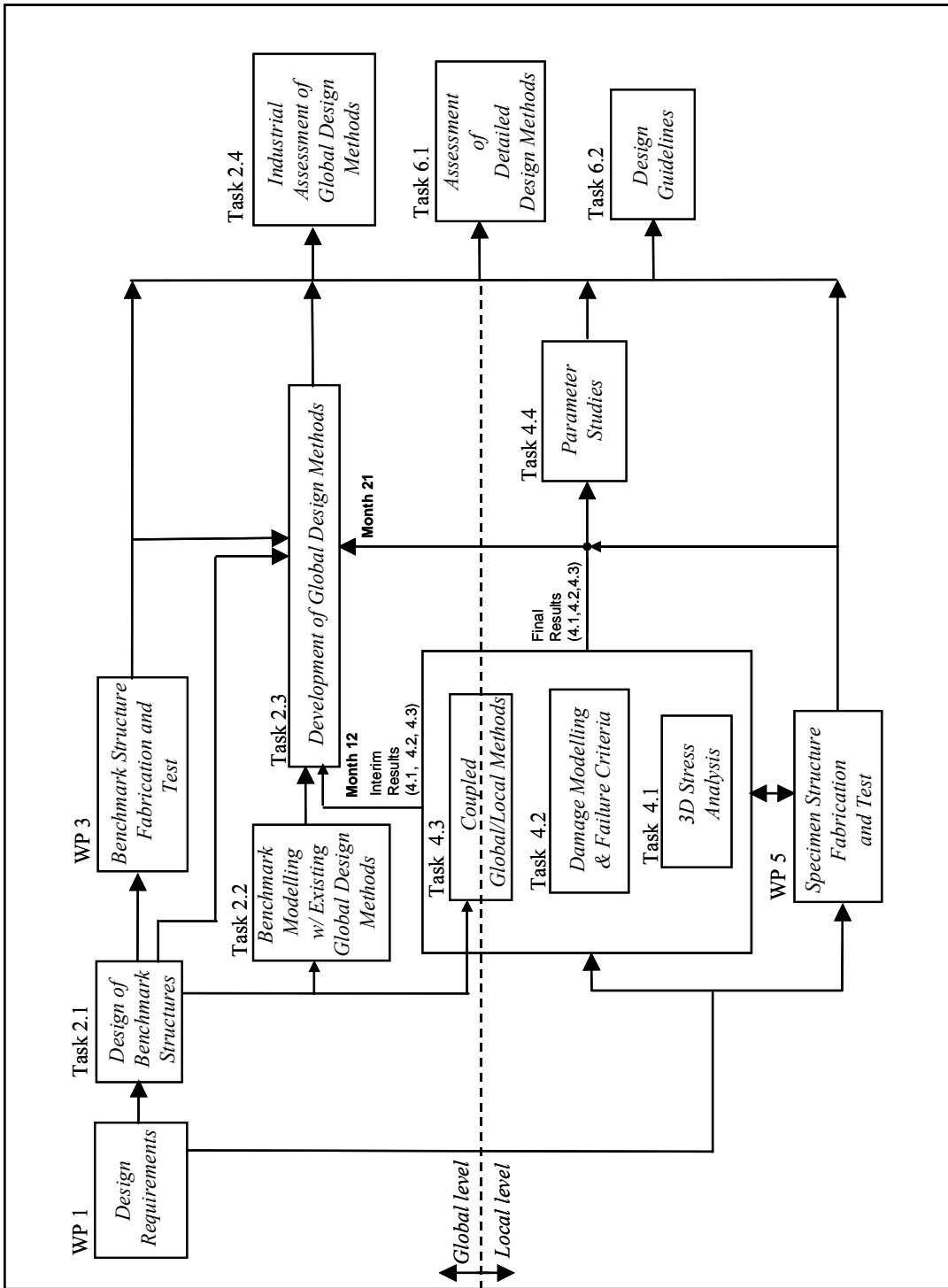


Fig. 3.2 BOJCAS Programme Structure

## 2 Scientific and Technical Description of the Results

The results description is split along workpackage lines, since this is still the most logical breakdown. In some cases, the reader may wish to change the sequence in which the material is read (e.g. WP 3 - benchmark experimental results before Tasks 2.3 and 2.4 - benchmark model results), but this is probably not necessary.

### 2.1 WP 1: Design Requirements

This short (2 month) workpackage was devoted to determining the broad details of the benchmark structures to be tested in WP 3. Detailed sizing was left to Task 2.1. The benchmark structures were to be complex, multi-bolt joints, suitable for providing a challenging test for the Global Design Methods of WP 2, and the Global-Local Methods of Task 4.3.

The three aircraft manufacturing partners (AUK, AD, and SAAB) were involved in this task, and the three resulting series of structures became known as the **BAe benchmark structures**, the **DA benchmark structures** and the **SAAB benchmark structures**. Despite name changes to two of these partners in the course of the project, these names for the benchmark structures were retained to avoid confusion.

#### WP 1: Airbus UK

The BAe benchmark joints were selected to be representative of the high load transfer joints that would be required for joining the metallic and composite wing skins of a hybrid wing box. They were relevant to the design of the TANGO lateral wingbox (contract No. G4RD-CT-2000-00241). A hybrid lateral wingbox with a CFC outboard wingbox is regarded as a potential weight saving structure provided that an efficient overall structure can be designed. The whole CFC outboard wing box needs to be developed to provide an efficient design and one part of this structure is the joint. The joint design has to be optimised to retain any benefit from the use of a hybrid wing.

Fig. 4.1.1 shows the basic concept behind the selection of the benchmark joints. The stringer-stiffened aluminium alloy and composite skins are joined via splice plates. The benchmark test specimens represent a slice of joint with one line of bolts. Two types of joint can be identified in Fig. 4.1.1: a joint between stringer blades and a joint between skins. Both these types of joint were represented in the chosen benchmark series, with the stringer blade joints having protruding head fasteners, and the skin joints having countersunk fasteners (for aerodynamic reasons). In addition joints representative of the top skin (to be loaded in compression) and of the bottom skin (to be loaded in tension) were included. The bottom metallic skin is a fatigue-driven design, so fatigue tests were planned for this type of joint.

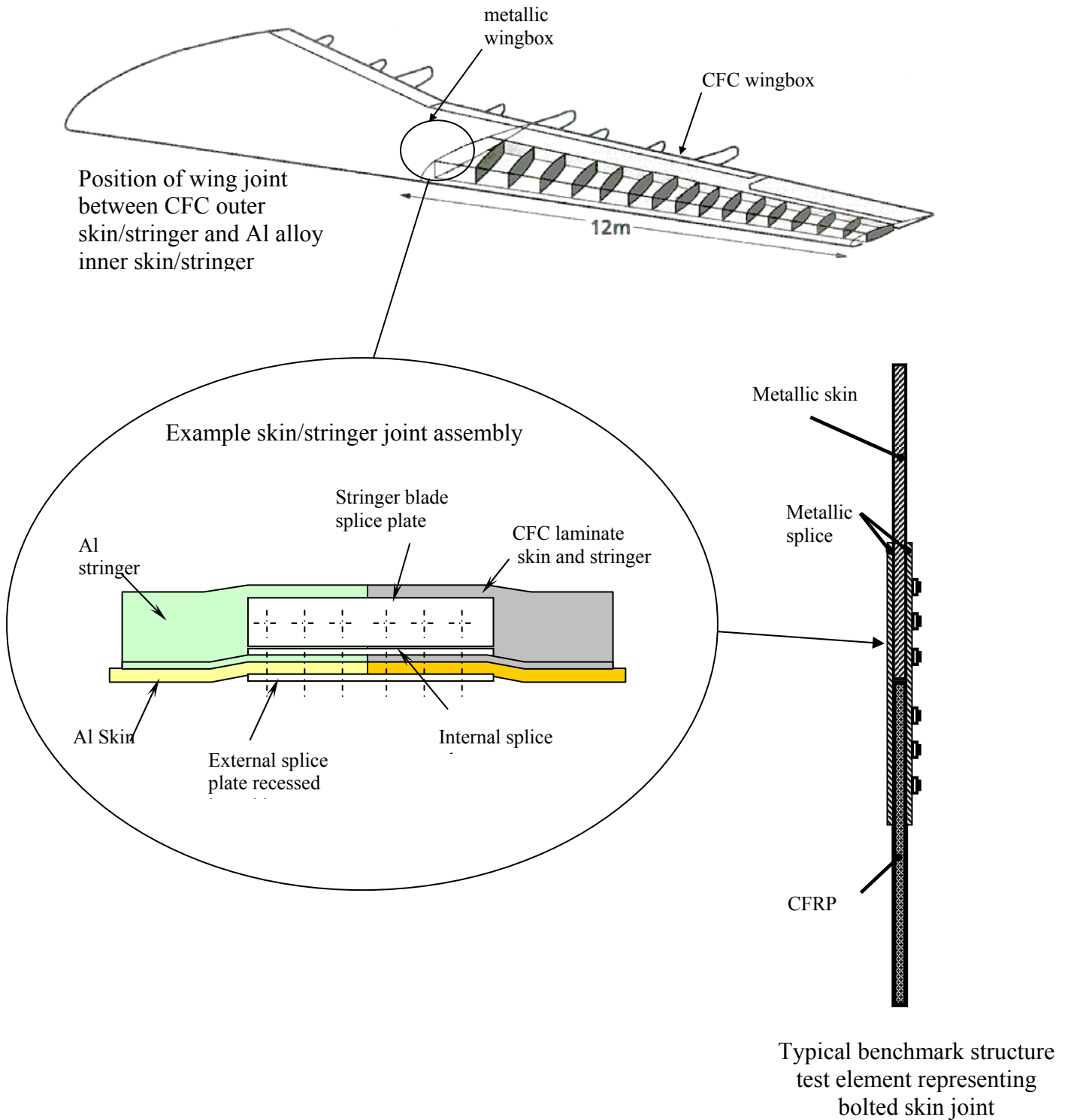


**Figure 4.1.1 Location of wing joint & typical configuration of BAe benchmark structure**

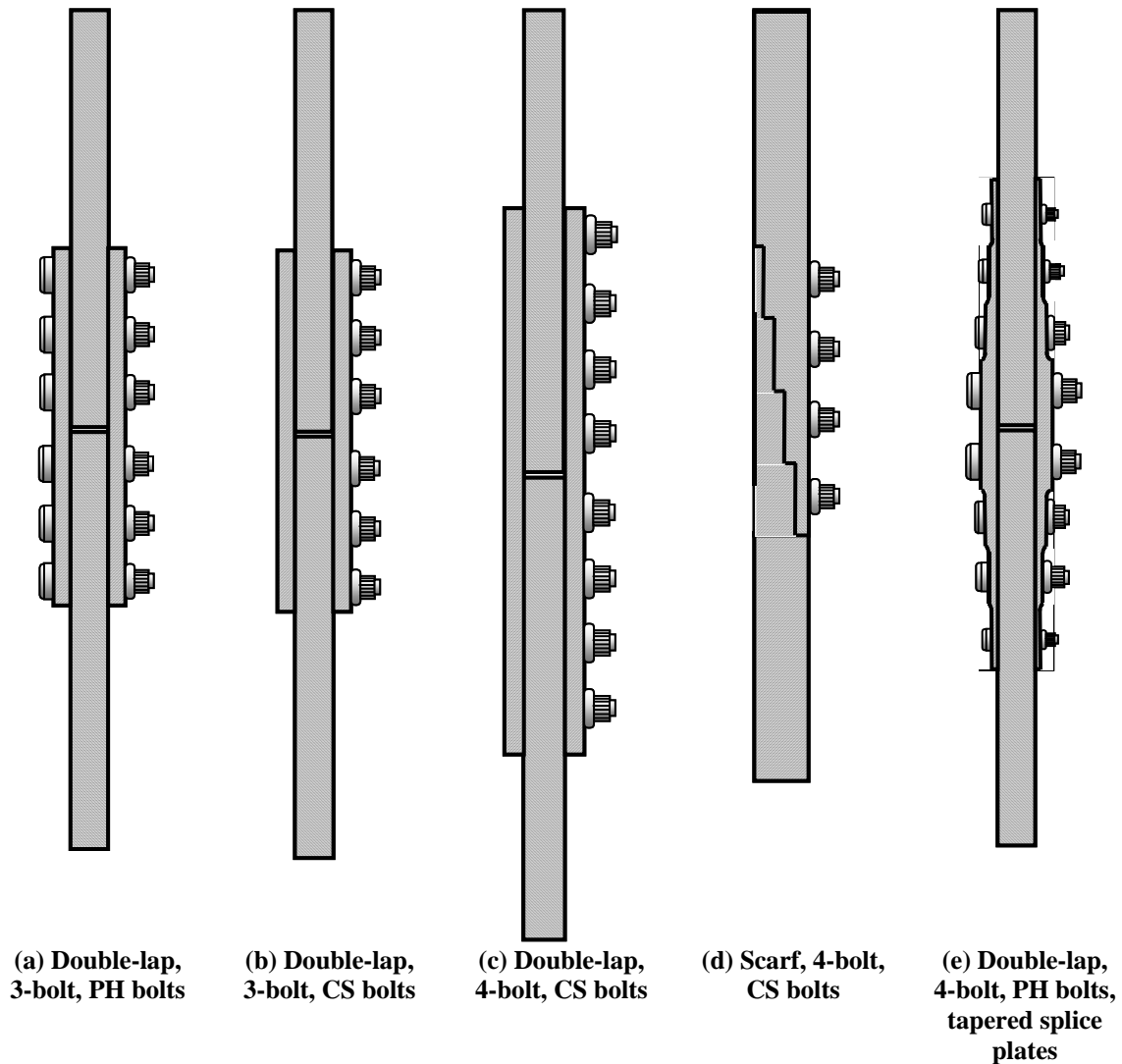


**Figure 4.1.2 Some of the BAe benchmark configurations selected**

Three different joint configurations (single-lap, double-lap and scarf) were considered, and the advantages and disadvantages were described in D1.1. Single-lap joints were rejected due to the large skin joggle and fastener sizes required due to secondary bending. Both double-lap joints and scarf joints were included in the series. Fig. 4.1.2 illustrates some of the configurations chosen. The joint in Fig. 4.1.2(e) featured tapered splice plates and graded fastener sizes, in an effort to tailor the load transfer to achieve weight saving.

In all, ten different benchmark configurations were selected. Relevant wing loads were extracted to allow panel loads to be determined. Preliminary drawings were produced and included in D1.1.



### **WP 1: Airbus Deutschland**

The DA benchmark structures focused on bolted repairs of composite structures. For many damage scenarios standard repair configurations and procedures have been developed and tested by the Aircraft Manufacturer (OEM). These standard repairs are described in the Structure Repair Manual released by the OEM. Tests of repaired parts generally result in a higher strength level compared to the original structure, but regarding optimisation of repair designs, there is limited potential due to the fact that bolt patterns are pre-defined by geometry needs (e.g. stiffener spacing), and part thickness by stiffness requirements. In particular, thin stiffened panels are not designed for strength but for stiffness requirements.

Nevertheless bolted composite repair configurations were included in the benchmarking exercise within BOJCAS because improved analysis of repairs will considerably reduce testing needed for the certification of repair configurations and procedures to be given as standards within the Structure Repair Manual. The repairs also represent complex multi-bolt joints, loaded in compression, which provide a severe test for modelling methods. The defined benchmark configurations were thus principally based on the standards given in the SRM. The testing conditions however, and the detailed design, needed to allow for an initial failure at the repaired section and not in the area of the original structure. For this reason the benchmark structure designs were not completely conformable to the guidelines given in the SRM.

An outline design was given in deliverable D1.2 for four different DA benchmark joint configurations representing bolted composite skin and skin/stringer standard repairs for the Airbus A330 fin-box shell including panel geometry, materials, lay-ups, loads and test configurations. The bolted repair benchmark specimens were defined from the cut-out panels shown in Fig. 4.1.3 as follows:

from area R10-R13/P2-P6: two standard skin repairs:

**DA-BM-1-T:** temporary repair using metallic parts and blind rivets

**DA-BM-1-P:** permanent repair using all composite parts and HILOK bolts

from area R3-R4 / P9-P13: two standard skin/stringer repairs:

**DA-BM-2-T:** temporary repair using metallic parts and blind rivets

**DA-BM-2-P:** permanent repair using all composite parts and HILOK bolts

The principle features of the skin and skin-stringer repairs are shown in Figs. 4.1.4 and 4.1.5 respectively. Fig. 4.1.6 illustrates the differences between the temporary and permanent repairs – note the flush external surfaces on the permanent repairs. Finally Table 4.1.1 summarises the proposed specimen tests, indicating a total of 4 static tests and 2 fatigue tests.

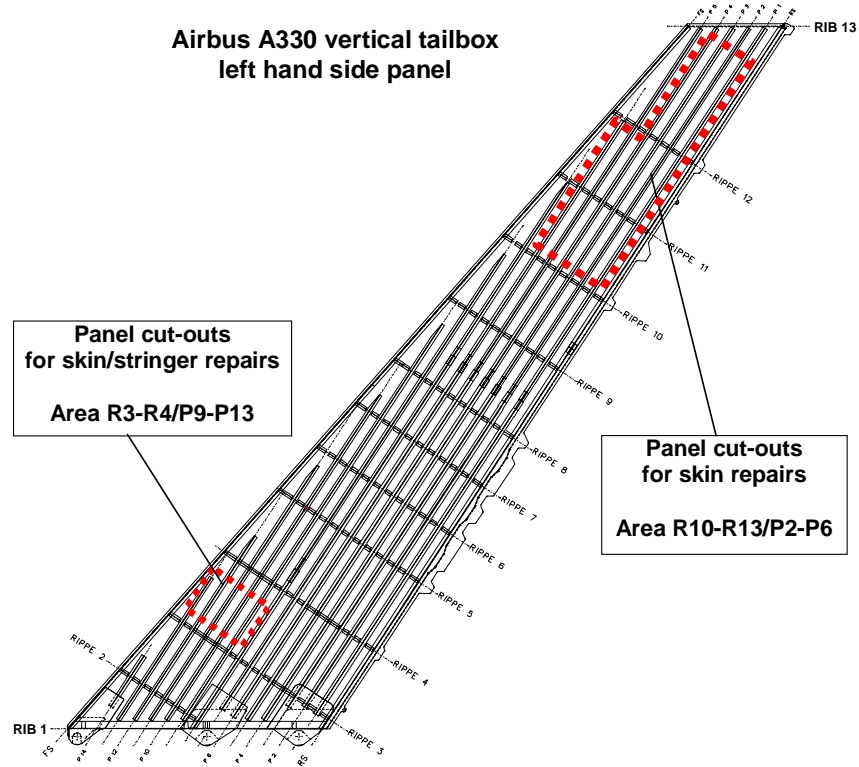


Figure 4.1.3 Location of panel cut-outs for DA benchmark bolted composite repairs

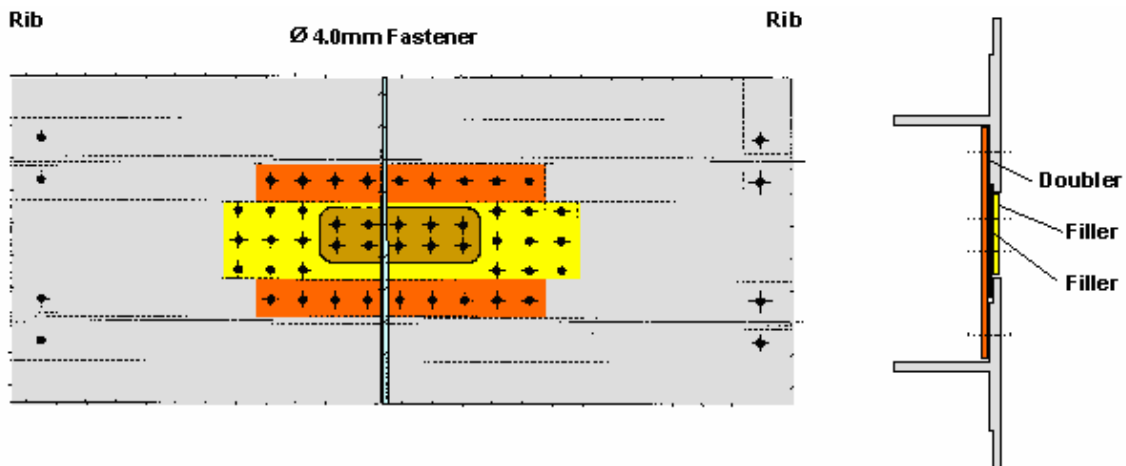
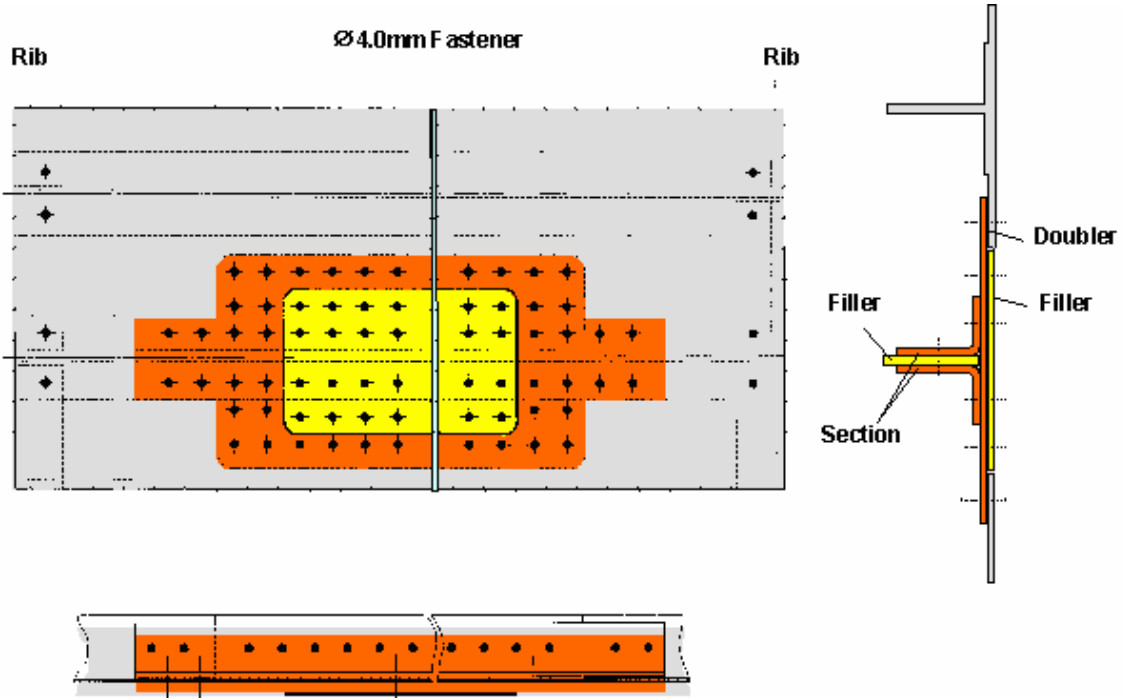


Figure 4.1.4 Repair principle for DA skin repair benchmark



**Figure 4.1.5 Repair principle for DA skin/stringer repair benchmark**

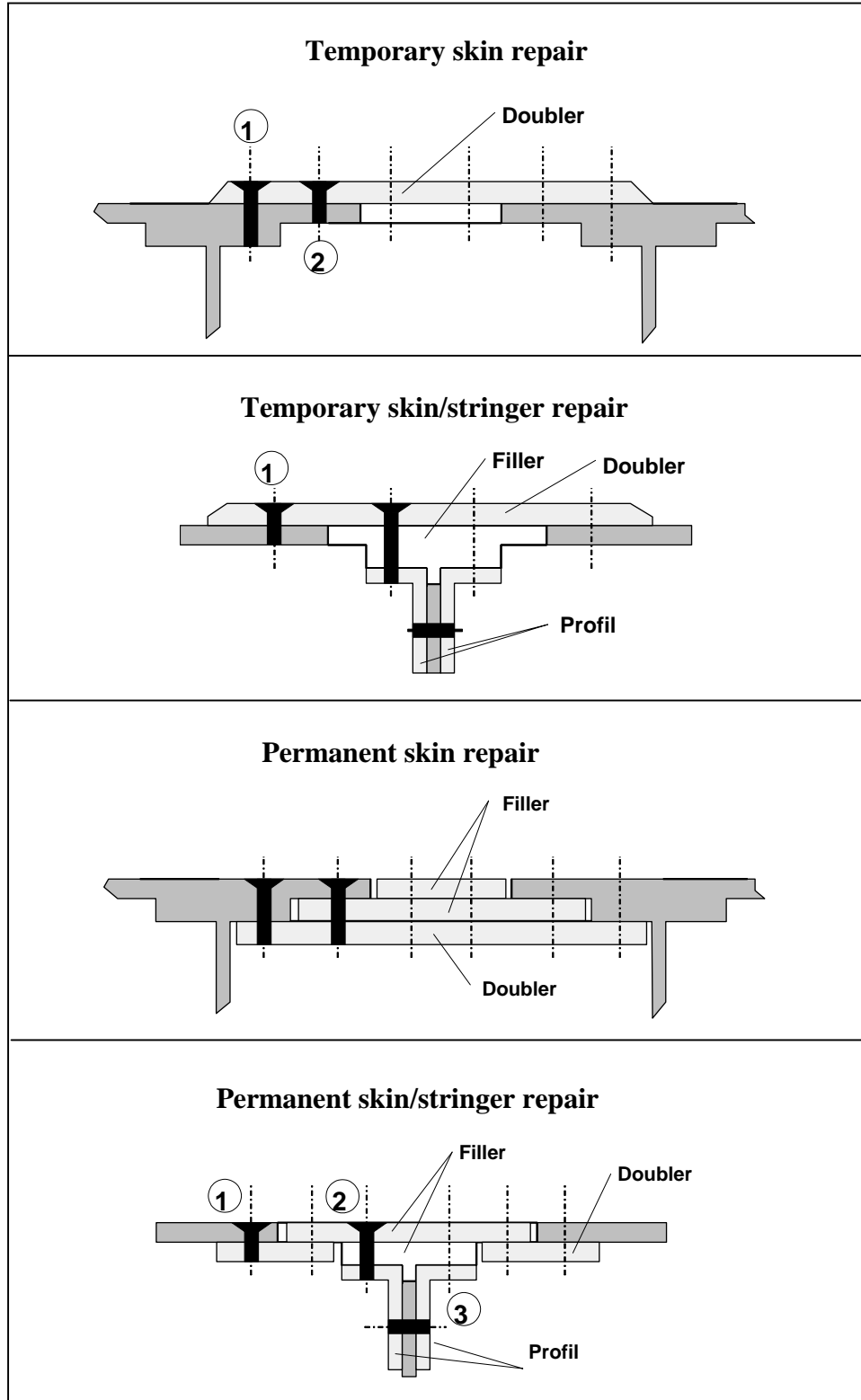


Figure 4.1.6 Design principles of temporary and permanent DA repair benchmark configurations

Benchmark Reference	<i>DA-BM-1-T</i>	<i>DA-BM-1-P</i>	<i>DA-BM-2-T</i>	<i>DA-BM-2-P</i>
Type of Repair	Temporary skin repair	Permanent skin repair	Temporary skin/stringer repair	Permanent skin/stringer repair
skin thickness	1.75 mm	1.75 mm	3.5 mm	3.5 mm
stringer flange thickn.	4.66 mm	4.66 mm	4.66 mm	4.66 mm
stringer foot thickness	1.58 mm	1.58 mm	1.58 mm	1.58 mm
bolt types ( 4mm diam. )	NAS1921-5	HL1011/HL94-5	NAS1919-5 NAS1921-5	HL1011/HL94-5 HL1012VF5/HL94-5
fatigue loading	-	compression R=0.01 50.000 cycles 0.62 % UL	-	compression R=0.01 50.000 cycles 0.62% UL
static loading	compression	compression residual strength	compression	compression residual strength

**Table 4.1.1: Summary of DA benchmark test specimens**

**WP 1: SAAB**

The SAAB benchmark structures were not intended to represent real aircraft structures, but instead were chosen to validate the developed modelling tools in a challenging way. Thus 20-bolt structures with two different bolt patterns, and two different joint configurations (double-lap and single-lap) were selected (see Figs. 4.1.7 and 4.1.8). Damage tolerance was to be addressed by removing some bolts. Tests in tension and compression were planned, under quasi-static and fatigue loading (see Table 4.1.2).

Test	Bolt pattern 1	Bolt pattern 2	Type of joint
Static tension	1	1	Single overlap
Static compression	1	1	Double overlap
Static tension with one missing bolt	1	1	Single overlap
Static tension with two missing bolts	1	1	Single overlap
Fatigue	2		Double overlap
Fatigue with missing bolt(s)	2		Double overlap
<b>Total number of specimens:</b>	<b>8</b>	<b>4</b>	

**Table 4.1.2 Overview of SAAB benchmark test programme**

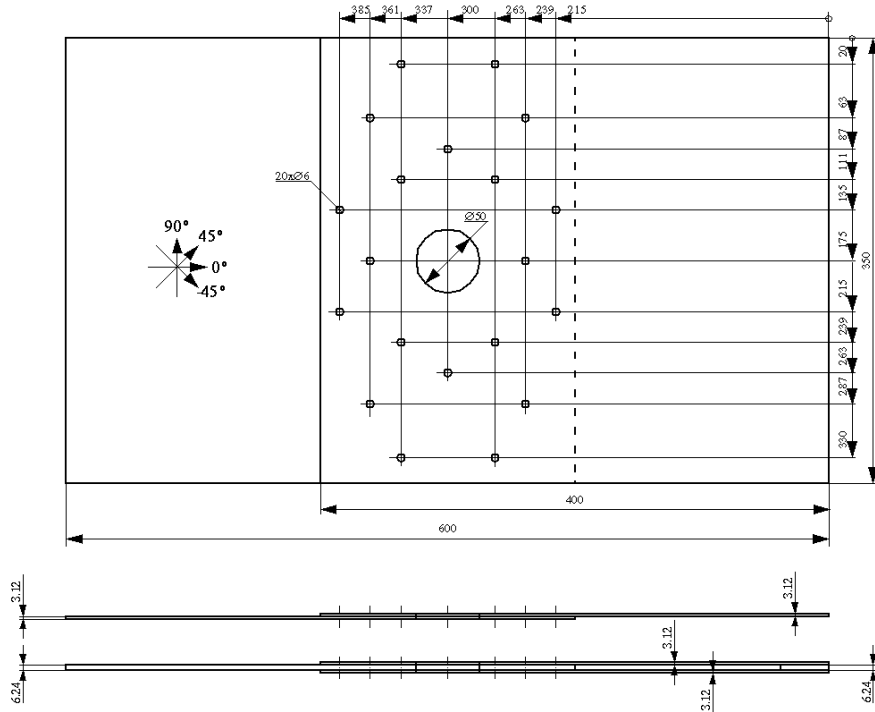


**Figure 4.1.7 Geometry/Bolt pattern for SAAB benchmark configuration 1, - both single lap and double lap joints are shown in the side view**

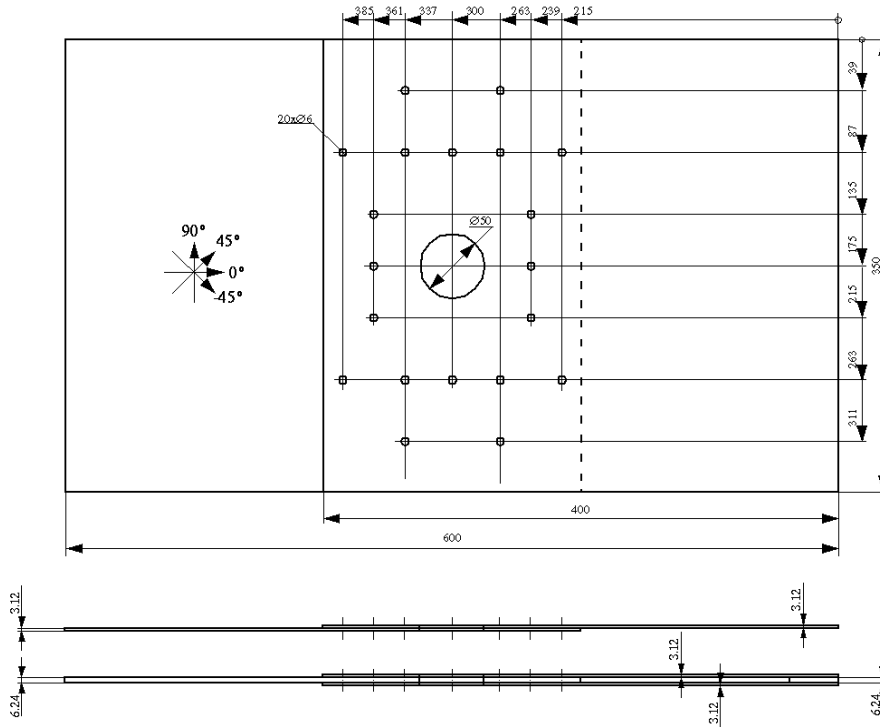


**Figure 4.1.8 Geometry/Bolt pattern for SAAB benchmark configuration 2, - both single lap and double lap joints are shown in the side view**

## 2.2 WP 2: Global Design Methods

### 2.2.1 Task 2.1 Design of Benchmark Structures

In this first task of WP 2, the objective was to perform detailed design of the benchmark structures, using “traditional” industry methods. These methods varied considerably between the three industry partners. The starting point was the outline designs from WP 1, and the outcome was to be engineering drawings to be used for specimen manufacture in WP 3. In addition, predictions were to be made of bolt load distributions and failure loads, again using “traditional” methods. Again, the three aircraft manufacturing partners (AUK, AD, and SAAB) were involved in this task

#### Task 2.1 Airbus UK

Airbus UK used a one-dimensional spring model (see Fig. 4.2.1) to determine the bolt load distributions in the ten BAe benchmark configurations. The model in Fig. 4.2.1 represents a quarter model of the joint in Fig. 4.1.2(a). Splice and skin stiffnesses were calculated from elementary equations of the form  $k = EA/l$ . Bolt stiffnesses  $Kb1$ ,  $Kb2$  and  $Kb3$  were calculated from equations for bolt shear, bolt bending, bolt bearing, splice bearing and skin bearing (Ref [1]).

From these loads, bearing and bypass stresses were determined for each hole and bearing/bypass diagrams of the type shown in Fig. 4.2.2 were produced for the critical locations. In this diagram, two lines bound the safe operating envelope. The horizontal bearing cut off line is the maximum bearing stress for the given lay-up. The diagonal line is plotted between the maximum bypass stress with zero bearing stress and the maximum bearing stress with zero bypass stress. Several correction factors for items such as hole size, edge distance, notch factors etc. have to be applied to determine the allowable values. This diagram allows the interaction that takes place between bearing and bypass loads to be taken into account, when determining the likely failure load at a particular location in a joint. In the example in Fig. 4.2.2, the plotted point falls just outside the envelope, resulting in a reserve factor of less than 1, indicating that this is a critical location in the joint.

The possibility of shear-out failure was also considered, while bolt-bending and secondary bending effects were not considered significant for the joints in question.

Based on these analyses, the detailed design of the ten configurations was done, and some of the details including reference codes are shown in Table 4.2.1. Finally, the bolt load distribution and failure loads and modes were predicted and are shown in Table 4.2.2.

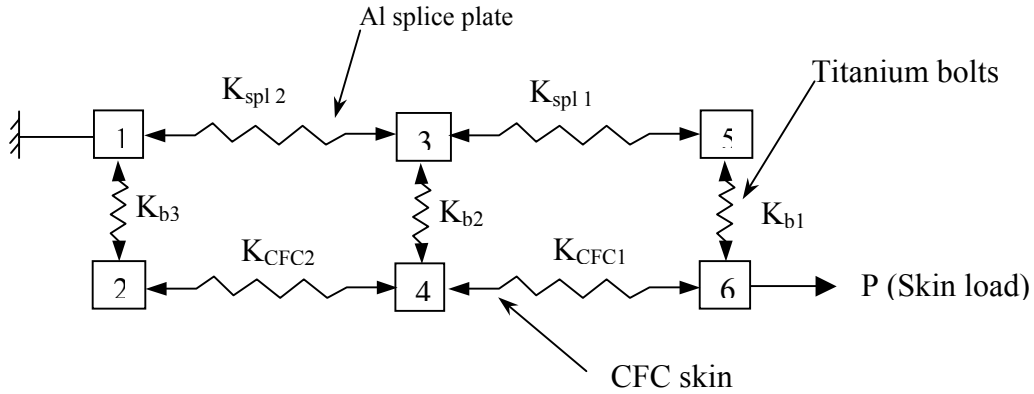


Figure 4.2.1 AUK’s spring element representation of CFC skin, splice plate and bolts

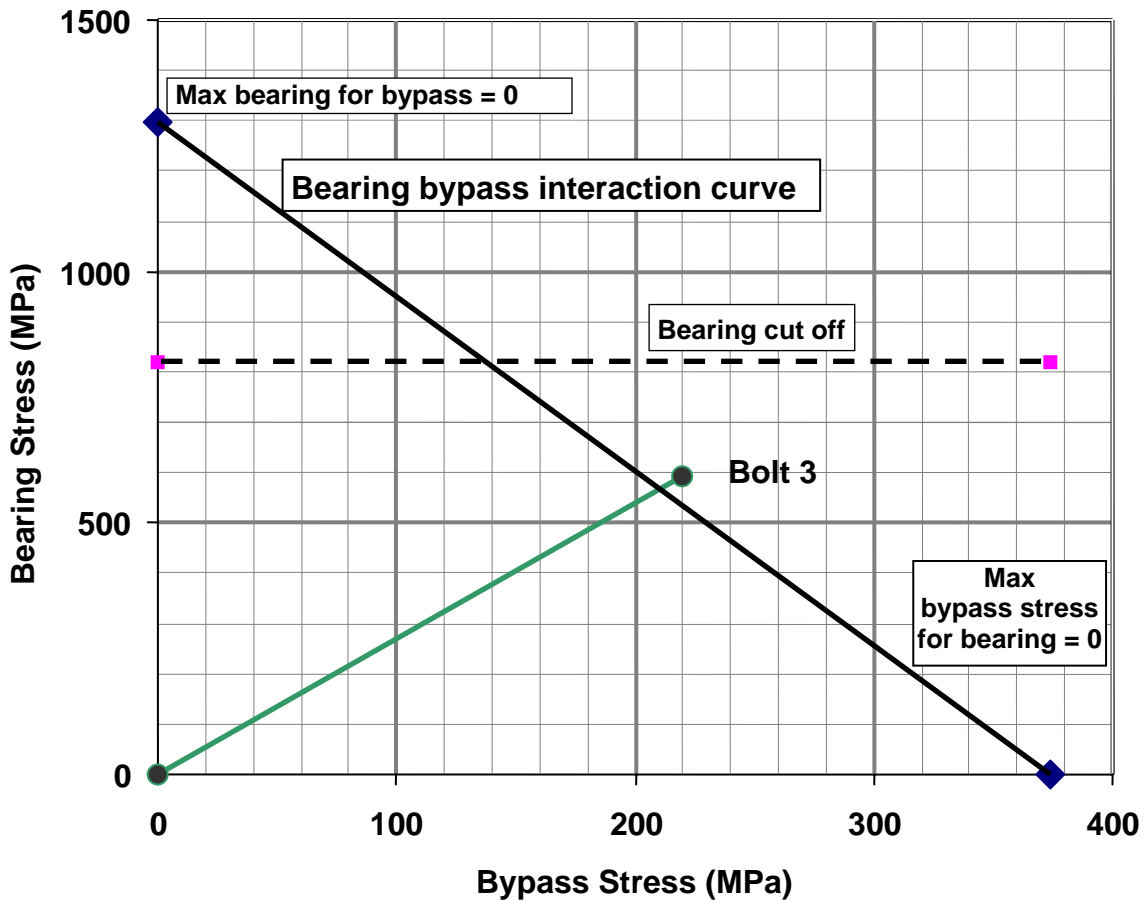


Figure 4.2.2 Typical Bearing-Bypass Diagram for used by AUK in Task 2.1



	1	2	3	4	5
Benchmark Ref	<b>BAE-BM-1T</b> Btm skin Stringer-Blade Joint	<b>BAE-BM-1C</b> Top skin Stringer-Blade Joint	<b>BAE-BM-2T</b> Btm skin Skin Joint	<b>BAE-BM-2C</b> Top skin Skin Joint	<b>BAE-BM-3T</b> Btm skin Skin Joint
Drawing No	MCWTR0488	MCWTR0489	MCWTR0490	MCWTR0491	MCWTR0492
Joint configuration	3 bolt double lap	3 bolt double lap	3 bolt double lap	3 bolt double lap	4 bolt double lap
No of specimens*	3T	3C	3T 3F	3C	3T 3F
Joint width (mm)	90	100	90	100	90
<i>Splice mat'l</i>	AS4 8552	AS4 8552	2024 T351	7150 T651	2024 T351
Splice thk (mm)	7.28	7.28	10	7	10
Inboard skin	AS4 8552	AS4 8552	2024 T351	7150 T651	2024 T351
Skin thk (mm)	14.56	11.44	14	10	14
Bolt dia (inch)	0.625 pr hd	0.625 pr hd	0.625 Csk hd	0.5625Csk hd	0.625 Csk hd
Outboard skin	AS4 8552	AS4 8552	AS4 8552	AS4 8552	AS4 8552
Skin thk (mm)	14.56	11.44	14.56	10.4	14.56
Bolt dia (inch)	0.625	0.625	0.625	0.5625	0.625

	6	7	8	9	10
Benchmark Ref	<b>BAE-BM-3C</b> Top skin Skin Joint	<b>BAE-BM-4T</b> Btm skin Skin Joint	<b>BAE-BM-4C</b> Top skin Skin Joint	<b>BAE-BM-5T</b> Btm skin Stringer-Blade Joint	<b>BAE-BM-6C</b> Top skin Skin Joint
Drawing No	MCWTR0493	MCWTR0494	MCWTR0495	MCWTR0496	MCWTR0497
Joint configuration	4 bolt double lap	4 bolt scarf	4 bolt scarf	3 bolt blade joint, tapered splice	4 bolt double lap tapered splice
No of specimens*	3C	3T 3F	3C	3T	3C
Joint width (mm)	100	90	100	75	100
Splice mat'l	7150 T651	-	-	2024 T351	7150 T651
Splice thk (mm)	7	-	-	4/4.5/5	5.5/6/6.5/7
Inboard skin	7150 T651	2024 T351	7150 T651	2024 T351	7150 T651
Skin thk (mm)	10	10/12/14/16	10/12/14/16	10	10
Bolt dia (inch)	0.5625 Csk hd	0.75 Csk hd	0.75 Csk hd	0.4375/0.5/ 0.5625 pr hd	0.4375/0.5/0.5 /0.5625 Cskhd
Outboard skin	AS4 8552	AS4 8552	AS4 8552	AS4 8552	AS4 8552
Skin thk (mm)	10.4	15.6/13.52/ 11.44/9.36	15.6/13.52/ 11.44/9.36	10.4	10.4
Bolt dia (inch)	0.5625	0.75	0.75	0.4375/ 0.5/0.5625	0.4375/0.5/ 0.5/0.5625

\* C = compression      T = tension      F = fatigue  
pr hd = protruding head bolts  
Csk hd = countersunk head bolts

**Table 4.2.1 Summary of BAe Benchmark Structure Dimensions & Materials**

	1	2	3	4	5
Benchmark Ref	<b>BAE-BM-1T</b> Btm skn	<b>BAE-BM-1C</b> Top skin	<b>BAE-BM-2T</b> Btm skin	<b>BAE-BM-2C</b> Top skin	<b>BAE-BM-3T</b> Btm skin
Basic config	3 bolt double lap	3 bolt double lap	3 bolt double lap	3 bolt double lap	4 bolt double lap
Splice mat'l	AS4 8552	AS4 8552	2024 T351	7150 T651	2024 T351
Inboard skin	AS4 8552	AS4 8552	2024 T351	7150 T651	2024 T351
Outboard skin	AS4 8552	AS4 8552	AS4 8552	AS4 8552	AS4 8552
Loading	Tension	Comp	Tension	Comp	Tension
Running Load Ultimate (N/mm)	4000	4000	4000	4000	4000
Joint width (mm)	90	100	90	100	90
Load Ultimate (N)	360000	400000	360000	400000	360000
R.F.	0.98	0.94	0.96	0.80	1.0
Failure mode	Net section 1 <sup>st</sup> bolt splice	laminat compression failur bolt1	splice brg 1 <sup>st</sup> bolt	laminat compression failur	Net section 1 <sup>st</sup> bolt laminat
Failure load (N)	352800	376000	345600	320000	360000
Bolt Postion	% Load distribution on the bolts				
1	34.8	36	33.3A 36.5C	33.3A 36C	25.0A 30.3C
2	30.4	31	33.3A 30.5C	33.3A 31C	25.0A 22.7C
3	34.8	33	33.3A 33.0C	33.3A 33C	25.0A 21.3C
4	-	-	-	-	25.0A 25.7C

	6	7	8	9	10
Benchmark Ref	<b>BAE-BM-3C</b> Top skn	<b>BAE-BM-4T</b> Btm skin	<b>BAE-BM-4C</b> Top skin	<b>BAE-BM-5T</b> Btm skin	<b>BAE-BM-6C</b> Top skin
Basic config	4 bolt double lap	4 bolt scarf	4 bolt scarf	3 bolt blade joint, tapered splice	4 bolt double lap tapered splice
Splice mat'l	7150 T651	none	none	2024 T351	7150 T651
Inboard skin	7150 T651	2024 T351	7150 T651	2024 T351	7150 T651
Outboard skin	AS4 8552	AS4 8552	AS4 8552	AS4 8552	AS4 8552
Loading	Comp	Tension	Comp	Tension	Comp
Running Load Ultimate (N/mm)	4000	3000	3300	3000	4000
Joint width (mm)	100	90	100	75	100
Ultimate Load (N)	400000	270000	330000	225000	400000
R.F.	0.88	1.01	1.03	0.71	0.82
Failure mode	laminat compression failur 1 <sup>st</sup> bolt	Al skin brg bolt 1	laminat bolt1	splice brg bolt1	splice brg bolt1
Failure load (N)	352000	272700	339900	159750	328000
Bolt Postion	% Load distribution on the bolts				
1	25.0A 29.5C	23.9	23.8	25.3A 32.0C	19.0 A 26.5C
2	25.0A 23.0C	24.8	24.8	33.0A 30.2C	24.8A 22.8C
3	25.0A 21.8C	25.3	25.4	41.7A 37.8C	24.8A 22.8C
4	25.0A 25.7C	26.0	26.0	-	31.4A 27.9C

Note: Load distribution xxA = Aluminium side xxC = composite side

**Table 4.2.2 Predicted loads and failure modes for BAe benchmark structures**

### Task 2.1 Airbus Deutschland

The special problem with the detailed repair benchmark design was, that the standard design methods for repairs were closely related to the parameters given in the standard repair manuals *SRM*. These designs generally result in a higher strength level in the repaired region than in the original structure. The benchmark test panels on the other hand should allow for an initial failure at the repaired section and not in the area of the original structure. For this reason the benchmark designs were not completely conformable to the guidelines given in the *SRM* and required some additional analysis compared to the current design practice,

Therefore two different design methods were applied by DA and described in the deliverable report D2.1-2:

- **For the temporary repairs:** Classical strength justification based on design charts and stress handbooks.
- **For the permanent repairs:** Finite Element Method combined with stress handbook method.

Due to the much more complex configurations of the permanent repairs with fillers and doublers in addition to the patches, the Finite Element modelling was needed for dimensioning the repair for failure in the riveted region.

Fig. 4.2.3 illustrates the classical techniques used for the temporary repairs. The actual rivet forces depend on the position of the individual rivet within the doubler. It was assumed that each rivet in the first two rows carries an equal part of the tension or compression loading or in the other direction an equal part of the shear loading. This results in the equations shown in the figure and allows a quick estimate of the location of the most critical fastener(s). Allowable bearing strength for the laminate was then determined using several correction factors for effects such as finite width, finite edge distance, environmental conditions, bolt material, material lay-up etc., and the allowables for the aluminium doublers were taken from a stress handbook.

For the permanent repairs, several FE-models of the panels were created to estimate the resulting rivet forces and bearing stresses. Pre- and post-processing was done with MSC.Patran, using MSC.Nastran for linear and non-linear analysis. The models consisted of QUAD4 elements with composite material properties according to the laminate stacking sequences and RBARs for the connection of skin and stringer as well as for the modelling of the repair riveting. Between each rivet position there were three QUAD4 elements. All opposite nodes of doubler, filler and skin between the rivet positions were also coupled in translation normal to the shell by RBARs. To reduce the number of elements in the model the meshing outside the area of interest was coarser. The fine mesh was tied by RSPLINEs. The models were loaded in compression using a displacement of max. 3.2 mm at the outer edge ( $\gg 4 \text{ ‰}$  global strain). Fig. 4.2.4 illustrates the models and the resulting deformation and bolt loads at the doubler for both skin and skin/stringer repairs.

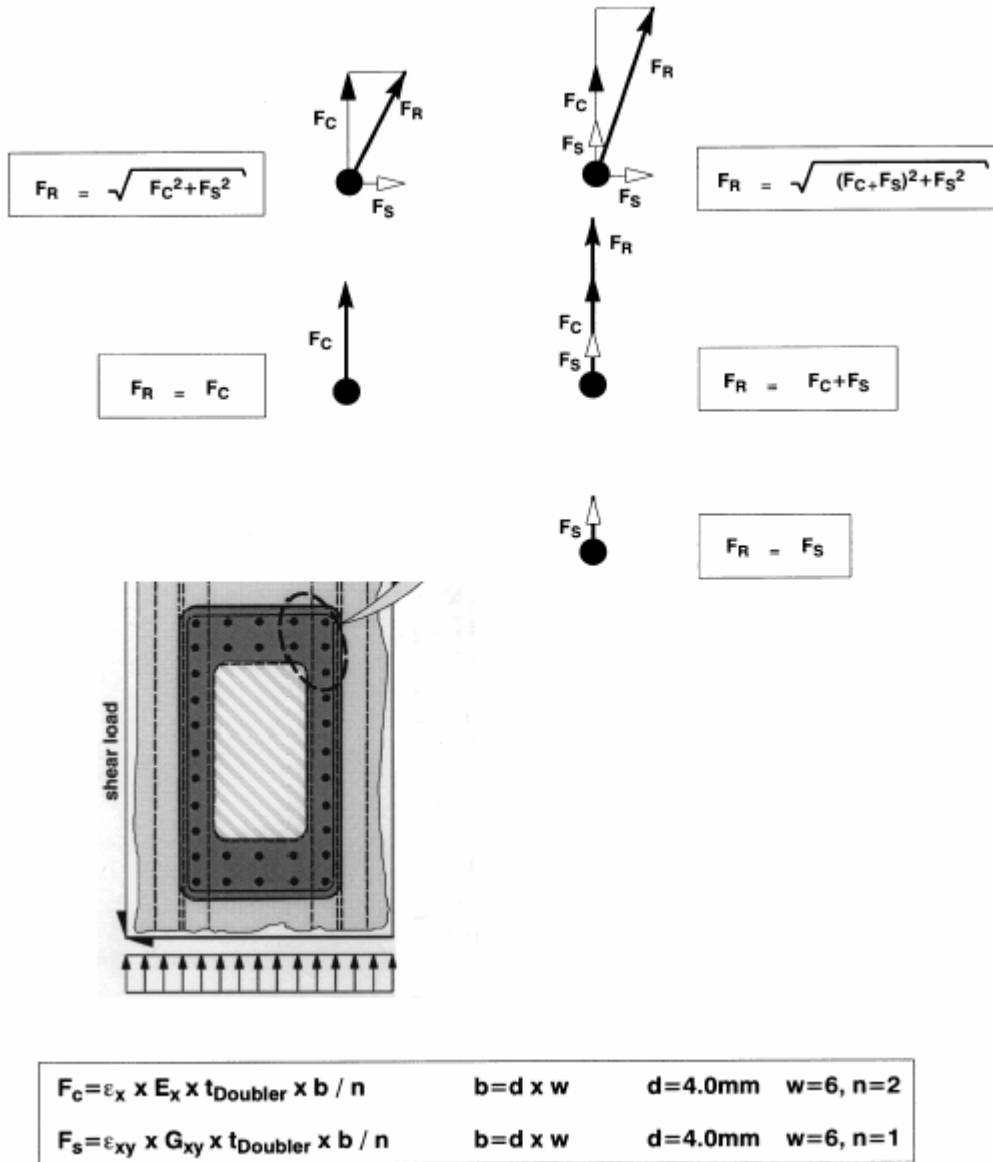
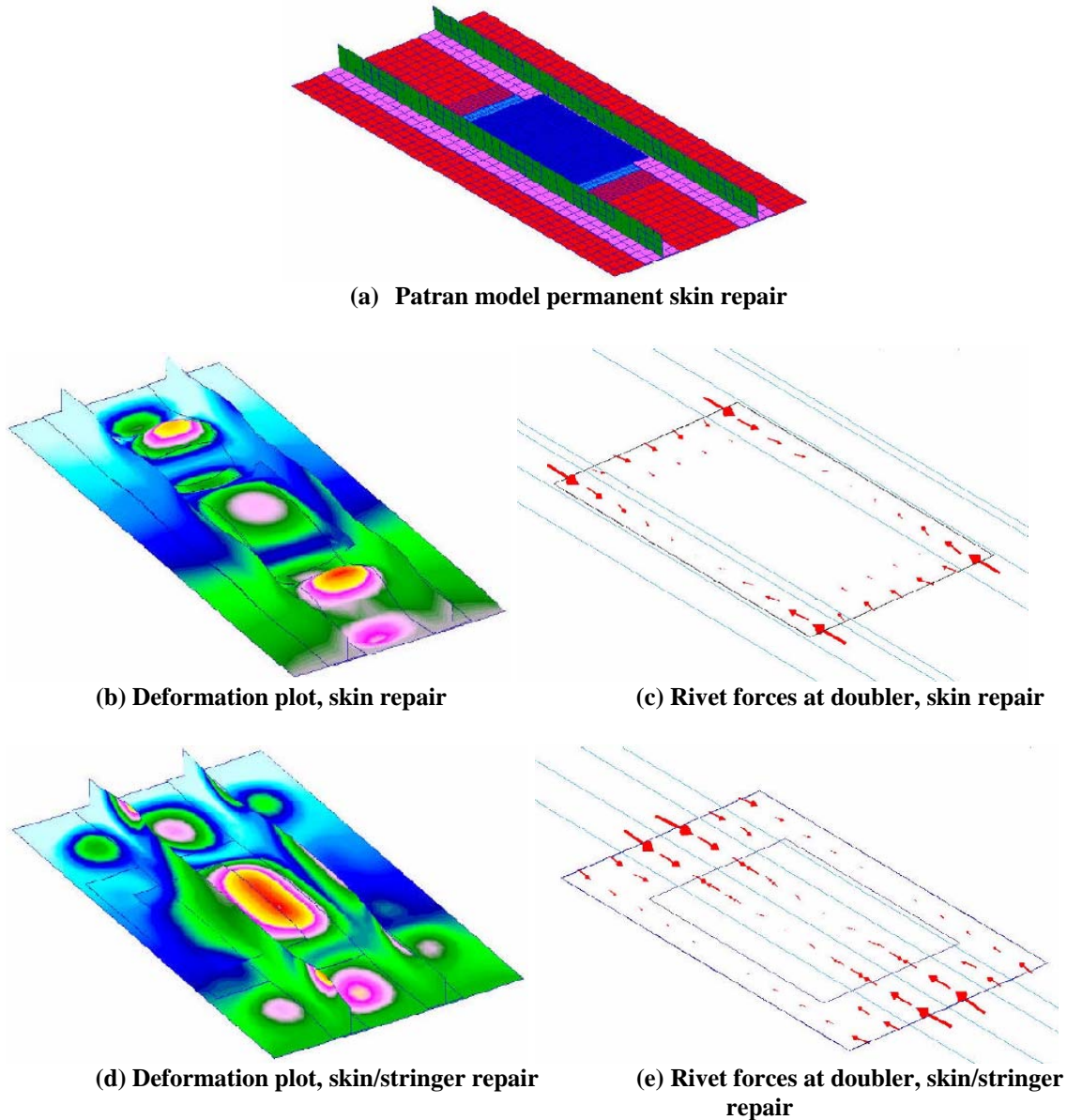


Figure 4.2.3 Calculation of rivet forces for temporary DA repair benchmark panels



**Figure 4.2.4 Models of DA permanent repairs**

For both repairs, the compression stiffness of the skin is considerably less than the stringer stiffness, so most of the applied compression load will be transferred through the stringer. Therefore it proved difficult to find a “bad” repair solution that will fail within the maximum strain level of the panel. For example, for the skin repair, it turned out that the only rivets that might fail by bearing stresses are the edge rivets at the stringer flanges, on condition that the doubler has a high stiffness and low thickness. For this reason, doubler lay-up and thickness had to be selected in a way, which was not conformable to the existing SRM rules for bolted composite repairs. The details of the lay-ups and thicknesses selected are given in D2.1-2. Finally, Figs. 4.2.5 and 4.2.6 show the predictions of failure locations and strains for the four DA benchmark structures.

Repair: Permanent skin  
Location: Doubler laminate  
Strain: 2,0 ‰

Temporary skin  
Skin laminate  
2,5 ‰

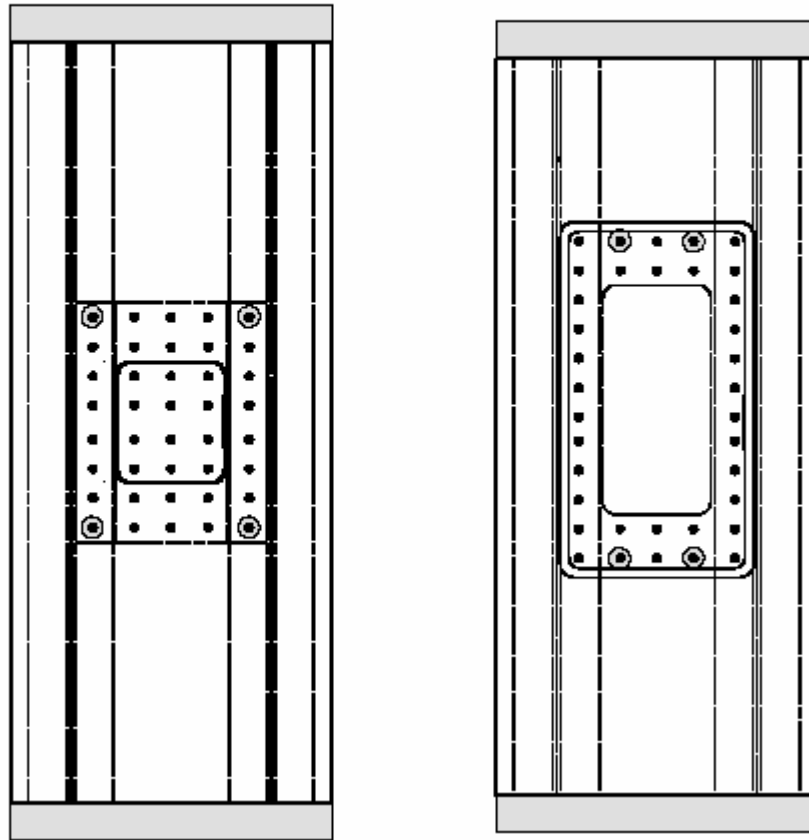
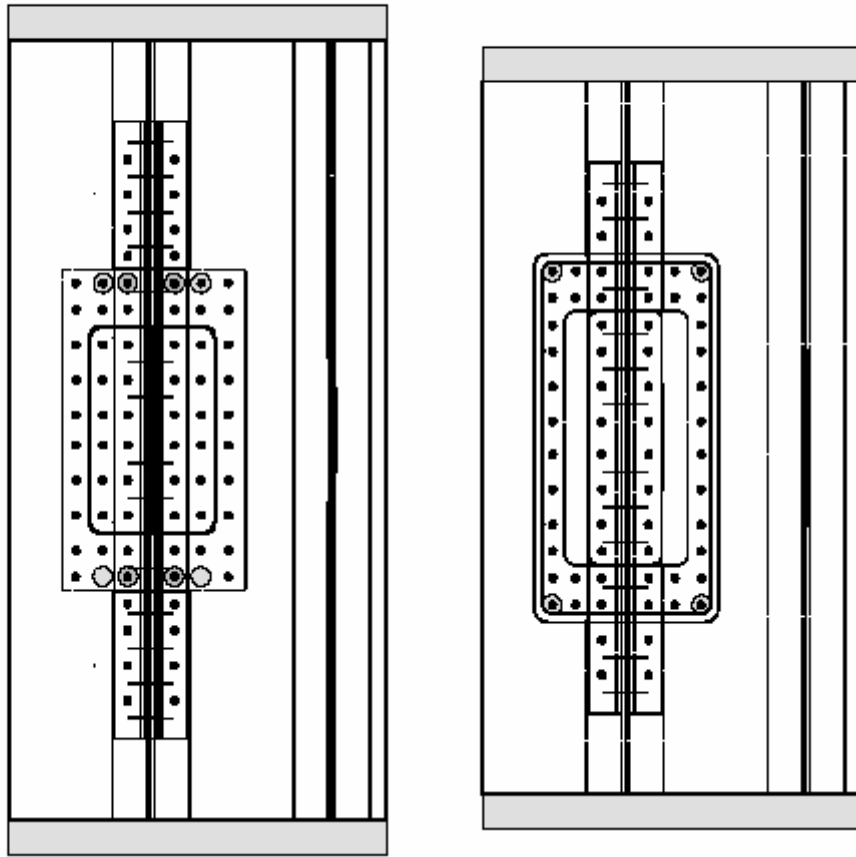


Figure 4.2.5 Predicted failure locations and strains for the skin repair panels

Repair: Permanent skin/stringer  
Location: Doubler laminate  
Strain: 1,5 ‰

Temporary skin/stringer  
Skin laminate  
2,5 ‰



**Figure 4.2.6 Predicted failure locations and strains for the skin/stringer repair panels**

### **Task 2.1 SAAB**

SAAB used three different methods to calculate the load distribution in the SAAB benchmark structures: an analytical method and two different finite element methods.

The analytical method used an in-house tool, BARROIS, based on an article in ref. [2]. The method bears some similarities to the AUK spring method (see Fig. 4.2.1 above). The method assumes a linear relation between the deflection,  $y$ , and the applied load,  $P$ :

$$y = f \cdot P$$

where  $f$  is the fastener flexibility.

Furthermore, the program calculates fastener flexibilities and stress concentrations for bearing pressure and countersunk holes. If the fastener flexibilities are known, they can also be given as input data and the program will only calculate load distributions and stress concentrations at countersunk holes. For simplicity, a simple one-dimensional model is used, which assumes there is a resultant fastener flexibility for each *row* of fasteners. Thus, the result shows the load transferred per row and does not describe the load transferred by single fasteners within the rows. The program has options to account for different types of fastener fixation, ranging from clamped with large rigid heads, to simply-supported with pins. Friction between the plates is neglected, as is bending stiffness of the joint.

For the FE method, the contact between the fastener and the parts was ignored. The hole was degenerated to a point (node) and the fastener was represented in one case by a beam (Fig. 4.2.7) and in the other case by a spring element.

This is typical of current industry practice for global joint modelling. However, as outlined in SAAB's deliverable D2.1-3, there are several difficulties with this method. For example, the flexibility to assign to the fastener beam element may be estimated from experiments, but it is not sufficient to just assign the experimental value to the fastener element since the deformation determined from the test includes both fastener and part deformation and these are not separable in practice. In the same way the deformation in the FE model depends on both the deformation in the element representing the fastener and the elements representing the parts. The latter is not equal to the experimental value because of the simplified connection used in the FE model, i.e. the omission of the hole. In addition, the flexibility of the parts is strongly dependent on the coarseness of the mesh. If the mesh in the parts is refined, it becomes more flexible and a stiffer modelling of the bolt is required to obtain the correct overall flexibility in the joint. To minimise these problems, a number of recommendations were given in D2.1-3, but the problems cannot be completely eliminated, because the hole is not modelled.



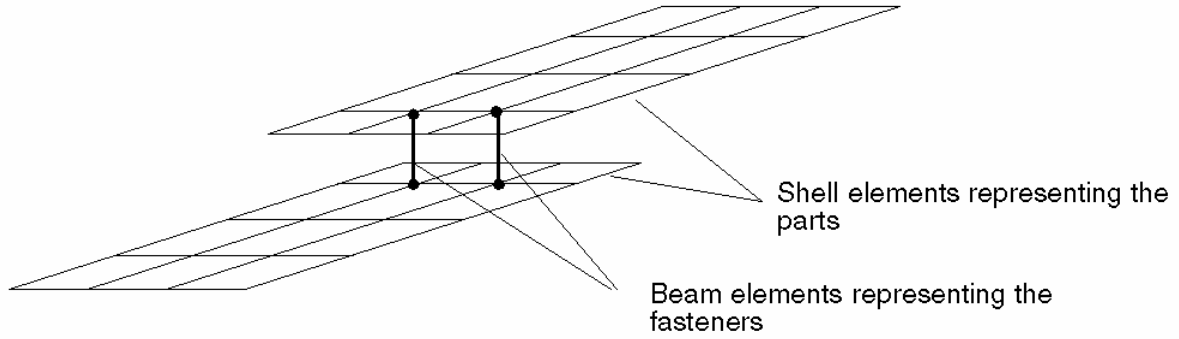


**Figure 4.2.7 FE method used in Task 2.1 by SAAB: holes degenerated to points and fasteners represented by beams**

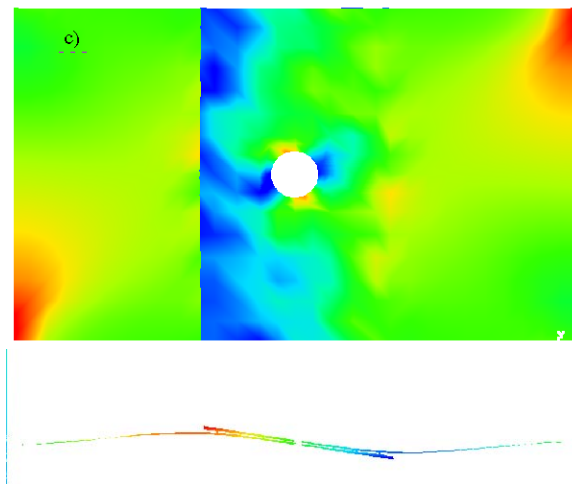


**Figure 4.2.8  $\sigma_{xx}$  and displacement for single-lap model with beam elements representing fasteners ( $\sigma_{xx}$  calculated at mid-plane of the shell elements)**

Fig. 4.2.8 shows the distribution of  $\sigma_{xx}$  and displacement for a single-lap joint when beams are used to model the fasteners. Note, from the out of plane deflections that secondary bending effects can be captured when beam elements are used. When spring elements are used for the fasteners (not shown here), no secondary bending effects can be modelled.

To avoid repetition, the load distribution results are not shown here, but are deferred to Task 2.2, where they are shown together with a fourth modelling method.

SAAB also performed failure analysis of the SAAB benchmarks for the two most important failure modes (net tension and bearing). An in-house code called COBOLT was used, and the results from the FE models were fed into this. COBOLT uses a variation of the “Point Stress Criterion” [3]. In simple terms, failure occurs when the strain at a fixed distance  $r_0$  from the hole boundary reaches a critical value which

depends on the ratio between the radial and tangential moduli,  $E_r/E_t$ , see Fig. 4.2.9. For more details see deliverable D2.1-3. The failure predictions are not shown here, as they were somewhat meaningless due to later changes in the geometry of the structures.

**Point “Strain” Criterion:**

Failure occurs if  $\epsilon_t(r_0) \geq \epsilon_0$

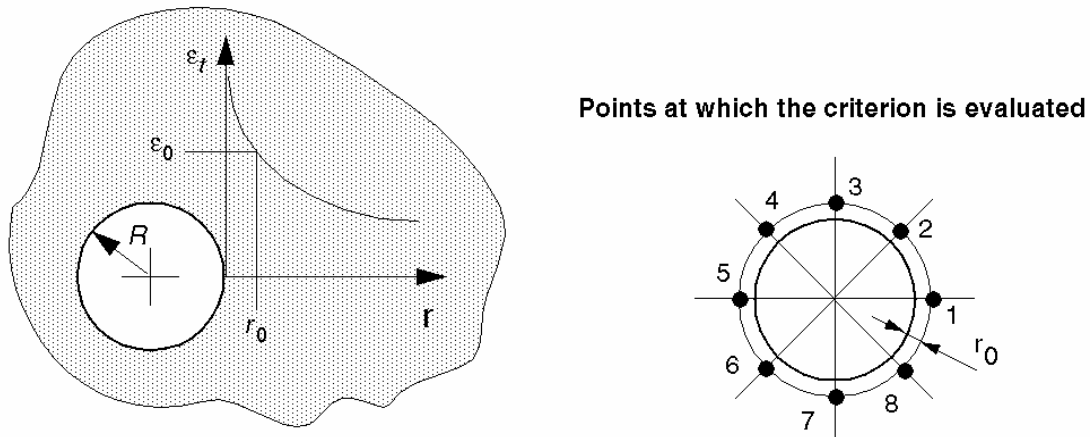


**Figure 4.2.9 Illustration of Failure Criterion used by SAAB in Task 2.1**

### 2.2.2 Task 2.2 Benchmark Modelling with Existing Global Design Methods

In this task, the objectives were to model the benchmarks using “existing” global methods. As can be seen from the previous section, some modelling already took place in Task 2.1, so the line between these two tasks was not as clear-cut as might have appeared at the proposal stage. Nevertheless, different methods *were* used in this task compared to Task 2.1.

The partners in this task were SAAB, QinetiQ and NLR. The same partners were involved in Task 2.3 where their global methods were to be improved. It is fair to say that the three partners did not begin at the same starting point. SAAB had the most advanced method coming into the project, namely their “Joint Element” developed in Swedish national research projects and EDAVCOS. QinetiQ and NLR did not really have an “existing” method beyond the FE methods described in Task 2.1, so they had to do some development in Task 2.2.

Airbus UK and Airbus Deutschland also had a small involvement in this task, interacting with QinetiQ and NLR respectively, to ensure that any methods developed were suitable for implementation later by the industry partners in Task 2.4. AUK's involvement basically just involved a number of meetings at which QinetiQ updated AUK on the work. On the other hand, AD developed a tool for rapid global modelling within MSC.Patran based on pre-existing PCL-codes for modelling of stiffened panels with defects. This tool was given to NLR as a starting point for the global modelling. This was done to ensure that AD would be able to implement the improved global design tool to be developed by NLR in WP 2.3 back into AD's own MSC.Patran environment, later in Task 2.4.

### **Task 2.2 SAAB**

In this task SAAB used their Joint Element to re-calculate the load distribution in the SAAB benchmark joints. The Joint Element is an attempt to address the problems described above with the method where the hole is not modelled explicitly (Fig. 4.2.7), *without* incurring a large penalty in computational cost.

The Joint Element is illustrated in Fig. 4.2.10. At the start of BOJCAS, the tool could handle *two* components bolted together. It is implemented in ABAQUS as an 18-noded macro-element which includes the two joined components modelled with 4-noded general-purpose shell elements utilising reduced integration, and the fastener modelled as a beam *structure* (not just a single beam) with linear beam elements. Further details are shown in Fig. 4.2.11. Contact between fastener and hole and between the components is achieved using interface elements (ABAQUS designation INTER1) and gap elements (ABAQUS designation GAPUNI). Lateral constraints are imposed by MPC (Multi-Point Constraint) equations at the nodes at the hole boundary and at the adjacent nodes ( $z_1 - z_2 = 0$  where index 1 refers to the upper component and index 2 to the lower component). All other translations at the hole boundary are handled by the interface elements. Rotations at the hole boundary are not constrained. Depending on the mesh refinement around the Joint Element, MPC equations can also be used at the edges to join the Joint Element with the surrounding mesh, which are illustrated in Fig. 4.2.11 as *possible* sites for MPC equations. Rigid body rotation is prevented through SPC (Single-Point Constraint), equations ( $F_z = 0$ ) at the two beam element hubs in the components.

The macro-element is capable of handling both straight and curved components. In the first case, linear interpolation is used when the mesh is generated and in the latter case, quadratic interpolation is used, i.e. the nodes are assumed to lie on an arc of a circle. The macro-element is automatically generated by a pre-processor called PREJOINT. To use PREJOINT, the user supplies the information given in Fig. 4.2.12. PREJOINT reads the ABAQUS input file and inserts the new cards containing the Joint Elements. All other cards remain unchanged.

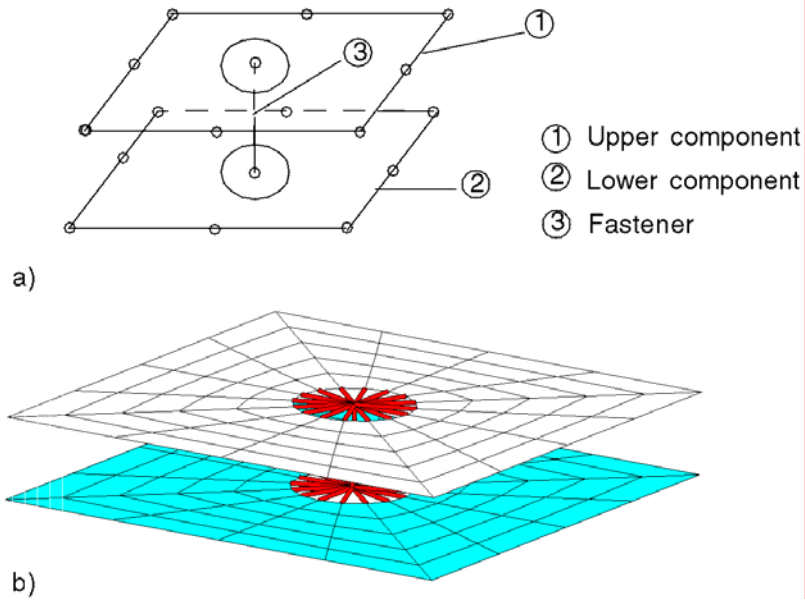


**Figure 4.2.10 (a) Schematic sketch of the Joint Element  
(b) Picture taken from a model where the joint element has been used**

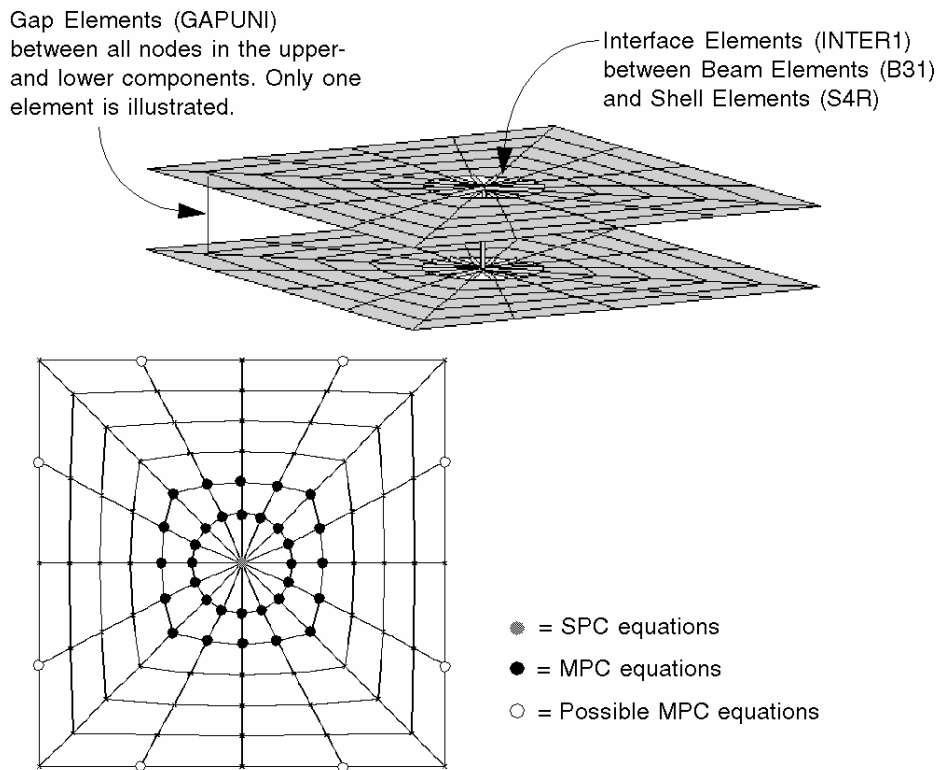


**Figure 4.2.11 Modelling details of the Joint Element**

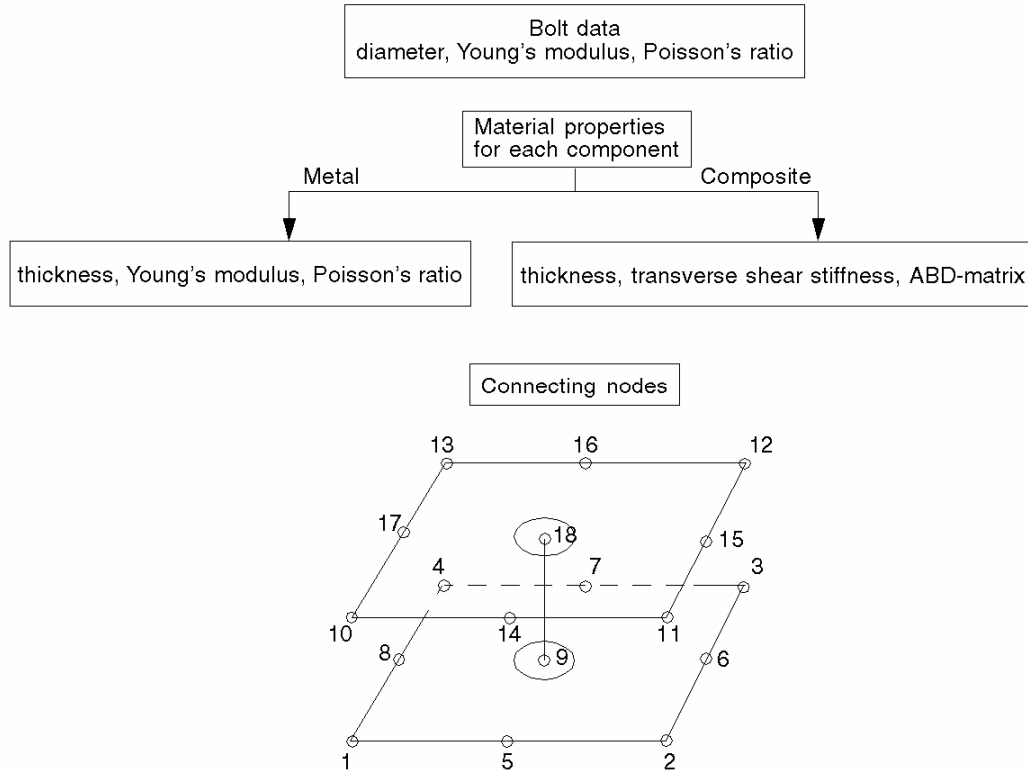


**Figure 4.2.12 User input to pre-processor PREJOINT**

A post-processor called POSTJOINT has also been developed. POSTJOINT calculates the normal and shear load intensities in both components on the edges of a cut-out around each fastener using the section forces and moments from the FE model. Bolt loads and bolt load angles are calculated from the beam elements representing the fasteners. The bolt loads,  $F$ , and bolt load angles,  $\alpha$ , are calculated according to Equation (4.2.1).

$$F = \sqrt{F_x^2 + F_y^2}, \quad \tan \alpha = \frac{F_y}{F_x} \quad \dots(4.2.1)$$

where  $F_x$  and  $F_y$  are the sums of the beam element loads in the x and y directions for each fastener. POSTJOINT also calculates the secondary bending using the strains at the AGARD points. The output from POSTJOINT enables the user either to move on directly to sizing or to make a more detailed local analysis.

The Joint Element was used to recalculate the bolt load distribution in the SAAB benchmark joints. The two configurations were modelled leaving areas for Joint Elements according to Fig. 4.2.13. The pre-processor PREJOINT was then run which introduced the Joint Elements according to Fig. 4.2.14.

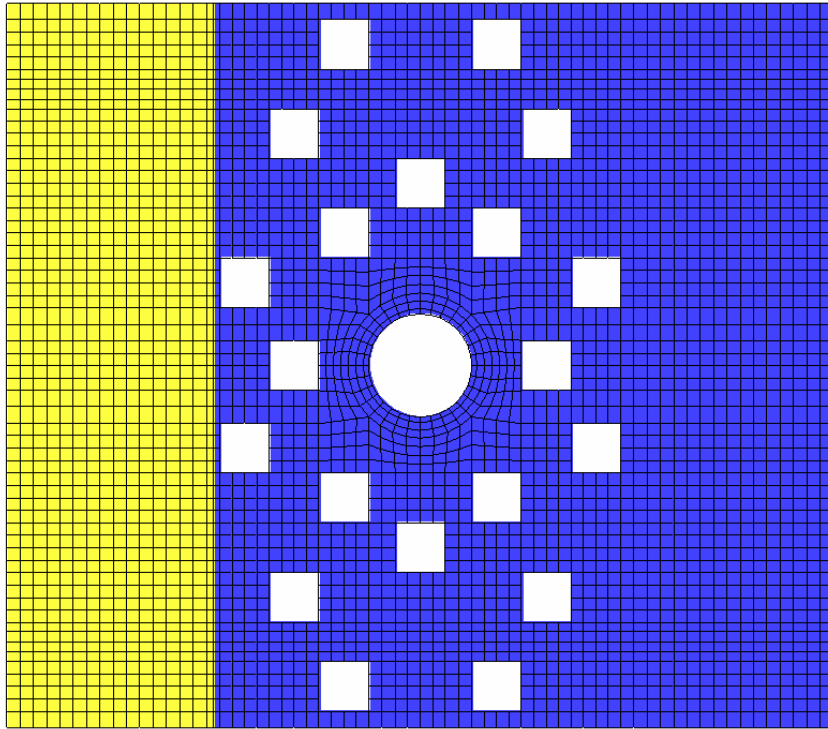


**Figure 4.2.13 FE model of Configuration 1 before the Joint elements have been introduced**

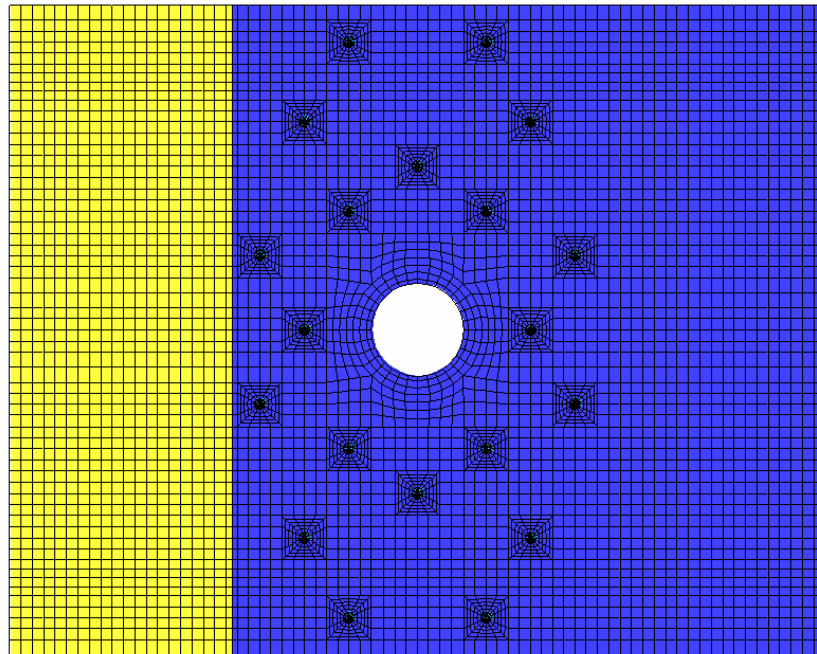


**Figure 4.2.14 FE model of Configuration 1 after the Joint Elements have been introduced using PREJOINT**

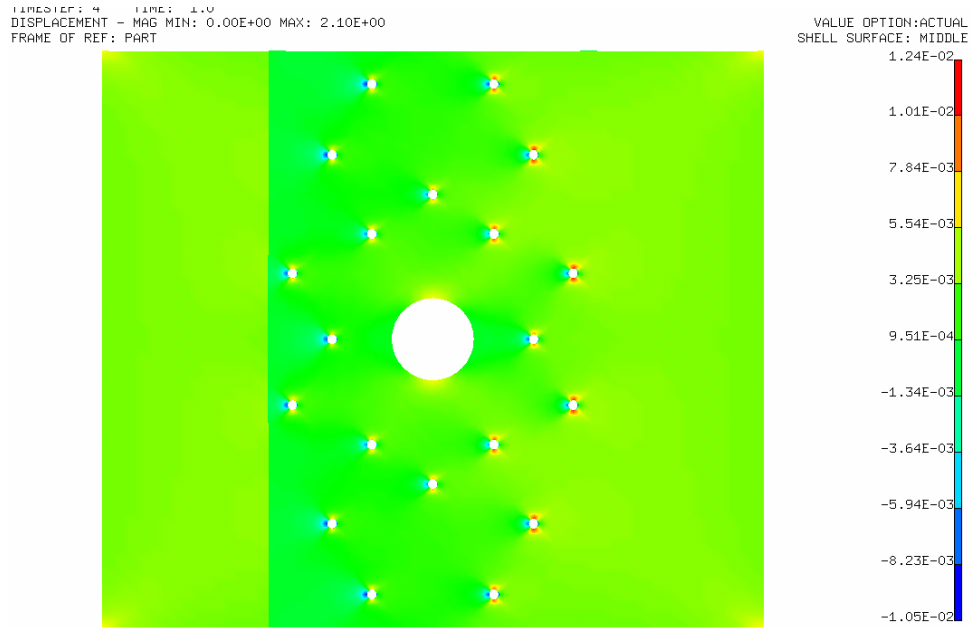


**Figure 4.2.15 Results showing strain in the global x-direction for Configuration 1**

Results for  $\epsilon_{xx}$  from Configuration 1 are shown in Fig. 4.2.15. Comparing with Fig. 4.2.8, the qualitative improvement in the distributions around the holes obtained by modelling the holes explicitly is apparent (although the comparison is a little unfair since the scale in Fig. 4.2.8 does not show the stresses around the hole in the best light).

The load distribution results from the four methods used (analytical, FE – beam elements for fasteners, FE – spring elements for fasteners, and FE – with Joint Elements) are shown in Figs. 4.2.17 and 4.2.18 (Fig. 4.2.16 gives the key to the bolt numbering). Note that between Tasks 2.1 and 2.2 there was a change made to the free length of the joint by NLR for testing purposes, so the results for all the “traditional” methods of Task 2.1 were all re-calculated here.

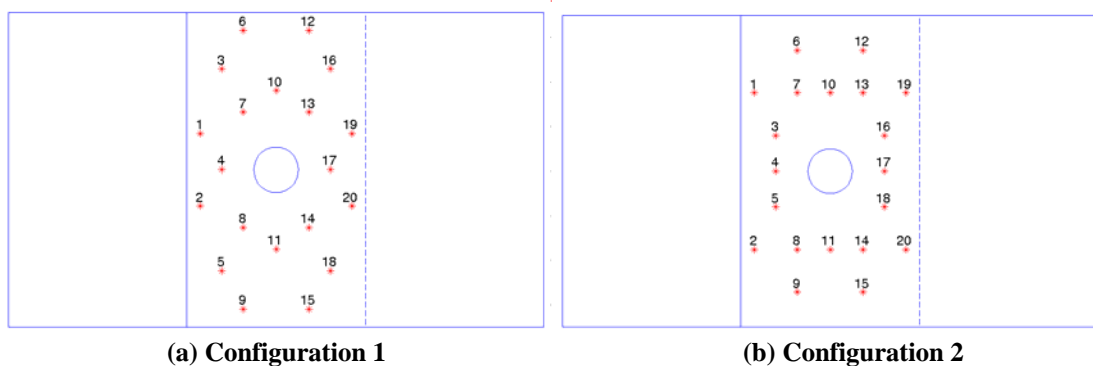
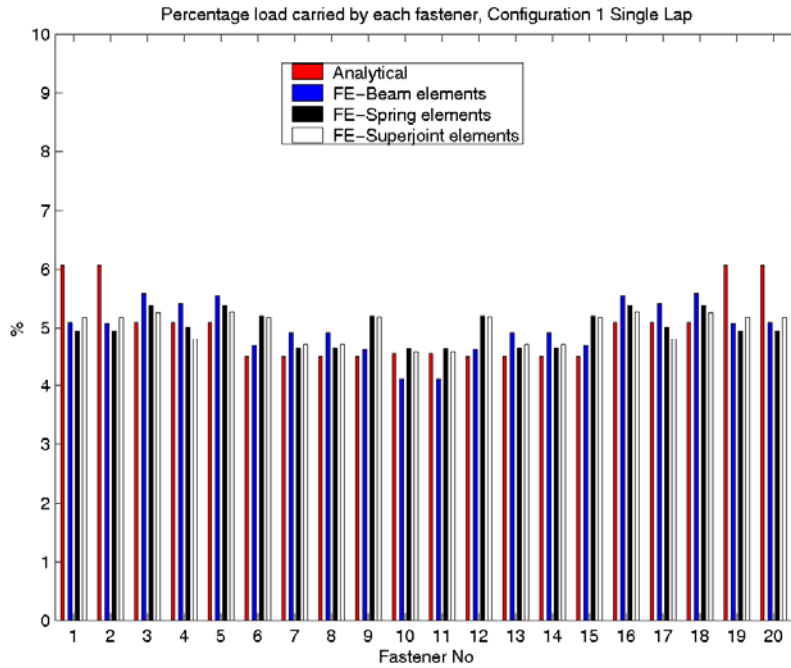
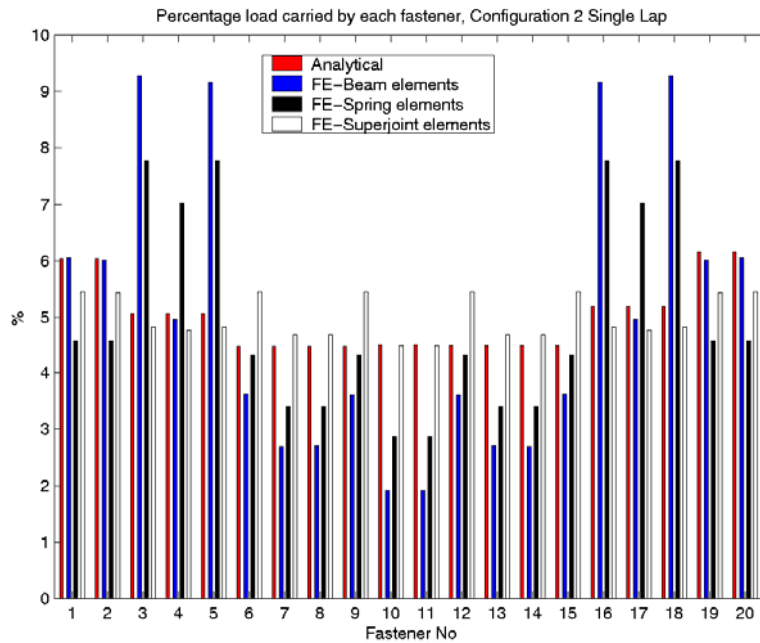


**Figure 4.2.16 Numbering of fasteners (for fastener load results in Figs. 4.2.17 and 4.2.18)**



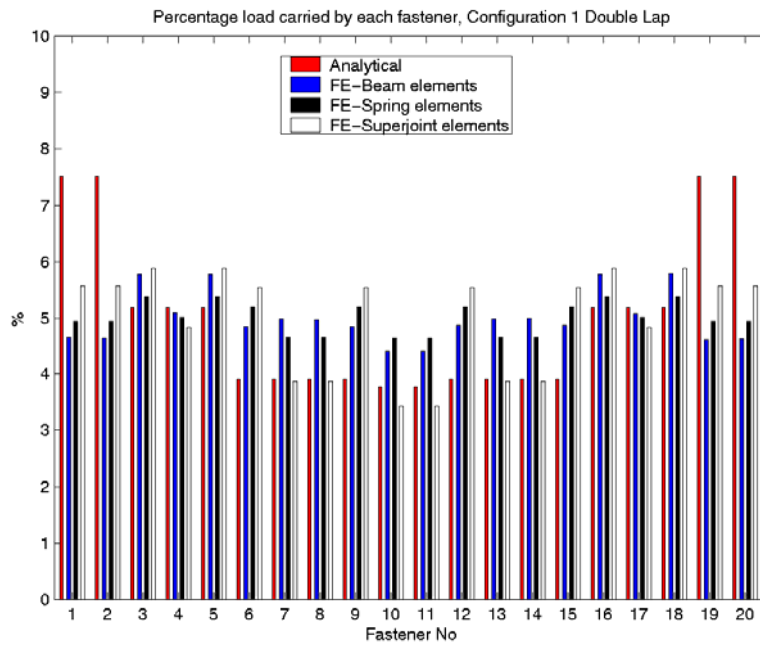
(a) Configuration 1



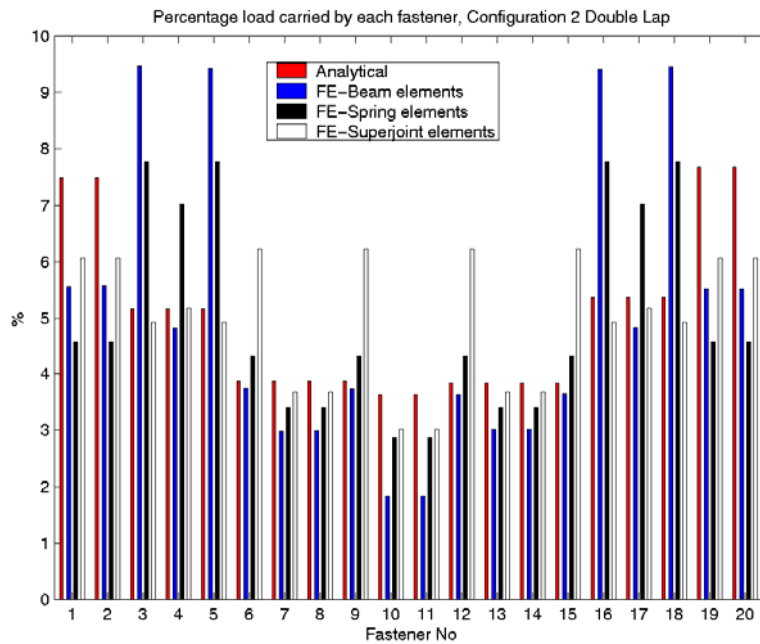
(b) Configuration 2

**Figure 4.2.17 Percentage load carried by each fastener for the SINGLE LAP joints. The first, red bars show the analytical prediction, the second, blue bars show FE prediction with beam elements, the third, black bars show FE prediction with spring elements, and the fourth, white bars show FE prediction with Joint Elements**





(a) Configuration 1



(b) Configuration 2

**Figure 4.2.18 Percentage load carried by each fastener for the DOUBLE LAP joints. The first, red bars show the analytical prediction, the second, blue bars show FE prediction with beam elements, the third, black bars show FE prediction with spring elements, and the fourth, white bars show FE prediction with Joint Elements**

The results show significant differences between the more advanced Joint Element method and the traditional methods. The traditional methods predict a more uneven load distribution, particularly for Configuration 2. Based on the traditional methods, one would expect a much lower failure load for Configuration 2 than Configuration 1, but the Joint Element results do not indicate such a big difference. The greater unevenness of the load distribution from the traditional methods could be expected since the fastener loads in the traditional methods are introduced in discrete points while the introduction is smoother with the Joint elements.

The plots show only the *amount* of load transferred in each fastener, not the load *angle*, since only the FE methods can determine the angle. This is a weakness in the analytical method since fastener load angle may not be so important for isotropic materials but is often critical for composite materials, as a small deviation in the load angle affects the strength significantly.

The strength analysis method outlined above (see Fig. 4.2.9) was used here to predict the failure load and failure mode for each configuration. Results from using the Joint Element method as the load distribution method are summarised in Table 4.2.3 - the predicted failure mode was bearing in all cases. The strains at the open hole were, even with these high loads, below 1% and were not considered critical.

	Configuration 1 Single-Lap	Configuration 1 Double-Lap	Configuration 2 Single-Lap	Configuration 2 Double-Lap
Ultimate Load [kN]	169	505	159	481

**Table 4.2.3 Predicted ultimate total load for the different configurations (using Joint Elements)**

**Task 2.2 QinetiQ**

At the outset of BOJCAS, QinetiQ had relatively little experience of global modelling of multi-fastener joints. As a consequence, the ‘existing’ method reported on in Task 2.2 was relatively crude, but did provide a useful baseline against which improved methods could be evaluated later.

The method used plate-elements to represent the composite laminates and metallic plates, and spring elements to represent the bolts. It thus was similar to the method in Fig. 4.2.7 and suffered from all the problems associated with that method outlined in Task 2.1 above. Fig. 4.2.19 shows one of the models. Neutral-axis offsets and varying element thicknesses were used to represent the stepped splice-plate features that are present in some of the benchmarks.

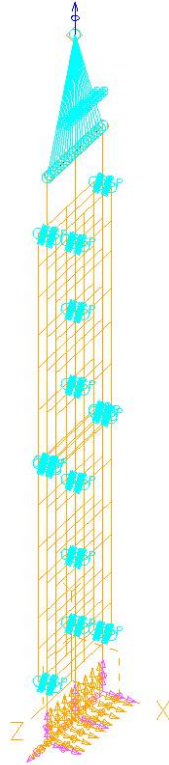


**Figure 4.2.19 QinetiQ’s “existing” global analysis method – plates and springs**

The fasteners were represented by three-dimensional spring elements. The stiffness of these springs was calculated using the BF2 software obtained from BAe Systems (Warton). At each bolt location, separate springs were used to represent the axial, longitudinal, and transverse bolt and foundation stiffness. Failure predictions were made using the Point Stress Criterion and the Average Stress Criterion [3] for the composite laminates within the tension-loaded benchmarks. Results are shown in Table 4.2.4. Comparing with Table 4.2.2, the results are similar for joints 2T and 3T but differ significantly for joints 4T (the scarf joint) and 5T (the tapered splice plate joint). Some of these differences are due to the method used to calculate the spring stiffnesses. The stiffness predicted by BF2 is suitable for use in a 1D environment. The spring represents both the bolt deflection and the extra deflection due to the local effects in the laminate foundation (hole stretching). When the springs are applied in a 2D environment, there will be local deformations in the laminates at the load introduction points (spring attachments). These deformations will be in addition to the local laminate deflections that are already accounted for in the 1D spring representation. If the local deformations in the laminates at the load introduction points are significant compared to those of the spring, then the bolt foundation will be artificially compliant. These problems served to further illustrate the problems with “traditional” global methods.

Benchmark	Plate	Matl	w (mm)	t (mm)	d (mm)	Bolt No.	Bolt load (N)	Bearing load (N)	Bearing stress (Pa)	Bypass load (N)	Bypass stress (Pa)	Point stress (Pa)	Average stress (Pa)	RFpoint	RFaverage	% difference	RFbearing	Failure load (kN) (min)
2T	cfrp skin 1	AS4 8552	90	14.56	15.875	1	70843	70843	3.065 E+08	109156	1.011 E+08	4.74E+08	4.89E+08	2.02	1.96	3.03	2.68	353
			90	14.56	15.875	2	48982	48982	2.119 E+08	60174	5.575 E+07	2.92E+08	3.01E+08	3.29	3.19	3.03	3.87	
			90	14.56	15.875	3	60174	60174	2.603 E+08	0	0	1.92E+08	1.98E+08	4.99	4.86	2.73	3.15	
3T	cfrp skin 1	AS4 8552	90	14.56	15.875	1	65193	65193	2.820 E+08	114808	1.064 E+08	4.69E+08	4.83E+08	2.05	1.99	3.00	2.91	357
			still ok	90	14.56	15.875	2	34896	34896	1.510 E+08	79912	7.404 E+07	2.92E+08	3.01E+08	3.29	3.19	2.96	
		90	14.56	15.875	3	30571	30571	1.323 E+08	49341	4.572 E+07	2.09E+08	2.15E+08	4.60	4.46	3.07	6.20		
		90	14.56	15.875	4	49341	49341	2.135 E+08	0	0	1.58E+08	1.62E+08	6.09	5.93	2.72	3.84		
4T	CFRP skin	AS4 8552	90	15.6	19.05	1	78004	78004	2.625 E+08	192996	1.744 E+08	6.75E+08	6.83E+08	1.42	1.40	1.19	3.12	381
			90	13.52	19.05	2	58346	58346	2.265 E+08	134650	1.404 E+08	5.56E+08	5.62E+08	1.73	1.71	1.17	3.62	
			90	11.44	19.05	3	57979	57979	2.660 E+08	76671	9.446 E+07	5.12E+08	5.18E+08	1.88	1.85	1.18	3.08	
			90	9.36	19.05	4	76671	76671	4.300 E+08	0	0	4.19E+08	4.20E+08	2.29	2.28	0.38	1.91	
5T	cfrp skin 1	AS4 8552	75	10.4	11.1125	1	70843	70843	6.130 E+08	109156	1.643 E+08	7.56E+08	7.97E+08	1.27	1.20	5.14	1.34	217
			75	10.4	12.7	2	48982	48982	3.709 E+08	60174	9.287 E+07	4.79E+08	4.99E+08	2.00	1.92	4.01	2.21	
			75	10.4	14.2875	3	60174	60174	4.050 E+08	0	0	3.14E+08	3.23E+08	3.06	2.97	2.73	2.02	

**Table 4.2.4 Reserve factor and strength predictions for composite laminates in tension-loaded BAe benchmark joints using QinetiQ’s “existing” method**

**Task 2.2 NLR**

Similarly to QinetiQ, NLR did not have any “advanced” global modelling tool for joints at the start of BOJCAS. In Task 2.1 AD had modelled the two permanent repair benchmarks using RBARs, which are rigid links implemented by using multi-point constraints to couple the nodes at the bolt locations in the different parts of the assembly. In this task, NLR modelled all four DA benchmark structures, firstly using RBARs, and then using flexible beams. NLR first calibrated the two methods using the joint that became known as the “*Multi-Bolt Benchmark*” for the project, BAE-BM-2C (see Task 2.4). Fig. 4.2.20 shows the four RBAR models. Note that the beam models used a coarser mesh than this, since the beam stiffnesses were calculated from a semi-empirical formula derived by Grumman [4], which is based on the use of two shell elements between bolts.

The configuration of the skin/stringer repairs is different to that shown in Fig. 4.1.5 and 4.2.6. This is because the original configurations were later changed in order to allow for symmetric loading conditions. Instead of a specimen with two stringers, the revised benchmark configuration shows three stringers, the centre one with the repair.

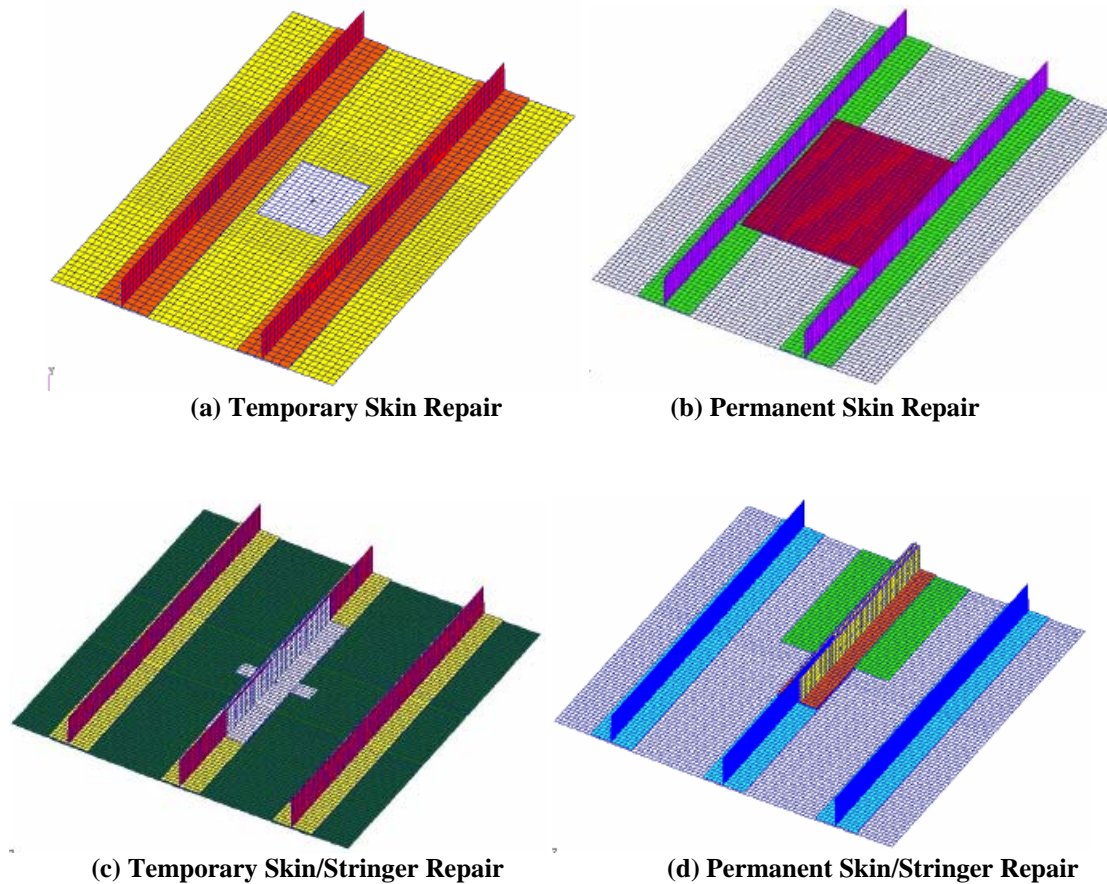


**Figure 4.2.20 NLR models of four different DA benchmark structures**

Compressive axial loading was applied via a prescribed axial displacement on the nodes at one end of the specimens. Anti-buckling guides at the side edges of the panels were represented by simple supports ( $U_Z, R_Y, R_Z = 0$ ). Calculation of the beam stiffnesses was based on the Grumman formula [4] as well as some simple modelling of single beam elements. This work is described in detail in D2.2-3.

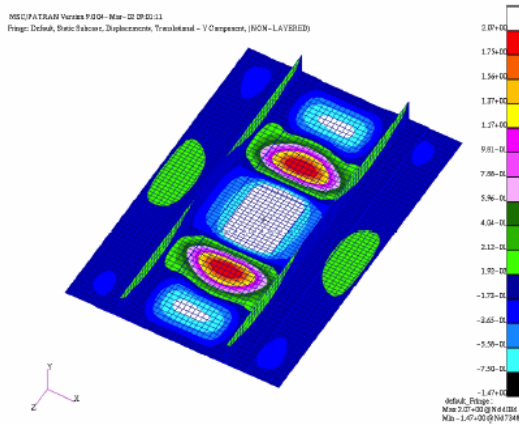
For each model, the out-of-plane displacements, axial displacements, stress distributions and bolt load distribution were calculated. Results for the Temporary Skin repair are shown in Fig. 4.2.21. In general, for all the models, due to the lower stiffness of the BEAM elements, the maximum resultant forces in the BEAM elements were lower than the MPC (Multi Point Constraint) forces in the models using RBARs. Compared to the MPC forces, the resultant BEAM forces were also more evenly distributed over the bolts.

A failure analysis was performed on all structures, in which bearing failure of composite and metal parts, as well as shear failure of bolts was considered. The lowest far-field strain value ( $\epsilon_{xx}$ ) triggering any of these three types of failure was regarded as the failure strain. The predicted failure strains are shown in Table 4.2.5, while the predicted failure locations are given in Fig. 4.2.22. From Table 4.2.5, it is seen that in all cases, the beam models predicted higher failure strains. Comparing with AD's predictions for the skin repairs in Fig. 4.2.5, the failure strain for the temporary skin repair is quite similar, while the failure location is different. On the other hand, for the Permanent Skin Repair, the failure location is the same as AD's prediction, while the failure strain is much higher in NLR's predictions (especially when using beams). No comparison with AD's results can be made for the stringer repairs, since the structures analysed here are completely different.

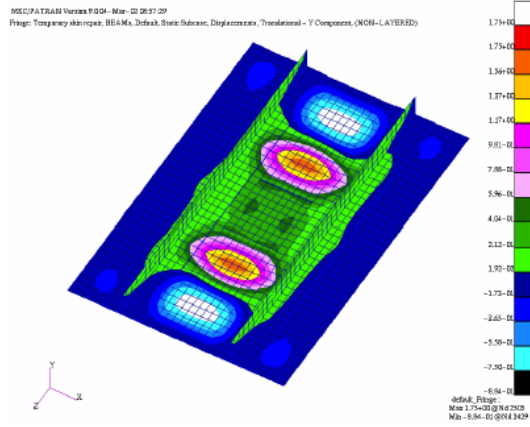
The finite element models developed by NLR were used by SMR for their work on global-local modelling techniques in WP 4.

Repair Model	Temporary Skin		Permanent Skin		Temporary Stringer		Permanent Stringer	
	RBAR	BEAM	RBAR	BEAM	RBAR	BEAM	RBAR	BEAM
$\epsilon_{xx}$ (%)	0.29	0.32	0.36	0.68	0.22	0.32	0.32	0.66

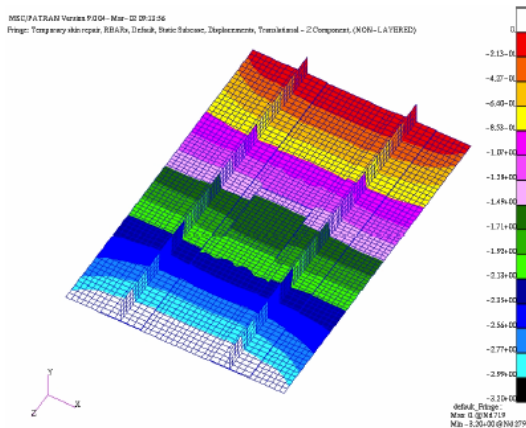
**Table 4.2.5 Predicted global strains at first failure (NLR models of DA benchmarks)**



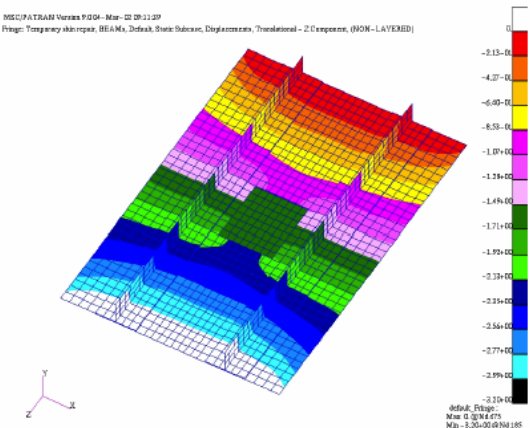
(a) Out of plane displacements, RBARs



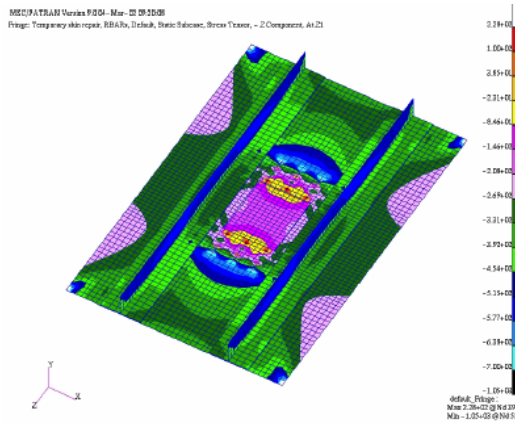
(b) Out of plane displacements, Beams



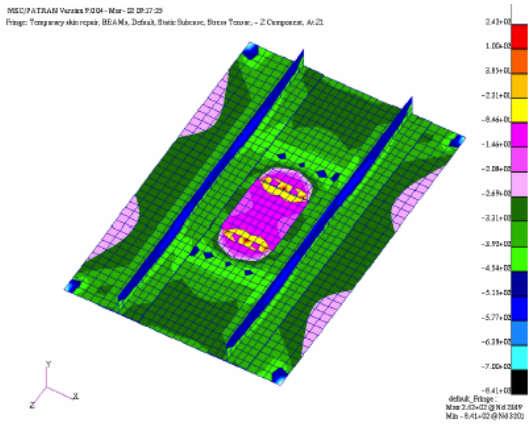
(c) Axial displacements, RBARs



(d) Axial displacements, Beams

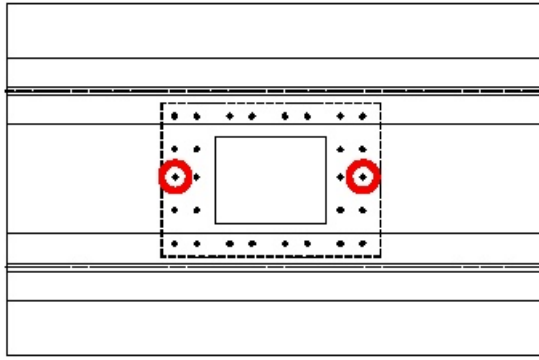


(e) Average Stress SZ, RBARs

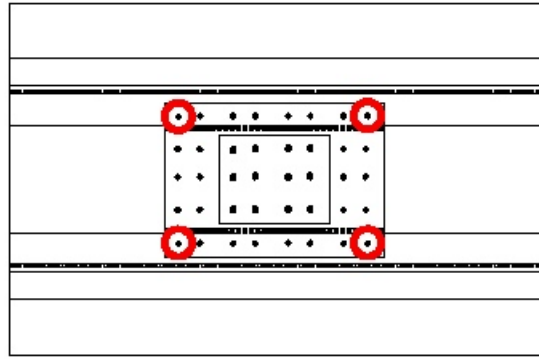


(f) Average Stress SZ, Beams

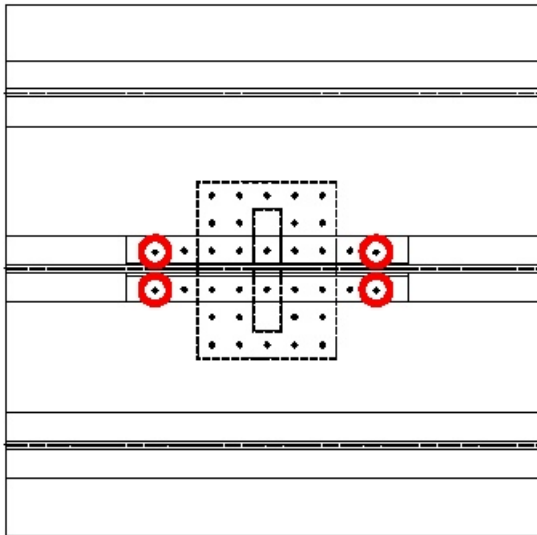
Figure 4.2.21 NLR model results for Temporary Skin Repair



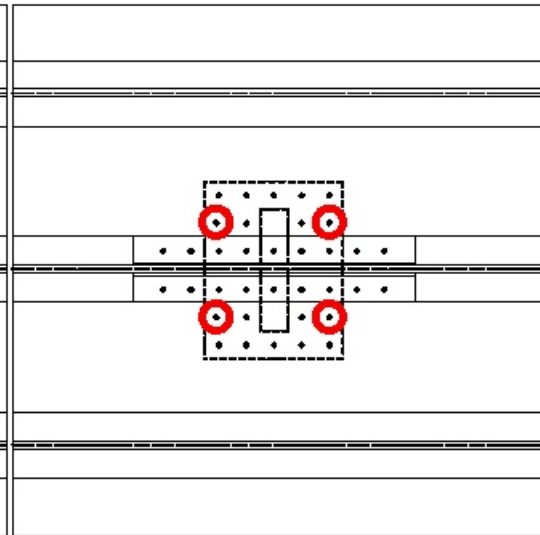
(a) Temporary Skin Repair (RBARS & BEAMS)



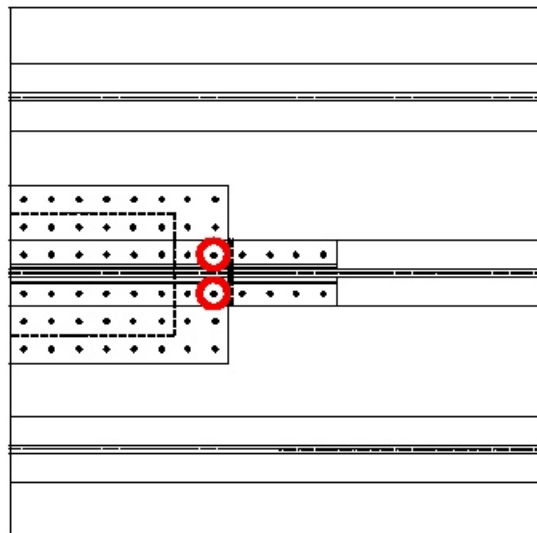
(b) Permanent Skin Repair (RBARS & BEAMS)



(c) Temporary Stringer Repair (RBARS)



(d) Temporary Stringer Repair (BEAMS)



(e) Permanent Stringer Repair (RBARS & BEAMS)

Figure 4.2.22 Predicted first failure locations from NLR models of DA benchmarks



## 2.2.3 Task 2.3 Development of Global Design Methods

In this task, global methods were to be developed beyond the state-of-the-art demonstrated in Task 2.2. QinetiQ, SAAB and NLR were again involved, with AUK and AD playing a consulting role.

In the end, NLR did not develop their method any further than that described above. This was due to budget overruns primarily in their experimental testing work in WP 3 and WP 5. The work on development of the beam representation of fasteners (calibrated using the project *Multi-bolt Benchmark* BAE-BM-2C) did represent a development beyond NLR's state-of-the-art (which was the spring method), and actually matched their original Description of Work in Task 2.3. Thus, NLR's final report in Task 2.2 (D2.2-3) and Interim Report in Task 2.3 (D2.3-3) were combined into a single deliverable. However, no post-test validation and improvement of the method was done, so no final report was produced and no further description of their work in Task 2.3 is given here. This change to the work description was described in an amendment to Annex 1, which was approved by the EU in Autumn 2002. The primary effect on the rest of the project was on AD's work in Task 2.4, which is discussed in the Section 4.2.4.

This section is thus devoted to the development and validation of SAAB and QinetiQ's methods. Because SAAB started from a more advanced position than QinetiQ they were able to devote a considerable effort to validation.

### Task 2.3 SAAB

SAAB implemented a number of improvements to their Joint Element. Firstly, the previous limitation of two member plates was removed, and the tool can now handle an arbitrary number of parts. This enables joints that are non-symmetrical through the thickness to be modelled. In addition, joints like the double-lap SAAB benchmark (see Fig. 4.1.7), had to be modelled in Task 2.2 with symmetry conditions (at a plane halfway through the thickness), but could now be modelled without such simplifying conditions.

Secondly, improved capabilities to handle anisotropic material properties were implemented. Most post-processors on the market cannot handle stress components for shell elements with a general property description. It is also convenient to be able to use different material property definitions depending on what is available. For these reasons a new method of defining material properties has been incorporated in the pre-processor PREJOINT. It is now possible to define material properties in three different ways:

1. ISO (\*SHELL SECTION is used in ABAQUS)  
Required input: E modulus and Poisson's ratio are required
2. COMP (\*SHELL GENERAL SECTION is used in ABAQUS)  
Required input: Transverse shear stiffness (default values can be used), symmetric half of the ABD matrix in the order D11, D12, D22, D13, D23, D33, D14, ..., D44, D15, ..., D55, D16, ..., D66 (21 values).

3. ANISO (\*SHELL SECTION is used in ABAQUS), new option

Required input: Transverse shear stiffness (default values can be used), matrix in the order D1111, D1122, D2222, D1133, D2233, D3333, D1112, D2212, D3312, D1212, D1113, D2213, D3313, D1213, D1313, D1123, D2223, D3323, D1223, D1323, D2323 (21 values).

Thirdly, to simplify definition of the properties of the Joint Element, section properties can now also be defined from material properties. The definition of the Joint Element properties starts with definition of the bolt: diameter, E modulus and Poisson's ratio. The remaining definitions are then given with one of the following options:

- MATERIAL (new option)  
Material name and thickness, repeat for all member plates.
- PART  
Define all member plates directly and give thicknesses.

Fourthly, several new methods have been implemented for finding the nodes to connect to in the surrounding mesh for each Joint Element. For complex multi-bolt joints the effort involved in this can be tremendous, so these new methods have dramatically improved the user-friendliness of PREJOINT. The options are:

- OUTER NODES  
Required input: Element ID, all nodes in the Joint Element, see Fig. 4.2.23.
- EDGE (new option)  
Required input: Element ID, first edge node in lower member plate (enables desired orientation of the Joint Element), mid node in lower member plate, mid node in upper member plate, see Fig. 4.2.24. Mid nodes in interlaying member plates do not need to be defined.
- MID NODES (new option)  
Required input: Element ID, mid node in lower member plate, mid node in upper member plate, see Fig. 4.2.25. Mid nodes in interlaying member plates do not need to be defined.

Finally, to account for tilting of the bolt when the joint is not symmetric, a compensation of the load components in the axial beam load is needed before the resulting bolt load is calculated. The reason for this is that the section forces remain perpendicular to the beam element, see Fig. 4.2.26. The problem was identified when large deviations between SAAB and FOI predictions for single-lap joints were discovered and equilibrium between applied and transferred load was not achieved. To date, this compensation has been made in a MATLAB script, but it will be incorporated into POSTJOINT.

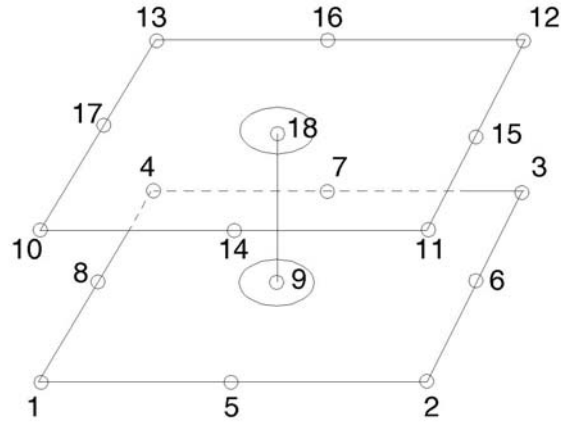


**Figure 4.2.23** Nodes to define when **OUTER NODES** is used (example with two member plates shown)

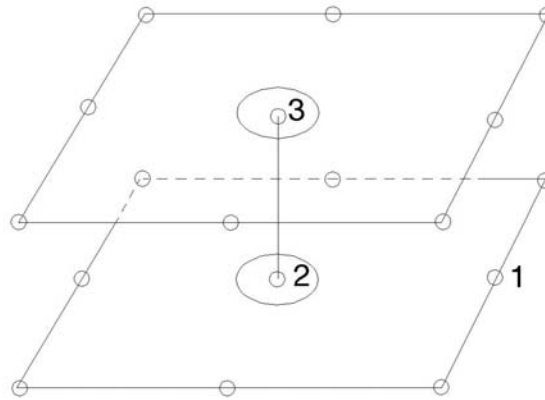


**Figure 4.2.24** Nodes to define when **EDGE** is used (example with two member plates shown)

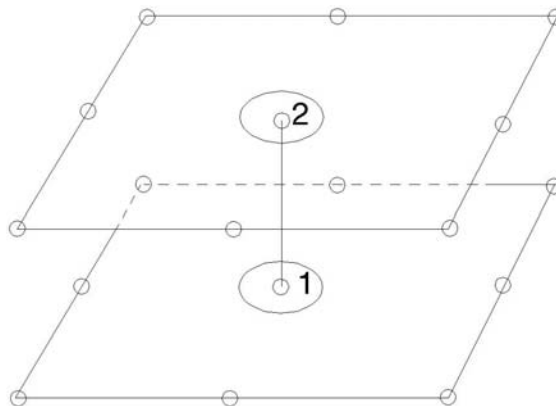


**Figure 4.2.25** Nodes to define when **MID NODES** is used (example with two member plates shown)

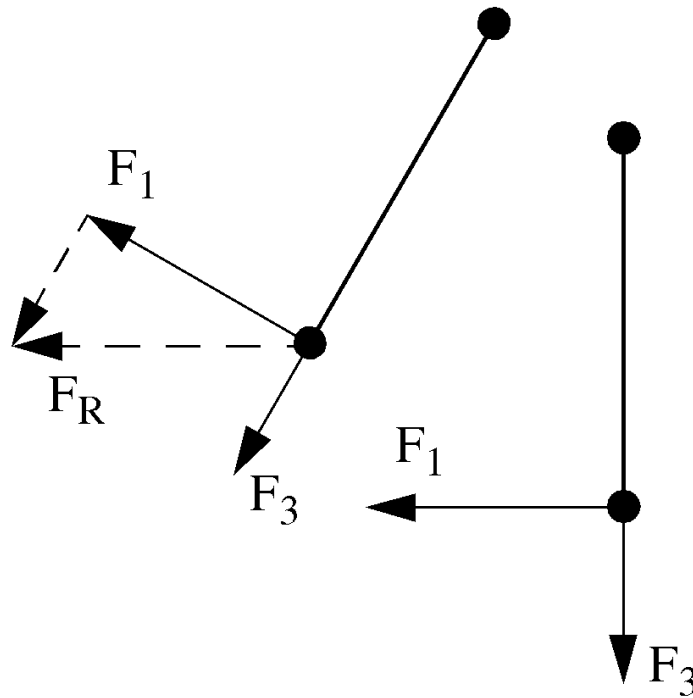


**Figure 4.2.26 Illustration of compensation of the resulting bolt load when the bolt tilts. Compensation is performed both in 1- and 2-direction with the axial beam load in the 3-direction**

To validate the SAAB method, comparisons were made both against NLR's experimental results and against FOI's full 3D hp-adaptive model, which gave a near exact mathematical solution to the problem (see Task 4.3). Taking advantage of the new ability to handle an arbitrary number of member plates, the double-lap SAAB benchmarks were re-modelled using three separate plate elements (see Fig. 4.2.27).

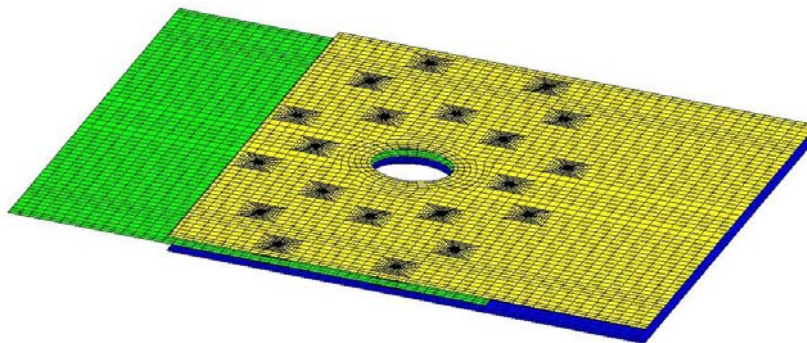


**Figure 4.2.27 Revised double-lap joint model with three separate plates**

Fig. 4.2.28(a) shows a comparison between the bolt load predictions from the SAAB method and FOI’s full 3D method for Configuration 1. If the FOI solution is regarded as virtually exact, the relative errors in the SAAB method are calculated according to:

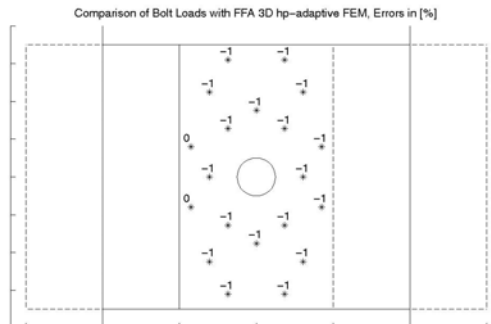
$$Error = \left( \frac{F_{SAAB} - F_{FFA}}{F_{SAAB}} \right) \cdot 100 \quad [\%]$$

Fig. 4.2.28(a) shows that the predicted loads from SAAB’s global method are almost identical to those from the detailed 3D hp-adaptive FE-solution.

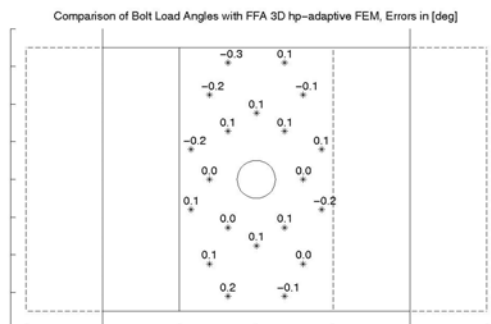
As noted above, bolt load angles are also very important to predict correctly when anisotropic materials are joined. The predicted bolt load angles are compared with those predicted by FOI’s 3D solution in Fig. 4.2.28(b). The numbers shown correspond to:

$$Error = \theta_{SAAB} - \theta_{FFA} \quad [\text{deg.}]$$

As can be seen only small deviations, maximum 0.3 degrees, exist between SAAB’s 2D FE-method and the detailed 3D hp-adaptive FE-solution. Further comparisons between SAAB’s global and FOI’s global-local model are given in Task 4.3.



(a) Bolt load magnitudes



(b) Bolt load angles

**Figure 4.2.28 “Errors” in bolt load magnitudes and angles predicted by SAAB’s global method, when compared to FOI’s full 3D method in Task 4.3 (Configuration 1, double-lap)**

Next a comparison between measured and predicted strain gauge readings was performed. Fig. 4.2.29 shows the strain gauge locations and numbering in the tests performed by NLR. Note that not all these gauges were present in all tests. For bolt numbering see Fig. 4.2.16. The selected load level for comparison was 250 kN for the single-lap joints which were tested in tension, and –200 kN for the double-lap joints which were tested in compression. The reason for the lower load level for the benchmarks loaded in compression is that these specimens experienced stability problems at higher load levels even though anti-buckling guides were used.

Fig. 4.2.30 shows the comparison between experimental and predicted strains for the single-lap joint, loaded in tension with the Configuration 1 bolt pattern. The x-axis represents the width coordinate, with zero being the joint centreline. Three different cases are shown: all bolts present, one bolt missing, and two bolts missing. Fig. 4.2.31 shows a similar comparison for Configuration 2. With only a few exceptions, the agreement between experimental and predicted strains is excellent. The agreement for the double-lap specimens in compression was also good (see D2.3-4).

Fig. 4.2.32 shows the scan lines over which a laser displacement transducer measured the out-of-plane displacement in the experiments. The lines were 15, 80 and 145 mm from the centre of the specimen. Fig. 4.2.33 shows the comparison between the predicted and experimentally measured out-of-plane displacements along these scan lines for the single-lap joint, with Configuration 2 bolt pattern, loaded in tension at 250 kN. The agreement between experiment and model is seen to be good.

Fig. 4.2.34 shows a plot of the predicted change in bolt load distribution as first one, and then two bolts are removed. No experimental results are available for comparison. In addition, margins of safety were plotted for each bolt in each configuration, so the critical bolts could be identified (see D2.3-4).

The experimental failure loads and modes are given in Table 4.2.6. Comparing with Table 4.2.3, the single-lap, tensile loading predictions were below the experimental values and the double-lap, compressive loading predictions were above. A significant source of error in the single-lap predictions was that the correction of bolt load direction in Fig. 4.2.26 had not been made – with this correction the predictions improved. For the compressive specimens, buckling was a major problem despite the use of anti-buckling guides, and this could not be predicted by the failure analysis methods used.

Test	Failure Load (kN)	First Failure Mode	Remark
Single-lap, Tension, Configuration 1	359.6	Bearing	
Single-lap, Tension, Configuration 2	355.9	Bearing / Net Section combination	
Double-lap, Compression, Configuration 1	-232.8	Buckling	Stability problems
Double-lap, Compression, Configuration 1	-200.0	No failure	Stability problems, test interrupted

**Table 4.2.6 Experimental failure load and failure mode**

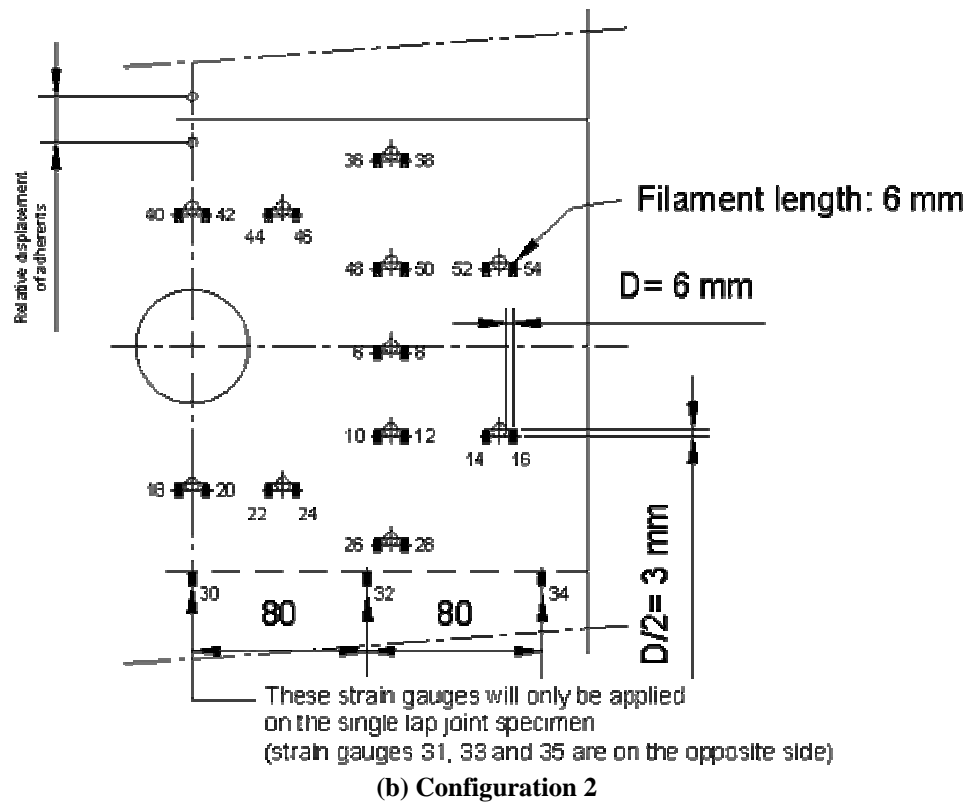
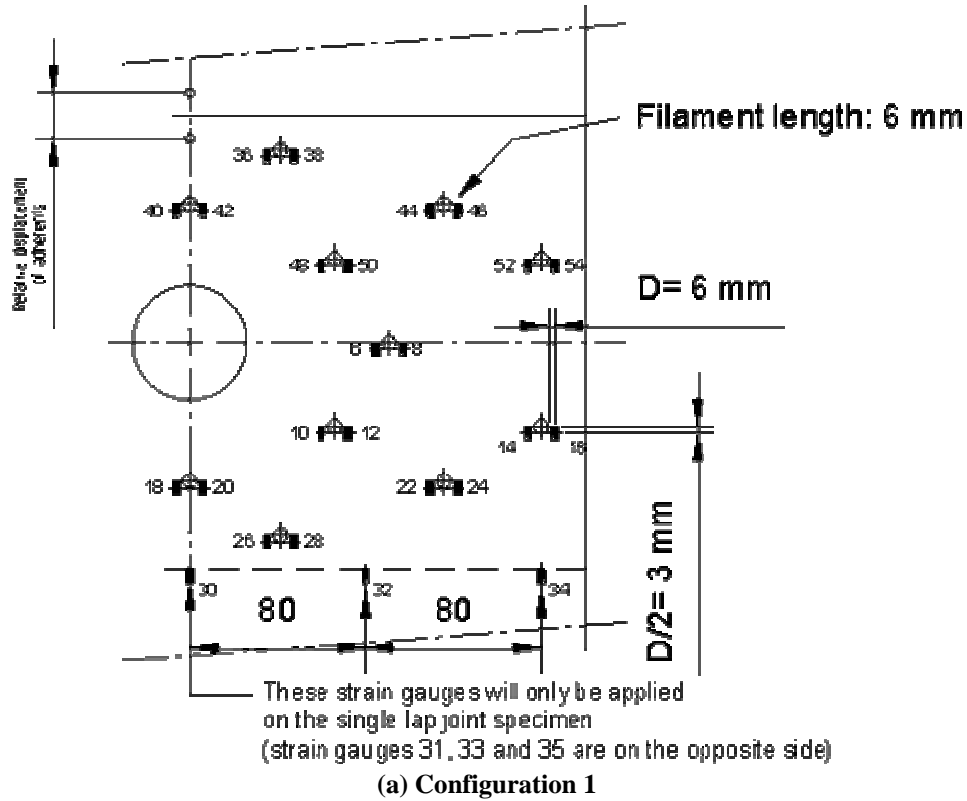
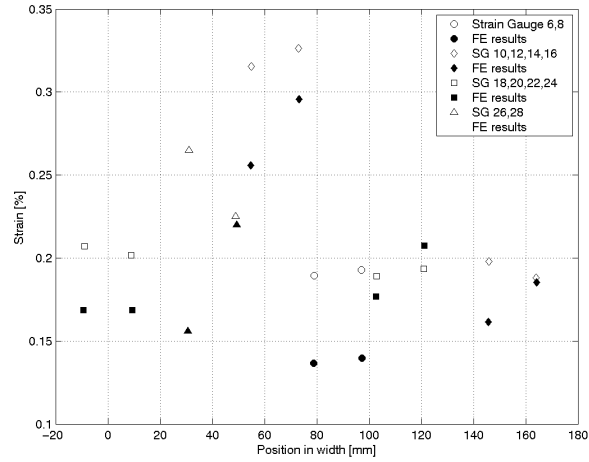
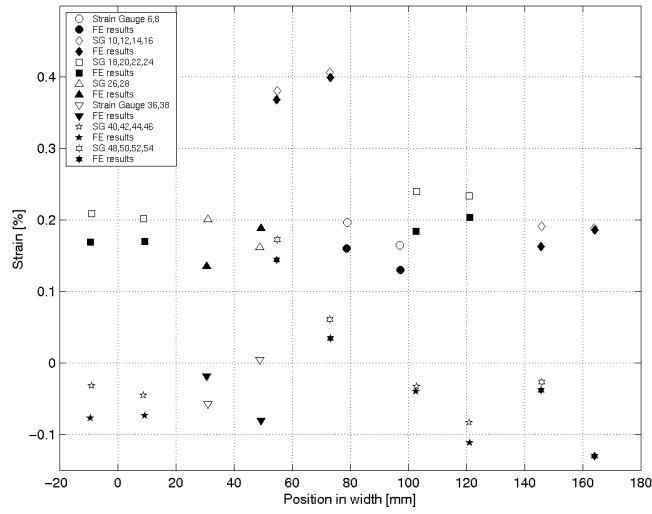


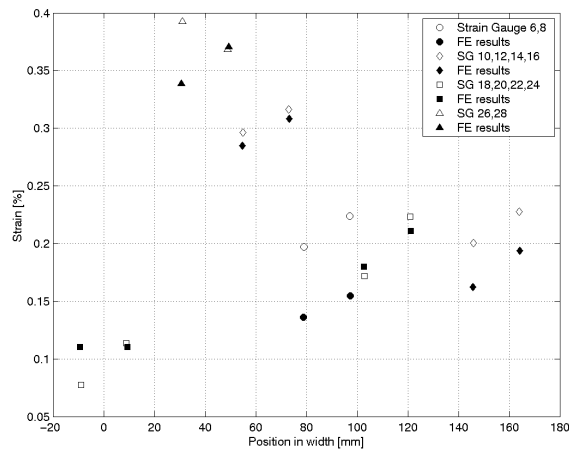
Figure 4.2.29 Strain gauge locations and numbering, SAAB benchmark



(a) All bolts present



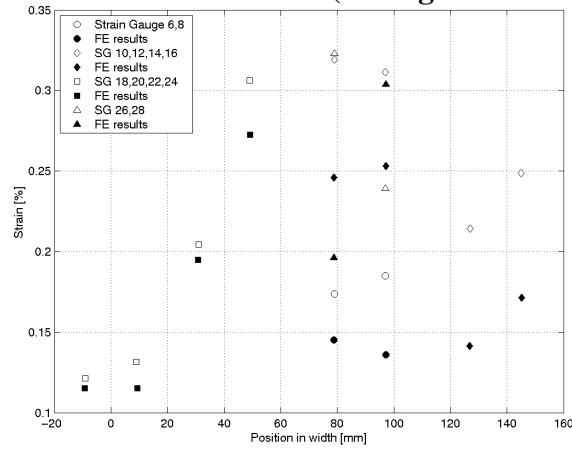
(b) Bolt 13 removed



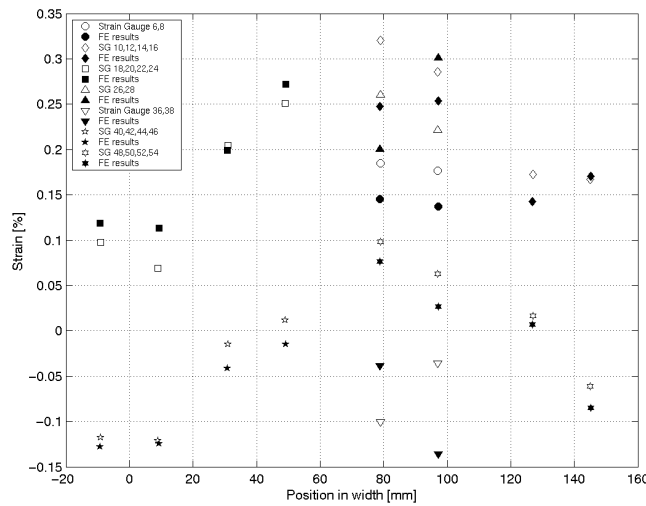
(c) Bolts 19 and 20 removed



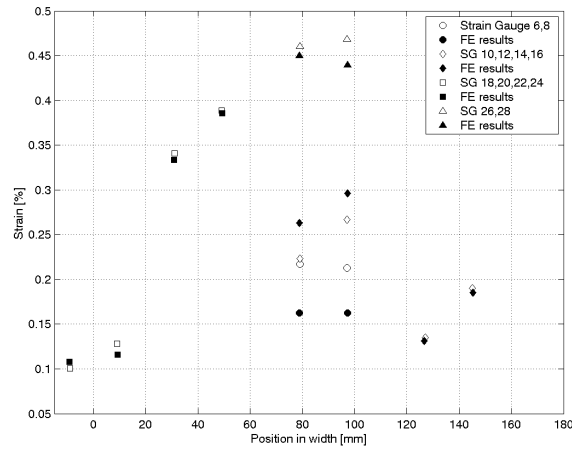
**Figure 4.2.30 Experimental versus Predicted Strain results – Configuration 1, Single-Lap joint loaded in tension at 250 kN (see Fig. 4.2.16 for Bolt Numbering)**



**(a) All bolts present**



**(b) Bolt 14 removed**



**(c) Bolts 16 and 19 removed**

**Figure 4.2.31 Experimental versus Predicted Strain results – Configuration 2, Single-Lap joint loaded in tension at 250 kN (see Fig. 4.2.16 for Bolt Numbering)**

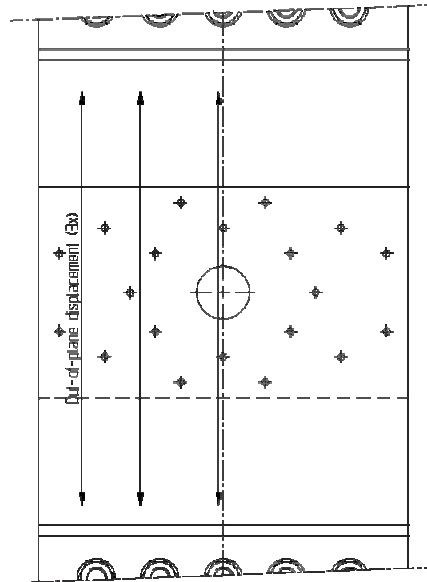


**Figure 4.2.32 Scanning lines used for laser displacement transducer measurements of out of plane displacements.**

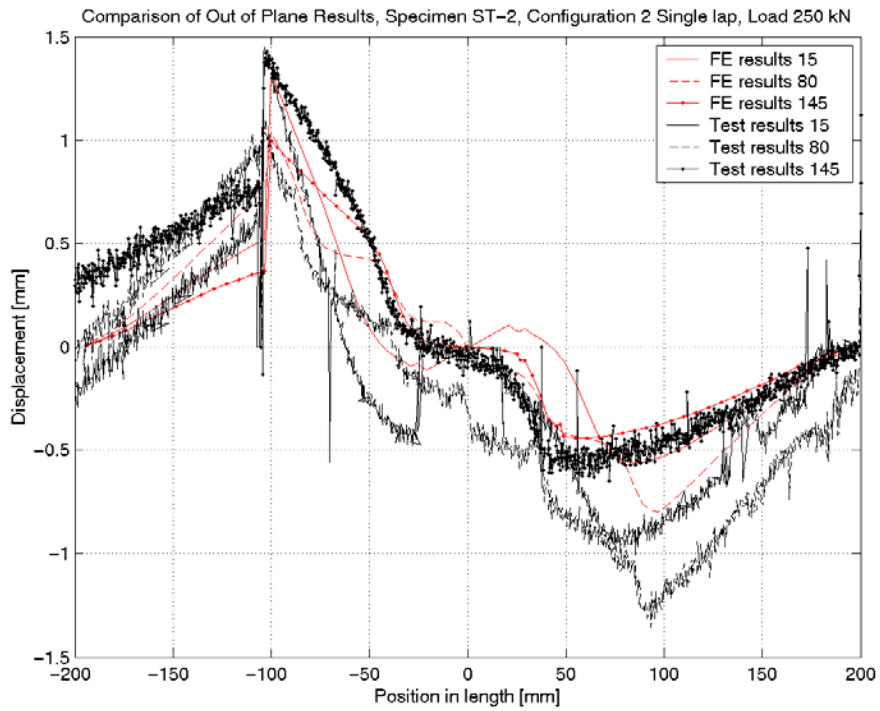


**Figure 4.2.33 Experimental versus predicted out of plane displacements for single-lap specimen, with Configuration 2 bolt pattern, loaded in tension at 250 kN**

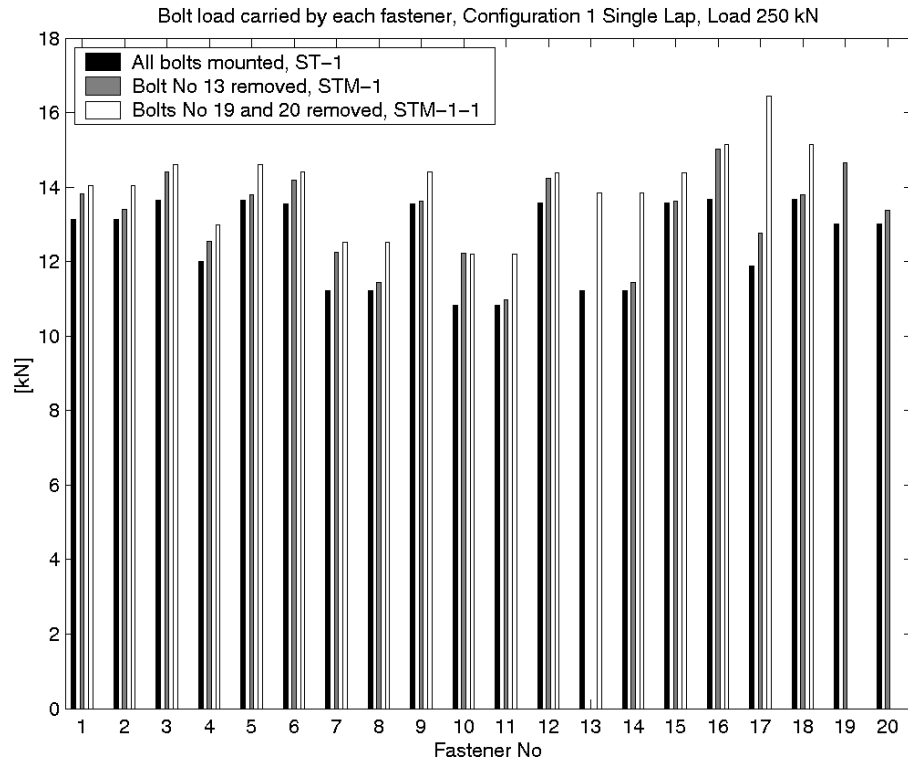


**Figure 4.2.34 Effect on bolt load distribution of removing one or two bolts (single-lap, Configuration 1, tensile load of 250 kN)**

### Task 2.3 QinetiQ

QinetiQ developed an entirely new global method in Task 2.3. The developed method can automatically add more robust representations of fasteners and their laminate foundations to a shell-based global FEA model. Two methods of representing the bolt-foundation were developed – a shell-based method and a solid-based method. A particular feature of QinetiQ’s method is it works within structures with arbitrarily curved surfaces.

The major considerations in the development of the improved methods are listed below.

- Work within Task 2.2 indicated the improved methods must contain distinct representations of the fastener and the hole (laminate foundation), and must represent the contact between them.
- The reliance upon empirical methods to define the stiffness of the fastener and the foundation was to be eliminated. This suggested that the method should be able to represent the effects of fastener tipping under single-shear loading, and that the method should be usable in global shell models of arbitrary geometry.
- The method should be fast to solve.
- The method should impose minimal restrictions on the meshing of the global model, which was a weakness in the methods of the other BOJCAS partners.

- The method should work with commercial packages and take advantage of their increasing power, but it should also be independent of any particular packages.
- The method should be compatible with the global-local coupling approach developed in Task 4.3.

The solution to these requirements was met, and is described below. An overview of the toolset is given in Fig. 4.2.35.

The requirement to keep the method independent of commercial packages was met by developing FORTRAN software (*Q\_global\_bolt*) that can be modified to act on the input and output files of most standard FEA packages. This also kept the method largely independent of the pre-processing software, because most pre-processing packages can export standard FEA files.

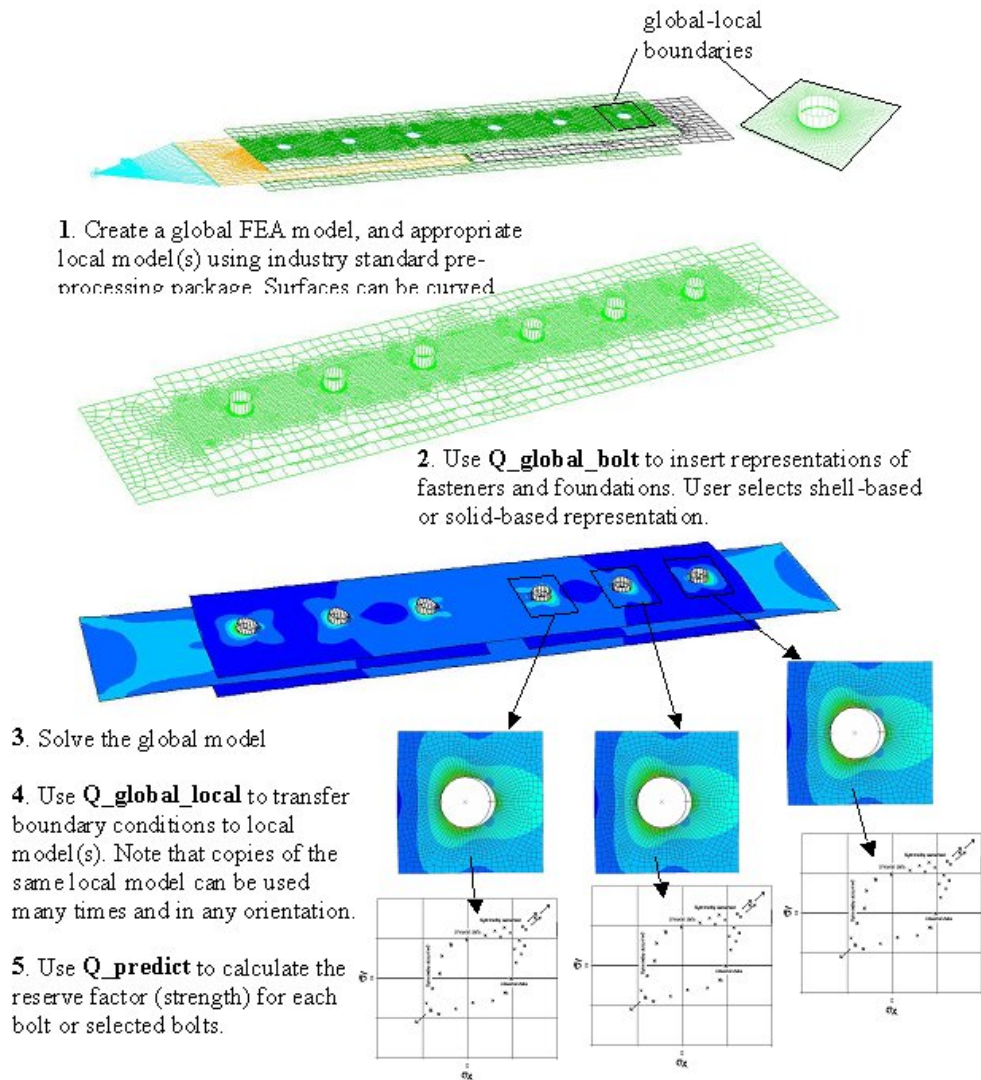


**Figure 4.2.35 Function of QinetiQ’s modelling toolset**

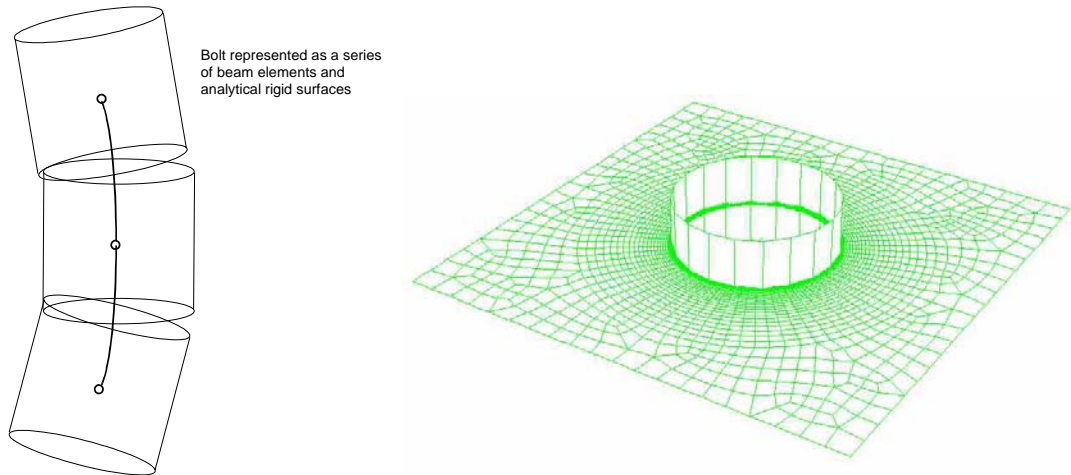
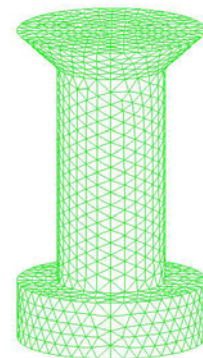
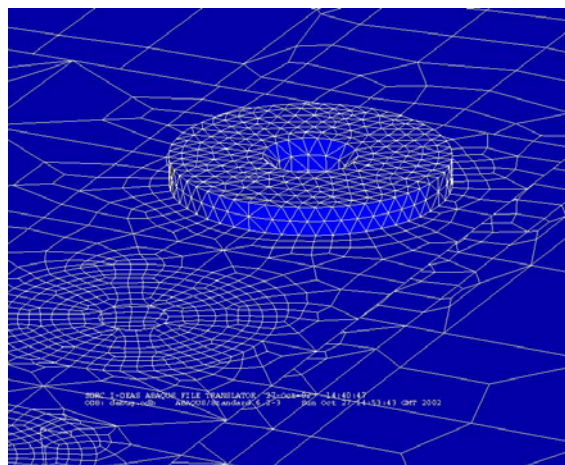
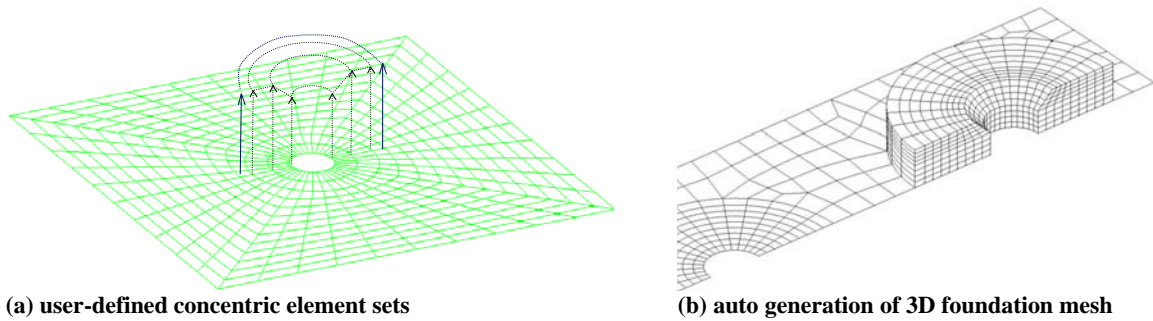


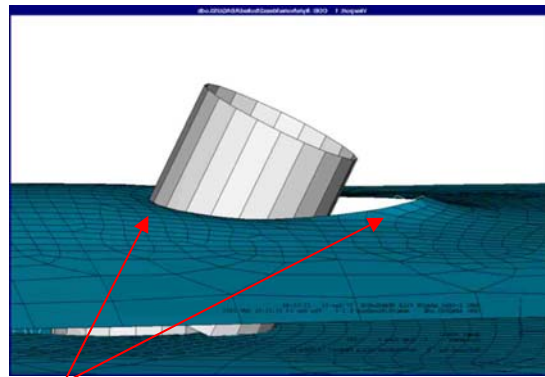
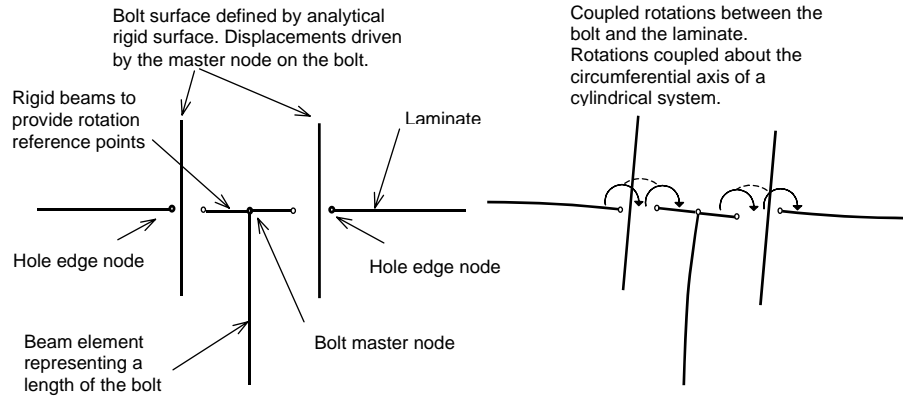
**Figure 4.2.36 “Shell-based” Method: Bolt represented as beams and rigid surfaces. Foundation represented by shells.**



(c) 3D model of critical bolt within 2D model

(d) Solid element representation of fastener

**Figure 4.2.37 “Solid-based” method: 3D bolt and foundation representation in a global 2D model**



Rotation induced in the laminate by tipping of the bolt.

Note:

- Displacements have been greatly magnified
- This model has no out-of-plane constraint, such as that which would be caused by a clamped fastener or neighbouring plate. In such cases the global rotation of the laminate may not be visible, but it would affect the stiffness of the joint.

#### Figure 4.2.38 Coupled displacements in shell-based method to capture fastener tipping

In the “shell-based” method, the problem of representing the fasteners and foundations was overcome by using beam-elements and analytical rigid surfaces to represent the fasteners, and by including the bolt-holes within the original shell mesh (Fig. 4.2.36). Thus the user ensures that the original global shell mesh contains representations of the bolt-holes when it is created. This is convenient because the power of the commercial pre-processing packages can be brought to bear in locating and creating the bolt-holes.

In the “solid-based” method, the bolt and the foundation are represented by 3D finite elements (Fig. 4.2.37).

When pre-processing, the analyst identifies boundaries within the global model that represent the perimeter of the bolt-hole and other details such as the extent of the countersink and the extent of the region to be converted to solid elements (for the solid method only – see Fig. 4.2.37(a)). If global-local coupling is required (see Task 4.3) then the analyst defines boundaries that represent the extent of the relevant local model (Fig.

4.2.35). All these boundaries are defined using node-set definitions, which are a standard feature of the majority of solvers and pre-processors.

When adding representations of fasteners and foundations, Q\_global\_bolt reads parameters from a simple text file that is created by the user. This file is called the ‘configuration file’, and contains parameters that describe the configuration of each single-bolt joint within the global model. Examples of these parameters include the material of the bolts, the diameter of the bolts, and the friction coefficients.

The configuration file and the global FEA file are submitted to the Q\_global\_bolt program, which inserts the relevant FEA representations of the fasteners and their foundations into an updated global FEA file. The updated global FEA file is then submitted to the solver (currently ABAQUS) to obtain the overall loading and deformation within the structure

One of the major limitations of other shell-based methods is their inability to capture the tipping behaviour of the fastener under single-shear loading without recourse to semi-empirical factors to modify the stiffness of the fastener. QinetiQ overcame this problem by coupling the tipping of master nodes on the fastener to the through-thickness rotations of the shell-elements around the boundary of the hole (see Fig. 4.2.38)

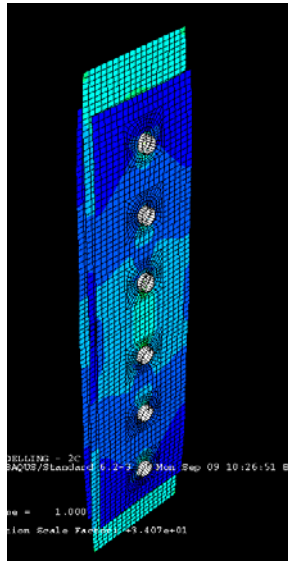
These improvements were assessed by re-modelling two of the BAe benchmark joints using the shell-based method (see Fig. 2.39(a)). One of the results is shown in Table 4.2.7. It can be seen that the shell-based method matched the experimental results more closely than the spring-based method. In addition, the shell method was far more flexible and easy to use than the spring method of Task 2.2. The method was also validated against BAE-BM-2C which became the *Multi-Bolt Benchmark* in BOJCAS. These results are discussed with the results from other partners in Task 2.4.

Benchmark	Applied load (kN)	Predicted stiffness (kN/mm)	Test stiffness (kN/mm)	Ratio of stiffness	CPU time (sec)	Bolt number	Predicted load (kN)	Predicted load (%)	BAe test load (%)	QinetiQ spring method (%)
BM1C	400	157	83	1.89	485	1	153.5	38.4	44	36
						2	109.9	27.5	27	28
						3	136.6	34.2	29	36
						4	136.6	34.1	30	36
						5	110	27.5	28	28
						6	153.5	38.4	43	36

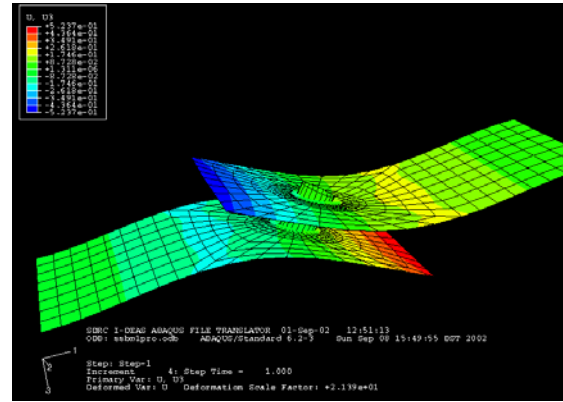
**Table 4.2.7 BAE-BM-1C predicted bolt loads – shell-based method, spring method and experimental results from WP 3**

A difficulty with validating against the BAe benchmarks was concern over the accuracy of the experimental results. Thus, as another validation, the *Single-Bolt Benchmark* (see Task 4.1) was modelled. Greatest confidence existed with this benchmark, as it was well controlled, and both experimental and 3D-solid FEA results were available. QinetiQ’s model approached the accuracy ULIM’s 3D solid model, and the solution was obtained in a fraction of the time (Table 4.2.8).





(a) BAE benchmark joint



(b) Single-Bolt Benchmark

Figure 4.2.39 Validation of QinetiQ’s shell-based method

Model	Stiffness (kN/mm)	CPU time (sec)	Increments	Cut backs	Iterations
ULim solid	34.6	~3600			
SAAB shell	23.2	?			
QinetiQ shell 1st order med.	34.68	78	4	2	28
QinetiQ shell 1st order fine	34.59	346	4	2	38
QinetiQ shell 2nd order med.	34.50	247	4	2	33

Table 4.2.8 Stiffness predictions for the Single-Bolt Benchmark

It has not been possible to demonstrate the solid element method within the duration of the BOJCAS programme due to bugs within the complicated geometric routines that create countersinks within solids with arbitrarily curved surfaces. However, this method goes beyond the original work plan for Task 2.3.

In an additional piece of work to that laid down in the Work Description, QinetiQ applied Q\_global\_bolt to the DASA temporary skin repair benchmark (Fig. 4.2.40). This enabled QinetiQ to apply Q\_global\_bolt to a more complex joint. A range of techniques that could be used to speed-up the creation of the configuration file was identified, and the method was demonstrated with reasonable success despite a mistake that affected the convergence of the solution. Final results were not available in time for this report.

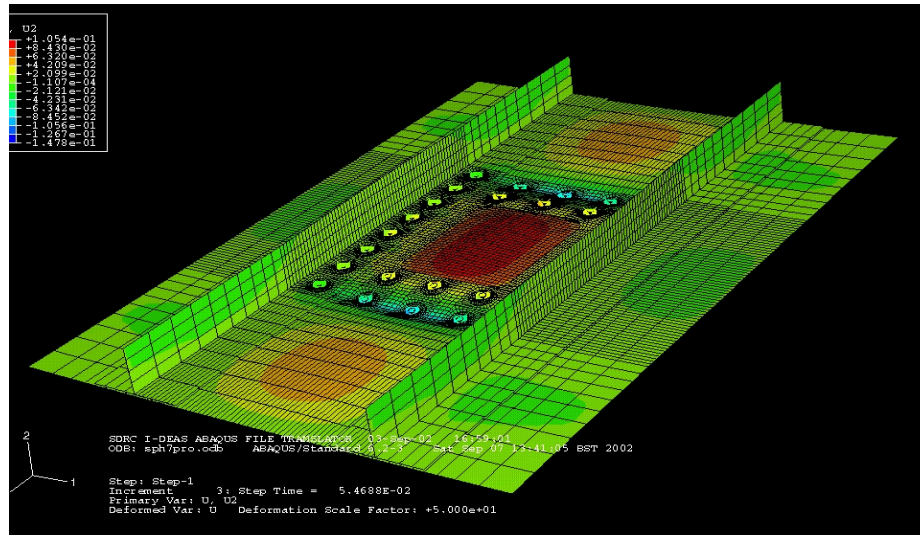


**Figure 4.2.40 QinetiQ's shell-based model of the DA temporary skin repair benchmark**

## 2.2.4 Task 2.4 Industrial Assessment of Global Design Methods

In this task, the three industrial partners were to evaluate the global design methods developed in Task 2.3. AUK was to evaluate QinetiQ's method, AD was to evaluate NLR's method, and SAAB was to evaluate their own method. AUK and AD were to provide contributions to a single report D2.4-1, to be finalised by SAAB.

Because NLR did not produce a significantly new method in Task 2.3, AD could not evaluate their method. Thus, an alternative plan was drawn up whereby AD implemented SMR's *global-local* method of Task 4.3 in their own environment and evaluated this instead. This plan was described in an amendment to the Work Description (Annex 1), which was accepted by the EU in Autumn 2002.

### Task 2.4 Airbus UK

QinetiQ supplied AUK with FORTRAN 90 source code for the programme Q-Bolt and associated demonstration files. The source code was compiled on a Hewlett Packard m-class super computer, the same machine that is used for all Airbus UK's finite element analysis work. The demonstration files ran and worked without any problems.

Execution of the code requires two files: an ABAQUS input file, complete except for the bolts, and a control file that contains the bolt definitions and the names of the ABAQUS files input to the code and output by the code.

Minor problems occurred when MSC.Patran was used to write the ABAQUS file that was to be used by Q-Bolt. This was due to some differences in the input written by IDEAS, QinetiQ's pre-processor, and MSC.Patran, Airbus UK's pre-processor. This

required minor alterations to the code and the executable is now available on the m-class super computer.

Q-Bolt was used to model all ten of Airbus UK's tension and compression benchmark structures and predict bolt load distributions. One example, joint BAE-BM-3T, is given here with a comparison to the spring method of Task 2.1 and experimental results.

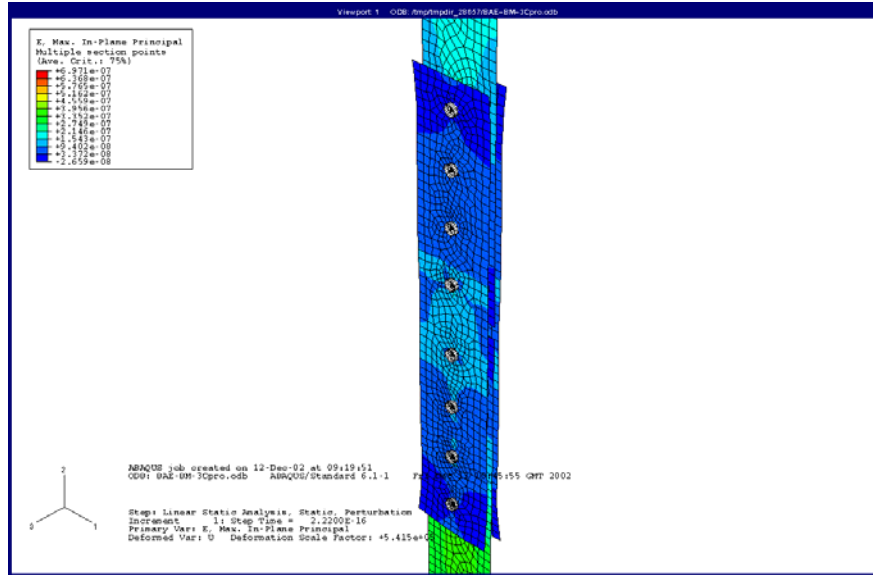
BAE-BM-3T is a plain double-lap joint with one side made from AS4-8552 CFRP and the other 7150-T651 aluminium alloy. The splice plates were also made from 7150-T651 aluminium alloy and the bolts made from titanium alloy. The structure was tested in tension with strain gauges to measure bolt load distribution.

Fig. 4.2.41 shows the deformation and principal strain in the structure. Fig. 4.2.42 shows the load distribution in the joint as predicted by the spring method of Task 2.1, QinetiQ's shell-based method and experimental results.

Unfortunately, the experimental results are questionable since the strain gauge method used to measure bolt load distribution was not valid (as discussed in WP 3 and 5). The best experimental results for BAe benchmarks were from BAE-BM-2C for which instrumented bolts were used. For this reason, this joint was chosen as a *Multi-Bolt Benchmark* for the project, and results for this benchmark are shown under SAAB's contribution in this task (see Task 2.4 SAAB below).

Disregarding the experimental results in Fig. 4.2.42, we can see that the shell-based method gives a much more uneven load distribution than the 1D method, especially on the composite side of the joint. This was generally true of all the joints modelled by AUK, and does not tally with the results obtained by QinetiQ using their own method, so there seems to have been some problem with the implementation at AUK. The reasons for this were not available at the time of writing this report, but are under investigation.

Despite this problem, the potential of the method was clear to AUK. The real advantage this method has over the traditional method is that more complex bolt arrangements, loads and patterns can be analysed with fewer assumptions and therefore reduced conservatism. The "in-line" BAE benchmark joint arrangements used in this programme were intentionally simple and did not fully demonstrate the advantages of the new method. More complex joints such as the SAAB or DA benchmarks would show the true worth of the method.



**Figure 4.2.41 Model of BAE-BM-3T created by AUK using QinetiQ’s shell-based method**

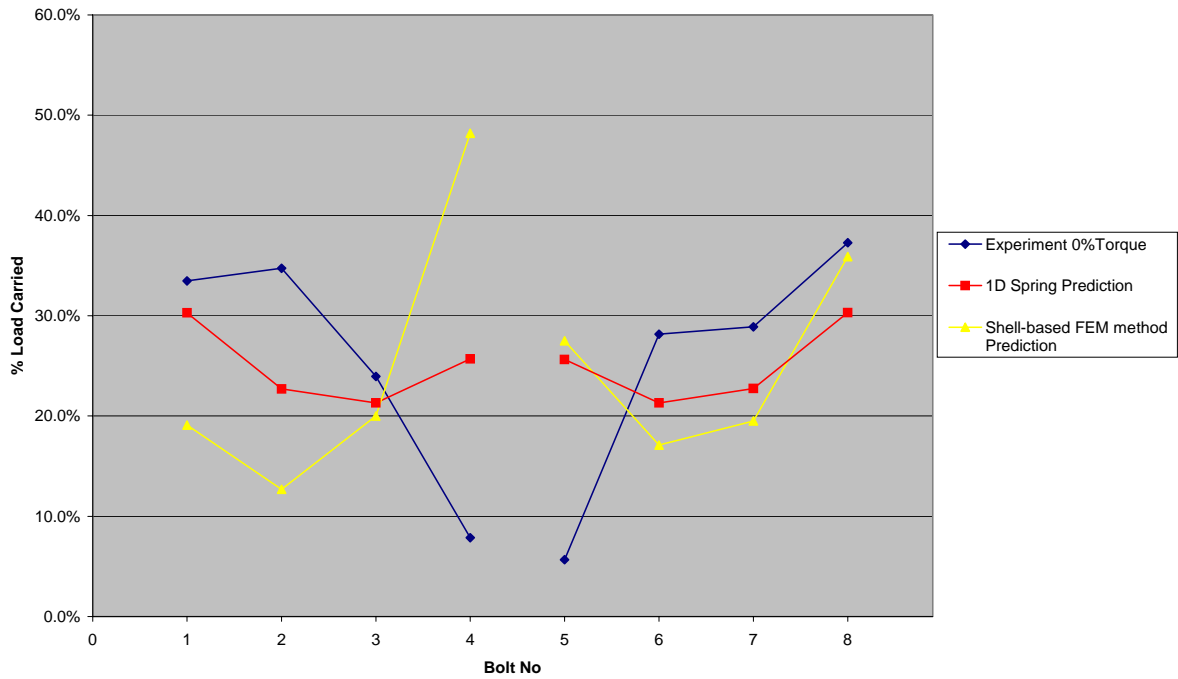


**Figure 4.2.42 Bolt Load distribution in BAE-BM-3T**

### Task 2.4 Airbus Deutschland

As stated above, according to the original work plan AD was not directly involved in the development of new methods. By close consultation with NLR, it was planned that implementation of the any new method developed in Task 2.3 into AD's environment would be relatively straightforward.

However, in the revised work plan, no significantly improved global method was available from NLR, so AD decided to work on implementation of a global-local methodology based on SMR's developments in Task 4.3.

Due to the fact that SMR results were not available in MSC.Patran/Nastran environment, it was not possible to port SMR's FORTRAN source, so AD decided to develop a tool within the ANSYS programming language (APDL), directly based on experiences and recommendations from Task 4.3.

A parameterised ANSYS/APDL tool C\_LOBO was therefore created for generation of local bolt models in global panel models (see Fig. 4.2.43). The tool enables automatic generation of all necessary FE geometries and contact definitions of the local model. The material definitions for composite parts of the model could not be fully automated due to complex definition conditions for that material. By using semi-automated routines and manual corrections this problem was bypassed. A flowchart for C\_LOBO is shown in Fig. 4.2.44.

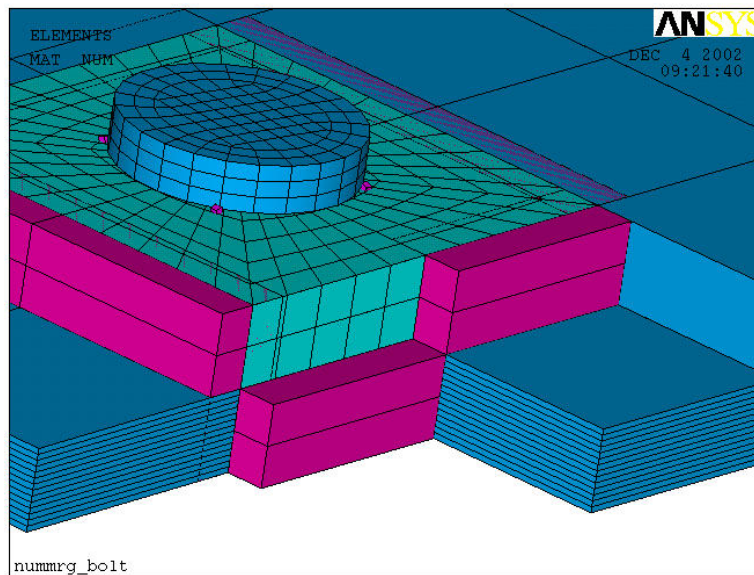


**Figure 4.2.43 Local 3D-Model within global 2D-Model - Transition Zone with Real Element Thickness**

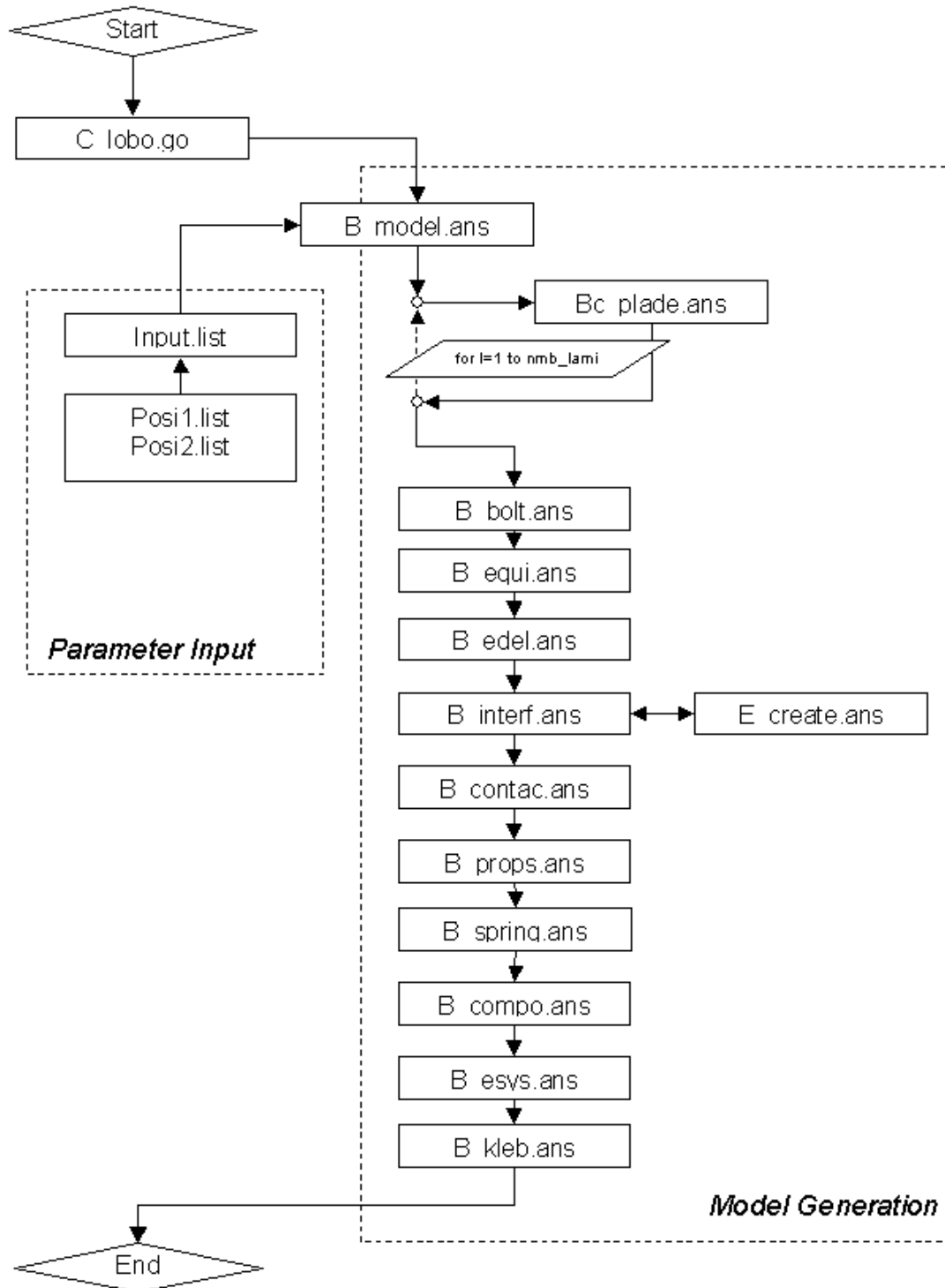


**Figure 4.2.44** Flow-chart of semi-automatic process for local 3D-model generation within global model

The C\_LOBO local bolt model was implemented into the DA Temporary Skin Repair model to assess a possible application of this approach (see Figs. 4.2.45 and 4.2.46). Several linear and non-linear simulations were performed, studying the convergence behaviour and the influence parameters of the model. It was found that attaching the repair patch to the panel skin by a sliding contact definition instead of constrained equation coupling results in more stable convergence behaviour. Generally in all analyses the displacement shapes and stress levels in panels with an implemented local bolt model were not disturbed appreciably compared to a global model without local bolt modelling. Therefore the general applicability of the global-local approach used here was shown.

Due to the fact that the simulations were only loaded by small enforced displacements into the initial post-buckled state, a general statement on the applicability of this global-local approach on an industrial scale cannot be given. Non-linear panel benchmark analyses providing large local model rotations due to distinctive buckling behaviour of the panel at displacements on a large scale could not be realised because of the very short time frame for Task 2.4. Nevertheless by comparing results of sub-model analyses at large deformations it can be stated that this global-local approach has in principle the potential to fulfil the requirement of robustness, stable convergence behaviour and accuracy also for post-buckling problems undergoing large rotations.

Generally it can be stated that application of local bolt models in an industrial development environment would be desirable and feasible. It would give further information about stress and load distribution in these highly loaded structural regions to stress engineers. Nevertheless an application of local 3D-modelling is presuming a user-friendly, automated and self-correcting tool for local model creation. Otherwise the time needed to build up and check the models would be unacceptable in the design process.

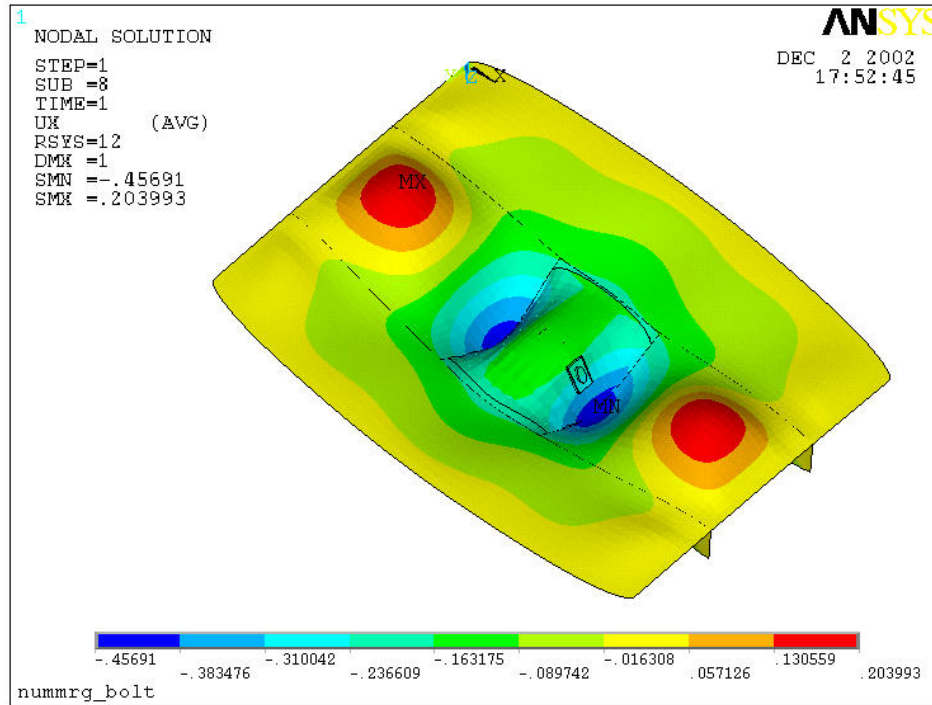


Figure 4.2.45 DA temporary skin repair with single local 3D bolt model created using C\_LOBO

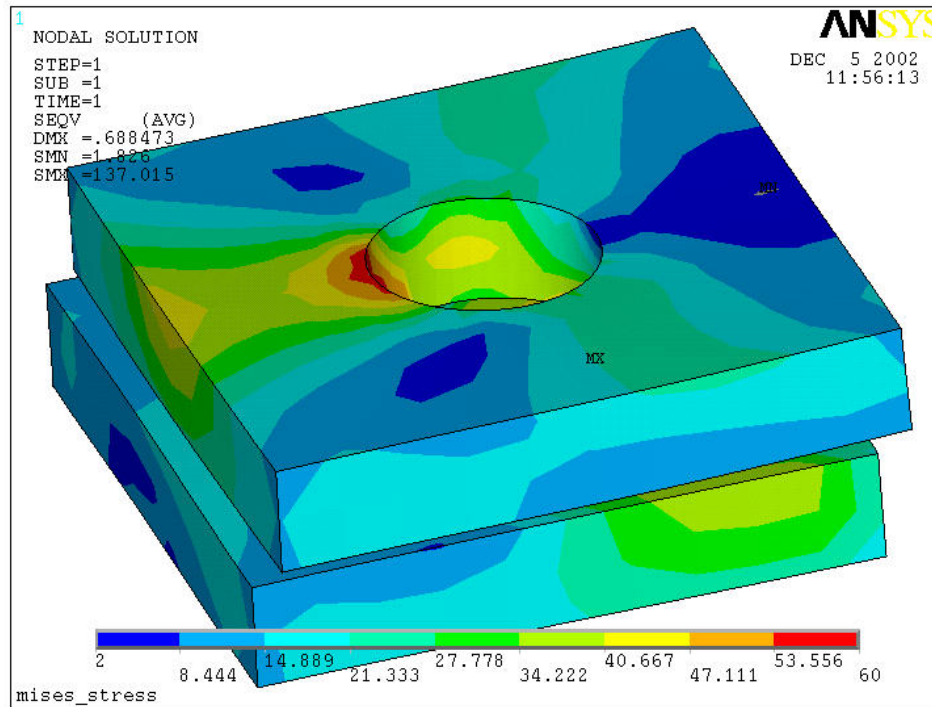


Figure 4.2.46 Stress distribution in local bolt foundation



## 2.4 SAAB

As WP 2 leader, SAAB co-ordinated an effort to compare different global methods on a single joint, which became known as the *Multi-Bolt Benchmark*. The chosen structure was BAE-BM-2C, which is illustrated in Fig. 4.2.47. The structure was tested by AUK with instrumented bolts in both tension and compression. It was modelled using global analysis methods by SAAB, QinetiQ, and NLR, and was also modelled in full 3D by ULIM – further details on the 3D model are given in ULIM’s contribution in Task 4.4. Fig. 4.2.48 illustrates SAAB’s model.

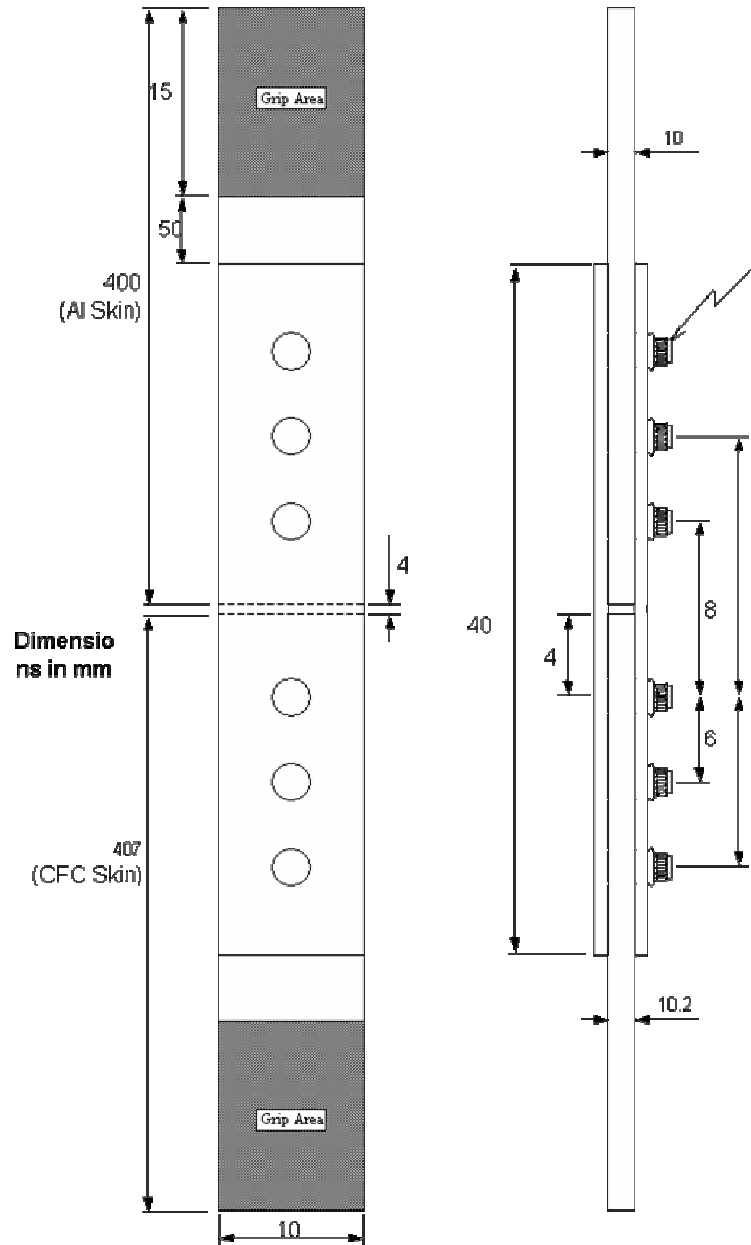
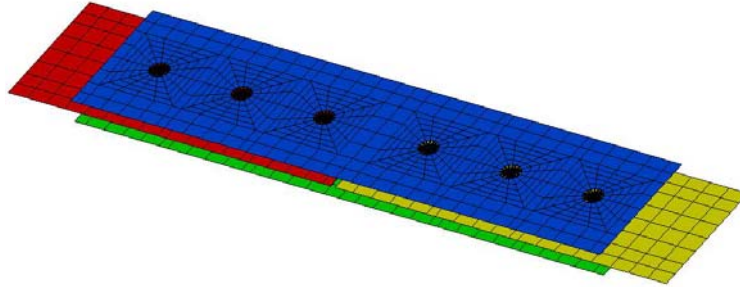


Figure 4.2.47 The *Multi-Bolt Benchmark* BAE-BM-2C



**Figure 4.2.48 SAAB's model of the *Multi-Bolt Benchmark***

The predicted results have been compared with test results and predictions with the 1-D spring method used by AUK. The results for tensile and compressive loading are summarised in Fig. 4.2.49(a) and (b) respectively. It can be seen that all methods predict quite similar bolt load distribution results, which are in good agreement with the instrumented bolt results (the instrumented bolt result for Bolt 5 in the tensile case seems likely to be in error, since it disagrees with all the modelling methods). The NLR method predicts a more uneven load distribution than the other methods.

The stiffness measured in the test is not really a valid stiffness to use when comparing with model stiffnesses, since it was based on the machine stroke, which includes a large amount of compliance besides that in the specimen (see WP 5 for more on this subject). If the 2-D methods are compared with the 3-D method, the 2-D methods predict similar stiffness under compressive loading, but show a large scatter for stiffness under tensile loading – the tensile stiffness from SAAB's method is closest to the stiffness predicted with the 3-D method.

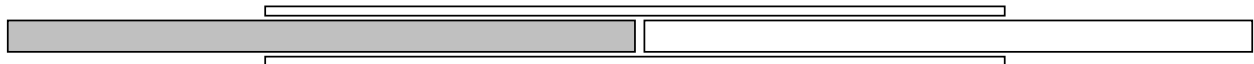
As part of its industrial implementation, SAAB has already used its method in another project to predict the load distribution in a real aircraft structure (Airbus A380) in a complex bolted joint where a spreader plate is used to enable transfer of more load in a highly loaded metallic structure (see Fig. 4.2.50).

In summary, SAAB has developed a user-friendly tool that improves the load distribution analyses in complex bolted joints. When comparison with 3D-analyses is made, the tool seems to predict the numerical load distribution for symmetrical joints very well, while at high deviations from symmetry (single lap joints are extremes) a discrepancy can be expected (about 20% in bolt load). Such high deviations are on the other hand unusual in real aircraft structures where support is to be expected from the surrounding structure. The measured and predicted strains, out of plane displacements and failure behaviours are in good correlation. The usefulness of the tool has already been demonstrated in industrial use.

Bolt Load Distributions for BAE-BM-2C-3 (using existing FE methods)								
TENSION	CFC			Al alloy			Load (kN)	Disp (mm)
	Bolt 1	Bolt 2	Bolt 3	Bolt 4	Bolt 5	Bolt 6		
Predicted (1D model)	36%	31%	33%	33%	30,5%	36,5%	-	-
Instd Bolt (0% torque)	39%	27%	34%	33%	34%	33%	111	1,5
SAAB (FE)	39%	29%	32%	33%	29%	38%	190,5	1,5
QinetiQ (FE)	39%	28%	33%	33%	27,5%	39,5%	245	1,5
NLR (FE)	42%	25%	33%	32%	25%	43%	369	1,5
ULIM (3D FE)	37.2%	29.7%	33.1%	32.6%	29.3%	38.1%	183.5	1.5

CFC	1	2	3	4	5	6	Al alloy
-----	---	---	---	---	---	---	----------

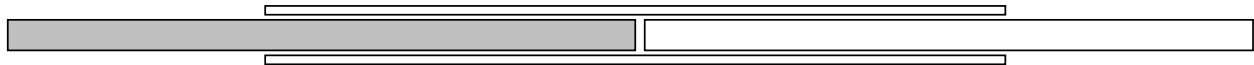


(a) Tension loading

Bolt Load Distributions for BAE-BM-2C-3 (using existing FE methods)								
COMPRESSION	CFC			Al alloy			Load (kN)	Disp (mm)
	Bolt 1	Bolt 2	Bolt 3	Bolt 4	Bolt 5	Bolt 6		
Predicted (1D model)	36%	31%	33%	33%	30,5%	36,5%	-	-
Instd Bolt (0% torque)	42%	25%	33%	33%	29%	38%	-90	-1,24
SAAB	39%	28%	33%	34%	28%	38%	-237	-1,5
QinetiQ	37%	30%	33%	33%	29,1%	38,3%	-203	-1,5
NLR	40%	26%	34%	34%	25%	41%	-221	-1,5
ULIM (3D FE)	37.7%	28.1%	34.1%	33.7%	27.7%	38.6%	-230	-1,5

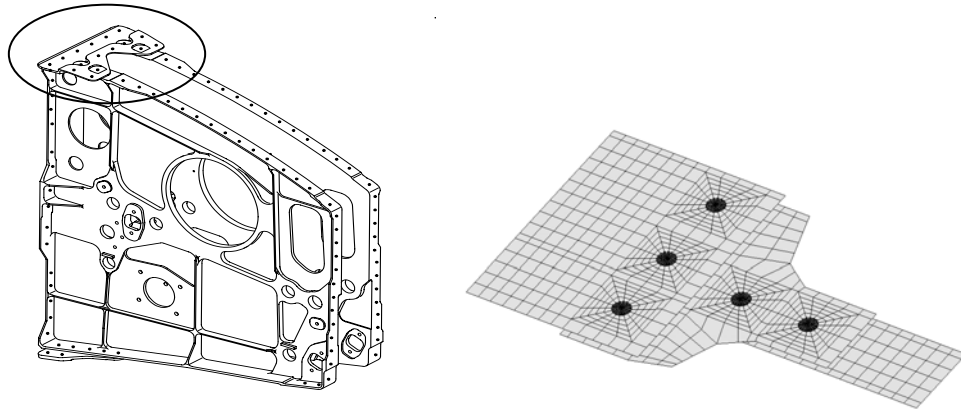
  

CFC	1	2	3	4	5	6	Al alloy
-----	---	---	---	---	---	---	----------



(b) Compression loading

Figure 4.2.49 Comparison of results from different partners on the *Multi-Bolt Benchmark*



**Figure 4.2.50 Example of use of SAAB's method in a real aircraft structure**

## 2.3 WP 3: Benchmark Structure Fabrication and Test

In this WP, AUK performed manufacture and test of the BAe benchmark joints and NLR did the same for the SAAB and DA benchmarks. AD provided the panels for the repair benchmarks. Descriptions of these benchmarks were given above in WP 1 and Task 2.1. The results were to be used for validation of the global and global-local analysis methods.

### WP 3 Airbus UK

The ten BAe benchmark configurations were detailed in Table 4.2.1 and illustrated in Fig. 4.1.2. AUK manufactured 39 test specimens – 30 for quasi-static testing and 9 for fatigue testing. The quasi-static tests are described first.

Three specimens of each of the ten configurations were tested, giving 15 specimens in tension and 15 in compression. A number of methods for determining the bolt load distributions were explored including strain gauges, photoelastic coating and instrumented bolts. Moiré fringe methods were also experimented with to determine the displacements between each of the bolts under load, however this work was unsuccessful.

Results from each configuration were documented in detail in D3-7. To illustrate the results produced, the configuration BAE-BM-2C (which became the *Multi-Bolt Benchmark* for comparison of load distribution methods in the project) is discussed here. Then a summary discussion of all configurations is given.

BAE-BM-2C is a 3-bolt double-lap joint with one CFC skin, one LA skin, two LA splice plates, and countersunk head fasteners. It was designed to be loaded in compression and is representative of a top wing skin joint (see Fig. 4.3.1).

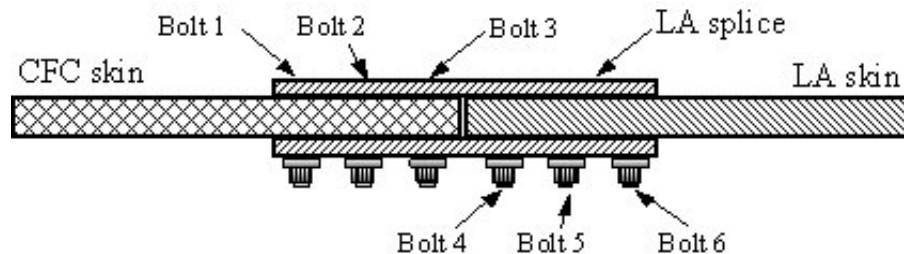


**Figure 4.3.1 BAE-BM-2C joint**

Specimen 2C-1 was loaded to failure with no instrumentation, 2C-2 had photoelastic coating bonded to the splice plates, while 2C-3 had strain gauges bonded to the AL splice plates and six instrumented bolts to measure bolt load distribution. Thus 2C-3 produced the most data for modellers. Load was applied in 25kN compressive increments to an approximate load of 125kN using the maximum safe instrumented bolt load of 40kN as a limit to avoid damaging them. The instrumented bolts were then removed before loading the joint to failure.

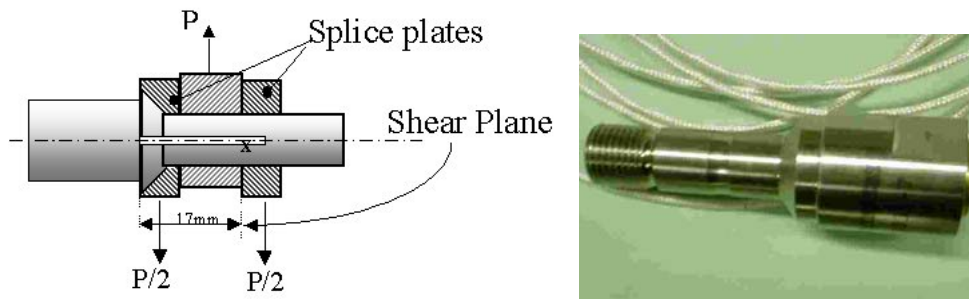


**Figure 4.3.2 Instrumented bolts for measuring shear load between splice and skin plates**

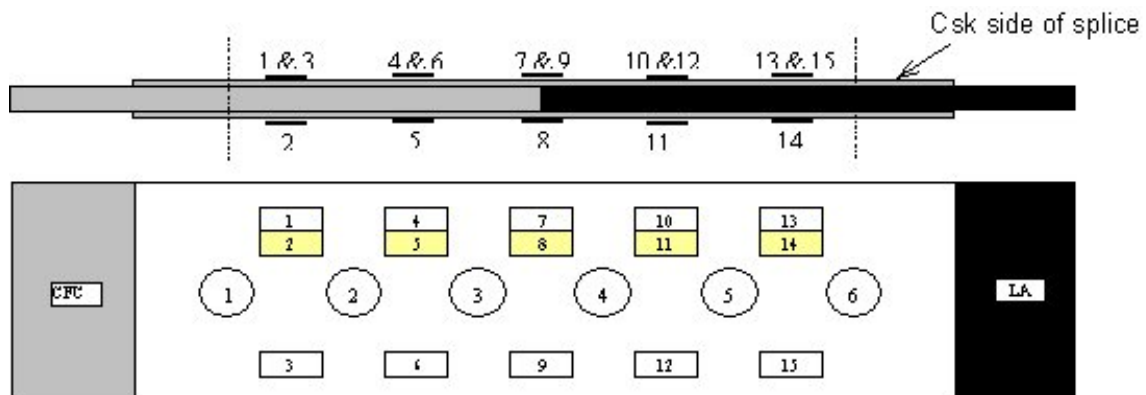


**Figure 4.3.3 Schematic showing strain gauge positions on AL splice plates for 2C-3**



**(a) Instrumented Bolts and Strain gauges**



**(b) Anti-buckle guides**

**Figure 4.3.4 Test Set-up**

The instrumented bolts measured shear strain on one plane only, which is the interface between the splice plate (without a countersink) and the skin, see Fig 4.3.2. Due to the specific geometry of the bolts they could only be used for specimens 2C and 3C.

Fig 4.3.3 shows the positions of the strain gauges on the AL splice plates, which were also used for calculating bolt load distribution. The gauges were positioned longitudinally midway between the bolt-hole centre lines, and laterally midway between the edge of the splice plate and the bolt-hole centre line. The gauges coloured yellow in the figure were bonded in the same position but on the opposite (non-countersunk) splice plate. Fig. 4.3.4 shows the test set-up with instrumented bolts, strain gauges and anti-buckling guides in position.

Fig. 4.3.5 shows the damage in joint 2C-3 after final failure. The ultimate failure mode was net compression failure at Bolt 1 which was the mode predicted, but bearing damage was visible on all the AL and CFC bolt holes. In addition, the AL skin started to buckle adjacent to Bolt 6, where the anti-buckle guides did not support the assembly.

Fig. 4.3.6 shows the load-displacement curves for the three tests. Displacement in this graph is from the machine stroke. The joint 2C-2 was the first joint tested and it had severe buckling problems. In the remaining two tests, the free length between the splice plates and the hydraulic grips was reduced from 50 to 10 mm in an effort to avoid buckling. The unevenness in the 2C-3 curve is due to the use of manual displacement control in this test.

The failure loads for 2C-1, 2C-2 and 2C-3 were -426 kN, -317 kN, and -399 kN respectively. The average of 2C-1 and 2C-3 is 413 kN which is 29% above the predicted net compression load (-320 kN).

The bearing and bypass stresses at the actual failure load of each joint were calculated based on the bolt load distribution prediction from the 1-D spring model (Fig. 4.2.1), and are shown in Table 4.3.1. Note that the bearing stresses for the CFC skin are above the bearing allowable for joints 2C-1 and 2C-3, so the bearing failures occurring prior to the final net compression failures are not surprising.

Before being tested to failure, joint 2C-3 was tested in both tension and compression in the linear region (i.e. at loads that should not produce damage). The bolt load distribution was measured using both the instrumented bolts and the strain gauges, for the cases of 0% and 100% bolt torque. The results are shown in Figs. 4.3.7 and 4.3.8 together with predictions from the 1D spring model. It can be seen that the results from the strain gauge method (especially for 0% torque) are significantly different from the other results. The main problem with the strain gauge method used here is that only one strain gauge has been used across the width. In fact the strain distribution varies substantially across the width in a way that is different for each location along the length. This almost certainly makes the method invalid. This issue is discussed further in ULIM's contribution to WP 5. Even though the strain gauge readings did not give good bolt load distribution results they were still very useful in validating ULIM's 3D model of this joint in Task 4.4.

The agreement between the instrumented bolt results and the predicted results is generally quite good, with the instrumented bolt results indicating a slightly more uneven load distribution than the predictions. The worst comparison is for Bolt 5 with 0% torque under tensile loading (Fig. 4.3.8). The instrumented bolts indicate that the load in this bolt is higher than in bolts 4 and 6. As noted in Task 2.4 above, all the analysis methods contradict this, so it is felt this is an experimental error. Instrumented bolts are quite difficult to use correctly, as will be discussed in ULIM's contribution to WP 5.

Finally on BAE-BM-2C, Fig. 4.3.9 shows the load applied to the joint against instrumented bolt load for 2C-3 with 100% torque. The difference between the applied load and the total load seen by the instrumented bolts has been plotted as friction. The dotted lines show the load on the bolts as the applied load is reduced to zero. The results indicate a friction load of some 35kN and that the bolts do not see any load until the friction has been overcome.

Similar results were presented for the other benchmark configurations (though in less detail since instrumented bolts were only used in joints 2C and 3C). Fig. 4.3.10 shows the actual failure loads, and the failure loads predicted from the 1D spring method for the ten BAe benchmark configurations. Only *ultimate* failure load is shown – *initial* failure due to e.g. bearing failure at the holes is not presented. The failure load predictions given in D2.1-1 were based on net section by-pass stress, calculated from skin cross sectional area minus the area of the bolt hole. For reference, the predicted failure load based on gross section by-pass stress is also given, which is calculated using the full cross sectional area of the skin. This takes into account a hole size correction factor on the maximum bearing stress for zero by-pass that was not used in the original failure load predictions in D2.2-1.

For the tension specimens the "Net Section" failure loads were all within 12% and the "Gross Section" failure loads were all within 14%, of the mean test failure loads. For the compression specimens the "Net Section" failure loads were all within 32% and the "Gross Section" failure loads were all within 27% of the mean test failure loads. The predicted failure loads for compression are conservative, so there is good potential for optimising the performance of bolted CFC compression joints.

Table 4.3.2 shows joint weights, and ranks the joints in terms of efficiency according to failure load/weight ratio. The mean failure load for the tensile 3-bolt joint BAE-BM-2T was 389kN, which is higher than the mean failure load of the equivalent 4-bolt tension joint BAE-BM-3T of 379kN. For the same bolt diameter and skin/splice thickness the static performance is not improved by adding an extra bolt, due to the higher bypass stresses seen in the 4-bolt joint. The extra bolt increases the joint weight by 25%. The mean failure load for the composite/composite tension 3-bolt joint BAE-BM-1T was 395kN, which is slightly greater than the 389kN for the equivalent composite/aluminium joint BAE-BM-2T. The 1T joints weighed 38% less than the 2T joints. The 1T joint has protruding head fasteners, and countersunk fasteners in the CFC splice would have higher stress concentration factors, causing a failure at a lower load. However this shows good potential for a weight benefit of using carbon fibre composite over an equivalent strength metallic joint. Further conclusions can be found in D3-7.



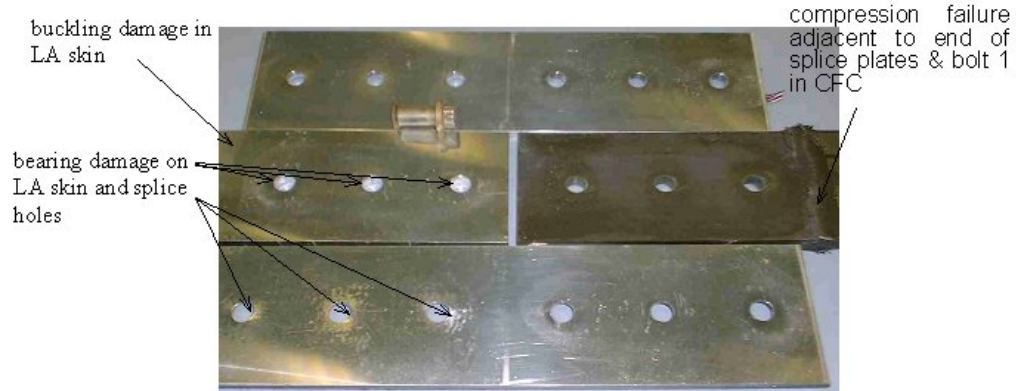
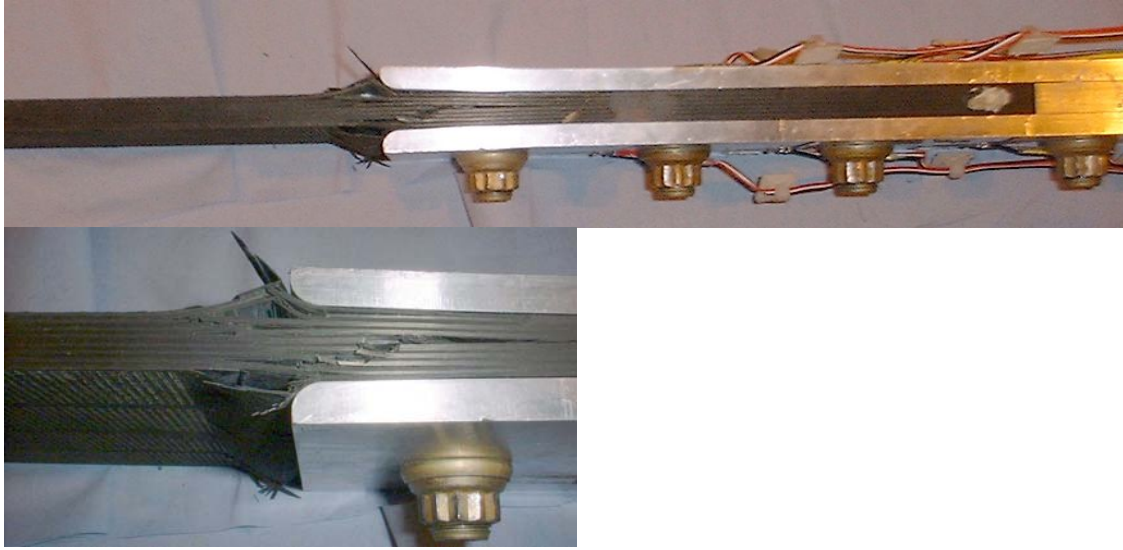


Figure 4.3.5 Details of damage in failed 2C-3 joint

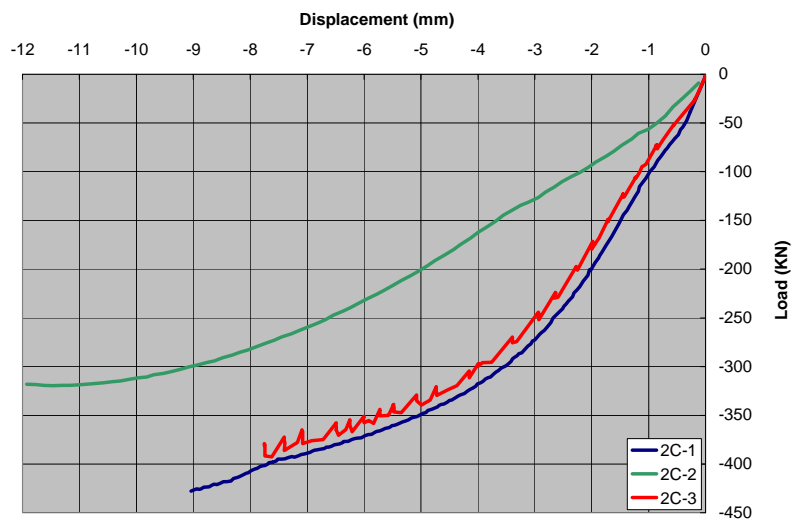
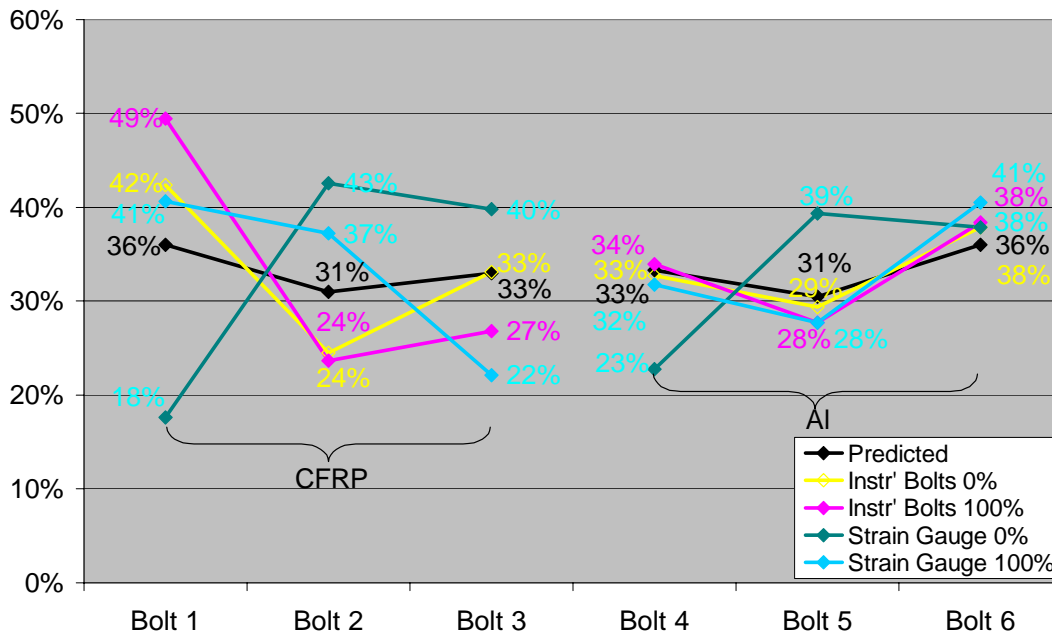


Figure 4.3.6 Load-Displacement for BAE-BM-2C joints

	2C-1			2C-2			2C-3		
	Bolt 1	Bolt 2	Bolt 3	Bolt 1	Bolt 2	Bolt 3	Bolt 1	Bolt 2	Bolt 3
Predicted Load (%)	36.0	31.0	33.0	36.0	31.0	33.0	36.0	31.0	33.0
Bolt Load (kN)	-153	-132	-141	-114	-98	-105	-143	-124	-132
<i>CFC skin</i>									
$\sigma_{Brg}$ (MPa)	-1032	-889	-946	-768	-661	-704	-966	-831	-885
$\sigma_{Byp}$ (MPa)	-262	-135	0	-195	-101	0	-245	-126	0
<i>LA Splice</i>									
$\sigma_{Brg}$ (MPa)	-767	-660	-703	-571	-491	-523	-717	-618	-657
$\sigma_{Byp}$ (MPa)	0	-110	-204	0	-82	-152	0	-102	-191

**Table 4.3.1 Bearing and by-pass stress based on actual failure load and predicted bolt load distribution (from 1-D spring model) for BAE-BM-2C**



**Figure 4.3.7 Bolt load distribution for bolts 1 to 3 in the CFC side and bolts 4 to 6 in the AL side of the joint based on strain gauges and instrumented bolt measurements for BAE-BM-2C at -100kN compression**

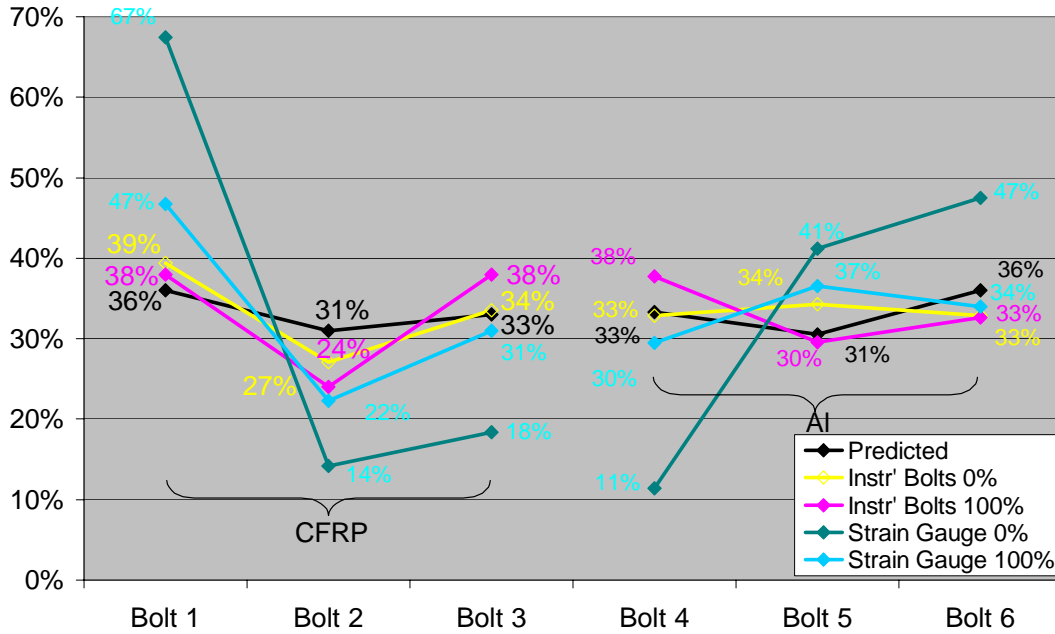


**Figure 4.3.8 Bolt load distribution for bolts 1 to 3 in the CFC side and bolts 4 to 6 in the AL side of the joint based on strain gauges and instrumented bolt measurements for BAE-BM-2C at 110kN tension**

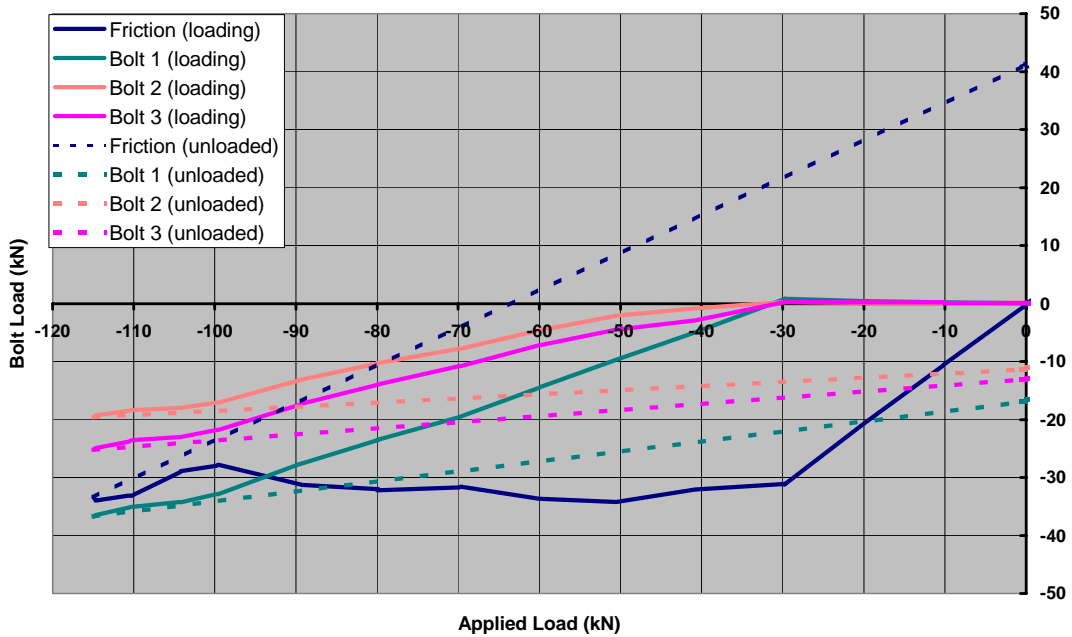


**Figure 4.3.9 Graph showing frictional effects at 100% torque for compression specimen BAE-BM-2C**

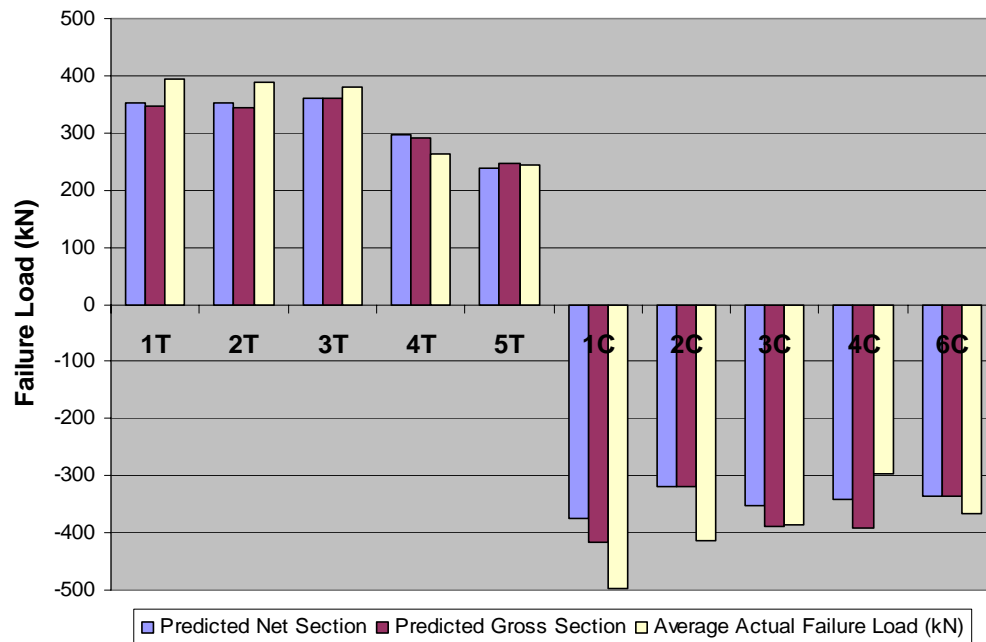


**Figure 4.3.10 Summary of predicted (from 1D spring model) and actual *ultimate* failure loads for the 10 Airbus UK benchmark configurations**

Benchmark Ref	Weight (kg)	Failure load (kN)	Index	Rank
BAE-BM-1T	3.11	395	127	2
BAE-BM-2T	4.98	389	78	7
BAE-BM-3T	6.21	379	61	10
BAE-BM-4T	4.12	262	64	9
BAE-BM-5T	2.19	244	111	4
BAE-BM-1C	2.99	497	166	1
BAE-BM-2C	3.57	413	116	3
BAE-BM-3C	4.42	386	87	6
BAE-BM-4C	4.55	296	65	8
BAE-BM-6C	3.96	367	93	5

**Table 4.3.2 Efficiency of each benchmark joint structure assembly**

Turning to the fatigue tests, nine joints (3 each of 3 different configurations) were tested. The joint configurations were representative of bottom wing skin joints predominantly working in tension and therefore sensitive to fatigue. The three tested configurations were labelled BAE-BM-2F, BAE-BM-3F and BAE-BM-4F, which were identical to the quasi-static configurations BAE-BM-2T, BAE-BM-3T and BAE-BM-4T, except the holes in the AL splice plates and skin were cold worked and interference fits were used on the AL side of the joint (which enhances fatigue life in metals). The three joints are illustrated in Fig. 4.3.11. Testing for all joint assemblies was in tension/compression at

constant amplitude with an R ratio of  $-1$ . The equal tension/compression cycle crudely simulates the ground-air-ground flight cycle, giving a mean stress of zero. The assemblies were tested without anti-buckle guides, however the distance between the end of the splice plates and the hydraulic grips was reduced from the originally specified 50mm to 10mm to ensure no instability problems were experienced.

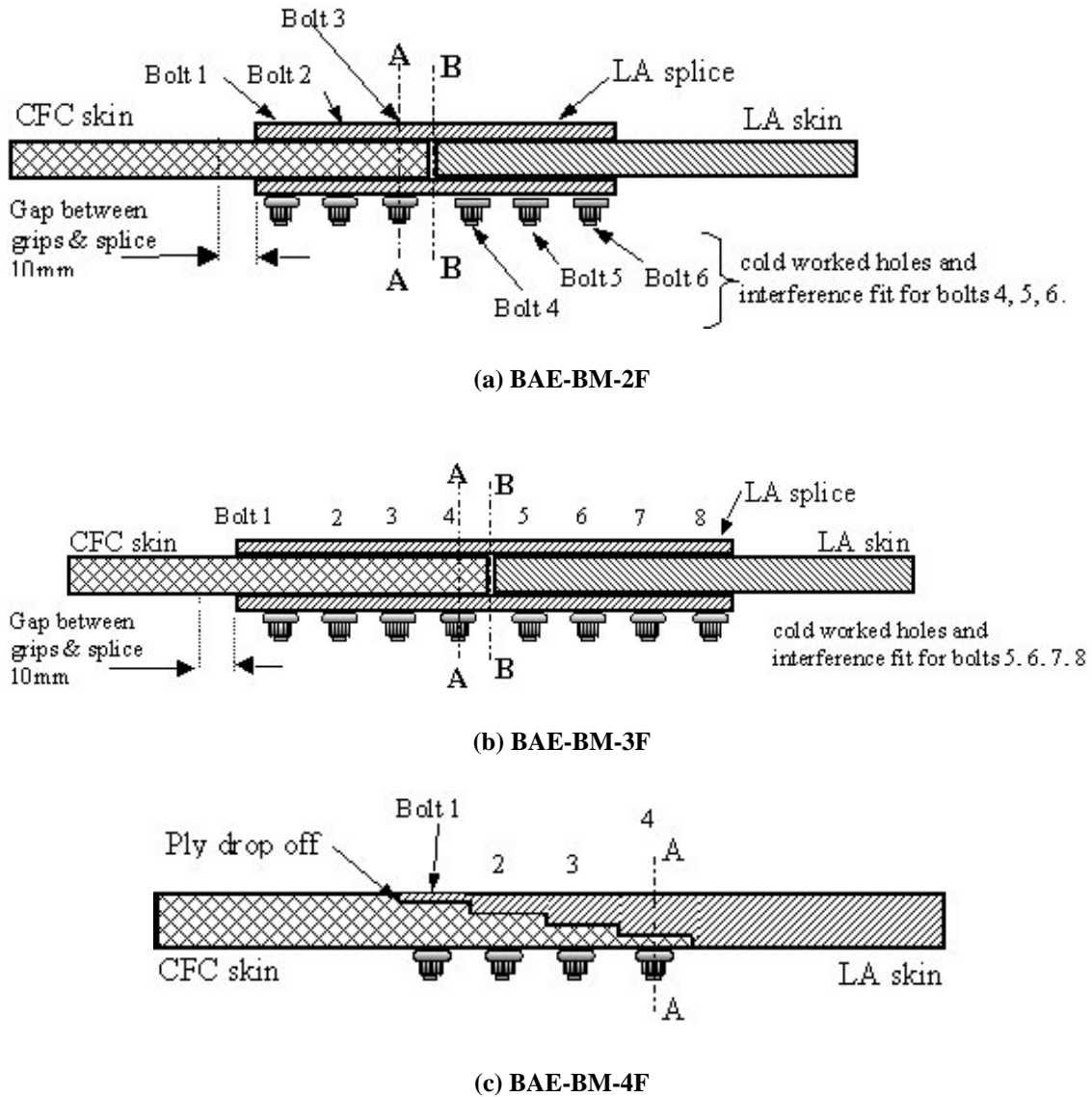


**Figure 4.3.11 BAE fatigue benchmark configurations**

The results are quite difficult to interpret, since three different failure modes occurred, depending on the configuration and loading (see Fig. 4.3.12):

- Mode A – failure at expected location in AL splice plates (CFC side of the joint), crack initiating at point X, (see Fig. 4.3.12).

- Mode B – failure in AL skin member ahead of bolt hole closest to the gripped end of the joint, crack initiating at point Y (or at least passing through point Y) in Fig. 4.3.12.
- Mode C – failure in CFC skin for the scarf joint design.

Specimen 2F-1, tested at  $\pm 115$  kN, had a fatigue endurance of 1,453,228 cycles to failure, which is very promising at a load level of 30% of the average static tensile failure load. For 2F-2 and 2F-3, tested at  $\pm 200$  kN load level (51% of the average static failure load) the average cycles to failure was 52,695, which is a considerable decrease in fatigue performance. Two of the 2F specimens failed in Mode A, one in Mode B.

All the 3F benchmarks were tested at the same  $\pm 200$  kN load level, which is 53% of average static tensile failure load. The benchmarks underwent an average of 67,670 cycles to failure, notably higher than the two 2F benchmarks tested at the same load level. The maximum bypass stress for 2F and 3F is the same, but the bearing loads are higher for 2F (one fastener less). Again, two of the 3F specimens failed in Mode A, one in Mode B.

Specimens 4F-1 and 4F-2 were tested at  $\pm 100$  and  $\pm 90$  kN respectively which is 38% and 34% of the average static tensile failure load. They underwent an average of 318,700 cycles to failure and failed in Mode B. The net skin stress (92 and 82 MPa) is similar to that of 2F-1, which underwent over 1.4 million cycles to failure. This implies that the secondary bending effects contributed to the reduced endurance of 4F-1 and 4F-2. Specimen 4F-3 was loaded too highly and the onset of delamination and ply failure (Mode C) was rapid (2710 cycles).

In conclusion the majority of failures were in the AL splice plates as expected (Mode A failure). Mode B and C could be a result of test procedure/set-up (e.g. due to bending at that section of the joint). Normally, in service, all these joint configurations would be supported by ribs that would resist out of plane bending. Life for the 2F (3-bolt) and 3F (4-bolt) joints seems to be approximately the same for the same splice plate net stress. Mode C CFC fatigue failure of 4F should be investigated in conjunction with static strength of such joints. Further work is recommended for the Mode B failure to determine the initiation site and whether the type of failure is a result of the test method/set up.

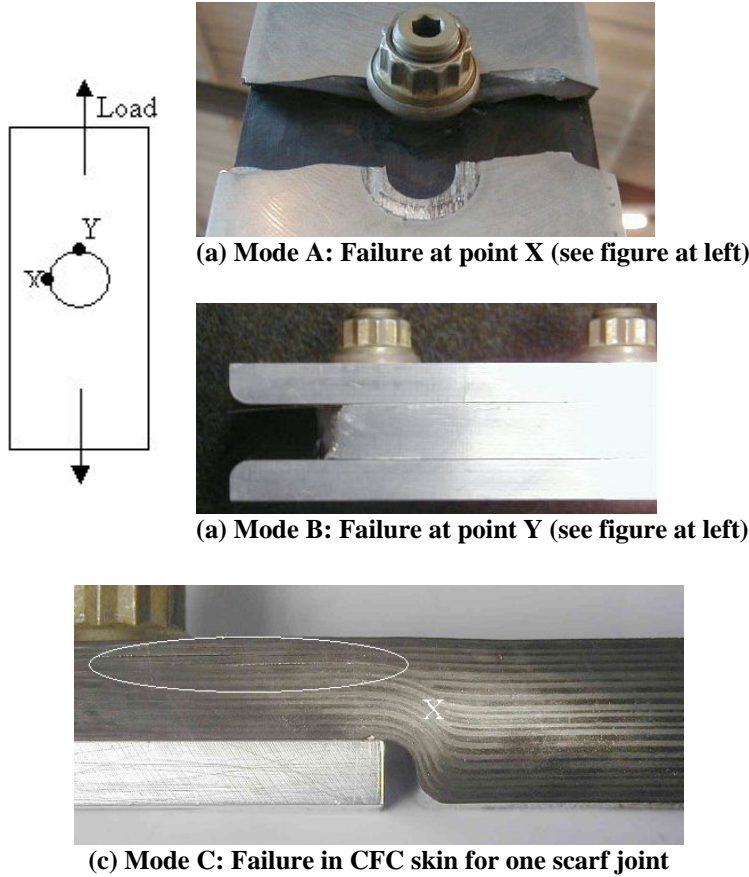


**Figure 4.3.12 Failure modes in BAe fatigue benchmark specimens**

**WP 3 NLR – Part 1: SAAB benchmarks**

The SAAB benchmark joints have been already illustrated in Figs. 4.1.7 and 4.1.8. The summary of the test programme is repeated here in Table 4.3.3 for convenience. Note that the single-lap joints were tested in tension and the double-lap joints were tested in compression and fatigue. The loading fixture for one of the specimens is shown in Fig. 4.3.13. The compression and fatigue specimens used anti-buckling guides.

Test	Bolt pattern 1	Bolt pattern 2	Type of joint
Static tension	1	1	Single overlap
Static compression	1	1	Double overlap
Static tension with one missing bolt	1	1	Single overlap
Static tension with two missing bolts	1	1	Single overlap
Fatigue	2		Double overlap
Fatigue with missing bolt(s)	2		Double overlap
<b>Total number of specimens:</b>	<b>8</b>	<b>4</b>	

**Table 4.3.3 Overview of SAAB benchmark test programme**

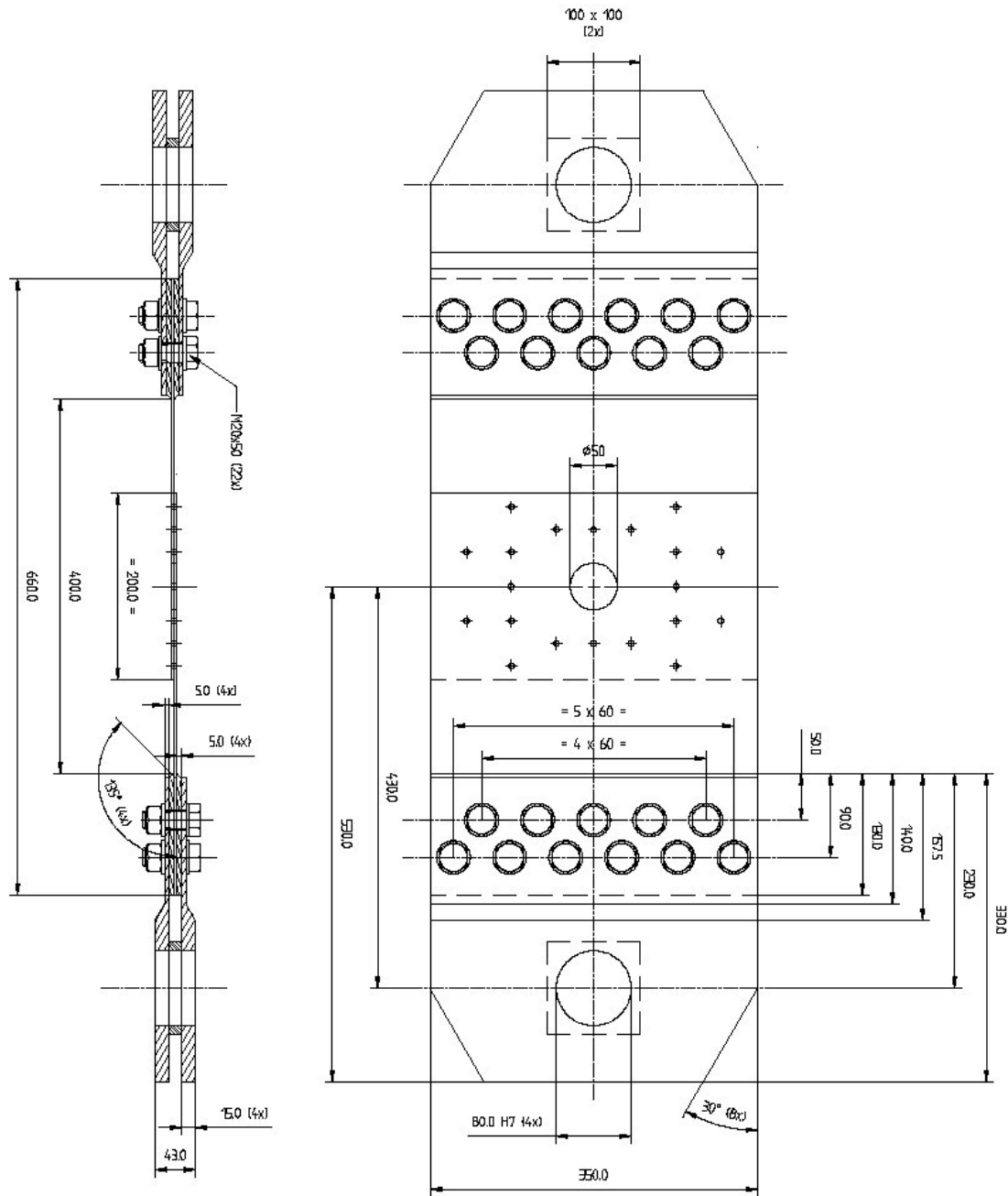


**Figure 4.3.13 Test fixtures for SAAB single-lap specimen with bolt pattern 2 (dimensions in mm)**

Strain gauges were used to measure strains close to the holes, as shown previously in Fig. 4.2.29, and out of plane displacements were measured using a laser displacement transducer mounted on a linear guide rail, as shown in Fig. 4.2.32. The relative displacement between the adherents was also determined, and on some specimens, photoelastic coatings were used.



For the specimens with one missing bolt, loading up to 75 kN was performed, with the missing bolt in 16 different positions (i.e. 16 repeats of the experiment). Strain gauge and displacement transducers were recorded to evaluate the effect of the position of the missing bolt on the strains and displacement in the structure. This generated a very large volume of data that was transmitted to the modellers (SAAB and FOI). Finally the specimens were tested to failure with the missing bolt in one position. Fig. 4.3.14 illustrates the photoelastic results from one of these tests (Bolt Pattern 1) with the missing bolt in the position used for the test to failure. The specimens with two missing bolts were tested once only to failure.

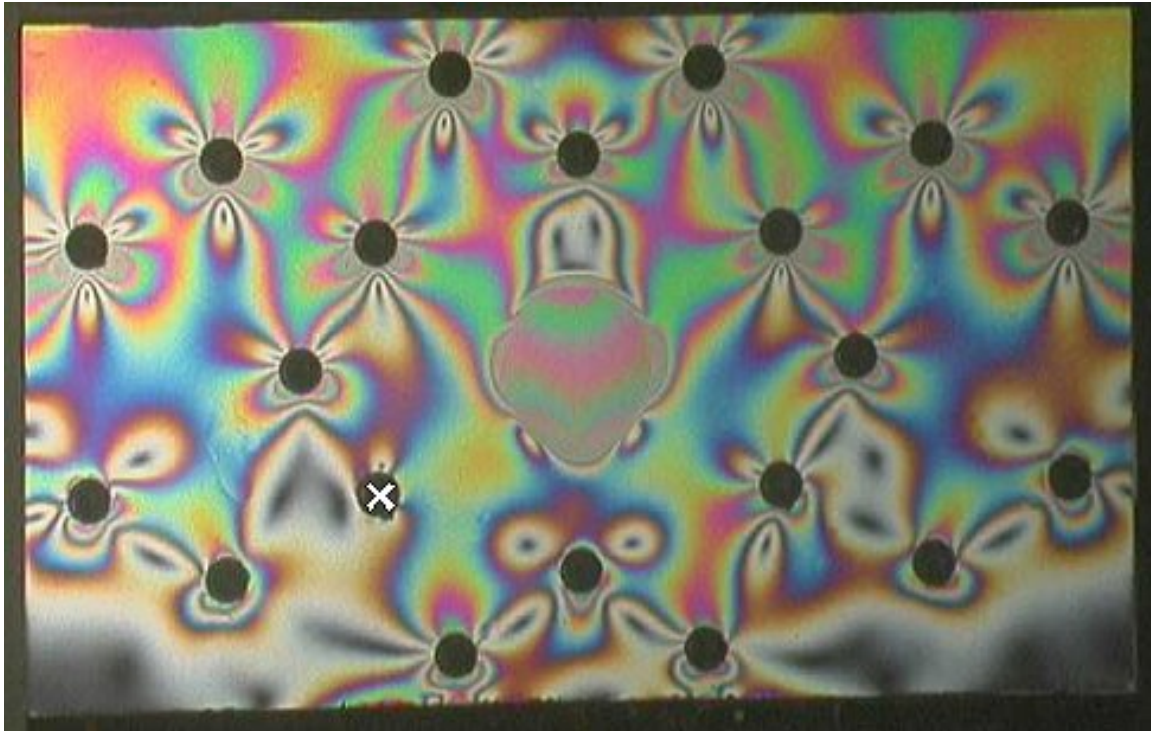


**Figure 4.3.14 Photoelastic fringe pattern for single-lap specimen with Pattern 1, and one missing bolt (location marked with an X), at an external load of 200 kN**

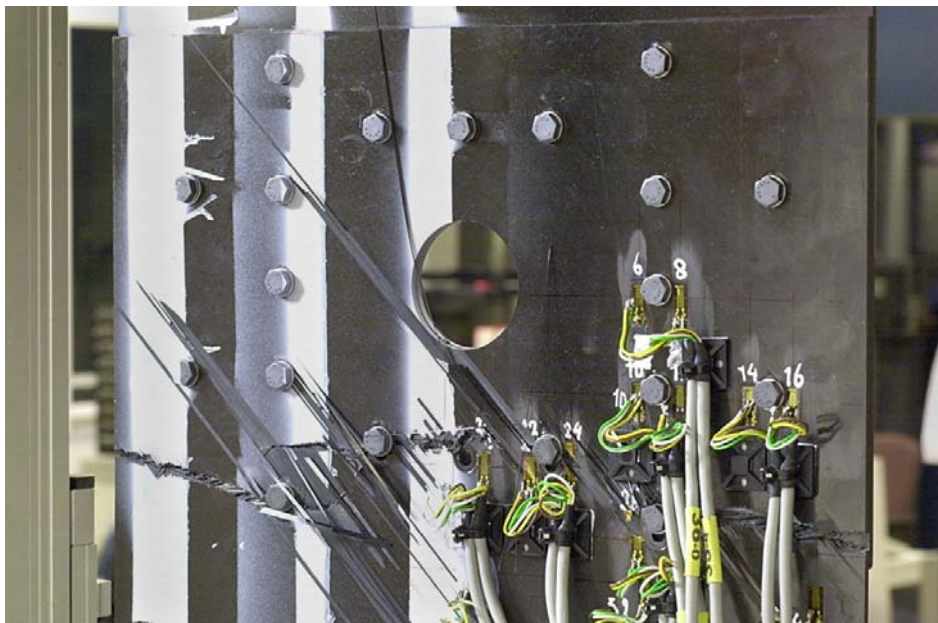
Table 4.3.4 summarises the ultimate failure loads of the quasi-static tension specimens. The failure load for the two bolt patterns with no missing bolts was nearly the same. However, the failure modes were different. The specimen with Pattern 1 failed in bearing followed by failure of a number of bolts, while the specimen with Pattern 2 failed by net section failure in combination with bearing failure at a number of bolts (see Fig. 4.3.15). The failure loads in the specimens with missing bolts were 9-13% lower than the specimens with no missing bolts. For Pattern 2, the specimen with two missing bolts failed at a lower load than the specimen with one missing bolt, but for Pattern 1, the failure load was the same with one and two missing bolts.

Test	Bolt pattern 1	Bolt pattern 2
Static tension	360	356
Static tension with one missing bolt	310	327
Static tension with two missing bolts	309	310

**Table 4.3.4 Ultimate failure loads of single-lap joints loaded in tension**



**(a) Bolt Pattern 1 showing bearing failure and subsequent bolt failure**



**(b) Bolt Pattern 2 showing net section failure at first bolt row + bearing failures at some bolts**

**Figure 4.3.15 Failure of SAAB benchmarks with no missing bolts**

The first quasi-static compression test was performed on the specimen with Bolt Pattern 1 (a double-lap joint, all bolts present). The specimen failed at –233 kN, but unfortunately (despite using anti-buckle guides), the failure was initiated by buckling failure of one of the thinner adherends. The specimen with Bolt Pattern 2 was then tested, but it was decided to abort the test when it was observed that a similar deformation pattern to the first test was occurring, and failure due to buckling was likely again. Despite these problems, both tests gave valuable information to the modellers as they were fully instrumented, as described above.

Four fatigue tests with Bolt Pattern 1 were performed, two with all bolts present and two with 2 bolts missing. The loading was sinusoidal with  $R = -0.2$ . The strain gauge and displacement transducer data were recorded during the first 30 load cycles, and after 100, 300, 1000, 3000 and 10000 loading cycles. This data were also recorded after failure of one or more bolts.

The first specimen with all bolts present was tested at loads varying between –115 kN and 575 kN (calculated to be 80% of static strength). Final failure occurred after 2265 cycles. A number of bolts failed before final failure. The second specimen with all bolts present was tested at loads varying between –99 kN and 495 kN (calculated to be 70% of static strength). Final failure occurred after 10828 cycles. Again, a number of bolts failed before final failure.

Both specimens with two missing bolts were tested at loads varying between –99 kN and 495 kN (calculated to be 80% of the static strength with two bolts missing). Both specimens had the same bolts missing. Final failure occurred after 2140 cycles for the first specimen and after 3957 cycles for the second specimen. A number of bolts failed before final failure.

Thus the tests at 80% of static failure load failed between 2000 and 4000 cycles, while the test at 70% of static failure load failed at 11000 cycles. For the tests at the same absolute load level (-99 to 495 kN), the effect of the missing bolts was to reduce the fatigue life from 11000 to 2000-4000 cycles.

Finally, some interpretations of the very large volume of data generated in the SAAB benchmark test series were given in D3.9 and D3.12. For example, the effect of removal of a bolt on the strain gauge readings was determined and visualised to allow for a direct assessment of the changes in the strain distribution. The change of the strain gauge readings as function of the number of fatigue cycles was determined and visualised to allow for a direct assessment of the changes in the cyclic strain distribution.

### **WP 3 NLR – Part 2: DA benchmarks**

The DA benchmark joints have been described in WP 1 and WP 2. Fig. 4.2.20 best illustrates the four final configurations. There were four configurations: temporary and permanent skin repairs and temporary and permanent stringer repairs. AD delivered the structural parts and NLR made these into specimens, carried out the repair, instrumented

the specimens and performed the tests. All specimens were tested in static compression, under dry and room temperature conditions. Two fatigue tests originally planned were cancelled due to budget overruns – this was agreed with the EU Officer after the 24-month meeting.

All specimens were extensively instrumented using techniques similar to those used for the SAAB benchmark (strain gauges, out-of-plane displacement transducers, photoelastic coatings, LVDTs etc.). The instrumentation for the Permanent Stringer Repair is illustrated in Fig. 4.3.16.

The temporary skin repair benchmark failed at a compressive load of 275 kN. The failure, illustrated in Fig. 4.3.17, involved skin failure in compression at the first rivet row and at the top of the cut-out on one side of the specimen. The stringers also failed in compression at the same location as the skin. The panel failed at the first rivet in the stringer foot.

The permanent skin repair benchmark also failed by net section compression at the first bolt row of the repair, with a failure load of 333 kN. The temporary stringer repair benchmark failed without significant failure of the repair, at a failure load of 605 kN. Further details can be found in D3-8.

The permanent stringer repair benchmark failed at 595 kN. Pictures of the failed specimen are shown Fig. 4.3.18. As can be seen, the angle section on both sides of the central stiffener failed in net-section compression at the last rivet before the end of the original stringer. Both outer stringers were completely separated from the skin. From the figure on the right it can be seen that the doublers on each side of the web and the end of the filler also failed in compression.

For all specimens, data were presented in D3-8 on load-displacement, relative displacement between the parts (e.g. patch and skin), out-of-plane displacement and strains. Fig. 4.3.19(a) illustrates one of the out-of-plane displacements over one scan line for the temporary skin repair – the interruption in the readings is due to the cut-out. A local buckling pattern is evident. Fig. 4.3.19(b) illustrates a photoelastic fringe pattern for the permanent skin repair – the bolt positions are clearly visible.

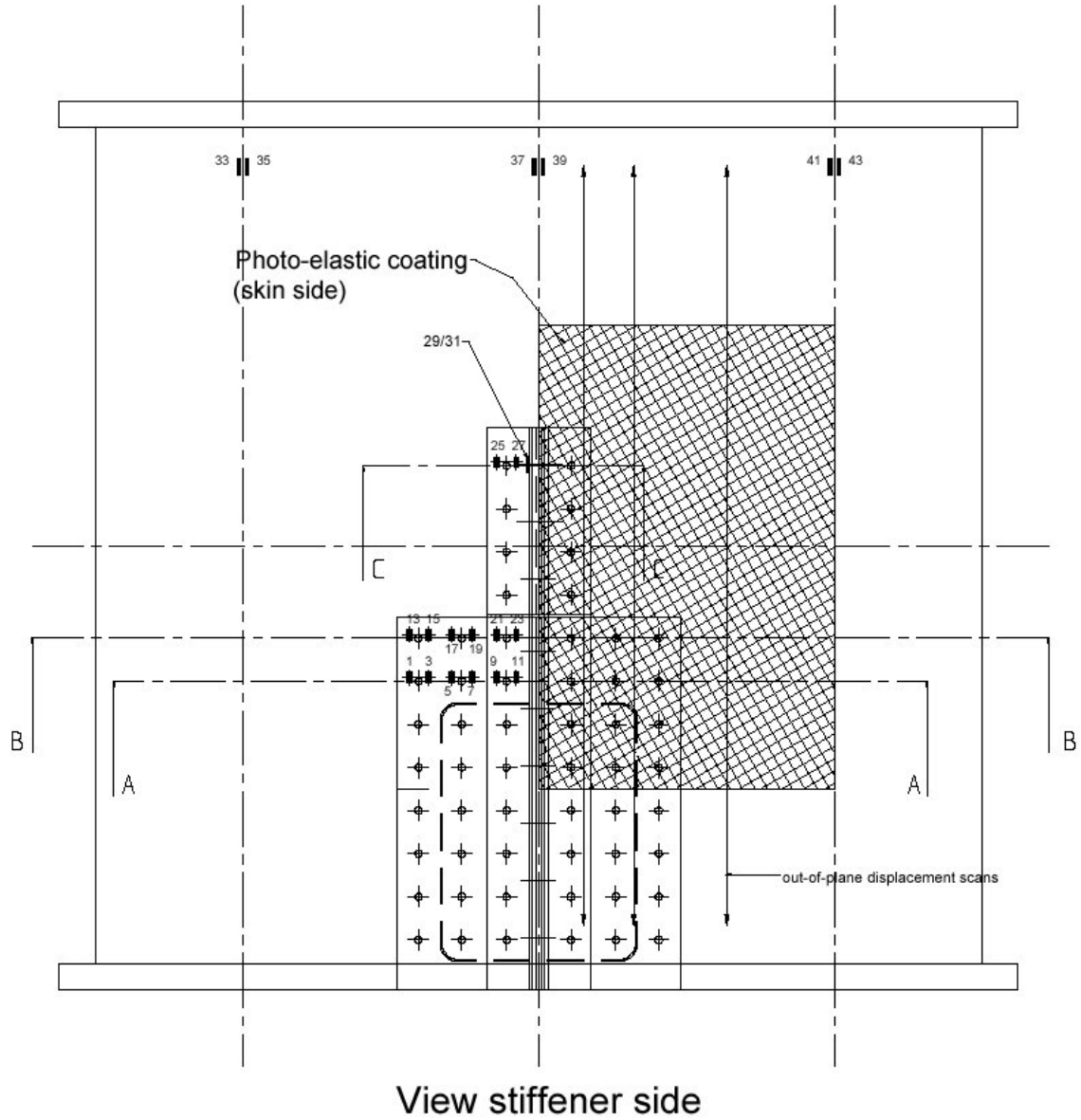
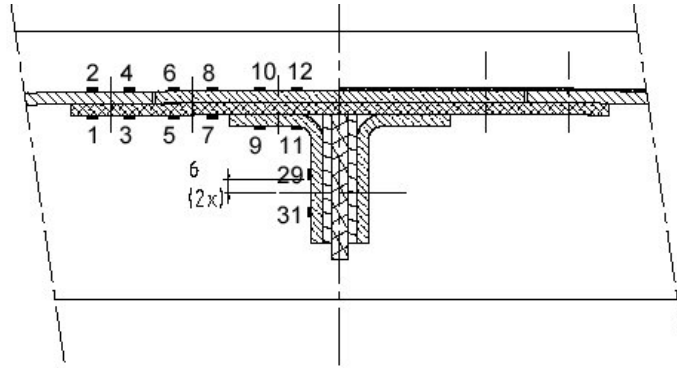
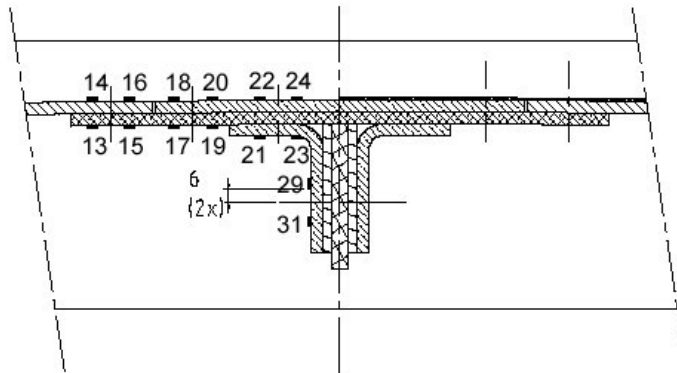


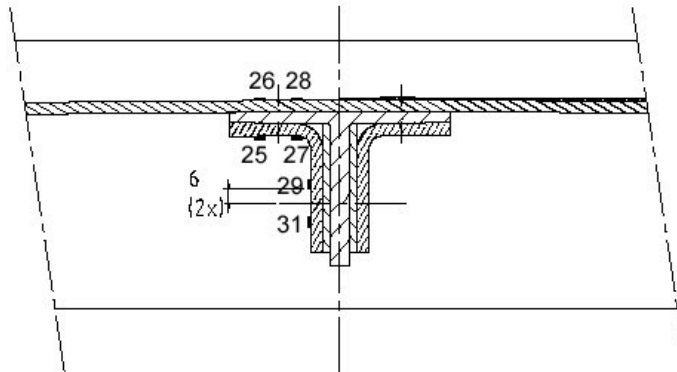
**Figure 4.3.16 Overview of instrumentation on Permanent Stringer Repair (continued overleaf)**



Cross section A-A  
(scaled)



Cross section B-B  
(scaled)



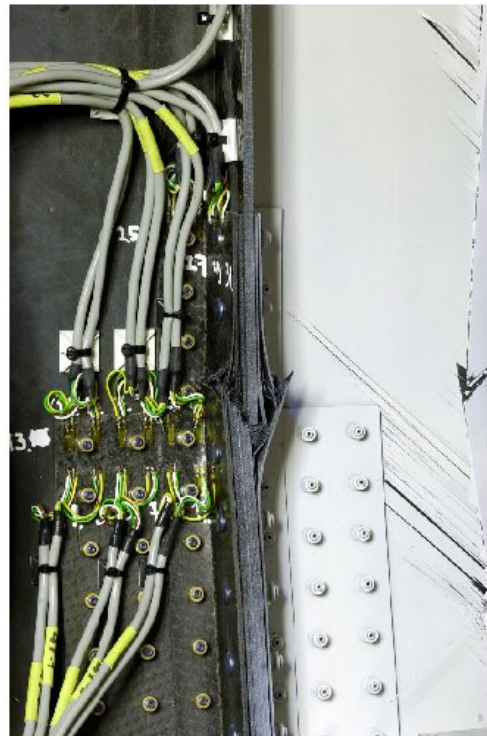
Cross section C-C  
(scaled)

Figure 4.3.16 (continued) Overview of instrumentation on Permanent Stringer Repair

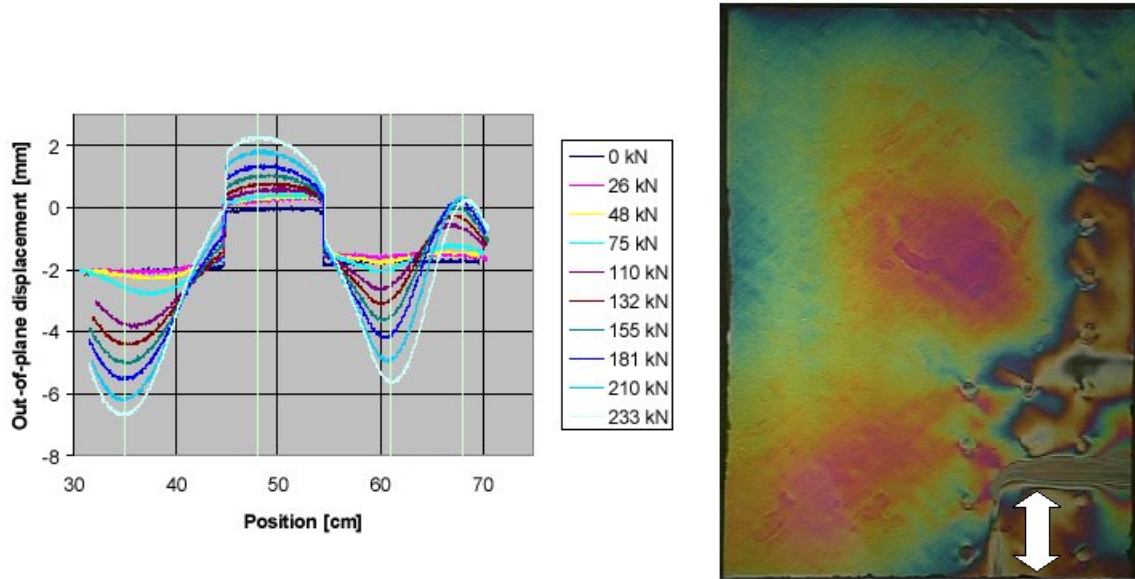




**Figure 4.3.17 Failure mode of Temporary Skin Repair**



**Figure 4.3.18 Failure mode of Permanent Skin/Stringer Repair**



**(a) Out-of-plane displacements for temporary skin repair benchmark**

**(b) Photoelastic fringe pattern for permanent skin repair at 305 kN. Loading direction indicated by arrow**

**Figure 4.3.19 Some of the data obtained from instrumentation on the DA benchmarks**



## 2.4 WP 4: Detailed Design Methods

### 2.4.1 Task 4.1 Three-dimensional stress analysis

In this first task of WP 4, ULIM and KTH performed three-dimensional stress analysis of composite bolted joints. They also developed pre-processors for the creation of such models. ULIM worked in an MSC.Patran/MSC.Marc environment and created a tool named BOLJAT (Bolted Joint Analysis Tool), while KTH worked with ABAQUS. ULIM validated their methods by focusing on the effects of bolt-hole clearance and comparing their results with experiments in WP 5. KTH focused on composite-metallic joints and also validated their results against experiments from WP 5.

#### Task 4.1 University of Limerick (ULIM)

The baseline geometries for the joints studied by ULIM in this task are shown in Figs. 4.4.1 and 4.4.2. The single-bolt joint in Fig. 4.4.1 became known as the *Single-Bolt Benchmark* for the project, and several partners modelled this joint to compare results from different codes and techniques. Table 4.4.1 provides details of the four different bolt-hole clearances studied, coded C1, C2, C3 and C4. The clearances used in the models are shown in the last column. Clearance C2 is near the upper end of the clearance allowed for this hole size under aerospace tolerancing specifications. Clearances C3 and C4 are therefore outside normal tolerances, although clearances as large as C3 are allowed in larger holes.

ULIM began this task with a careful study of material property definition methods and particularly contact definition. Contact definition is crucial to the accurate and efficient modelling of the joint, and so was a vital ingredient to get right before developing an automated model creation tool. Composite material properties were modelled via layered solid elements. However, interpretation of results from these elements can be complex, so equivalent homogenised properties for the composite material were determined from a series of numerical experiments. The resulting in-plane homogenised properties were verified against classical laminate theory (out-of-plane properties cannot be obtained from laminate theory). With these homogenised properties it was easier to predict what the stress distribution at the hole should look like, and so tell if the contact was working properly.

Getting contact to work properly in MSC.Marc took several months of work. This was partly due to poor documentation in the manuals, and partly due to the fact that modelling bolted joints with very small variations in clearance requires a level of accuracy that would not be required in most applications. A very detailed description of the problems that ULIM encountered with contact, together with the solutions found is given in D4.1-2. This should be a very useful reference for anyone attempting to model contact in a joint using MSC.Marc. As an example, Fig. 4.4.3 illustrates the poor stress distributions obtained at the hole, if the optimum contact parameters are not used.

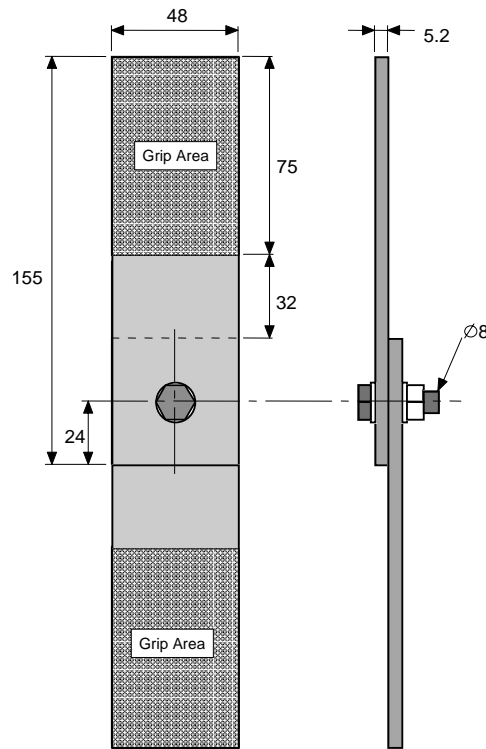


**Figure 4.4.1 Single-lap specimen geometry (all dimensions in mm). NOTE: This joint became the *Single-Bolt Benchmark* for the project**

Clearance Code	Reamer Min (mm)	Reamer Max (mm)	Bolt Min (mm)	Bolt Max (mm)	Min Clearance (µm)	Max Clearance (µm)	Clearance used in FE Model
C1	7.985	7.994	7.972	7.987	-2	22	10
C2	8.065	8.074	"	"	78	102	80
C3	8.14	8.149	"	"	153	177	160
C4	8.225	8.234	"	"	238	262	240

**Table 4.4.1 Range on reamer/bolt sizes and resulting clearances (on the diameter)**

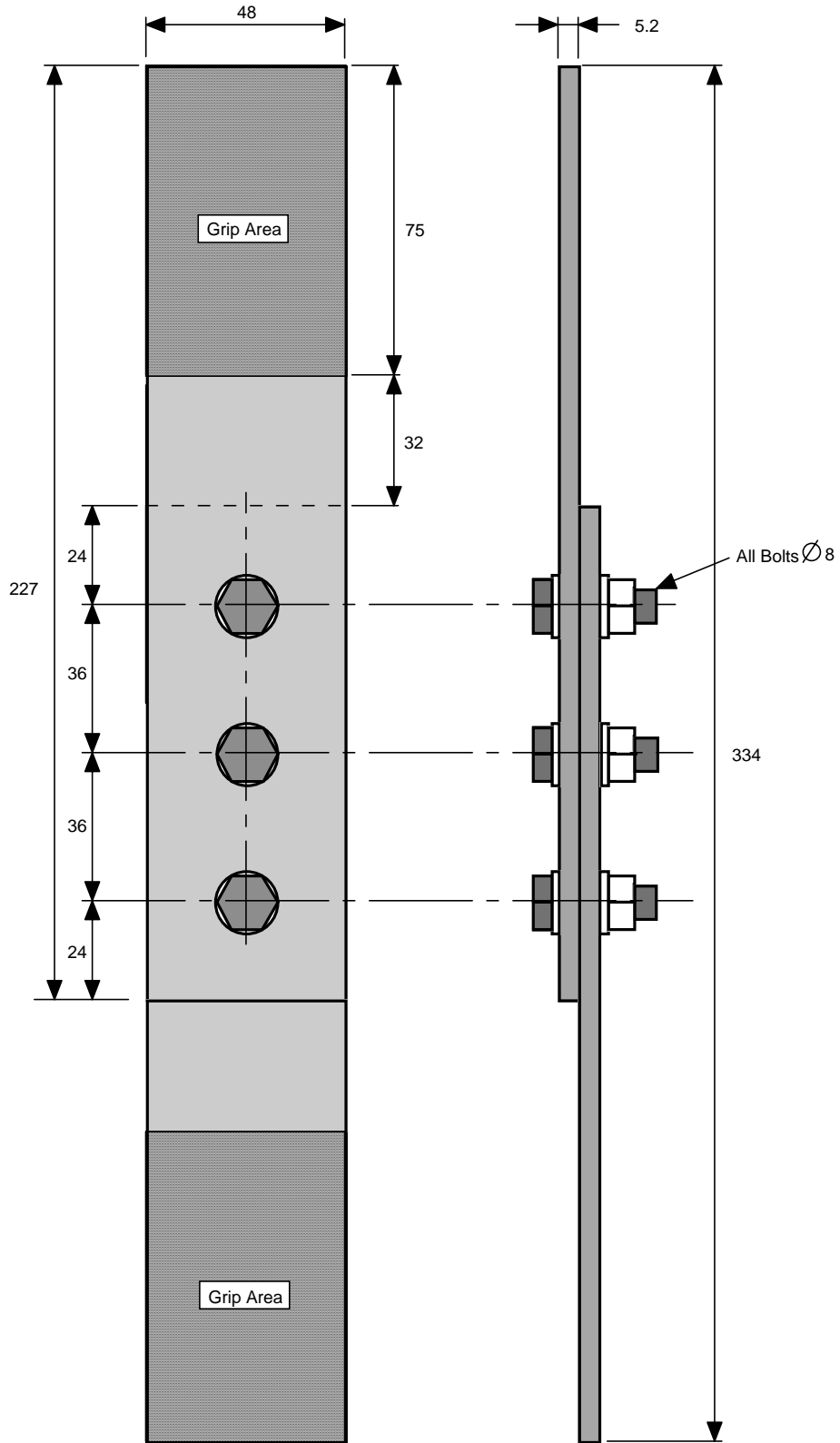
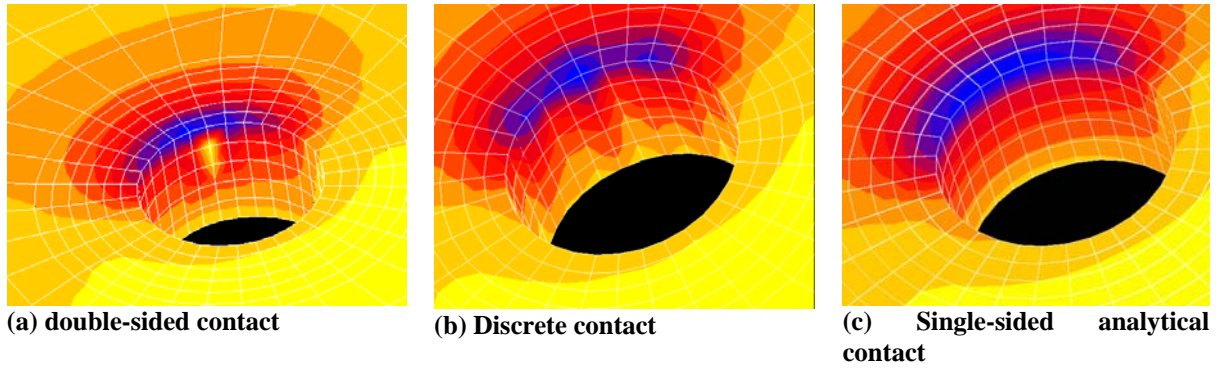
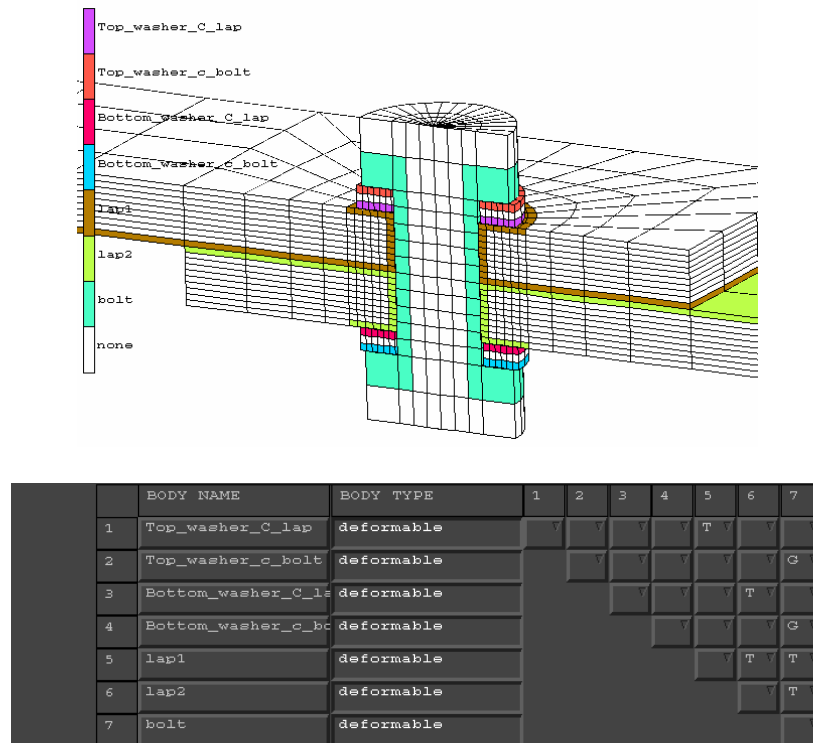


Figure 4.4.2 Single-lap multi-bolt geometry (all dimensions in mm)



**Figure 4.4.3 Anomalous stress distributions in (a) and (b), with correct distribution using optimum contact parameters in (c)**

As well as seeking accurate contact definition, efficiency was also important if multi-bolt joints were to be modelled later. Fig. 4.4.4 illustrates the use of contact bodies (subsets of the actual bodies containing only those parts likely to come in contact) and contact tables (which identifies which contact bodies have any likelihood of contacting each other). These features help to dramatically reduce run-time and were incorporated into the method implemented in BOLJAT for automatically setting up contact.



**Figure 4.4.4 Use of contact bodies and contact tables (later implemented into BOLJAT)**

ULIM next performed a 3D FE study of the effects of clearance in single-bolt joints. Fig. 4.4.5 shows the effect on the load-deflection curve of the joint. Note that, as in the experiments, the bolts were initially placed in the centre of the hole. The first effect then is a delay in load take-up in the larger clearance joint, as the bolt does not initially contact the hole. In real joints, bolts would not be centred in holes, but during operation under cyclic loading, such “dead-zones” would exist where the bolt was not taking any load, and during these periods, the other bolts would be taking all the load (in a multi-bolt joint), so the effect does have practical significance. The second effect is an increase in non-linearity in the load-deflection curve. Above about 1.5 kN load, the C1 curve is essentially linear, while in the C4 joint, the stiffness continues to increase with increasing load. The third effect is that the stiffness of the C4 joint is less than that of the C1 joint. Even at higher loads this is the case.

The reasons for these latter two effects are shown in Fig. 4.4.6. In the C1 joint the contact area between the bolt and the hole gets up to its final value quite quickly, and is then relatively constant (hence so is the stiffness of the joint) with increasing load. In the C4 joint, the contact area increases more gradually and continues to increase with increasing load (hence so does the joint stiffness). The final contact area is larger in the C1 joint than the C4 joint, so the C1 joint is stiffer. The findings are corroborated by experiments that showed a clear imprint of the bolt on the hole.

Fig. 4.4.7 illustrates the effects of clearance on the stresses in the laminate (when homogenised properties are used). It can be seen that, in the larger clearance case, the radial stress is concentrated over a smaller area, and is more peaked; the peak tensile tangential stress shifts towards the bearing plane and compressive tangential stresses form at the bearing plane. These findings are consistent with those of previous researchers who used 2D analysis.

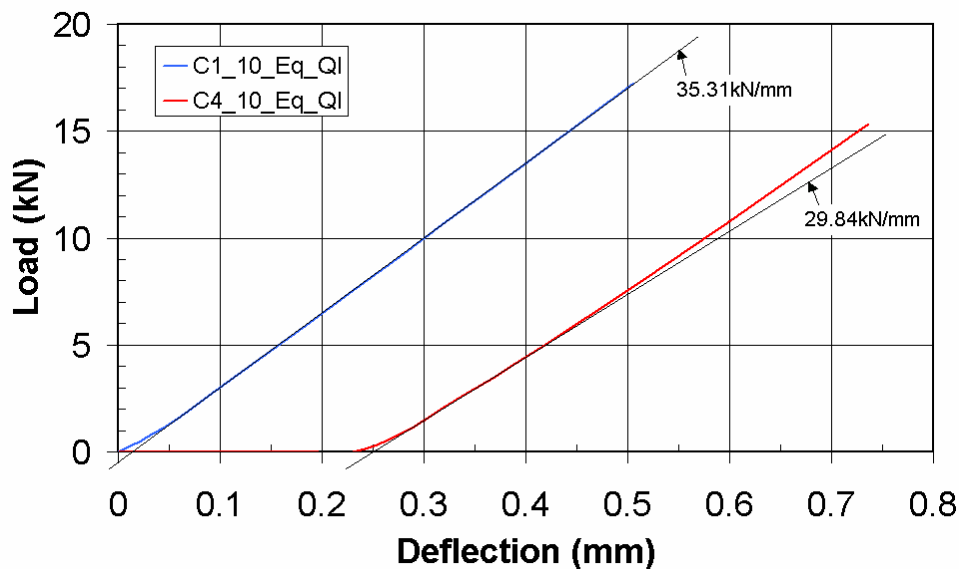


**Figure 4.4.5 Effect of clearance on load-deflection curve – C1 versus C4 clearance**

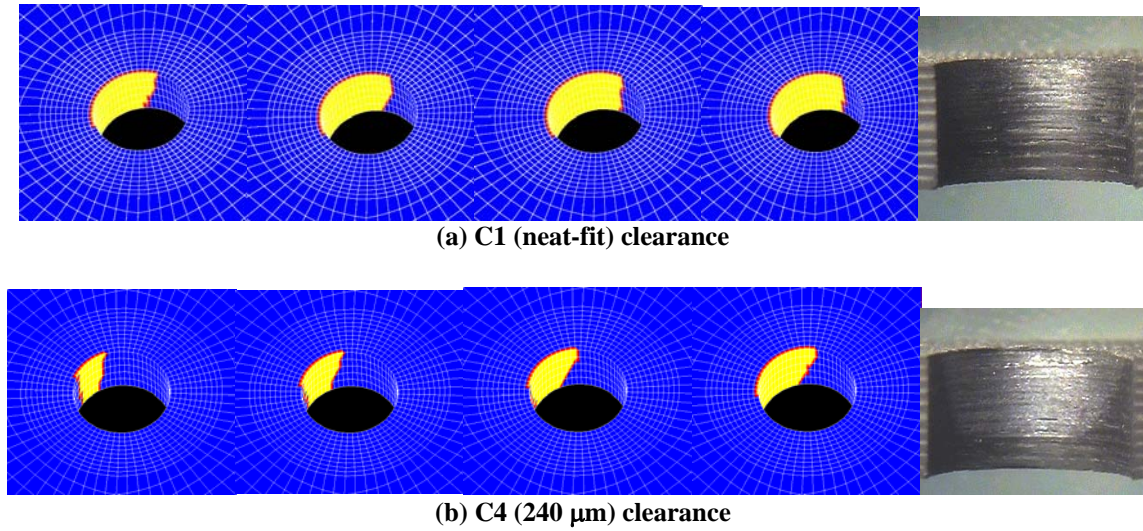


Figure 4.4.6 Growth of contact area with increasing load, with comparison with final contact area obtained from imprint of bolt on hole in tests

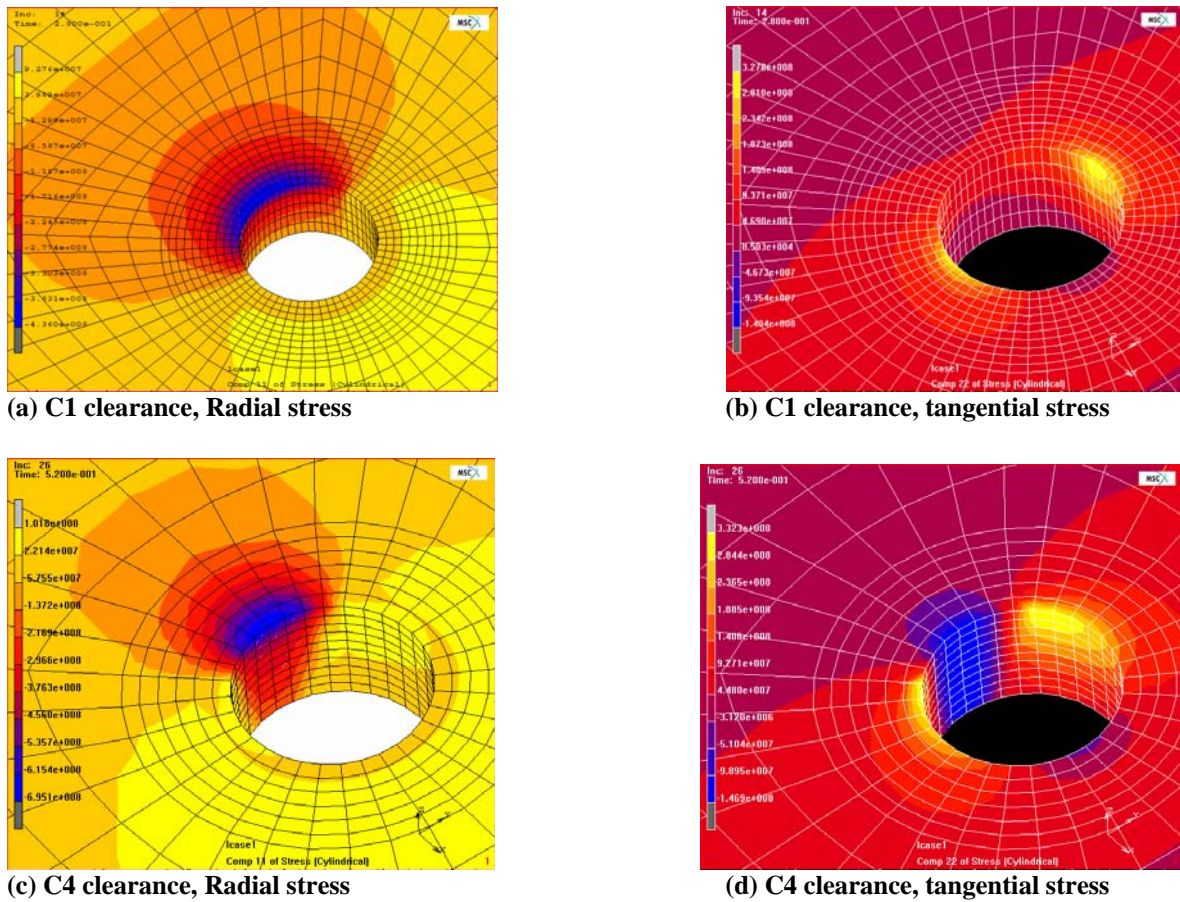


Figure 4.4.7 Effect of clearance on hole stresses



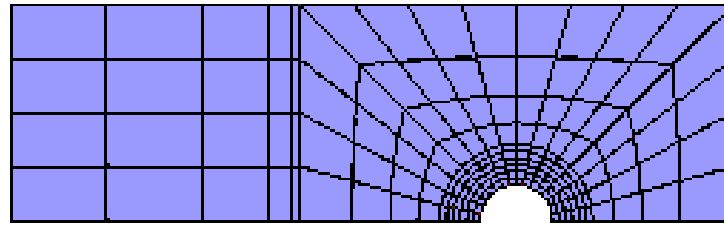
As mentioned above, the single-bolt joint in Fig. 4.4.1 (with a C1 or neat-fit clearance) was selected as a *Single-Bolt Benchmark* for comparison of different modelling methods by several partners. At the 12-month meeting, four partners presented models of this joint. The four partners were ULIM (using MSC.Marc), KTH (using ABAQUS), FOI (using STRIPE) and CIRA (using ANSYS). For a comparison of joint stiffness, the load at 0.5 mm joint deflection was given by each partner and the results were in quite close agreement, ranging from 16 – 17.5 kN. However, the value from ULIM's experiments was 10 kN. Clearly this represented a big discrepancy, and ULIM undertook a detailed experimental and numerical study to try to determine the reasons for this.

The experimental work is covered in WP 5, but the significant finding was that using machine stroke as a measure of joint displacement gives very poor results. Using LVDTs, and extensometers it was found that a large correction needs to be made to the machine stroke to obtain the true joint stiffness (to allow for compliances in the system other than that of the joint). Having said that, even after this correction there was still a considerable discrepancy between the numerical and experimental stiffnesses. Thus ULIM undertook an extensive numerical parameter study to investigate this. So that the focus was not purely on stiffness, ULIM also modelled several strain-gauged joints, and compared the effects of the parameters on the joint strains as well as the joint stiffness. Of considerable value in this study was a very detailed model created by FOI with 1 million degrees of freedom, which gave a virtually exact reference solution for the mathematical problem (see Task 4.3).

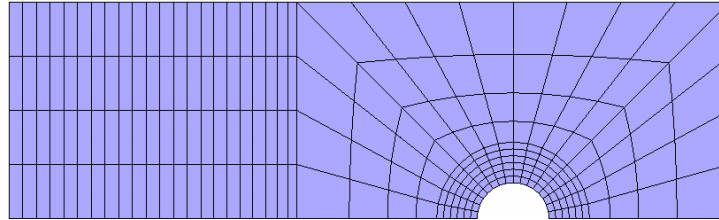
Some of the parameters investigated were:

- Use of different material properties in tension and compression. Available material data suggests that the compressive stiffness of the composite material used is less in compression than in tension. A user subroutine was written to allow this to be modelled.
- Mesh refinements (see Fig. 4.4.8)
- Use of 2<sup>nd</sup> order elements
- Use of assumed strain formulation in 1<sup>st</sup> order elements. This allows 1<sup>st</sup> order elements to approximate bending behaviour better, without the expense of going to 2<sup>nd</sup> order elements (similar to incompatible modes formulations in ABAQUS).
- Calibration of pre-stress from instrumented bolts
- Modelling the clamped portion of the joint, i.e. not assuming perfect clamping (see Fig. 4.4.9).

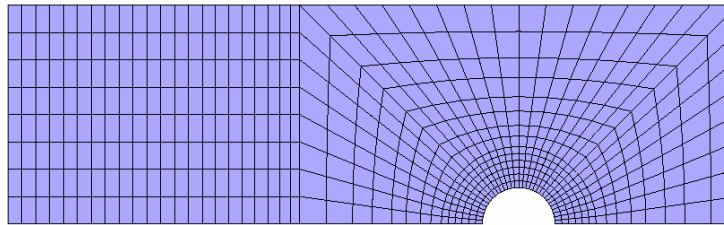
Mesh Refinement 1 (non-overlap region only) was found to considerably improve the agreement with the experimental strains in this region, with a negligible increase in run time. Mesh Refinement 2 improved the strains throughout the joint, but at the expense of a 6-fold increase in run-time (due to the large increase in elements in contact). Second-order elements gave similar results as Mesh Refinement 2, but at an even larger computational expense. Mesh Refinement 1 with the assumed strain formulation gave almost identical results as Mesh Refinement 2, but with negligible increase in run-time – hence this was found to be the best solution.



(a) Standard mesh



(b) Refinement 1: Refined non-overlap region



(c) Refinement 2: Refined overlap and non-overlap regions

**Figure 4.4.8 Mesh refinements in ULIM parameter study**

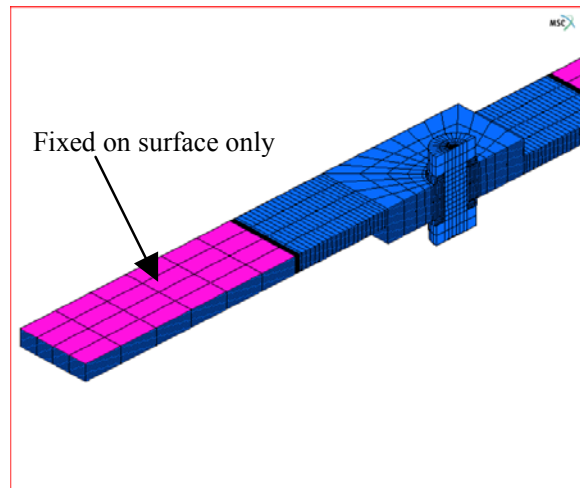


**Figure 4.4.9 Modelling the clamped portion of the joint**



Overall it was found that with an improved model incorporating the following parameters:

- Separate tensile/compressive properties
- Mesh refinement in non-overlap region
- Assumed Strain Formulation
- Correct Bolt Pre-Stress
- Modelling Clamped Area

the difference in stiffness between the experiments (using extensometers) and simulations reduced from 24% to just 12%. In addition the improvements in strain values outlined in Table 4.4.2 occurred, further confirming that the “Improved” model was a much closer match to the real joint.

Gauge Number	Experiment (microstrain)	Standard Model (microstrain)	Improved Model (microstrain)
1	-1.8	231	149
2	760	548	633
3	-349	-209	-244
4	-488	-374	-438
5	-400	-302	-346
6	-218	-191	-182
7	-367	-430	-414
8	-353	-302	-346

**Table 4.4.2 Strains in “Improved Model” at an applied load of 5 kN**

As noted above, clearance causes a loss in joint stiffness. Table 4.4.3 quantifies this effect, as predicted by the models and as measured by experiment. The results indicated that the models are capable of accurately predicting this stiffness loss. Joints with countersunk bolts were also tested and modelled. Fig. 4.4.10 shows countersunk models, showing the difference in bolt rotation, when the clearance changes. Table 4.4.4 shows the predicted stiffness loss due to clearance for a countersunk joint versus the measured value – again the agreement is excellent.

Turning to the multi-bolt joint in Fig. 4.4.2, the load distribution for six different clearance cases (see Table 4.4.5) was determined experimentally using instrumented bolts (see WP 5). Three-dimensional FE models of each case were created and the obtained load distribution was compared with experiment. Fig. 4.4.11 shows two cases, and the agreement is seen to be excellent (as the for the single-bolt joints, the models were slightly stiffer than the experiments). The agreement was in fact excellent in all six cases. The results showed the quite dramatic effect that clearance can have on the load distribution in multi-bolt joints. Generally in such a joint, it would be assumed that the load is distributed as in the C1\_C1\_C1 case, but clearly, with variable clearances, the actual distribution can be quite different.

Protruding Head, Quasi-Isotropic, 0.5Nm Torque				
	C1	C2	C3	C4
Percentage change from C1 (Models)	-	-4.2%	-8.5%	-11.7%
Percentage change from C1 (Experiments)	-	-1.9%	-7.3%	-10.4%

**Table 4.4.3 Reduction in joint stiffness as a function of bolt-hole clearance – simulations versus experiments (protruding head bolts)**

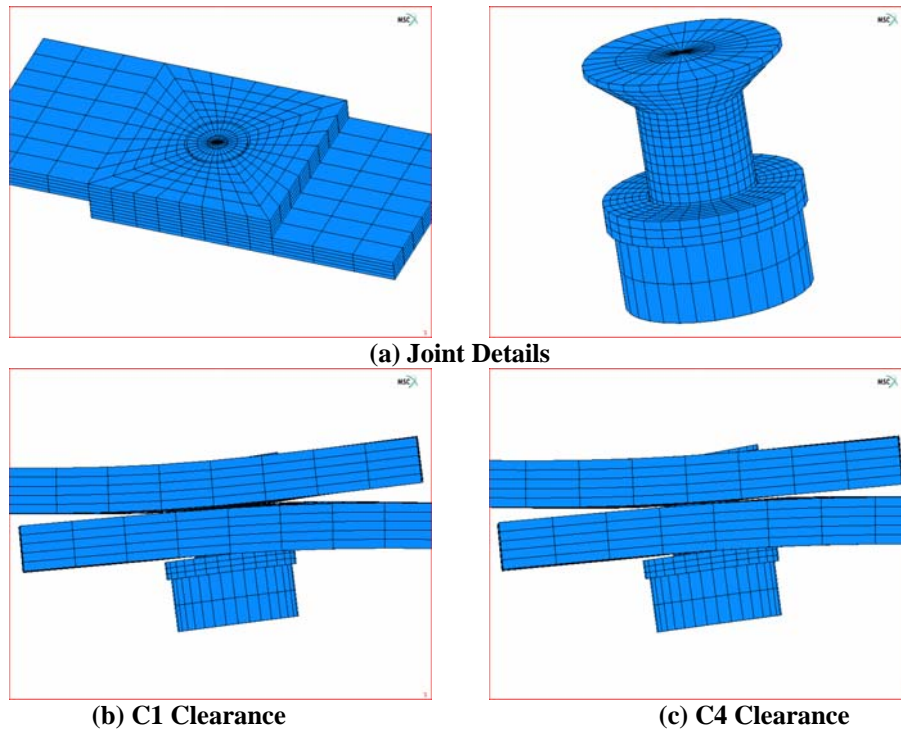


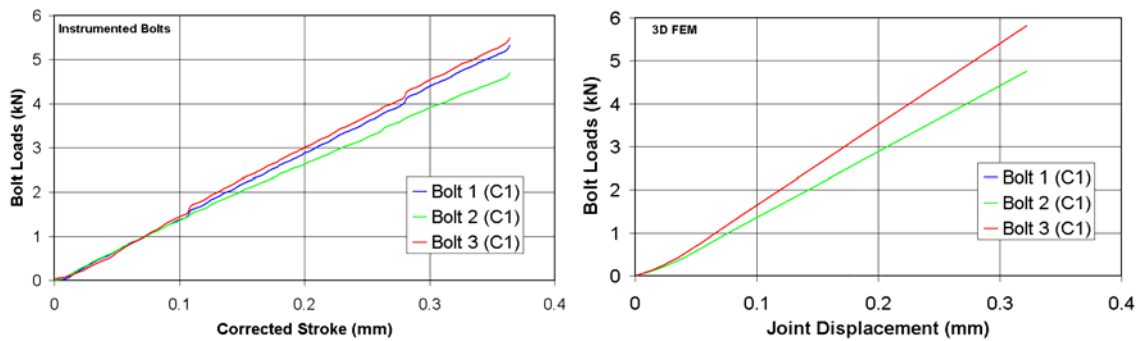
**Figure 4.4.10 Rotation of the countersunk bolt within the hole for two different clearances (shown at 5X Magnification)**

Countersunk Head, Quasi-Isotropic, 0.5Nm Torque		
	C1	C4
Percentage change from C1 (Models)	-	-11.7%
Percentage change from C1 (Experiments)	-	-10.8%

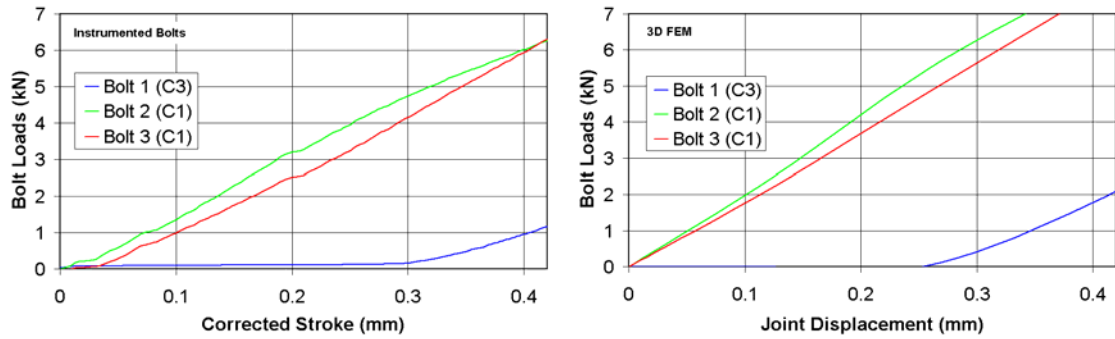
**Table 4.4.4 Reduction in joint stiffness as a function of bolt-hole clearance – simulations versus experiments (countersunk head bolts)**

Code	Nominal Clearance Hole 1 (µm)	Nominal Clearance Hole 2 (µm)	Nominal Clearance Hole 3 (µm)
C1 C1 C1	0	0	0
C2 C1 C1	80	0	0
C3 C1 C1	160	0	0
C4 C1 C1	240	0	0
C1 C3 C1	0	160	0
C3_C3_C1	160	160	0

**Table 4.4.5 Clearance cases for multi-bolt joints**



**(a) C1\_C1\_C1 case**



**(b) C3\_C1\_C1 case**

**Figure 4.4.11 Effects of clearance on load distribution in multi-bolt joints – Instrumented bolts and 3D FE**

To investigate if clearance effects could be included in simpler models, AUK’s 1-D spring model (Fig. 4.2.1) was implemented in MATLAB by ULIM. Some modifications were made which allowed consideration of variable clearances in multi-bolt joints. Adding clearance makes the problem non-linear, so an incremental solution with increasing load was needed. Fig. 4.4.12 shows a comparison between the load distribution obtained by 3-D FE and the extended 1-D spring model. The agreement both in load distribution and joint stiffness was very good.

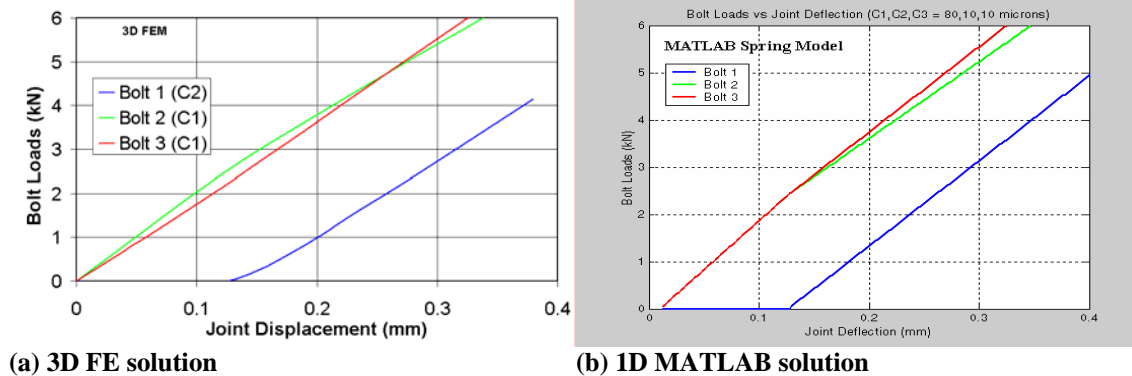


**Figure 4.4.12 3D FE solution versus 1D MATLAB solution to load distribution in C2\_C1\_C1 case**

Finally in Task 4.1, BOLJAT (Bolted Joint Analysis Tool) was developed for semi-automated creation of 3D FE models of bolted joints. The tool was developed from scratch as ULIM had no such tool at the start of BOJCAS. A recurring problem in the development of any modelling software is the wide range of finite element solvers in use. Since commercial providers of finite element pre-processing software already provide solutions to this problem, it was decided to develop the tool in the programming language of one of these pre-processors, rather than using a general-purpose language such as C++ or FORTRAN. The pre-processor chosen was MSC.Patran, and BOLJAT has been developed using the Patran Command Language (PCL). MSC.Patran was chosen because it is in wide use in the aircraft industry, and appears likely to remain so for the foreseeable future. It also interfaces with most finite element solvers in use in the industry.

In general, the basic steps for performing a bolted joint analysis including contact are as follows:

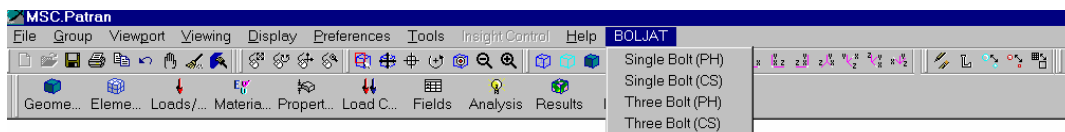
- Create the model geometry of the parts to be joined.
- Create the model geometry of the bolt(s), nut(s) and washer(s).
- Mesh all parts in a way that provides refinement only where it is needed.
- Determine contacting surfaces, in a way that results in the most efficient analysis possible (contact is the chief factor in overall execution time). Depending on the solver, these surfaces may need to be separated into e.g. “master and slave”, or “contacting and contacted surfaces”.
- Define several parameters that determine contact behaviour.
- Apply necessary boundary conditions.
- Define element material properties.
- Define solution options and load steps.
- Submit the problem to a finite element solver.
- Post-process the results.

Modern software works through graphical user interfaces (GUIs), so BOLJAT provides GUIs for most of the above steps. All inputs are parameterised, so joints with different geometry and materials can be modelled easily. The crucial contact steps are almost fully automated, which shields the user from the complications of this process. The steps for geometry and mesh creation in BOLJAT provide a mesh that can be used in any finite element solver. However, there are many different methods for modelling contact and each solver tends to use its own method. Thus, to date, the contact steps in BOLJAT have been aimed at one solver only (MSC.Marc); in the future it is planned to extend this to other solvers.

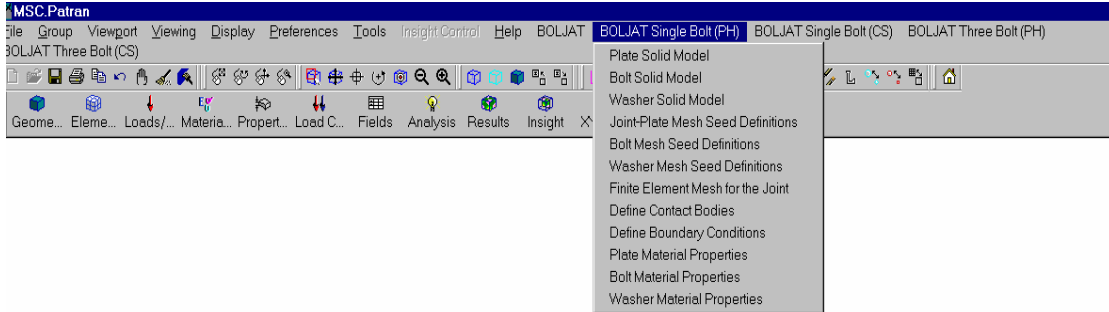
BOLJAT is described in detail in a User’s manual (D4.1-6). In fact, this user’s manual has been superseded by an updated version (version 2 delivered as an extra deliverable, coded D4.1-7, at the end of Task 4.4). A paper has also recently been published on BOLJAT in the journal *Composites Part A* [5], so only a few illustrative figures are given here.

Fig. 4.4.13 shows the BOLJAT main menu after installation in MSC.Patran. At the end of Task 4.1, there were four modules, covering *single-lap* joints with one protruding-head or countersunk fastener, or three protruding-head or countersunk fasteners. Selecting “Single-Bolt (PH)” brings up the menu in Fig. 4.4.14. GUIs for creation of solid models for joint plates, bolts and washers are available from this menu (e.g. see Fig. 4.4.15). All values are definable by the user, and solid models are then automatically created (e.g. see Fig. 4.4.16). The mesh of each part is also under user control (Fig. 4.4.17). Definition of all contact bodies and contact tables (like those shown in Fig. 4.4.4 above) is fully automated (see Fig. 4.4.18). Finally GUIs exist for defining boundary conditions and material properties (orthotropic for the plates, isotropic for the bolts and washers).

At the end of Task 4.1, BOLJAT was delivered to all partners. At that stage there were a number of manual steps needed (twelve in all) after exiting MSC.Patran before the job could be submitted to MSC.Marc. These mostly involved cutting and pasting some lines from standard input files supplied with the code and were not very time-consuming. Nevertheless, in Task 4.4, reducing the number of these steps was targeted. A number of other improvements were also made, which are described in Task 4.4.



**Figure 4.4.13 Patran main menu with BOLJAT**



**Figure 4.4.14 Patran main menu, with the BOLJAT module, “Single Bolt (PH)”, activated**

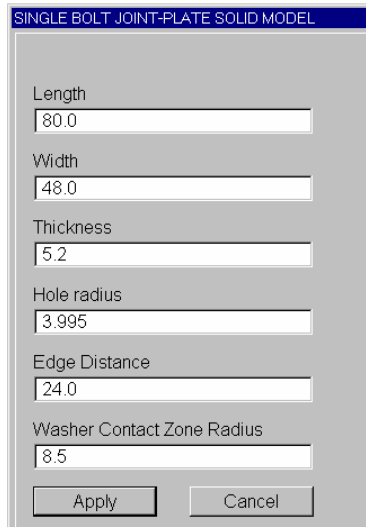


**Figure 4.4.15 GUI for creation of solid model for joint plate (single bolt, protruding head)**

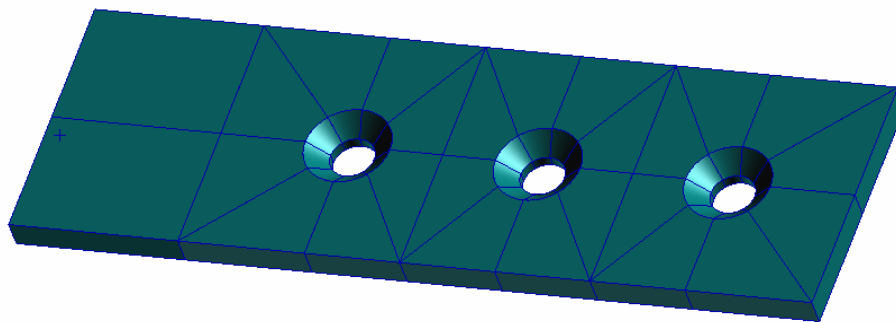


**Figure 4.4.16 Solid model of the upper plate (three bolt, countersunk)**

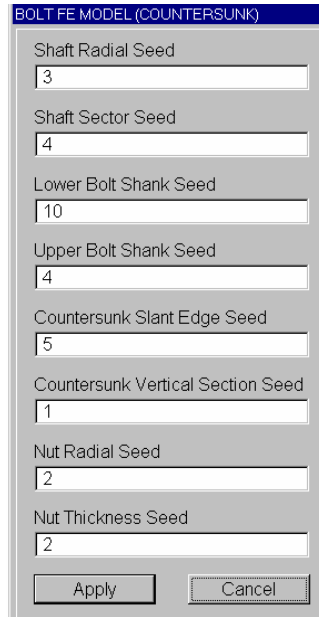


**Figure 4.4.17 GUI for creation of mesh seeds for the countersunk bolt (single bolt, countersunk)**

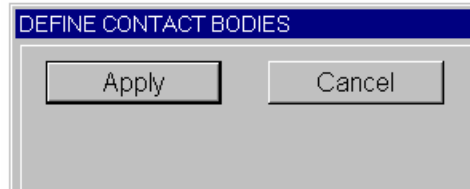


**Figure 4.4.18 GUI for creating the contact bodies (all configurations)**

#### **Task 4.1 Royal Institute of Technology, Stockholm (KTH)**

KTH's work in BOJCAS focused on composite-to-metal, multi-bolt, single-lap joints representing complex structural elements that are affected by numerous parameters. The baseline geometry is illustrated in Figure 4.4.19.

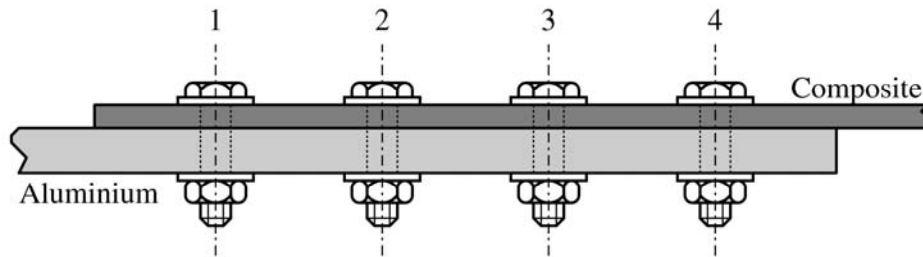


**Figure 4.4.19 KTH Composite-to-metal, multi bolt single-lap joint**

The overall objectives were to generate basic research information on the mechanisms and parameters that are important for the behaviour of this class of joints.

In Task 4.1, KTH developed a parameterised 3-D FE model of the structure in Fig. 4.4.19 and compared its results to experimental results from WP 5. KTH also developed a pre-processor for generating 3-D bolted joint models in ABAQUS. The pre-processor is described here first.

Conducting detailed 3D finite element analyses of bolted joints is a time-consuming process. A number of commercial pre-processors that can export ABAQUS input files are available. These are in general very powerful in terms of modelling capabilities but they rely heavily on user interactivity via a graphical user interface. This is in some cases not efficient when systematic changes of various parameters are required.

The aim was to develop software that reduces the time required to develop finite element models of bolted composite joints and that facilitates parametric studies of these joints. The program should handle 2-4 member plates bolted together by 1-4 countersunk or protruding head bolts. All geometrical dimensions of the plates and bolts were to be parameterised. The user should be able to control mesh density, element type, material properties, loads and boundary conditions. Contact surfaces should be automatically traced out and contact conditions specified for all contact pairs.

The program meeting these requirements was developed in Fortran 77 and is very fast and robust. It can be compiled and installed on any computer platform provided that there is a Fortran 77 compiler available. The program reads a text file that must be prepared by the user, in which a number of parameters are defined. A complete ABAQUS input file is then generated in a few seconds. An example is illustrated in Fig. 4.4.20. The geometry produced is of the fastener region (1-4 fasteners), containing all contact parameters, material properties etc. This can then be dropped into a mesh of the plates, where a cut-out has been left for the fastener region. This makes it quite flexible.

Changing the number of plates or bolts, the type of bolt, mesh density, element type, material properties, loads and boundary conditions is done by changing the parameters in the text file and re-running the program. The capabilities, usage and limitations of the program are given in D4.1.5.

The program can be used in conjunction with any commercial pre-processor that can import ABAQUS input files and has recently been used in its current state of development by SAAB on real aircraft structures outside the BOJCAS project. It forms a powerful and flexible basis for further development.



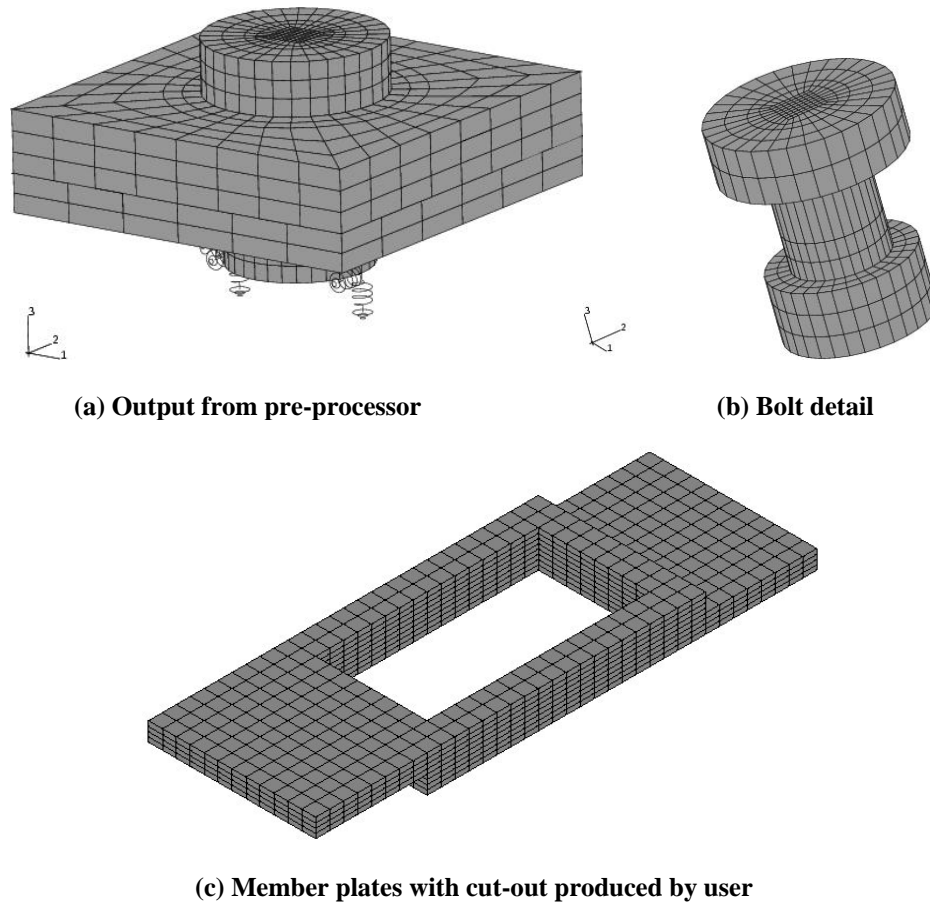


**Figure 4.4.20 Two member plates joined by a protruding head bolt. The pre-processor creates the mesh, contact etc. for the fastener region. This can then be merged with a model of the plates with a cut-out left for the fastener region. The bolt is attached to ground with weak springs to avoid rigid body modes**

The objective for the modelling in Task 4.1 was to develop an FE model that took into account all important physical mechanisms that were present in the real structure, and that was parameterised as generally as possible. As it turned out (see below), to model the experiments accurately, it was necessary to allow hole sizes and hole locations to be different within a member plate and also different for different plates. The ability to change dimensions for bolts and washers on an individual basis was also needed. This was in order to enable studies of bolt-hole clearances and hole eccentricity between the plates.

This ruled out the possibility to use the developed pre-processor, since it did not have some of the above capabilities and it automatically models the bolt, nut and the washers as one unit which was deemed to be too much of a simplification in some situations. Therefore, the commercial pre-processor ABAQUS CAE was used to generate the model.

Detailed validation of the model through comparisons with experimental results from WP5 was to be done in terms of load transfer, secondary bending and longitudinal stiffness. The validation was performed for a reference joint configuration only.

The developed model utilises non-linear kinematics, and general contact conditions, including friction, are specified for all relevant contact surfaces. The composite laminate was assumed homogenous and was given elastic properties in accordance with classical laminate theory. With homogeneous material properties, the structure was symmetric with respect to the longitudinal centre line, so only half the geometry had to be modelled, as illustrated in Fig. 4.4.21.

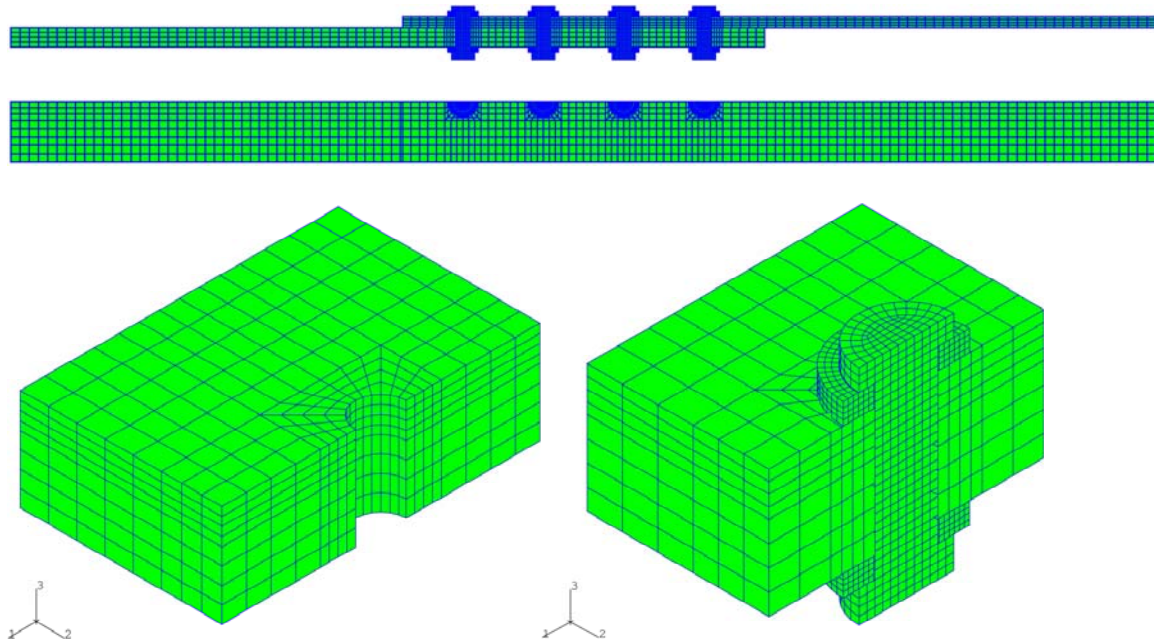


**Figure 4.4.21 Typical finite element mesh**

Loads and boundary conditions were applied according to the tensile tests in WP5. Load is transferred from one plate to the other by the bolts and by friction between the plates. Forces transferred by the bolts were measured with instrumented fasteners in WP 5, which enabled a direct comparison between FE results and experimental results. Individual bolt loads from the FE model and from the experiments during one load cycle are shown in Fig. 4.4.22.

The large discrepancy between FE results and experimental results was unexpected. The experimental technique used to measure the bolt loads had been validated by measuring the bolt loads simultaneously with strain gauges and had been found to be accurate. It was concluded that the discrepancy was due to incompleteness of the FE model and further refinement of the model was conducted. This resulted in no significant improvements, leading to the conclusion that the FE model generated accurate results.

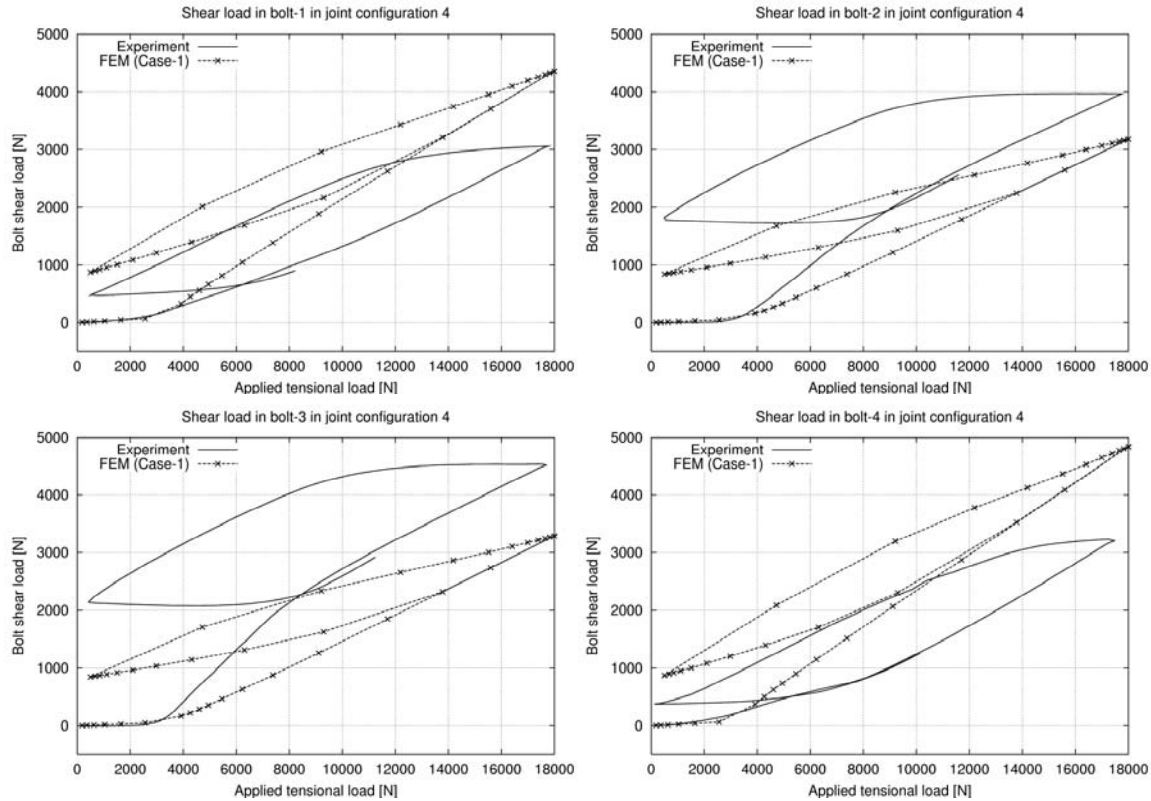


**Figure 4.4.22 Bolt loads from FE-model and experiments during one load cycle**

Focus was then placed on the geometries of the holes on a very local level. Detailed measurements on a small number of specimens with a coordinate measurement machine revealed that the holes in the composite and aluminium plates were different in size and also not perfectly concentric. The holes in the aluminium plate were slightly larger than the holes in the composite plate, and the holes were located in such a way that some of the load could be expected to be shifted towards the inner bolts. These deviations from nominal geometry were small, approximately  $20\mu\text{m}$ , but proved to be very important for the load distribution between the bolts.

Based on the knowledge of these geometrical deviations, two new FE-models were generated; one with bolt holes located to shift some load to the inner bolts (Case 2) and one where the load was shifted to the outer bolts (Case 3). Case 1 refers to the nominal geometry, i.e. concentric holes. Fig. 4.4.23 and Table 4.4.6 explain how Cases 2 and 3 were obtained. In Case 2, the holes in the aluminium plate were shifted, resulting in decreased  $ac_2$  for the inner holes, so that the inner bolts picked up load sooner, and increased  $ac_1$  for the outer holes, to delay the load pick-up for the outer bolts. The opposite was done for Case 3.

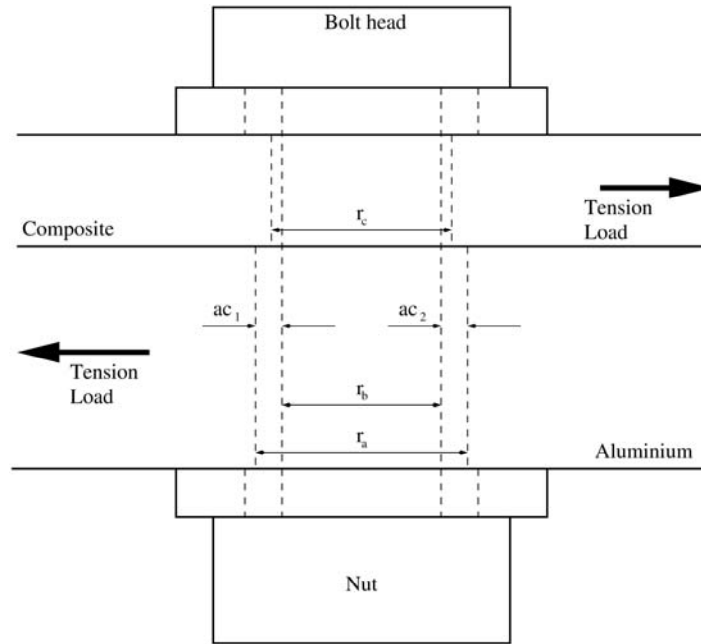


**Figure 4.4.23 Joint clearances**

	Case-1		Case-2		Case-3	
<i>Bolt</i>	$ac_1$	$ac_2$	$ac_1$	$ac_2$	$ac_1$	$ac_2$
1	$r_a - r_b$	$r_a - r_b$	$0.1(r_a - r_b)$	$0.9(r_a - r_b)$	$0.9(r_a - r_b)$	$0.1(r_a - r_b)$
2	$r_a - r_b$	$r_a - r_b$	$0.9(r_a - r_b)$	$0.1(r_a - r_b)$	$0.1(r_a - r_b)$	$0.9(r_a - r_b)$
3	$r_a - r_b$	$r_a - r_b$	$0.9(r_a - r_b)$	$0.1(r_a - r_b)$	$0.1(r_a - r_b)$	$0.9(r_a - r_b)$
4	$r_a - r_b$	$r_a - r_b$	$0.1(r_a - r_b)$	$0.9(r_a - r_b)$	$0.9(r_a - r_b)$	$0.1(r_a - r_b)$

**Table 4.4.6 Shift in clearances for Cases 1, 2, and 3**

Results from the three models and from experiments during tensional load-up are depicted in Fig. 4.4.24. It can be seen that Case 2 agrees well with the experiments, whereas Cases 1 and 3 show poor agreement. Thus, small deviations with respect to hole locations may significantly affect the distribution of load between the fasteners.

However, if the loads from all four bolts are added the three cases are very similar and agree well with the experiments. Hence the total amount of load transferred by the bolts and by friction between the plates is not affected by these small geometrical imperfections.

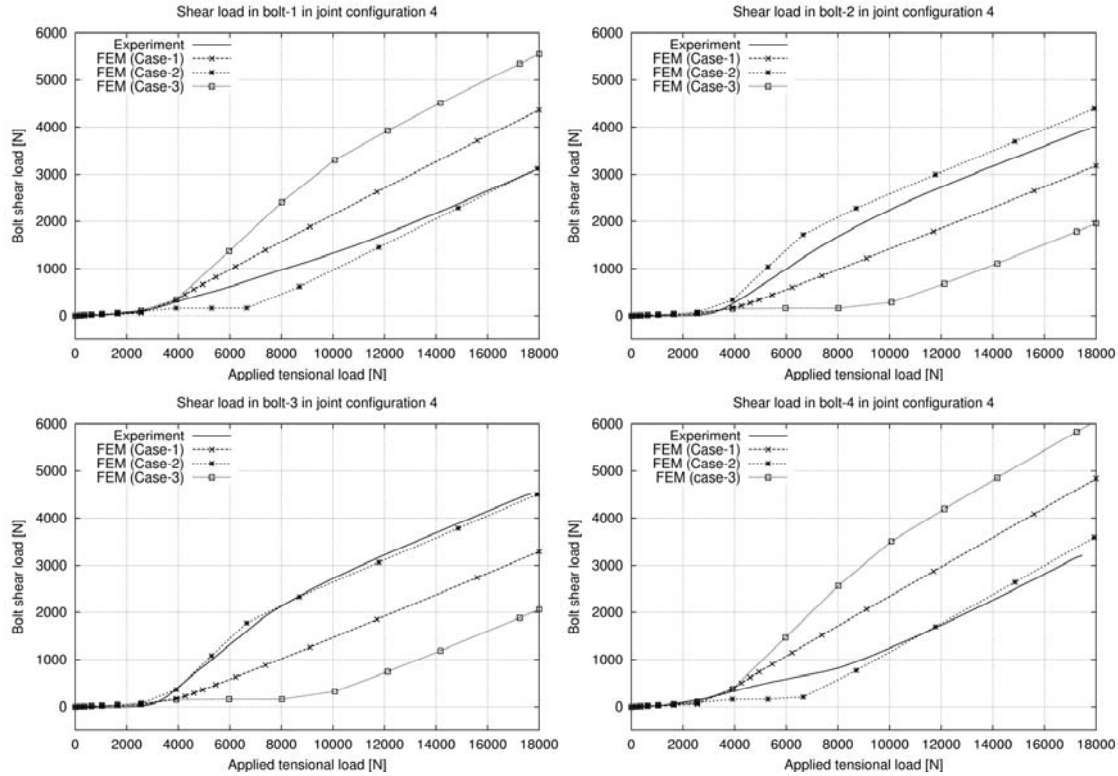


**Figure 4.4.24 Bolt loads from FE results and experiments. Cases 1-3 correspond to concentric holes, eccentric holes where load is shifted to the inner bolts, and eccentric holes where load is shifted to the outer bolts respectively**

Secondary bending (SB) is an important parameter that is related to the out-of-plane deflection of single-lap joints. The general definition is:

$$SB = \frac{\varepsilon_{bot} - \varepsilon_{top}}{\varepsilon_{bot} + \varepsilon_{top}} \quad \dots(4.4.1)$$

where  $\varepsilon_{bot}$  and  $\varepsilon_{top}$  are strains on bottom and top surfaces of the composites respectively. In effect, SB can be written as:

$$SB = \frac{\varepsilon_{bend}}{\varepsilon_{mem}} \quad \dots(4.4.2)$$

where  $\varepsilon_{bend}$  and  $\varepsilon_{mem}$  are strains pertaining to pure bending and pure tension (membrane strains) respectively.

Strains are generally measured with strain gauges at specific points, i.e. the AGARD points, on both sides of the plate, but the optical whole field measurement method used in

WP 5 enabled an alternative approach. The second derivative of the measured out-of-plane deformations corresponds to the curvature of the plate, which approximately corresponds to the bending strains on the surface according to:

$$\varepsilon_{bend} = -\frac{t}{2} \frac{\partial^2 z}{\partial x^2} \quad \dots(4.4.3)$$

where  $t$  is the thickness of the plate,  $z$  is the out-of-plane direction and  $x$  is the longitudinal direction of the plate.

Thus, an alternative definition of SB could be defined as

$$SB = \varepsilon_{bend} = -\frac{t}{2} \frac{\partial^2 z}{\partial x^2} \quad \dots(4.4.4).$$

The comparison between FE model and experiments using this definition of the secondary bending is shown in Fig. 4.4.25.

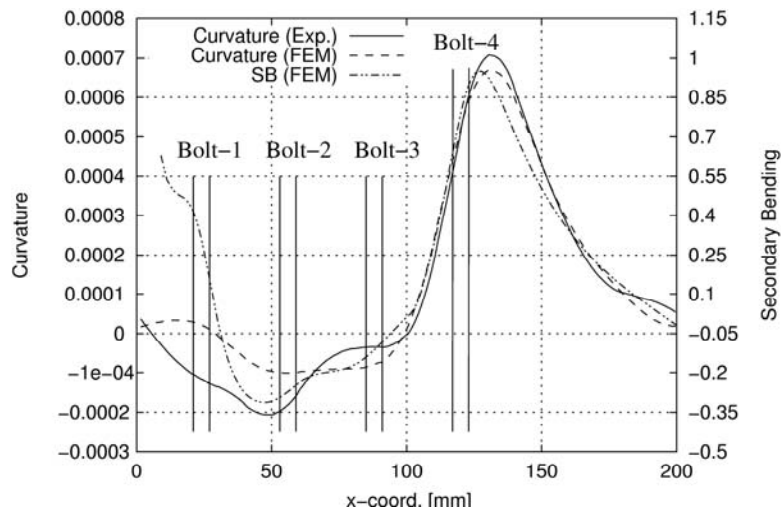


**Figure 4.4.25 Secondary bending based on curvature from FE model and experiments, and based on strains from FE model. The secondary bending is plotted along the length of the composite plate close to the edge**

Good agreement is evident especially at the critical region close to Bolt 4 (see Fig. 4.4.19 for bolt numbers) where the bending of the composite plate is severe. Also, SB based on equation (4.4.1) is included for the FE-model. It can be seen that the magnitude of the SB is different (use the right y-axis) but the information revealed about the joint is similar, i.e. that the SB is small everywhere except in the vicinity of bolt 4. The increase of SB close to Bolt 1 is due to the fact that the by-pass load, and therefore  $\varepsilon_{mem}$ , is approaching zero.

The FE model used in Fig. 4.4.25 had concentric holes, i.e. it corresponds to Case 1 above. The out-of-plane deformations for Cases 1-3 are plotted in Fig. 4.4.26. It can be seen that small amounts of hole eccentricity have only a minor effect on the out-of-plane deflection.

Regarding longitudinal stiffness, the experimental load displacement curve was measured based on measurements with an optical system, i.e. measurements directly on the specimen surface. This meant that the load displacement curve was not affected by compliances outside the specimen or slipping in the grips (thus avoiding the problems referred to by ULIM in WP 5). The longitudinal stiffness from the experiments and from the FE model is compared for Cases 1 and 2 in Figs. 4.4.27 and 4.4.28. The agreement between experiments and FEA is good in both cases for small loads, i.e. when load is transferred through friction. This implies that clamping force, coefficient of friction and overall stiffness of the FE model is comparable to the real structure. When the load exceeds 3 kN some small differences between the FE models as well as some deviation from the experiments are revealed.

In Case 1 (concentric holes and bolts) the FE-model suffers from a stiffness loss when the plates start to slide since there is no immediate contact between the bolts and the plates. At approximately 4 kN, contact is established simultaneously between all bolts and the plates and the joint becomes stiffer. After this point the FE-model is slightly stiffer than the experiments. In Case 2 (load shifted towards the inner bolts) the stiffness loss when the plates start to slide is smaller due to the almost immediate contact between the inner bolts and the plates.

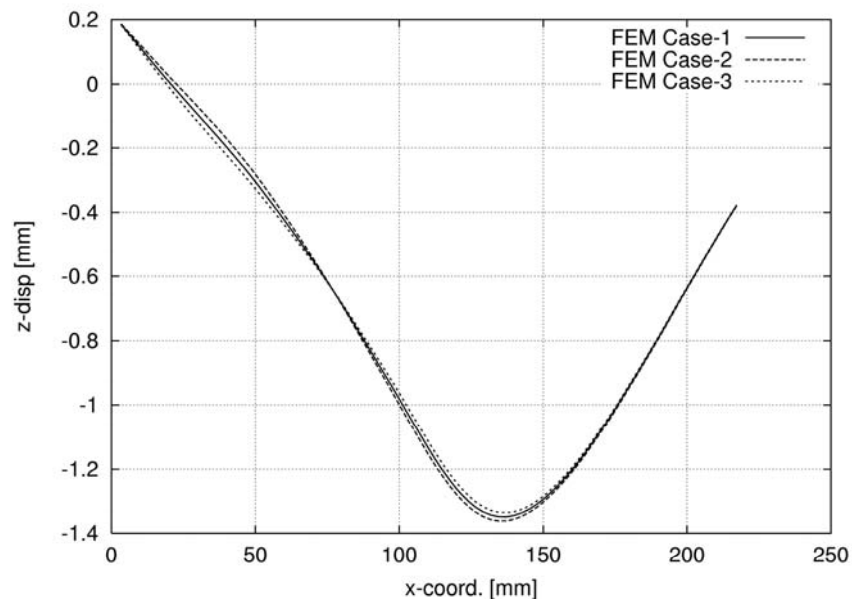


**Figure 4.4.26 Out-of-plane deformations for a joint with concentric holes (Case 1), a joint with eccentric holes and the load shifted to the inner holes (Case 2) and a joint with eccentric holes and the load shifted to the outer holes (Case 3)**

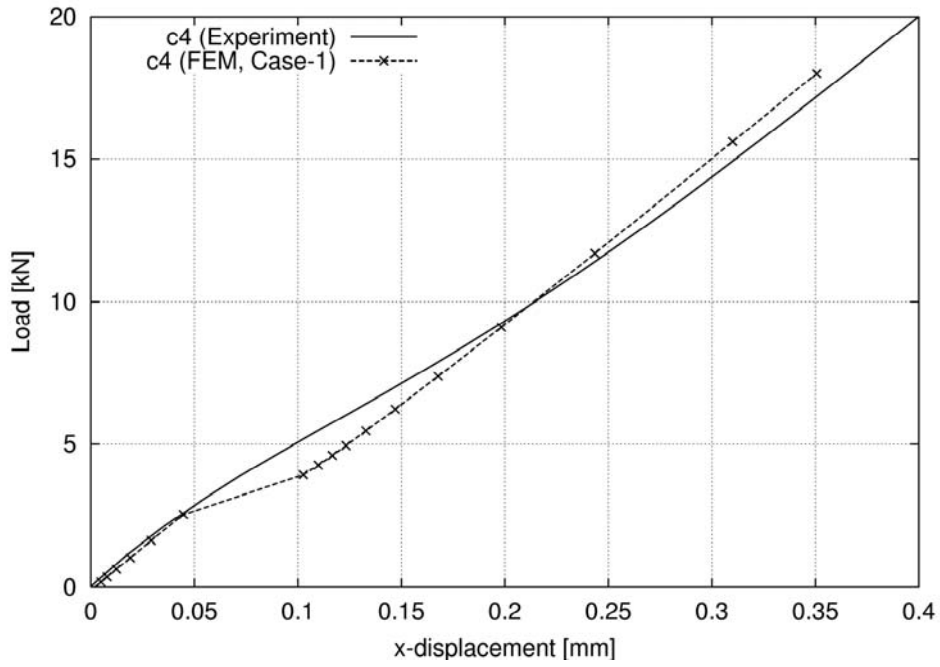


**Figure 4.4.27 Load displacement curves from experiments and FE model with concentric bolt holes (Case 1)**

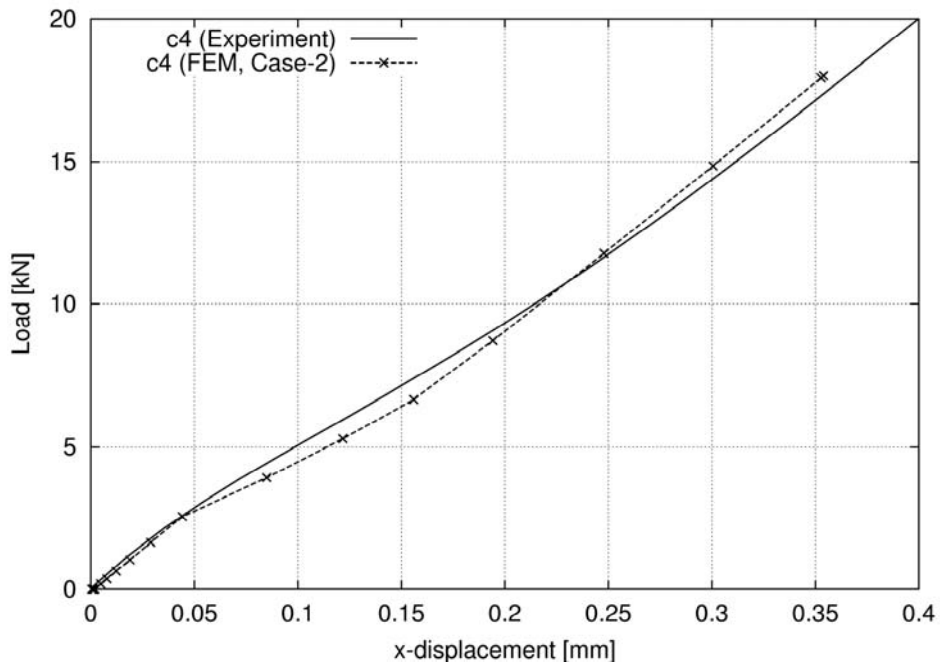


**Figure 4.4.28 Load displacement curves from experiments and FE model with eccentric holes in such a way that some load is shifted towards the inner bolts (Case 2)**



## 2.4.2 Task 4.2 Damage Modelling and Failure Criteria

The objectives of this task were to develop progressive damage modelling methodologies and a stress-based fatigue failure criterion. CIRA worked on progressive damage under quasi-static loading, with the support of SMR. ISTRAM developed a progressive damage methodology for fatigue loading. FOI developed a fatigue failure criterion for joints that fail by bolt failure.

### Task 4.2 CIRA

Using a Finite Element Approach, the CIRA main objective was to follow the progression of damage of composite joints in terms of fibres and matrix failure until the final collapse. The model was to be validated against CIRA's specimen tests in WP 5.

A three-dimensional geometrically non-linear FE model was developed. This model, developed initially within ANSYS in this task (implemented into B2000 in later tasks), was based on:

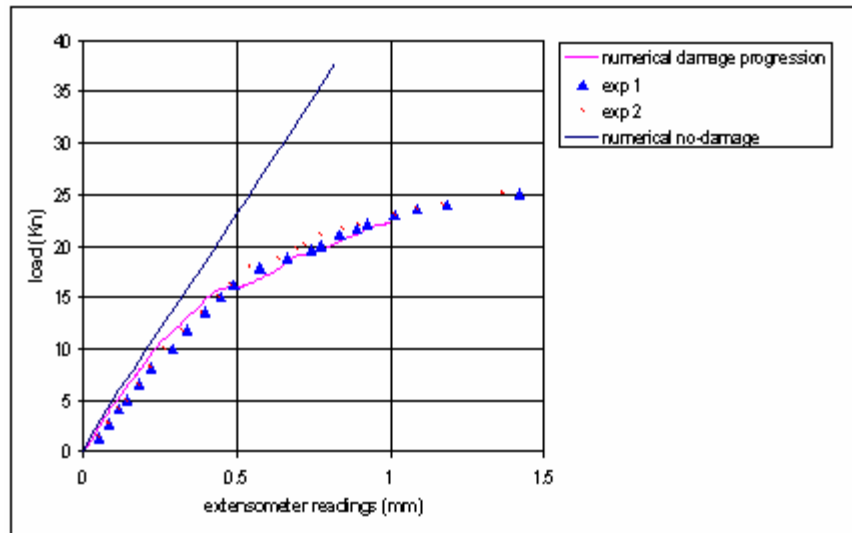
- Penalty method contact formulation
- Hashin's failure criteria
- Material property degradation rules

The Hashin failure criteria were used to check for failure inside the element at the ply level. The use of these criteria made it possible to distinguish among several failure modes. For each failure mode, sudden material property degradation rules were used to simulate the progression of damage inside the elements.

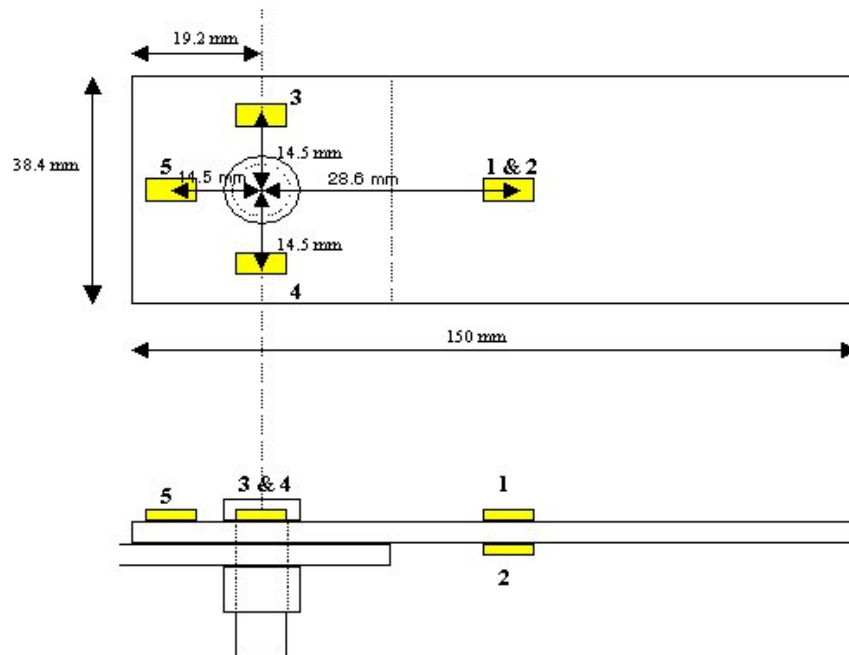
In the interim report D4.2-1 some three-dimensional analyses on the ULIM's single lap joint (the *Single-Bolt Benchmark* – see Fig. 4.4.1 above) were presented. The importance of contact between the sub-components of the joints was remarked upon and two different contact approaches were described in order to justify the choice of the penalty method approach in the computations. The numerical results in terms of deformed shape, strains, stresses and force-deflection curve were found to be comparable with those presented by ULIM. The same joint was then analysed using the proposed progressive damage approach. The damage onset and propagation in each lamina of the composite plates was investigated.

In the final report D4.2-4 the three-dimensional FE model introduced in D4.2-1 with some modifications was presented. The modifications addressed convergence problems found for high levels of load, and were focused on the modelling of property degradation rules. The proposed methodology was verified by using the experimental results found for the *Single-Bolt benchmark* and for three different configurations of single-lap CIRA specimens tested in tension. Preliminary non-linear no-damage analyses were performed in order to evaluate the deviation from experimental results. From comparisons with experimental tensile load vs. extensometer readings, the non-linear no-damage approach was found to be ineffective in predicting the real structural behaviour of the joints (after damage onset). On the other hand, the progressive damage approach demonstrated a

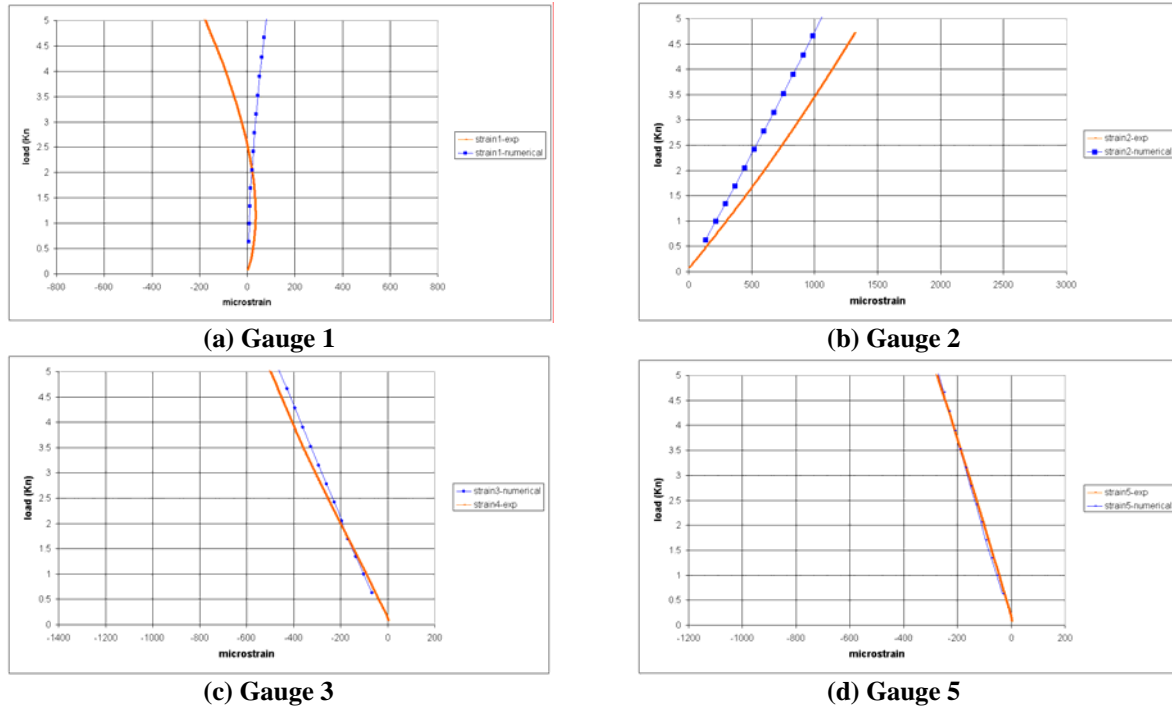
remarkable capability to follow the non-linear experimental trends as shown in Fig. 4.4.29.



**Figure 4.4.29 Single-Bolt Benchmark - applied tensile load versus deflection: experimental and numerical results with and without progressive damage**



**Figure 4.4.30 Positioning of strain gauges for CIRA single-lap specimen – Configuration 6**



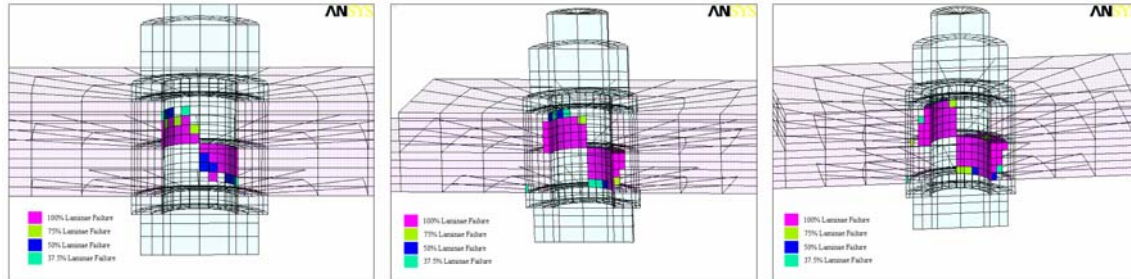
**Figure 4.4.31 Experimental and numerical strains for CIRA single-lap specimen – Configuration 6**

Fig. 4.4.30 shows the position of the strain gauges used on CIRA’s single-lap specimens (Configuration 6) and Fig. 4.4.31 shows the comparison between experimental and numerical strains. For Gauge 1, the strain is the sum of opposing effects: a tensile effect due to tensile loading applied to the joint and a compressive effect due to secondary bending of the joint. In Gauge 2, these two effects are both tensile, so they add together. Clearly, the secondary bending in the experiment is greater than in the simulation, since the difference between the Gauge 1 and Gauge 2 strains is higher in the experiment than in the simulation. In other words, the bending stiffness of the model is too high. ULM found the same result for their single-lap joints. On the other hand, the joint *longitudinal* stiffness (obtained by *adding* the strains in Gauge 1 and 2) is similar in the experiment and the model. The strains in the overlap region (Gauges 3 and 5) show excellent agreement between model and experiment for this configuration.

The numerical prediction of failed elements at different load steps showed that the damage progression was essentially the same for the three CIRA single-lap configurations studied (see Fig. 4.4.32). The damage onset was always located at the hole-edge near the interface between the plates (the “shear plane”) and propagation then occurred in the radial direction and towards the external surface of the plates. Some differences in the damage distribution, at the final stage of the loading process, between the composite-composite and the aluminium-composite joints were noticed. For the aluminium-composite joint, the damage distribution was rather constant through the thickness, while for the composite-composite joints a substantial decrease of damage

toward the external surfaces of the plates was evident. This difference was confirmed by NDE ultrasonic C-SCAN data in WP 5.

In conclusion the progressive damage approach developed in this task seems to be affordable and effective for detailed models of composite joints. In Task 4.3, the method was used in a global-local model, using SMR's developed global-local methodology. In Task 4.4, the full range of CIRA's experimental specimens were modelled.



**Figure 4.4.32 Quasi-isotropic configuration Percentage of broken plies in elements for three load steps**

#### Task 4.2 SMR

SMR's goals in WP 4 were to implement a global-local modelling capability into B2000 (Task 4.3) and support CIRA's efforts to implement damage modelling in B2000. As groundwork for this work, some improvements to the B2000 code were first necessary. The implementation of several detailed 3D local models into large global models results in systems with very large number of degrees of freedom. In addition, damage modelling involves time-consuming iterative procedures. In order to solve such problems, a very fast and efficient direct solver is needed, so SMR needed to improve the performance of its solver. In addition, contact modelling is crucial to successful 3-D modelling of bolted joints, so a new more efficient contact algorithm was needed.

SMR first implemented a new state-of-the-art sparse direct solver. The sparse direct solver was originally developed in an applied mathematics environment [6]. Thus, modifications were required to adapt the solver to a structural finite element environment.

About 50%-80% of the time of a non-linear continuation analysis is spent on the assembly and solution of the global system. The new sparse direct solver (with its own integrated assembler) requires approximately 50% of the memory compared to the traditional solver in case of 2D (shell) problems and 15% of the memory for 3D (volume) problems. On top of that the assembly and solution time are 10 to 20 times faster than for the old assembler and solver. The graphs in Figs. 4.3.33 and 4.4.34 show the substantial reduction in memory use and computation time in case of linear analysis of the DA temporary skin repair benchmark.

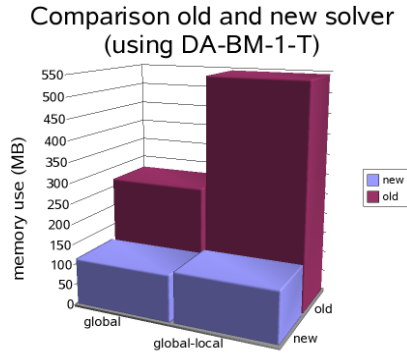


**Figure 4.4.33** Memory use for global and global-local model for old and new solver

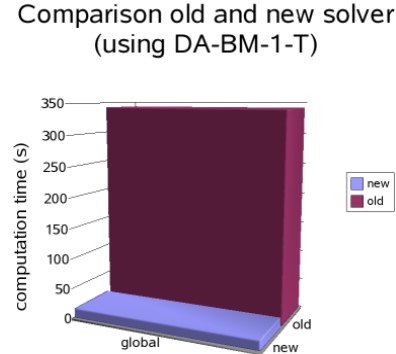


**Figure 4.4.34** Computation time of linear analysis of global model for old and new solver

SMR next implemented a new contact method. The method includes an advanced 3-stage contact detection algorithm [7] originating from the explicit finite element module in B2000. Fig. 4.4.35 shows a general contact problem. The contact definition is based on a master and a slave surface, where the slave surface nodes are not allowed to penetrate the master surface segments.

The contact search method uses a three-stage search, where the first two stages make use of a so-called bounding-box search as shown in Fig. 4.4.35. The first phase creates a box around the total master surface and searches for all nodes inside this bounding-box. This search is only done initially and after a fixed number of steps, depending on the displacement of the structure. In practice, this means that in most quasi-static cases the surface box search is performed only once. Any slave node outside this box (e.g. slave node 1) is no longer taken into account during the following analysis.

On this now limited set of slave nodes the local contact search is performed in two steps. First a bounding-box search is performed, similar to the one on the global surface. This gives for each master segment a set of nodes that have the potential to come into contact with the master segment. Some nodes are found only in the box of one particular segment (e.g. slave node 2), so that this slave node is only considered a potential contacting node for the corresponding master segment (in this case segment III). Other nodes are found to be in the overlap of two or more master segment bounding boxes (e.g. slave node 3). Finally, some nodes are not inside any of the local bounding boxes (e.g. slave node 4), so that they are no longer considered in the analysis until the next local search. This local search will usually take place more often than the above global bounding box search.

Finally, for each node within the bounding box of the master segment, the projection of the slave node on the master segment is computed. When the projection lies within the surface of the contact segment, the slave node is considered to be in contact with the master segment and is included in the computation of the contact force.

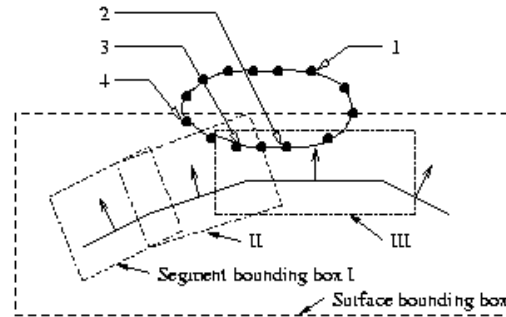


**Figure 4.4.35 Contact algorithm search strategy**

A beta version of B2000 containing the first version of the contact algorithm was delivered in Month 14. Combined with the sparse direct solver, this contact algorithm was shown to work very fast, allowing complicated models to be solved in a short period of time. However, in the case of multiple bolts and many potential contact pairs (many Lagrange-multiplier equations), the time to solve the Lagrange-multiplier system takes more time than the LU decomposition of the global stiffness matrix. Improvements need to be introduced to reduce the time of the contact iteration procedure.

#### **Task 4.2 ISTRAM**

ISTRAM has in BOJCAS developed a progressive fatigue damage model (PFDM) to predict the fatigue life and the macroscopic failure mechanisms of joints. The model and its results have been described in Deliverables D4.2-2 and D4.2-5. Additional work, done outside ISTRAM's obligation in BOJCAS, has been described in the extra deliverable D4.2-9.

The goal of the method was to predict the following parameters for a joint subjected to constant amplitude fatigue loading:

- the fatigue life of the joint,
- the macroscopic failure mechanism
- the fatigue damage accumulation as function of number of cycles

The model comprised the components of stress analysis, failure analysis and material property degradation.

The method was applied to a composite-to-metal single-lap joint described in [8]. Stress analysis was performed using ANSYS. A typical FE mesh of the joint is shown in Fig. 4.4.36. The modelling of the laminated plate has been done using layered linear solid elements. The metallic plate and the bolt were modelled using isotropic solid elements.

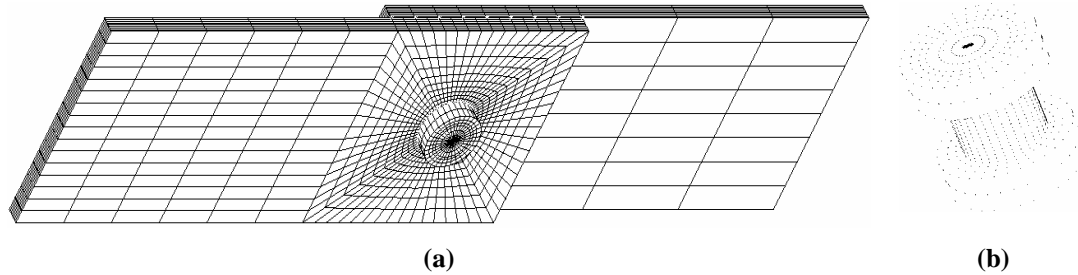


**Figure 4.4.36 (a) A typical FE mesh of the joint (b) Geometry and mesh of the protruding head bolt**

To simulate contact the node-to-surface 3-D CONTAC49 ANSYS element has been used. This element implements a combined penalty plus Lagrange multiplier contact method. The bolt, washer and nut have been considered as one unit to limit the number of contact elements in the model. Pre-tension of the bolts was achieved by temperature reduction in the bolt, which leads to bolt contraction and clamping of the plates.

Fatigue failure analysis was performed using a set of Hashin-type fatigue failure criteria (Table 4.4.7) for seven different damage modes. In the numerators of the criteria, the components of stress appear, while in the denominators, the relevant strengths appear, which are functions of the number of cycles  $n$ , stress state  $\sigma$  and stress ratio  $k$ . Both the stresses and strengths refer to the local layer coordinate system in which the x-axis is parallel to the fibres.

In fatigue loading cases, two types of material property degradation are applied: a sudden type, which is applied when a sudden fatigue failure mode is detected by the criteria and a gradual type, which is due to the nature of the cyclic loading and is independent of failure detection.

Sudden degradation is applied in terms of both stiffness and strength through the use of *sudden material property degradation rules* (Table 4.4.8). These rules were proposed in [9] for a unidirectional (UD) ply under a multi-axial state of fatigue stress.

Gradual degradation has been modelled by laws for *strength degradation*, *stiffness degradation* and *remaining fatigue life*, using a technique developed in [9]. The laws apply to a UD ply under a multi-axial state of stress and arbitrary stress ratio.

Mode of failure	Fatigue Failure Criterion
Matrix tensile cracking, for $(\sigma_{yy} > 0)$	$\left(\frac{\sigma_{yy}}{Y_t(n, \sigma, k)}\right)^2 + \left(\frac{\sigma_{xy}}{S_{xy}(n, \sigma, k)}\right)^2 + \left(\frac{\sigma_{yz}}{S_{yz}(n, \sigma, k)}\right)^2 \geq 1$ (1)
Matrix compressive cracking, for $(\sigma_{yy} < 0)$	$\left(\frac{\sigma_{yy}}{Y_C(n, \sigma, k)}\right)^2 + \left(\frac{\sigma_{xy}}{S_{xy}(n, \sigma, k)}\right)^2 + \left(\frac{\sigma_{yz}}{S_{yz}(n, \sigma, k)}\right)^2 \geq 1$ (2)
Fibre tensile failure, for $(\sigma_{xx} > 0)$	$\left(\frac{\sigma_{xx}}{X_t(n, \sigma, k)}\right)^2 + \left(\frac{\sigma_{xy}}{S_{xy}(n, \sigma, k)}\right)^2 + \left(\frac{\sigma_{xz}}{S_{xz}(n, \sigma, k)}\right)^2 \geq 1$ (3)
Fibre compressive failure, for $(\sigma_{xx} < 0)$	$\left(\frac{\sigma_{xx}}{X_C(n, \sigma, k)}\right) \geq 1$ (4)
Fibre-matrix shear-out, for $(\sigma_{xx} < 0)$	$\left(\frac{\sigma_{xx}}{X_C(n, \sigma, k)}\right)^2 + \left(\frac{\sigma_{xy}}{S_{xy}(n, \sigma, k)}\right)^2 + \left(\frac{\sigma_{xz}}{S_{xz}(n, \sigma, k)}\right)^2 \geq 1$ (5)
Delamination in tension, for $(\sigma_{zz} > 0)$	$\left(\frac{\sigma_{zz}}{Z_t(n, \sigma, k)}\right)^2 + \left(\frac{\sigma_{xz}}{S_{xz}(n, \sigma, k)}\right)^2 + \left(\frac{\sigma_{yz}}{S_{yz}(n, \sigma, k)}\right)^2 \geq 1$ (6)
Delamination in compression, for $(\sigma_{zz} < 0)$	$\left(\frac{\sigma_{zz}}{Z_C(n, \sigma, k)}\right)^2 + \left(\frac{\sigma_{xz}}{S_{xz}(n, \sigma, k)}\right)^2 + \left(\frac{\sigma_{yz}}{S_{yz}(n, \sigma, k)}\right)^2 \geq 1$ (7)

**Table 4.4.7 Fatigue failure criteria**

Sudden material property degradation rules		
Failure mode	Stiffness	Strength
Matrix tensile fatigue cracking	$\{E_{xx}, 0, E_{zz}, G_{xy}, G_{yz}, G_{xz}, 0, 0, \nu_{xz}\}$	$\{X_b, 0, Z_b, X_C, Y_C, Z_C, S_{xy}, S_{yz}, S_{xz}\}$
Matrix compressive fatigue cracking	$\{E_{xx}, 0, E_{zz}, G_{xy}, G_{yz}, G_{xz}, 0, 0, \nu_{xz}\}$	$\{X_b, Y_b, Z_b, X_C, 0, Z_C, S_{xy}, S_{yz}, S_{xz}\}$
Fibre tensile fatigue failure	$\{0, 0, 0, 0, 0, 0, 0, 0, 0\}$	$\{0, 0, 0, 0, 0, 0, 0, 0, 0\}$
Fibre compressive fatigue failure	$\{0, 0, 0, 0, 0, 0, 0, 0, 0\}$	$\{0, 0, 0, 0, 0, 0, 0, 0, 0\}$
Fibre-matrix shear-out	$\{E_{xx}, E_{yy}, E_{zz}, 0, G_{yz}, G_{xz}, 0, \nu_{yz}, \nu_{xz}\}$	$\{X_b, Y_b, Z_b, X_C, Y_C, Z_C, 0, S_{yz}, S_{xz}\}$
Delamination in tension	$\{E_{xx}, E_{yy}, E_{zz}, 0, G_{yz}, G_{xz}, \nu_{xy}, 0, 0\}$	$\{X_b, Y_b, 0, X_C, Y_C, Z_C, S_{xy}, S_{yz}, S_{xz}\}$
Delamination in compression	$\{E_{xx}, E_{yy}, E_{zz}, 0, G_{yz}, G_{xz}, \nu_{xy}, 0, 0\}$	$\{X_b, Y_b, Z_b, X_C, Y_C, 0, S_{xy}, S_{yz}, S_{xz}\}$

**Table 4.4.8 Sudden material property degradation rules.**



To simulate the residual *strength* of a UD ply under a general uni-axial fatigue loading (arbitrary state of stress and stress ratio) the following equation has been used:

$$R(n, \sigma, \kappa) = \left[ 1 - \left( \frac{\log(n) - \log(0.25)}{\log(N_f) - \log(0.25)} \right)^\beta \right]^{\frac{1}{\alpha}} (R_s - \sigma) + \sigma \quad \dots(4.4.5)$$

where  $R(n, \sigma, \kappa)$  = residual strength,  $R_s$  = static strength,  $n$  = number of applied cycles,  $\sigma$  = maximum stress,  $\kappa$  = stress ratio, and  $\alpha$  and  $\beta$  = experimental curve fitting parameters.

To simulate the residual *stiffness* of a UD ply under a general uni-axial fatigue loading the following equation has been used:

$$E(n, \sigma, \kappa) = \left[ 1 - \left( \frac{\log(n) - \log(0.25)}{\log(N_f) - \log(0.25)} \right)^\lambda \right]^{\frac{1}{\gamma}} \left( E_s - \frac{\sigma}{\varepsilon_f} \right) + \frac{\sigma}{\varepsilon_f} \quad \dots(4.4.6)$$

where  $E(n, \sigma, \kappa)$  = residual stiffness,  $E_s$  = static stiffness,  $\sigma$  = magnitude of applied maximum stress,  $\varepsilon_f$  = average strain to failure,  $n$  = number of applied cycles,  $N_f$  = fatigue life at  $\sigma$ , and  $\gamma$  and  $\lambda$  = experimental curve fitting parameters.

Considering that for each combination of the state of stress and stress ratio there is a fatigue life for a UD ply, to characterise the residual strength of a UD ply under arbitrary states of stress and stress ratios, a very large number of experiments must be performed. Many authors have restricted their failure criteria to a certain stress ratio to overcome this difficulty. However, assuming a certain stress ratio for the fatigue analysis of composite laminates is not always a realistic assumption. To remove this obstacle the fatigue life prediction model proposed in [9] has been used. The fatigue life  $N_f$  of the elements has been predicted by the equation:

$$u = \frac{\ln(a/f)}{\ln[(1-q)(c+q)]} = A + B \log N_f \quad \dots(4.4.7)$$

where  $A$  and  $B$  are the curve fitting constants,  $a = \sigma_\alpha / \sigma_t$ ,  $c = \sigma_x / \sigma_c$ ,  $q = \sigma_m / \sigma_t$ ,  $\sigma_x$  = the stress in the corresponding direction,  $\sigma_t$  = the tensile strength,  $\sigma_c$  = the compressive strength,  $\sigma_\alpha = (\sigma_{\max} - \sigma_{\min}) / 2$ ,  $\sigma_m = (\sigma_{\max} + \sigma_{\min}) / 2$

In order to calibrate the above gradual degradation laws, a complete characterisation of the composite material behaviour (stiffness, strength and fatigue life) under static and fatigue loading conditions is needed. This was beyond the scope of ISTRAM's work in BOJCAS and therefore, data for AS4/3501-6 from [10] were used. The experimental parameters, needed in above equations are summarised in Table 4.4.10. As normalising parameters of the fatigue material properties, the static material properties shown in Table 4.4.9 have been used.

Material Property	Magnitude
$E_{xx}$	147 GPa
$E_{yy}=E_{zz}$	9 GPa
$E_{xy}=E_{xz}$	5 GPa
$E_{yz}$	3 GPa
$\nu_{xy}=\nu_{yz}$	0.3
$\nu_{yz}$	0.42
$X_t$	2004 MPa
$X_c$	1197 MPa
$Y_t=Z_t$	53 MPa
$Y_c=Z_c$	204 MPa
$S_{xy}=S_{xz}$	137 MPa
$S_{yz}$	42 MPa

**Table 4.4.9 Material properties of the AS4/3501-6 lamina**

	Factors					
	Residual stiffness		Residual strength		Life prediction	
	$\lambda$	$\gamma$	$\alpha$	$\beta$	A	B
Longitudinal tensile	14.57	0.3024	10.03	0.473	1.3689	0.1097
Longitudinal compression	--	--	49.06	0.025		
Transverse tensile	14.77	0.1155	9.628	0.1255	0.999	0.096
Transverse compression	--	--	67.36	0.011		
In-plane shear	0.7	11	0.16	9.11	0.099	0.186
Out-of-plane shear	--	--	0.2	12	0.299	0.111

**Table 4.4.10 Summary of the experimental curve fitting data [10]**

In order to explain the way the residual strength, residual stiffness and fatigue life prediction models integrate to gradually reduce the material properties of the laminate due to cyclic loading, we consider a UD ply under a multi-axial state of stress and we assume that the mode that has to be verified is tensile fibre fatigue failure. Following the flowchart of Fig. 4.4.37 the following steps are taken. First the state of stress (stress analysis), stress ratio, and initial (static) material properties ( $X_b$ ,  $S_{xy}$ ,  $G_{xy}$ ,  $S_{xz}$ ,  $G_{xz}$ ) are determined. Then using the above *fatigue life prediction model* the number of cycles to failure for each stress state is calculated. With this as input, the residual material properties of the UD ply are calculated from equations 4.4.5 and 4.4.6. The gradually degraded material properties are then given as input to the next stress analysis and fatigue failure analysis.

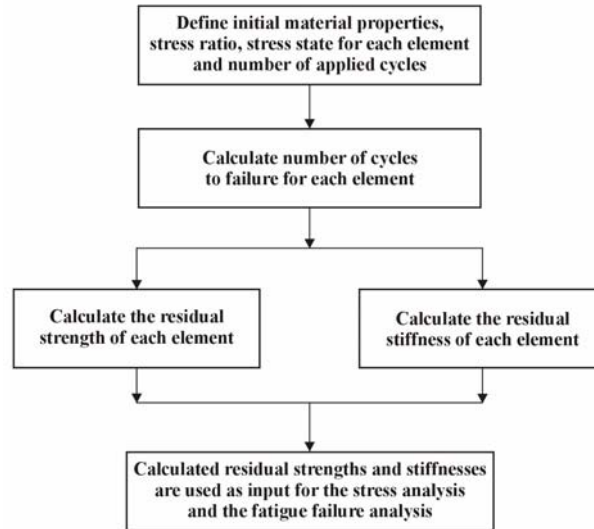


**Figure 4.4.37 Flowchart of the gradual material property degradation technique**

Fig. 4.4.38 shows the flowchart of the integrated PFDM. First the stress analysis must be performed (input: material properties, geometry, boundary conditions, maximum and minimum fatigue load, maximum number of cycles, increment of cycles). Next, based on the previous calculated stress field, the fatigue life, residual strength and residual stiffness of each element is calculated. Then sudden failure analysis is performed by examining the maximum stresses. If any sudden mode of failure is detected the material properties of the failed plied are degraded and a new stress analysis is performed with the same load to calculate the stress redistribution. Otherwise, the applied fatigue cycles are increased by a constant number and a new stress analysis is performed. The fatigue cycles increment has been selected such that the maximum number of steps needed is not large (e.g. 40 steps). This is necessary in order to keep the computing time realistic. The iterative procedure is terminated when final failure is reached.

In order to verify the PFDM, as a first step, two different cases of composite bolted joints incorporating different geometries and stacking sequences were considered. For these cases experimental results on life prediction and damage accumulation were available in the literature.

Figs. 4.4.39 and 4.4.40 show the comparison of the predicted and experimental S-N curves for the two cases. Predictions from using a coarse mesh with 2160 elements and a fine mesh with 8164 elements are shown. Note that the extensive post-processing analysis of the model, which is performed on an element basis, leads to a very large total space for data storage, and large CPU times. Clearly using the coarse mesh gives a satisfactory agreement in the first case. In the second case, the agreement is less satisfactory, especially at the low stresses. This can be explained by the fact that the material characterisation has been not performed at these small stress levels. A small improvement has been achieved with the fine mesh for both cases.

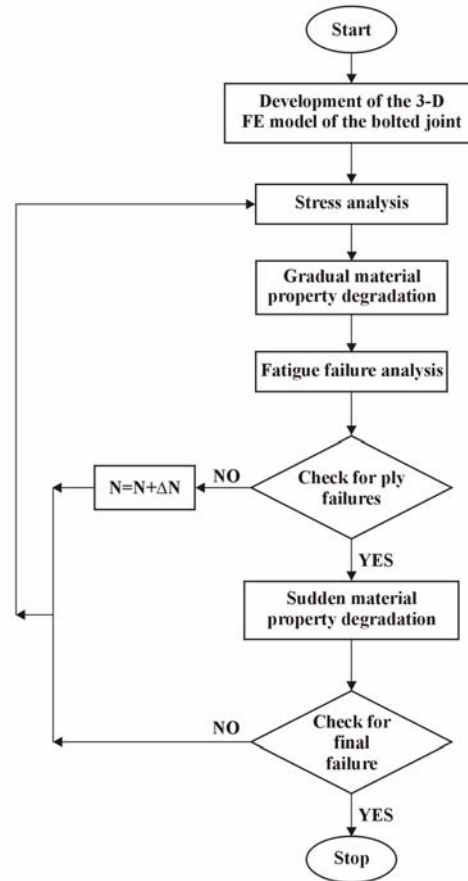


Figure 4.4.38 Flowchart of the PFDM

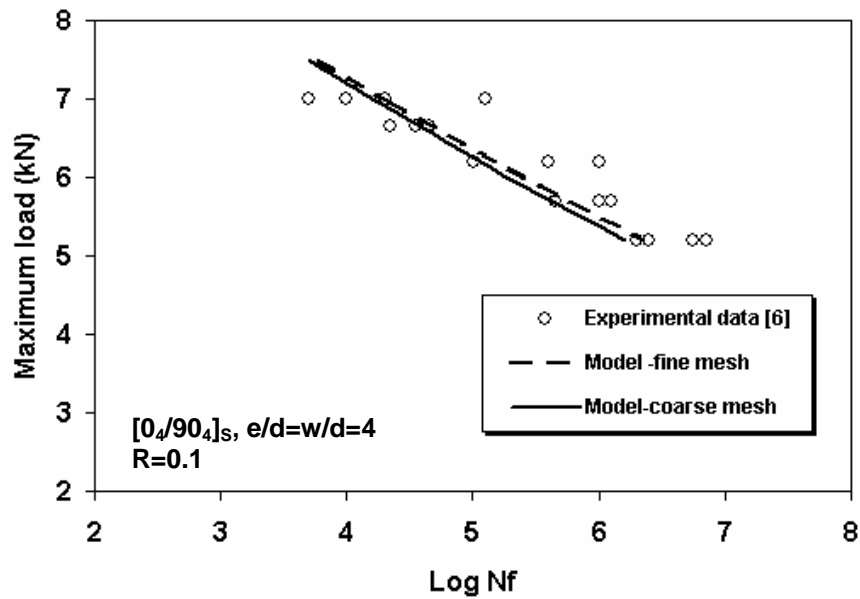
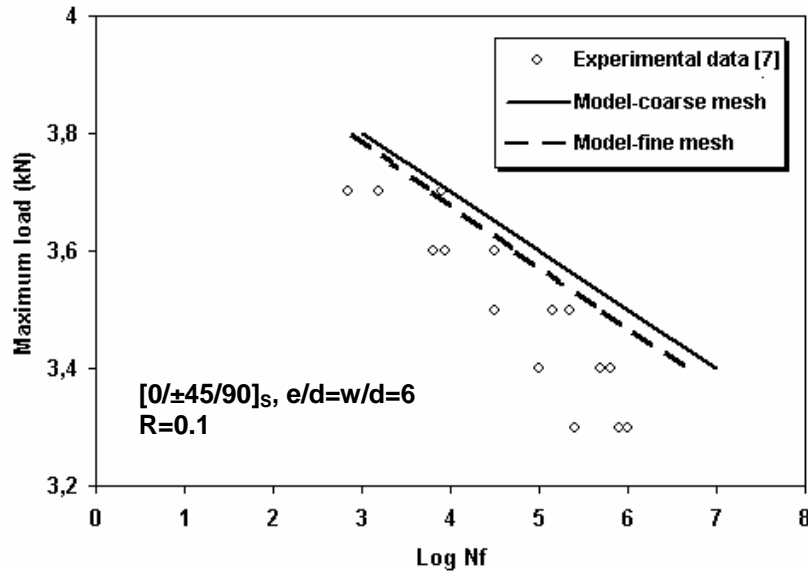


Figure 4.4.39 S-N curves of a bolted composite joint with a  $[0_4/90_4]_s$  laminate



**Figure 4.4.40 S-N curves of a bolted composite joint with a  $[0/\pm 45/90]_s$  laminate**

Based on the joint configuration of Fig. 4.4.36, three different geometries A, B and C described in Table 4.4.11 were modelled. These geometries were selected to lead to the three macroscopic failure mechanisms, namely tension, shear-out and bearing.

Bearing failure was defined as a bolt-hole deformation equal to 4% of the original hole diameter, (ASTM Standard D953 [11]). Tension and shear-out failure were defined to take place when damage propagated to the laminate outer edge.

Fig. 4.4.41 shows the predicted S-N curves for the three geometry cases obtained using the fine mesh. The maximum applied load has been normalised with the corresponding static strength of the joints. The results show a reduction of predicted life when moving from bearing to shear-out and finally the tension failure mode. This is consistent with findings on *static* tensile strengths of composite bolted joints, as discussed in [12].

Configuration	Stacking sequence	L (mm)	W (mm)	D (mm)	d (mm)	e (mm)	h (mm)	t (mm)
A	$[(\pm 45/0/90)]_s$	150	60	17.8	10.0	60	30	4.16
B	$[(\pm 45/0/90)]_s$	150	60	17.8	10.0	20	10	4.16
C	$[(\pm 45/0/90)]_s$	150	30	17.8	10.0	60	30	4.16

**Table 4.4.11 Geometrical data of the A, B and C joint configurations**

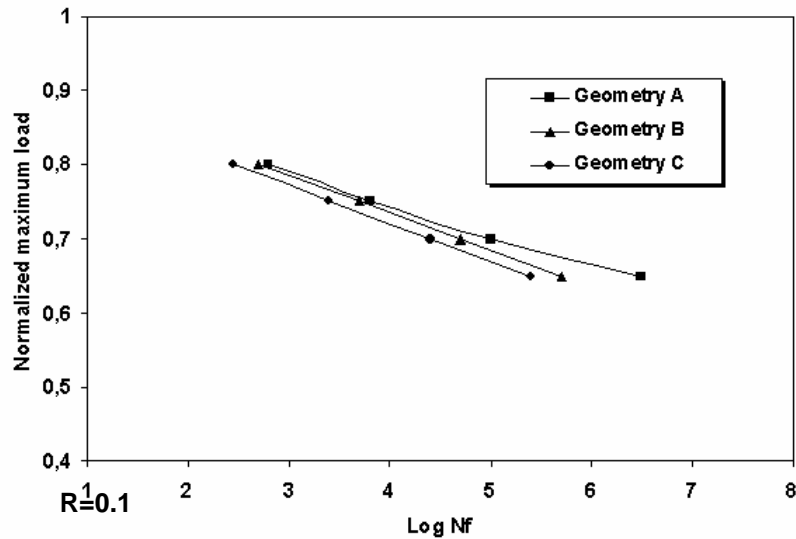


**Figure 4.4.41 Predicted S-N curves of the A, B and C configurations of the composite bolted joint with  $[(\pm 45/0/90)]_s$  laminate**

In conclusion, the developed progressive fatigue damage model has shown the capability to predict fatigue life of bolted joints, but only if material characterisation data are available for the specific load levels and modes. The model can be used in a global analysis system but it is believed that due to the three-dimensional and progressive nature of the modelling this will require a very large computing effort. Investigations on minimising model size and post-processing analysis, without loss of accuracy, are needed. It is important to note that the model needs further verification through extensive comparison with experiments, and consideration of the effect of several parameters on model results.

A drawback in the use of the PFDM is the requirement for a large amount of material characterisation data. This is reasonable if one considers the complexity of the problem solved. However, to use this model to predict the behaviour of new materials it is necessary to modify it in order to reduce the amount of material characterisation data needed. Investigation of this has been performed by ISTRAM and a modified progressive fatigue damage model, which requires input from a small number of experiments, has been proposed in the extra deliverable D4.2-9. The modified model has been satisfactorily applied in two different graphite/epoxy laminates subjected to tension-compression fatigue.

### Task 4.2 FOI

In this task, a fatigue failure criterion for bolted joints that fail through bolt failure has been developed. In earlier work on fatigue of bolted joints it had been observed that for joints with different number of bolt rows it was possible to obtain a master curve for predicting the fatigue life. If the applied load was divided with the number of bolt rows the fatigue data collapsed onto a master curve. The master curve worked for joints with different number of bolts and different lay-ups. In BOJCAS this concept was developed into a new fatigue failure criterion.

In parallel with the BOJCAS project joints were tested at constant amplitude loading and with occasional over loads. The joints with overloads had a longer fatigue life than the joints loaded at constant amplitude. This suggested that the fatigue life is governed by the fatigue life of the bolts and not by the composite. In BOJCAS an FE model was developed for the double-lap joints that were fatigue tested by FOI in WP 5, and for some earlier fatigue results. The model contained 29280 elements and is shown in Fig. 4.4.42. The washers were modelled and frictionless contact was used at all relevant contact surfaces. The model was solved with the in-house FE code STRIPE.

In experiments it has been found that the fasteners break at the centre of the specimens where the opening, tensile, stress is at its maximum. The maximum opening stress in the bolts were extracted from the FE solutions and the average was calculated. The joints had three rows and the bolts in the middle row had the lowest opening stress. However, during fatigue loading the loads in the fasteners will probably be redistributed due to hole wear. Therefore, the average opening stress in the bolts was used.

For each fatigue-loaded joint the average opening stress was plotted versus the fatigue life of the joint, see Fig. 4.4.43. Since the approach is based on metal fatigue of the titanium fasteners, fatigue data for rotating fatigue of the same titanium alloy as used in the fasteners was included in the figure. The joints with thin plates and 8 mm bolts failed due to hole elongation for which the fatigue failure criterion is not applicable. The remaining joints in the figure failed due to bolt failure and, as can be seen, they form a scatter band through which the rotating fatigue data passes. Thus, from this curve it is possible to predict the fatigue life of joints. This is the first fatigue failure criterion for joints developed to date.

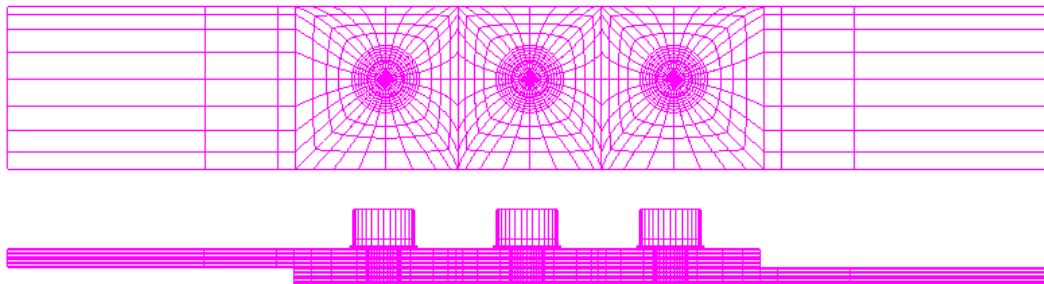


**Figure 4.4.42 FE mesh of joint with 6 mm fasteners and 3.12 mm thick outer plates**

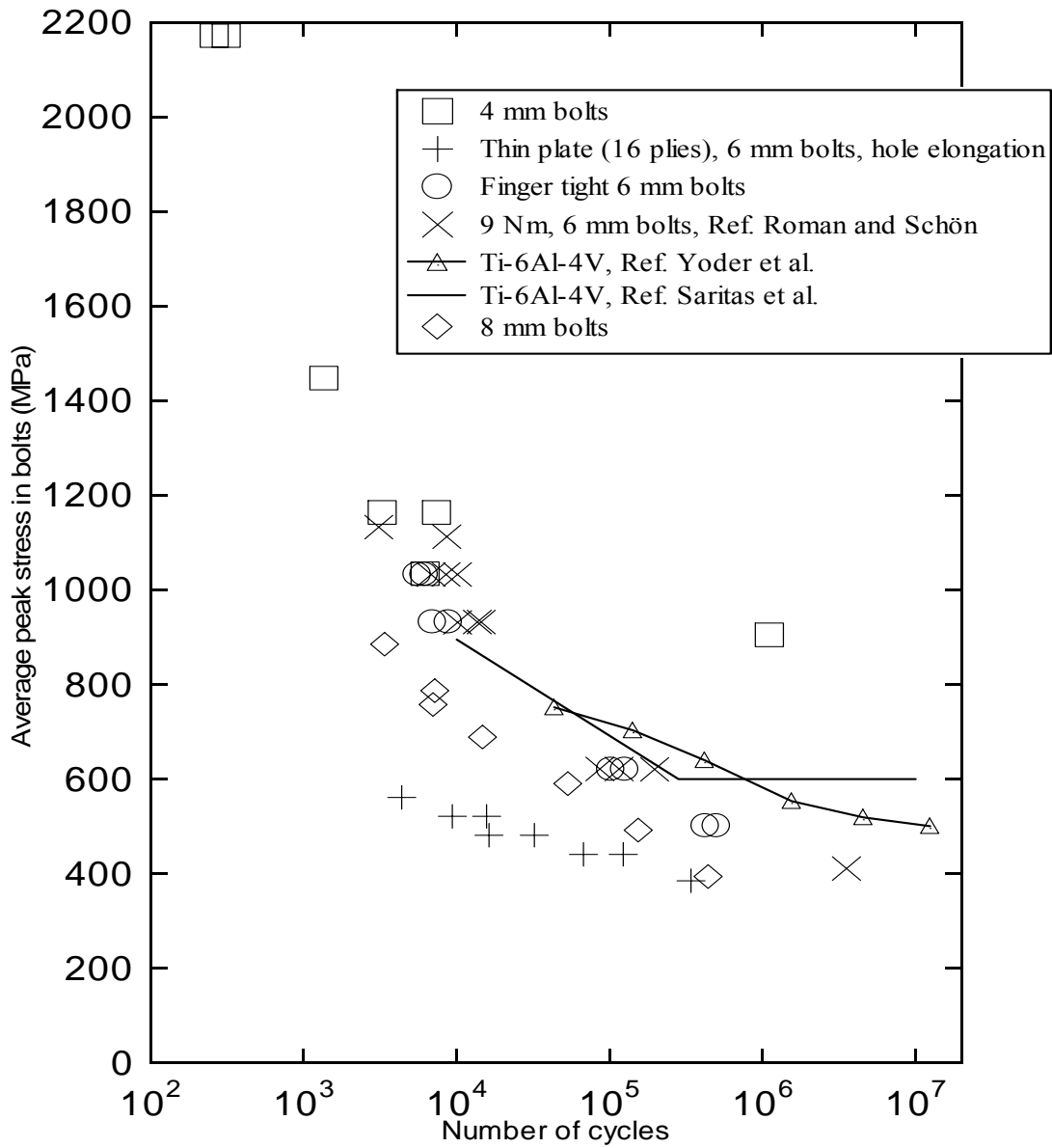


Figure 4.4.43 Average peak tensile stress in bolts versus number of cycles for six-bolt joints



## 2.4.3 Task 4.3 Coupled Global-Local Methods

In this task, the objective was to develop global-local methods and apply them to the benchmark structures. QinetiQ worked with the BAe benchmarks, as with their global methods in WP 2; FOI worked on the SAAB benchmarks, and SMR focused on the DA benchmarks. Near the end of this task, CIRA used SMR's developed global-local method and implemented damage modelling into the local model, showing that global-local analysis including damage was feasible.

### Task 4.3 QinetiQ

There are two primary methods of global-local modelling. The first is to perform separate global and local analyses in series (series method). Here, the global model includes simple representations of the local features. The representations are sufficiently refined to capture the stiffness of the local features but not the detailed stresses within them. Once a solution to the global model has been obtained, boundary conditions (displacements) can be transferred to isolated models of each local feature.

The second method is to embed refined models of the local features within a coarse global model and thereby solve the global and local models in parallel (parallel method). For example, refined 3D solid models of each bolt and its surrounding laminate foundations can be included within a shell model of the global structure. The critical fasteners can have a fine representation and the non-critical fasteners can have a coarse representation to minimise the size of the model.

The series method is attractive for structures that include a large number of bolts, many or all of which will be stressed using separate local models. This approach minimises the size of the mathematical problem. The parallel method is attractive where the number of bolts is small, or where the critical bolts are known in advance. Only the bolts that are believed to be critical need to be modelled in detail, and although the size of the mathematical problem is increased, it is still manageable because the number of detailed local features is small.

QinetiQ's aims for this task were:

- to create software for *series* coupling of global and local FE models of bolted joints
- to ensure the software could be easily modified to work with a wide range of commercial FEA packages
- to demonstrate the software on benchmark structures.

These aims were met through the development of a FORTRAN program called `Q_global_local`. Fig. 4.2.35 (in Task 2.3) shows how `Q_global_local` fits into the complete global-local tool-set.

`Q_global_local` is used to transfer boundary conditions from each fastener and foundation in the global model to a corresponding local model. `Q_global_local` operates on the global FEA file, a configuration file, and the local model FEA files. The configuration

file is a simple text file that identifies the boundary-condition mappings from the global model to the local models.

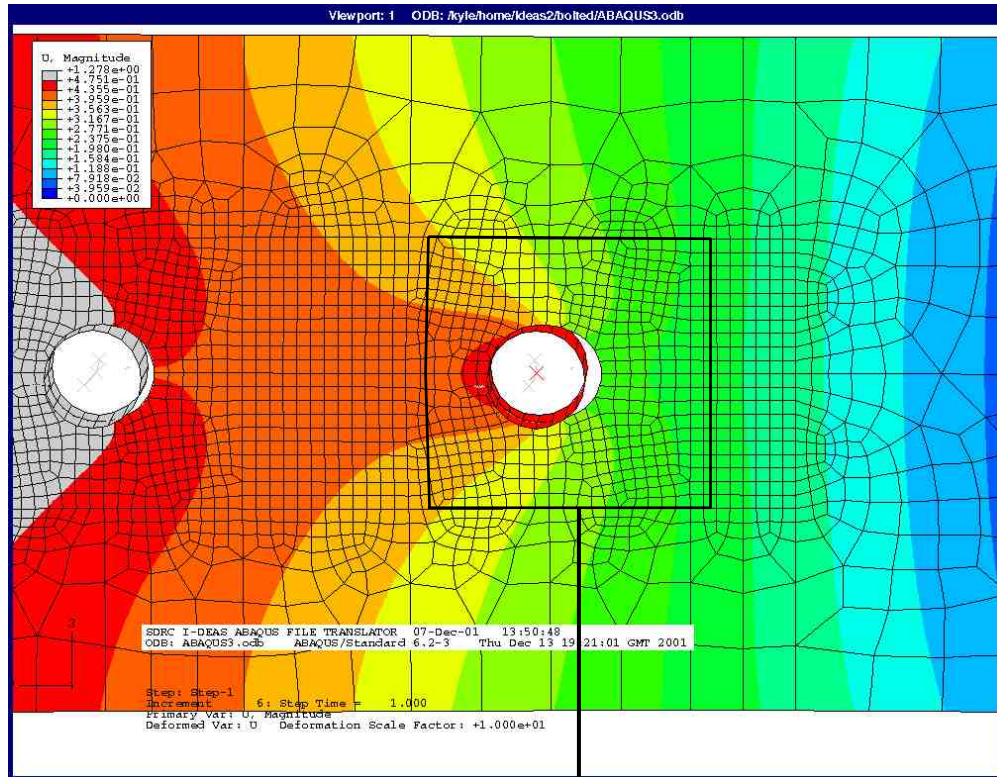
Each boundary is defined using a node-set definition. Node-set definitions are almost universally employed within pre-processing packages and FEA packages, and this ensures that Q\_global\_local is independent of any one package. A node-set is simply a named list of nodes, and operations can be performed on all the nodes in the set by giving its name. Modern pre-processors have very powerful methods of defining node-sets based on geometrical features. For example, it is relatively easy for the analyst to pick each boundary and hole centre and assign the associated nodes to a node-set.

Q\_global\_local allows the user to specify the same local model for several local regions (single-bolt joints) within the global model. In this case a set of updated local models are created. Each model is a copy of the original local model, and each has a different set of applied displacements. Another powerful feature of Q\_global\_local is that the local model need not be in the same orientation in space as the relevant region in the global model.

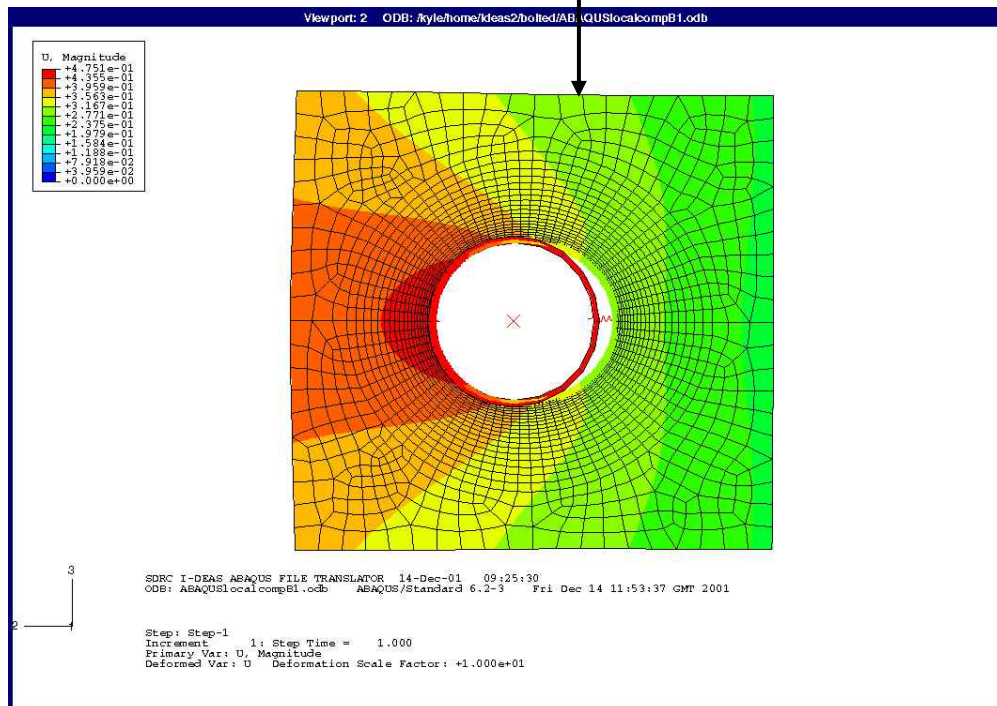
Figs. 4.4.44 and 4.4.45 show a demonstration of Q\_global\_local with a BAe benchmark structure. Fig. 4.4.44 shows a contour plot of the displacements within the foundation in the global model, and a corresponding plot of the displacements within the local model. The displacements are clearly equivalent. The refined mesh and the refined contour results within the local model are also evident. Figure 4.4.45 shows contour plots of the von-mises stress within the global and local models. The von-mises stresses are equivalent, but there is clearly greater resolution in the local model. The von-mises stress has no particular relevance to composites, and has only been used to give an indication of the overall loading in the joint. It is important to note that the contour plots of the local model also show that the stress at the boundary is not uniform. This shows that the global-local tool-set is able to capture the interaction between closely spaced bolts or the interaction between a bolt and an edge.

An interesting and unintentional bi-product of QinetiQ's work in Task 2.3, is that the solid-element version of Q\_global\_bolt can be used to create parallel global-local coupling. This is achieved by selecting a very fine mesh for the solid region rather than the coarse mesh that is acceptable for the prediction of stiffness in a global-model. This parallel procedure is very similar to that developed by SMR.

Note that the parallel method of global-local coupling has not yet been demonstrated because the solid version of Q\_global\_local is still being de-bugged. It is anticipated that this may be demonstrated in future work.

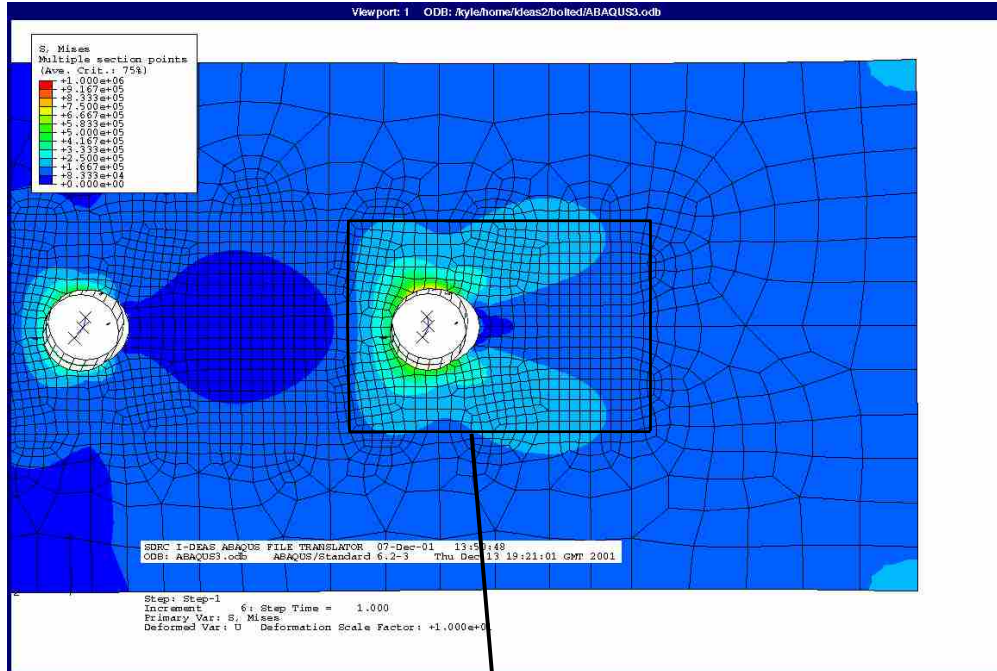


Resultant displacement in the global model

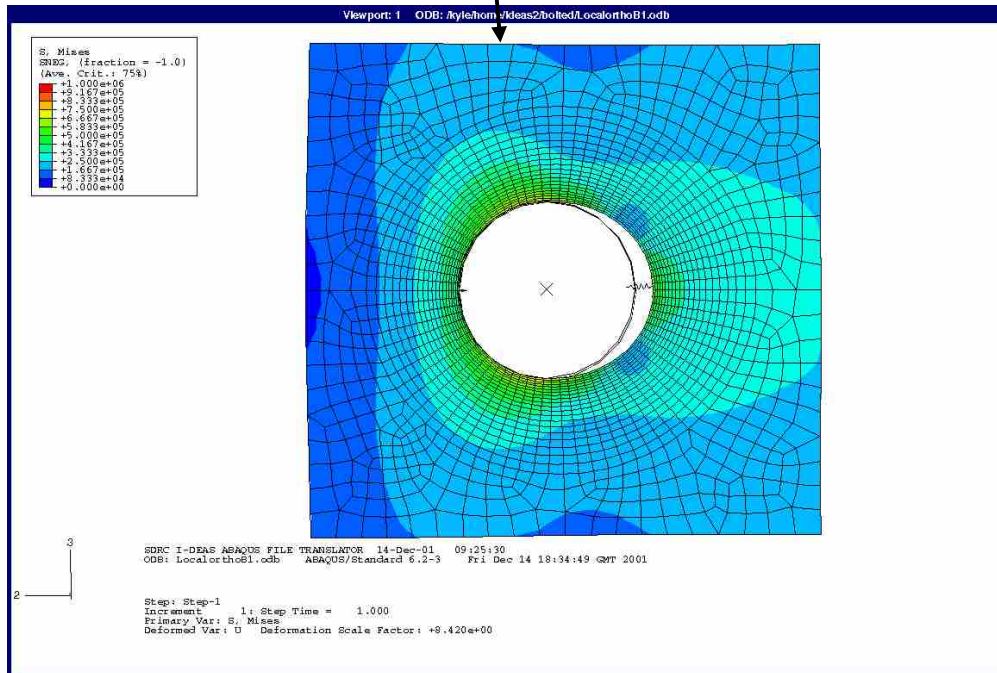


Resultant displacement in the local model

Figure 4.4.44 Validation of boundary-condition transfer using Q\_global\_local: displacements. Note that the mesh density that is used here in the global model is greater than that which would normally be required



Von-Mises stress in the global model



Von-Mises stress in the local-model

Figure 4.4.45 Validation of boundary-condition transfer using Q\_global\_local:  
induced stress

### Task 4.3 FOI

In Task 4.3, FOI developed a novel and reliable computational procedure for analysis of 3D bolted joint problems. The method is based on a mathematical splitting scheme, i.e. the problem to solve is split into several sub-problems and the final solution is obtained by superimposing several solutions.

The novel scheme developed by FOI is based on state-of-the-art methods in computational mathematics with a solid mathematical foundation including proofs of existence and convergence. It uses effective numerical schemes like the *hp*-version of the finite element method and schemes for error control. One of the key requirements for the method developed was that it be so efficient that it can be used in optimisation, damage tolerance and statistical analysis in Task 4.4.

It is foreseen that in a not too distant future, aircraft authorities will require such tools to be applied in analysis and design of aircraft structures. The work by FOI in Tasks 4.3 and 4.4 has resulted in methods that perhaps already today fulfil such (future) requirements.

The bolted joint problem was formulated as a set of partial differential equations with appropriate boundary conditions. The equations considered were the Navier 3D equations of elasticity with unknown contact surfaces. No damage modeling was attempted although the splitting method developed is ideally suited for analysis of several kinds of important damage in bolted joints.

Mathematical properties of the exact 3D solution, for *homogenised* material properties were first reviewed. In order to demonstrate that homogenised solutions can be used to derive important information about non-homogenised solutions a full 3D ply-by-ply analysis of a bolted joint was performed with control of the point-wise error in the solution with respect to the exact mathematical solution. Of special interest was to estimate sizes of regions controlled by *mathematical singularities* in the exact solutions. Since contact stresses theoretically are infinite in many regions in the joint, the question of what stress/strain measure to use is of outmost importance.

Fig. 4.4.46 illustrates the overall stress distribution in the *Single-Bolt Benchmark* (modelled by several partners in BOJCAS - see Fig. 4.4.1 above). At the washer-bolt, washer-plate, and bolt-plate interfaces, and interfaces between plies (at hole surfaces), the displacements are of the type  $u \sim r^\lambda$ ,  $\text{Re}[\lambda] < 1$ ,  $r$  being the distance to the edge. Hence, stresses and strains are infinite at these four types of edges *for arbitrarily small loads*. In the present analyses, an *hp*-version of FEM was used with very refined meshes near singular edges so all details could be captured.



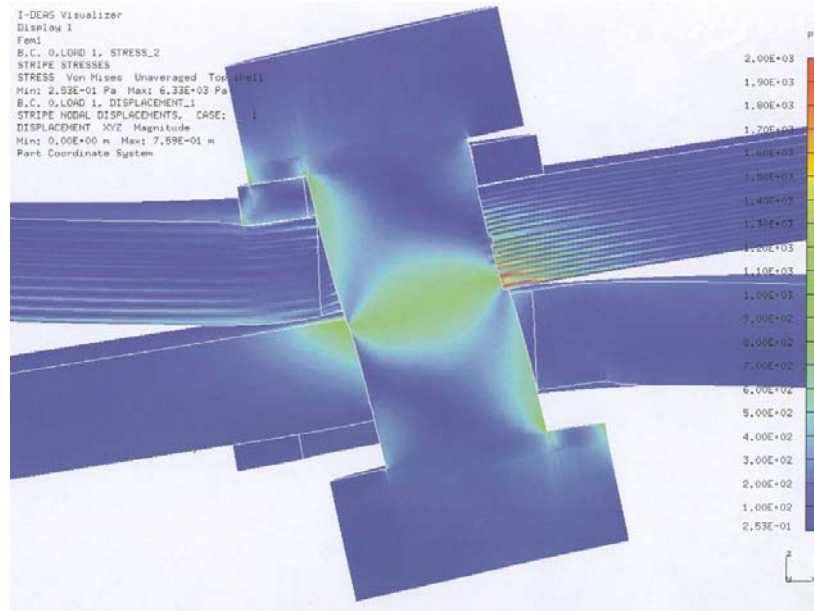


**Figure 4.4.46** Calculated stresses in single-bolt joint using a *hp*-version of FEM

Fig. 4.4.47 shows the radial stress distribution  $\sigma_r$  as function of the distance  $z$  from the contact surface between the two plates (the “shear plane”) at the circumferential angle where stresses are highest (the “bearing plane”). The solutions are converged. Stresses are singular at the material interfaces (filled black small circles) in all 40 plies. The stresses in the 0-degree plies are the largest, while stresses in +45/-45 plies are much smaller, and roughly the same. The stresses in the 90-degree plies are smallest. The large black circles show the *average stress* in a 45/0/-45/90 stack. This average is very close to the homogenised solution (open circles), except near the singular edge  $z=0$ . This implies that given a homogenised solution, the averaged radial stresses in the 45/0/-45/90 stack, can be obtained (except close to the singular edge  $z=0$ ). The size of the regions controlled by mathematical singularities depends on the mathematical model used, i.e. if homogenised data or detailed ply-by-ply data is used. Close to the edge ( $z=0$ ) where stresses are highest one sees that the singular stresses extend over a distance of order 2-3 ply thicknesses.

A main conclusion from this study was that the often-used technique of reporting (entirely FE-mesh dependent!) stresses at the singular edge (where stresses are infinite) must be avoided. For laminates having of the order 20 plies, FOI recommends that calculated stresses be characterised by a linear function (i.e. two scalars). The local singular behaviour can be calculated accurately from such a linear function (if needed).

The *reference solution* was used by other BOJCAS partners to compare solutions obtained using commercial FE packages and homogenised material data.

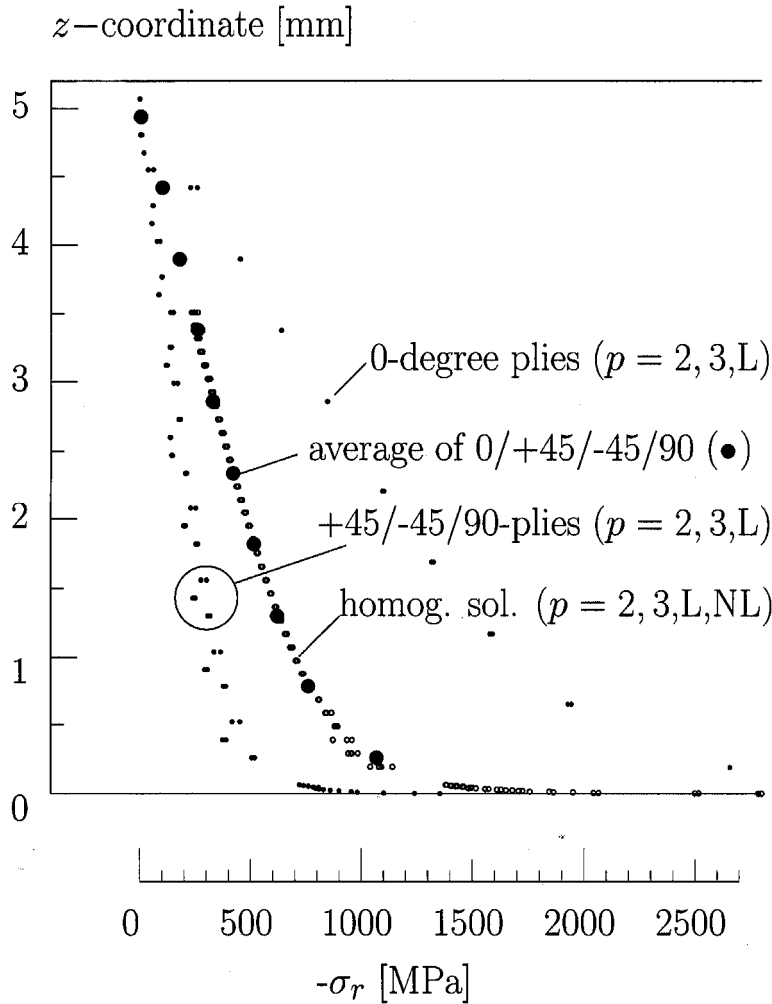


**Figure 4.4.47** Calculated radial stress  $\sigma_{rr}$  for different polynomial order  $p$  and linear and geometrically non-linear analysis as function of the distance  $z$  from the faying surface in 40-ply laminate (*Single-Bolt Benchmark*)

The major work in Task 4.3 was the development of a mathematical splitting method for solution of bolted joint problems of the complexity discussed above. Hence, a method was developed for *reliable* solution of 3D non-linear bolted joint problems of *real-life complexity* where point-wise stresses are determined (for homogenised material data) with high accuracy. Such a method did not exist previous to developments in Task 4.3.

The performed work consisted of the following parts:

- Invent a *very fast* and accurate method for solution of non-linear 3D contact problems (the splitting scheme)
- Derive mathematical proofs for the existence of a solution to the splitting scheme, together with its uniqueness and convergence properties
- Implement the splitting scheme on a cluster of SMP-computers

- *Verify* that the mathematical equations were solved correctly with control of error and high accuracy
- *Validate* the solution of the full 3D equations against experimental data

A novel scheme based on linear elastic fracture mechanics was used for solution of the contact problem. The lines separating areas of contact and no-contact are used as primary unknowns in the computational scheme. By using an iterative scheme the positions of the contact lines, satisfying the criteria that the first order edge and vertex stress intensity factors must be zero, are found with very high accuracy in only 3-4 iterations. In order to be computationally efficient, the method requires a solver that can solve the full 3D problem, for a-priori given contact surfaces, repeatedly to low cost. The splitting scheme is the basic tool used to achieve this objective. Tools for reliable extraction of edge and vertex intensity factors were available in the STRIPE-code used at the start of the project.

In the splitting scheme, the bolted joint problem with a-priori assumed contact surfaces is *split* into a number of problems and the solution is obtained by superposition. The discrete solution  $\tilde{u}$  to this problem is,

$$\tilde{u} = w_1 + \sum_{k=1}^n \beta_k \cdot w_2^{(k)} + \sum_{k=1}^n \beta_k \cdot w_3^{(k)} \quad \dots(4.4.8)$$

where  $\beta_k$  are scaling factors to be determined. The displacements  $w_1$  and  $\{w_2^{(k)}, w_3^{(k)} | k = 1, \dots, n\}$  are solutions to *local* and *global* problems.

Mesh design is an expensive and time-consuming part in FE-analysis. However, by employing the splitting scheme drastic simplifications are possible. The mesh for the local problem is designed for the *hp*-version of FEM (for an example see the mesh in Fig. 4.4.78 in the Task 4.4 description below). This mesh generation is time-consuming, the only advantage being that the same mesh can be used at all bolt locations.

However, the great advantage in mesh design is that on the global level, the mesh might be *very coarse*. In fact, the modelling of the bolts on the global model might be avoided completely (see Task 4.4 below)!

It was shown mathematically in D4.3-10A that coefficients  $\beta_k$  in equation (4.4.8) are uniquely determined and converge exponentially fast to the exact mathematical solution when employing the *hp*-version of the FE method. The non-linear solution scheme is based on the condition that stress intensity factors also converge extremely fast to the exact solution. In a benchmark example given in D4.3-10A, it was demonstrated, in the case of a 20-bolt joint, that a relative stress error in maximum bearing stress of  $10^{-4}$  could be obtained in only four iterations.



By using the *hp*-version of FE combined with the mathematical theory derived, the discretisation error in the non-linear contact solution, with respect to the exact mathematical solution, can be controlled. This is simply done by deriving a sequence of solutions for increasing polynomial orders  $p$  and refined *local* meshes and monitoring the convergence in the quantity of interest (which is exponential).

In order to verify that the splitting scheme was correctly implemented, a benchmark example having 20 bolts, was also solved using a direct approach, i.e., an extremely fine mesh was created and solved using the *hp*-version of FEM. The two solutions shown in D4.3-10A were in very close agreement, where the solution obtained using the splitting scheme most likely had lower error. This verification phase was very time-consuming but was considered to be a necessary part of the development work.

The splitting scheme has been designed to solve truly large-scale problems on a cluster of SMP-computers. A special version has been designed for optimisation studies, statistical analysis and damage tolerance analysis. The system exhibits excellent *scalability* and has been tested by solving problems with 212, 225 and 671 bolts. A large model to test the use of static sub-structuring with 250 bolts was also solved. Each of the 20 plies in the composite plates was modelled separately. The problem used to derive solution  $w_1$  in equation 4.4.8 had  $10^8$  degrees of freedom. Presently the system is being setup on the RED ASCII system at SANDIA Research Lab, Albuquerque, US, where test computations will be made using 4000 CPUs.

To validate the method against experimental results, the SAAB bolt pattern benchmarks were modelled. However, it turned out that all SAAB benchmark specimens tested exhibited large displacement effects. Since the splitting scheme is based on the assumption of linear kinematic conditions, it cannot be validated on cases where out-of-plane displacements are large. Non-linearities due to large displacements can be handled in an approximate way by first solving the kinematically non-linear problem without detailed analysis of the contact problems. Secondly, by using the tangent stiffness from the non-linear analysis, the contact problem can be solved virtually exactly. The splitting scheme is currently being developed in this direction to include kinematically non-linear effects. This is an ongoing effort that was not in the original BOJCAS plan.

Thus, instead of using the splitting method, straightforward non-linear 3D FE analysis using a  $p$ -version of the finite element method was used to analyse all specimens. This was done so that a comparison could be made of near exact 3D solutions with experimental results and with SAAB's Global Design method (see WP 2). As noted in WP 2, bolt load distributions and directions predicted by the global method were in good agreement with the 3D solution. Comparisons of strains close to several bolt-holes were also performed and presented in D4.3-10 Part B (see Fig. 4.2.29 for the location of the strain gauges).

The scatter plot in Fig 4.4.48 summarises results for six single-lap SAAB benchmark specimens (with all bolts present, one and two bolts missing, for two bolt patterns) at a tensile load of 250 kN. The figure shows that:

- The 3D mean strain error is practically zero ( $57 \mu$  strain) and four times smaller than for the 2D solution (SAAB Global Design Method).
- The standard deviation is  $380 \mu$  strain for the 2D solution and  $260 \mu$  strain for the 3D solution
- The 3D solution shows large discrepancies with the experimental data only for small strain levels

However, systematic differences between the 3D solution and the experimental data were found which have not been satisfactorily explained. Identified sources for this uncertainty are experimental scatter, damage formation and to a lesser degree discretisation errors. Fig. 4.4.49, which compares a photoelastic fringe pattern and the calculated maximum shear stress also indicates the accuracy obtainable when 3D analysis is used.

A critical question is if a good agreement between calculated and measured strains at gauges located 4 mm from the hole boundaries surfaces, as demonstrated above, is a sufficient condition for the stresses/strains near the bolt-plate contact surfaces to be accurately predicted too. The answer to this question depends on the size of the modelling error, which might be critically large for simplified global models. When the splitting method is employed, the discretisation errors can be made vanishingly small, at least for kinematically linear conditions. However, extensive damage formation near the bolt holes, which is presently not included in the mathematical model, might render the 3D splitting solutions less useful for prediction of joint failure.

These validation activities constitute a systematic and scientific approach to a better understanding of the predictive capability of composite joint failures for joints of real-life complexity.

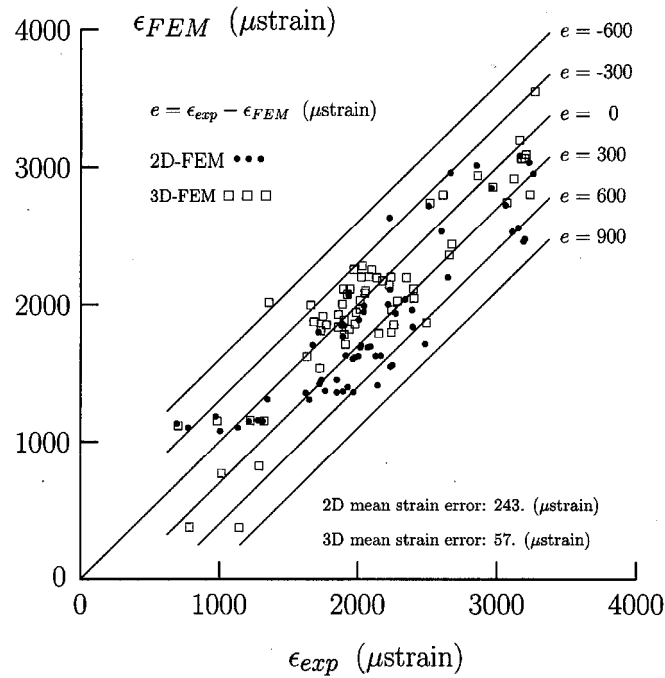


Figure 4.4.48 Scatter plot of calculated and measured strains at strain gauges near bolts in six single-lap specimens. Load is +250 kN

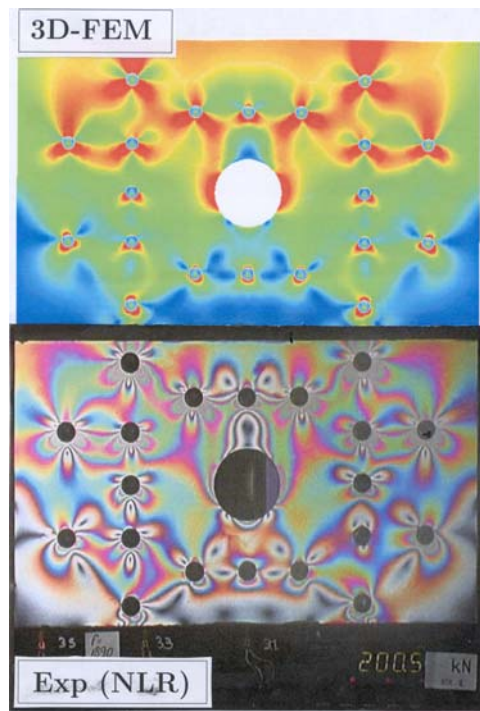
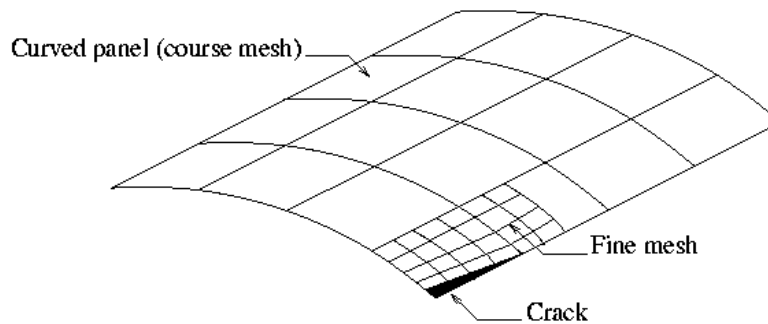


Figure 4.4.49 Comparison of calculated and experimental data for a single-lap specimen with one bolt removed

### Task 4.3 SMR

In this task SMR, collaborating with CIRA and the NLR, worked on different methods for global-local coupling. Based on a report by CIRA (D4.3-1), a method for coupling local 3D models with global shell methods was chosen and implemented. The developed global-local coupling was later evaluated by CIRA in combination with their progressive damage approach.



**Figure 4.4.50 Example where parallel global-local coupling is desirable**

As described above in QinetiQ’s Task 4.3 work, global-local modelling can be performed “in series” i.e. separate global and local models. However, in some cases, small details may have an impact on the global structure. In such cases it is desirable to integrate the local model directly into the global model (“parallel” method). An example of a situation where such integration is needed is the curved panel with a crack on one edge, shown in Fig. 4.4.50. When this panel is loaded in compression, the crack can have a large influence on the buckling behaviour and maximum loading of the global structure.

After discussions with CIRA, SMR decided to implement methods to couple a global shell mesh to a detailed shell or volume mesh.

In general, coupling of meshes is a complicated task, and is a topic of current research. In order to be able to apply it to any mesh, multi-node interface elements are developed, which use higher-order polynomials to follow curved edges. However, in aerospace engineering, shell elements and relatively simple geometries are often used. Considering the problems of interest, the following assumptions can be made. First, the global models are thin-walled structures, described by shell theory. Second, use can be made of four-node (linear) shell elements. These assumptions allow the connectivity between the coarse and the fine mesh to be expressed by means of linear constraints, because the displacement field along the edge of a linear shell element is a linear relation between the two nodes on this edge.

The developed global-local coupling allows the inclusion of detailed 3D volume models in a large global 2D shell structure. The integration avoids the use of separate models and creates an interaction between the global and local model without an iterative procedure.

Using the state-of-the-art direct sparse solver described in Task 4.2, the difference in computation time between the shell and shell-volume model was found to be negligible, except for the contact analysis.

The global-local coupling technique was evaluated by using the DA benchmark structures. Due to time constraints, delays in the delivery of the global MSC.Nastran models from NLR (which had to be corrected), and cancellation of the FE work by the NLR, only the temporary skin repair and the permanent skin-stringer repair were evaluated. During the introduction of the local models into the permanent skin-stringer repair, SMR discovered problems in the MSC.Nastran model. It was then decided to study the different steps of the global-local modelling in detail based only on the temporary skin repair structure. Further analyses could not be performed by SMR due to time and financial constraints.

Fig. 4.4.51 shows the DA benchmark structure without local models. Fig. 4.4.52 shows a slice of the model including a detailed 3D model of one of the bolts.

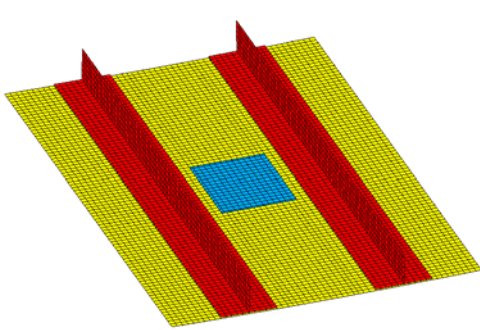


**Figure 4.4.51** DA-BM-1-T global model

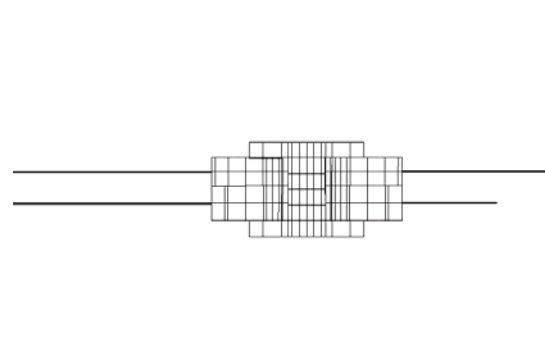


**Figure 4.4.52** 3D local model of bolt inserted into global benchmark structure

As outlined below, CIRA implemented their damage model in a new *progressive damage element* in B2000, with SMR's support. The original implementation by CIRA had been done with user-defined routines in ANSYS. By integrating the progressive damage directly in the FE solution procedure, CIRA aimed, among other things, to seriously reduce the computation time of the simulations. SMR provided the support for this implementation and the algorithms involved. After discussions with CIRA, it was decided to use the penalty method for contact, as already implemented by CIRA, instead of the newly developed Lagrange-multiplier method, in order to avoid the introduction of an additional iteration loop.

For the progressive damage equations to be evaluated inside the element routine, the Cauchy stresses need to be computed at each step of the non-linear analysis. The element used by CIRA is an eight-node total Lagrangian volume element based on the theory by Bathe. SMR modified the element routine to:

1. Compute the strains per layer
2. Compute the stresses (2<sup>nd</sup> Piola-Kirchhoff) in the material base system
3. Convert the PK2 stresses to Cauchy stresses

Finally, additional work was carried out to generate parameterised meshes in the B2000 input format for volume and shell meshes around a hole and to generate the mesh for a bolt. This allows for faster modelling of the local model. The code for these parameterised models was transferred to Airbus Deutschland to assist their developments in Task 2.4.

### **Task 4.3 CIRA**

CIRA was involved at the start and the end of Task 4.3. The first CIRA contribution was to give a preliminary overview of the different techniques to couple global and local models (D4.3-1). Both “series” and “parallel” methods were described. Though series methods can reduce CPU time, a strong interaction between the global and local models was recommended, to take into account the effect of detailed local results on global structural behaviour.

The second contribution was the development of a new *progressive damage element* in the B2000 FEM code, and on the validation of the global-local technique developed by SMR in progressive damage analyses.

In D4.3-6, the three-dimensional progressive damage ANSYS FEM model, introduced in Task 4.2, was implemented with substantial modifications as a new progressive damage element in B2000. As proof of the effectiveness of the developed numerical tool, the numerical results from a full 3D model of a notched composite panel, in terms of deformed shapes, force-deflection curve and progression of damage were compared with experimental and numerical results from the literature. The agreement between experimental/numerical results from the literature and the numerical results obtained with the 3D model was very good.

Next, a 2D-3D configuration (using the global-local technique developed by SMR) of the notched panel was numerically analysed (see Fig. 4.4.53). The 2D and 3D elements were joined by means of the global-local technique developed by SMR within Task 4.3. The two different models (full 3D and 2D-3D) were compared in terms of load-displacement curves (see Fig. 4.4.54) and damage progression in each ply (see Fig. 4.4.55), giving almost identical results.

In conclusion, the combined use of global-local coupling with damage modelling in the local model has been demonstrated. The method shows great promise as an effective way to reduce the amount of disk space and CPU cost required for analyses of large structures with progressive damage procedures. Finally, the implementation of the progressive damage approach into a new element in B2000 resulted in large gains in computational efficiency compared to implementation as a user subroutine in ANSYS.

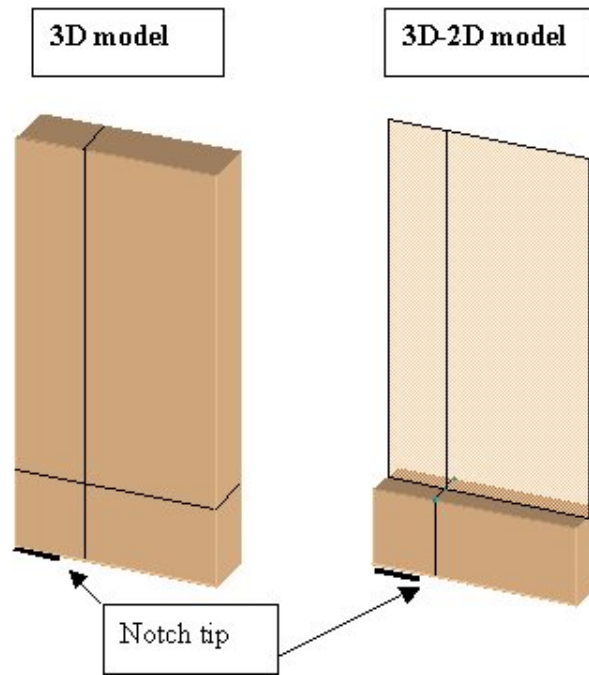


Figure 4.4.53 Schematic Representation of the 3D and 2D-3D models

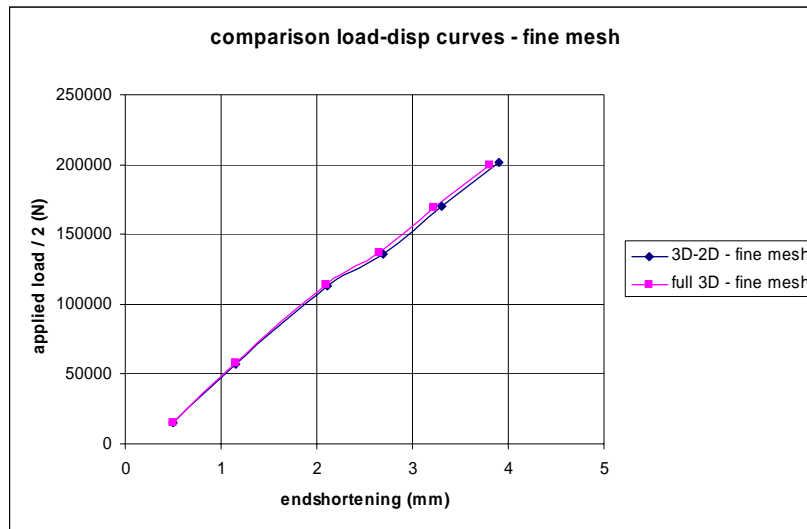
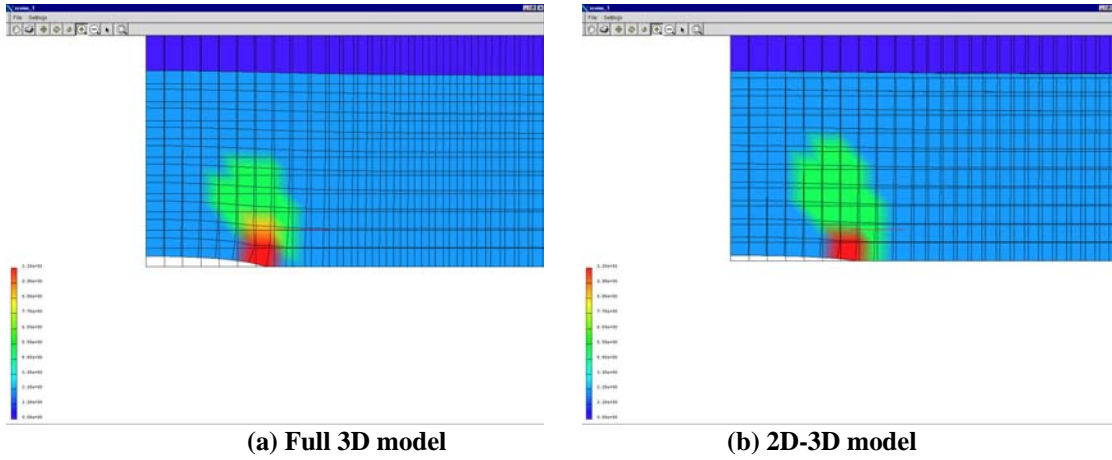


Figure 4.4.54 Applied tensile load versus displacement: comparison between 3D and 2D-3D models



**Figure 4.4.55 Numerical progression of damage in the 45° plies of the notched panel – 3D and 3D-2D models**



## 2.4.4 Task 4.4 Parameter Studies

In this task, ULIM, CIRA, KTH and FOI performed further development and/or validation of their techniques developed in Tasks 4.1 - 4.3.

### Task 4.4 ULIM

ULIM's activities in this task were:

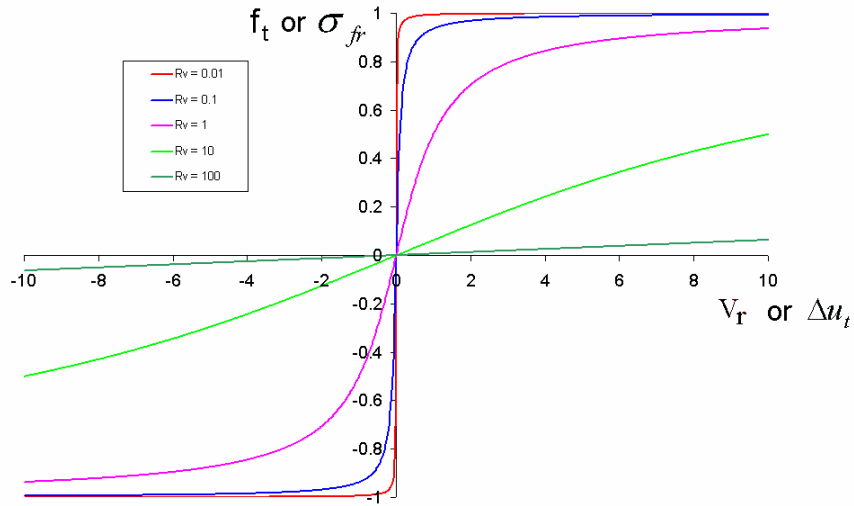
1. A study on the effects of friction in bolted joint models
2. A study of the ULIM *double-lap* multi-bolt joint with variable clearance
3. A study of the BOJCAS *Multi-Bolt Benchmark* (BAE-BM-2C) using 3D FE for comparison with the global methods of WP 2.
4. Further development of BOLJAT. This was not planned in the work programme but was deemed desirable.

In ULIM's study of friction, two models of friction available in MSC.Marc, were evaluated for their ability to:

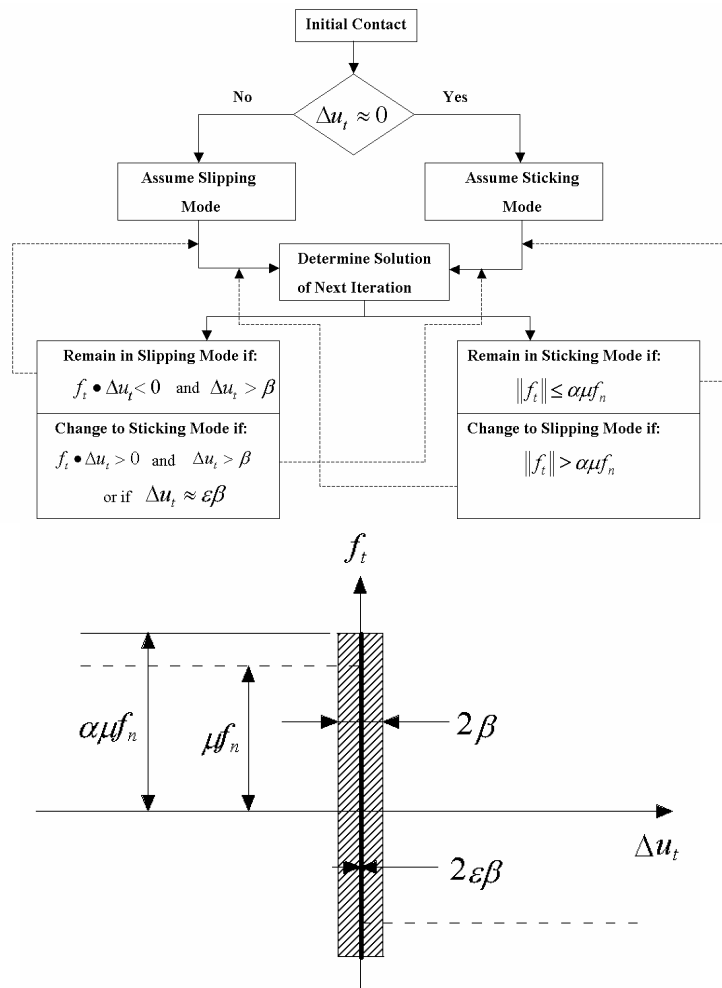
- a. successfully model friction effects in ULIM's torqued specimens in WP 5
- b. successfully match effects on stress distributions around the hole, previously reported (in 2D models) in the literature

The classical friction law due to Coulomb, widely known by all engineers as a relatively simple law, is not in fact simple to implement numerically, because it contains a discontinuity; namely the friction force always opposes the motion that all other forces are attempting to effect, and hence the friction force changes sign each time the direction of motion changes. Such a discontinuity makes it difficult to obtain converged solutions. For this reason, implementations in FE codes are approximations to the classical friction law. In MSC.Marc (typically of many codes) there are two implementations. The names in the MSC.Marc documentation are somewhat confusing, so we will refer to them here as the "Continuous Model" and the "Discontinuous Model". The two models are illustrated in Fig. 4.4.56. Briefly, the continuous model approximates the discontinuity by a continuous function, which can be considered as a smoothed step function. A parameter  $R_v$  controls how closely the true (discontinuous) step function is approximated. The closer the step function is approximated, the better the agreement with the classical friction law, but the more difficult it is to get a converged solution. This model is quite easy to use and get converged results for, so is popular with analysts. A point to note is that, unlike the classical law, there is no differentiation between static and kinetic friction; there is *always* some slipping, no matter how low the applied forces.

The discontinuous model is truly discontinuous, involving a series of IF-THEN statements to determine which regime the model is operating in. The convergence difficulties are handled by a "dead-zone", inside which "sticking" occurs, i.e. static and kinetic friction *are* differentiated. It is often more difficult (without some adjustment of parameters) to obtain converged solutions with this model, so it perhaps is not as popular with analysts.



(a) Continuous friction model



(b) Discontinuous friction model

Figure 4.4.56 The two friction models available in MSC.Marc

An extensive study was carried out on use of these two models for modelling the fully torqued single-bolt specimens in ULIM's test programme. The various parameters in these models were examined for their effects on the results, and the best match possible to the experimental results was obtained with each model. Fig. 4.4.57 shows the final results for the Continuous model. The joint modelled is a high (C4) clearance joint. There are thus three regions in the load-deflection curve:

- An initial high slope, no slip region, where applied load is resisted by static friction
- a transition region during which slippage occurs with no bolt-hole contact (due to the large clearance), so the load is resisted by kinetic friction forces only
- A final region after bolt-hole contact occurs, where the load is resisted by bolt-hole contact and friction

It can be seen that reducing  $R_v$  provides a better match of the initial (static friction) region (as would be expected from Fig. 4.4.56(a)). However, the force in the transition region becomes too high – adjusting the friction coefficients any further does not help the overall match. In addition, reducing  $R_v$  any lower than 17% leads to instability.

Fig. 4.4.58 provides some more insight into the apparently stable solution when  $R_v=17\%$ . It shows the contact normal stress, contact friction stress and the ratio of friction to normal stress (shown multiplied by ten so as to be visible on the graph), for a node located at the shear plane near the bolt. The ratio of friction to normal stress should of course equal the coefficient of friction (also shown) once the joint begins to slide. It can be seen that the contact normal stress remains fairly constant throughout the analysis. The contact friction stress rises in an unstable manner from an initially low value until it stabilises for a period before dropping off again. The ratio of friction to normal stress approaches but never quite reaches the actual friction coefficient value of 0.45, and indeed falls off towards the end of the simulation. This model, being at the cusp of stability, is the closest one can get to the ideal step function behaviour of the Coulomb friction law, with this Continuous model.

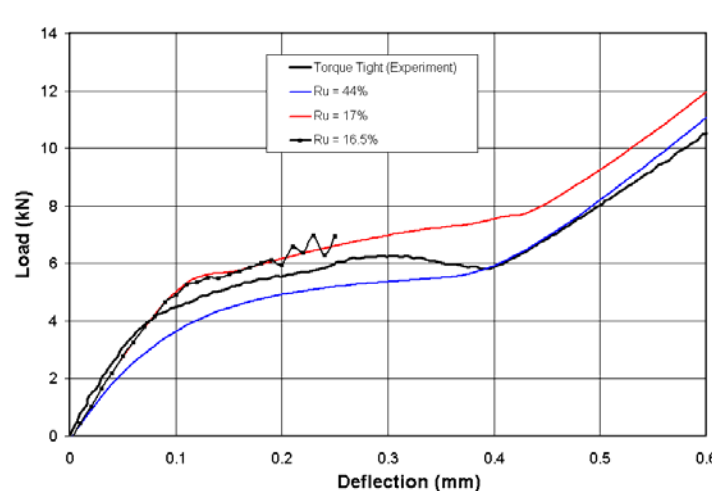


**Figure 4.4.57 Effect of  $R_v$  parameter in the Continuous model on the load-displacement curve**

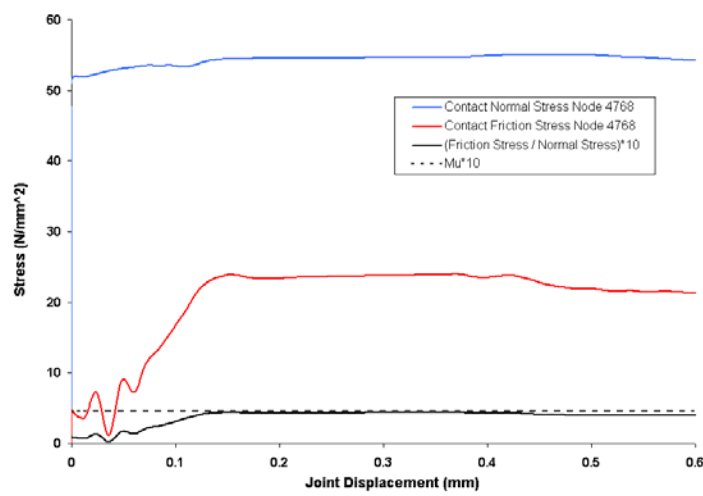


**Figure 4.4.58 Normal and friction stresses plotted against joint displacement for a node located at the shear-plane using the Continuous friction model**

Fig. 4.4.59 and 4.4.60 show the corresponding graphs for the Discontinuous model. The overall match of the load-deflection curve in Fig. 4.4.59 is better than for the Continuous model (especially the sharp transition from sticking to slipping at around 0.08 mm deflection). Equally importantly, when the solution is examined more closely in Fig. 4.4.60, it can be seen that the solution from the Discontinuous model is stable, and the ratio of friction to normal stress perfectly matches the friction coefficient. The Discontinuous model thus appeared to be preferable for matching the experimental load deflection curves of the joints from WP 5.

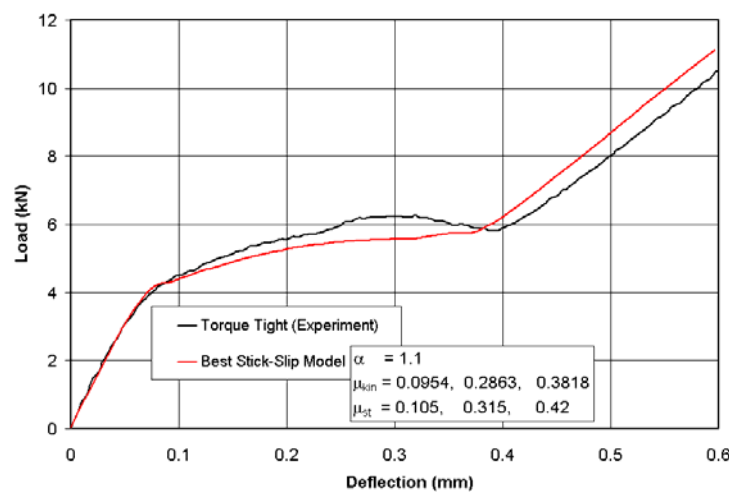


**Figure 4.4.59 Best Stick-slip model vs. Experiment**

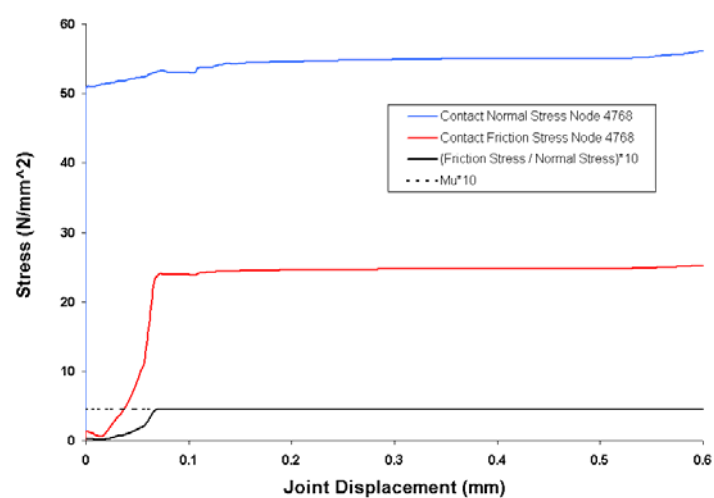


**Figure 4.4.60 Friction Stresses plotted against joint displacement for a node located at the shear plane using the Discontinuous friction model**

Load-deflection curves are not the only measure of interest when modelling bolted joints however. At least as important is the stress distribution around the hole, since this will determine failure of the joint. It was not possible to measure this experimentally, but results from analytical models are available in the literature. A classical study by Hyer et. al. [13] on a pin-loaded, orthotropic plate (with infinite dimensions) predicted the effects on the stress distribution shown in Fig. 4.4.61. In summary, the effect on the *radial* stress is to shift the peak away from the bearing plane ( $\theta = 0$  position), and also to increase the area over which radial stress exists (i.e. the contact area). The effect on the *circumferential* stress is to increase the peak value slightly (as well as slightly altering the position of the peak), and to greatly depress the circumferential stress at the bearing plane to the point where it actually changes sign. Finally, friction introduces a *shear* stress that is not present in the frictionless case.

ULIM modelled this pin-loaded plate, using a very large but finite w/d ratio, and an extremely fine (2D) mesh. The Continuous and Discontinuous friction models in MSC.Marc were used to try to predict the effects due to friction.

Fig. 4.4.62 shows the results for the radial stress from the Continuous model, for varying values of  $R_v$ . As can be seen, it was found to be impossible to match the results from Hyer et. al.'s analytical model, using the Continuous friction model. For low  $R_v$  values, the solution is unstable, while for very high values, the solution approaches the no friction case (as would be expected from Fig. 4.4.56(a)). There is no value of  $R_v$  that even comes close to giving a reasonable match of the analytical result. The same findings were found for the circumferential and shear stress.

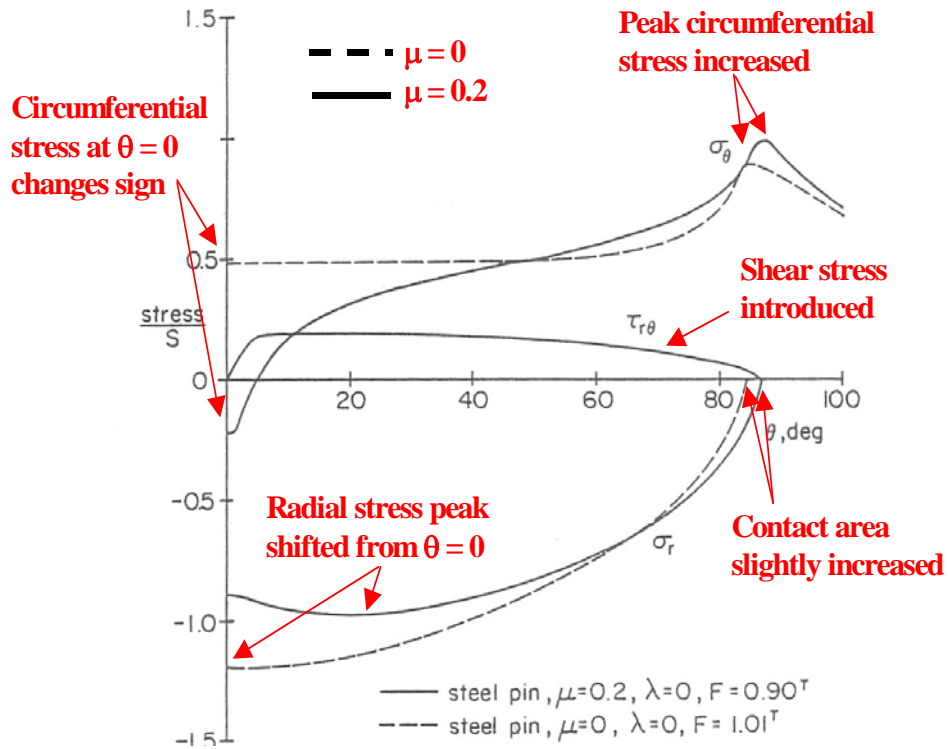


Figure 4.4.61 Effects of friction on hole stress distributions in a pin-loaded orthotropic plate (from Hyer et. al. [13] – annotations by ULIM)

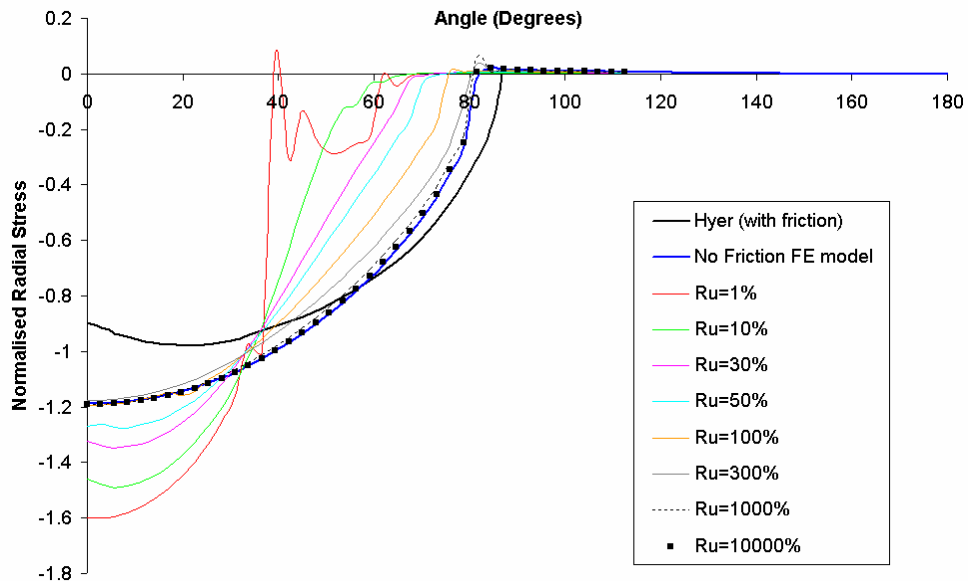
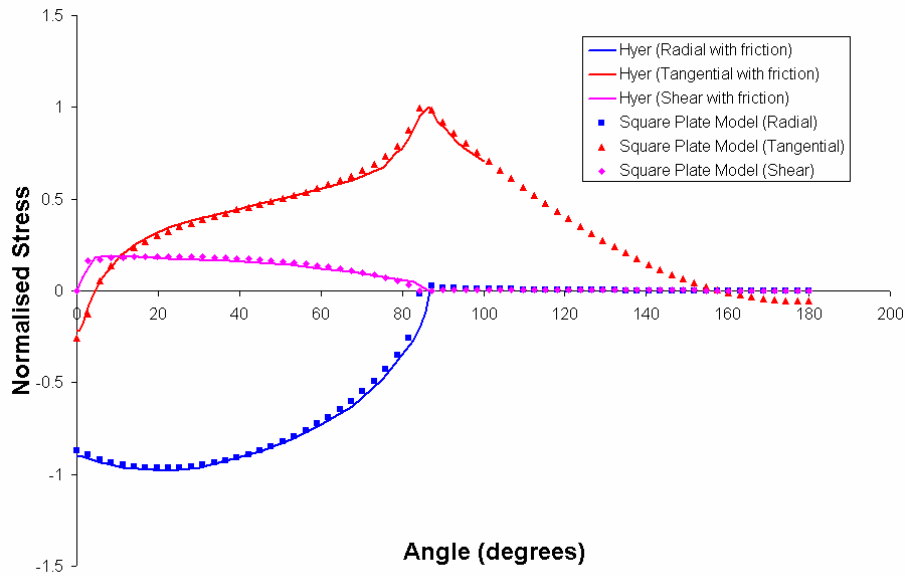


Figure 4.4.62 Comparison between square plate model and Hyer et al's solution [13] for the friction case using the “Continuous” model

In contrast, Fig. 4.4.63 shows that a near perfect match with the analytical results was obtained using the Discontinuous model. This, combined with the findings on the load-displacement curves of the joints tested in WP 5, led to a recommendation to use the Discontinuous friction model (called the “Stick-Slip” model in the MSC.Marc documentation) when modelling bolted joints.



**Figure 4.4.63 Comparison between square plate model and Hyer et al’s solution [13] for the friction case using the “Discontinuous” model**

ULIM next performed a study on their *double-lap*, multi-bolt joint tested in WP 5 (see Fig. 4.5.3 in WP 5 for the joint geometry). A new module for BOLJAT was created for this. A range of clearance cases, similar to (but not identical) to those in Table 4.4.5 above were examined. Fig. 4.4.64 shows the longitudinal strain ( $\epsilon_{xx}$ ) distribution in a C1\_C1\_C1 joint loaded in tension. Generally, the distribution is as expected. Looking closely, it is evident that, in the vicinity of the holes, the strain varies through the thickness of each plate, which is due to bolt bending. Clearly this cannot be captured by 2D modelling.

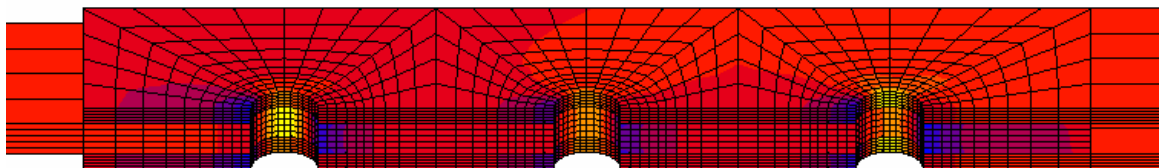


**Figure 4.4.64 Distribution of  $\epsilon_{xx}$  in C1\_C1\_C1 joint under tensile loading**

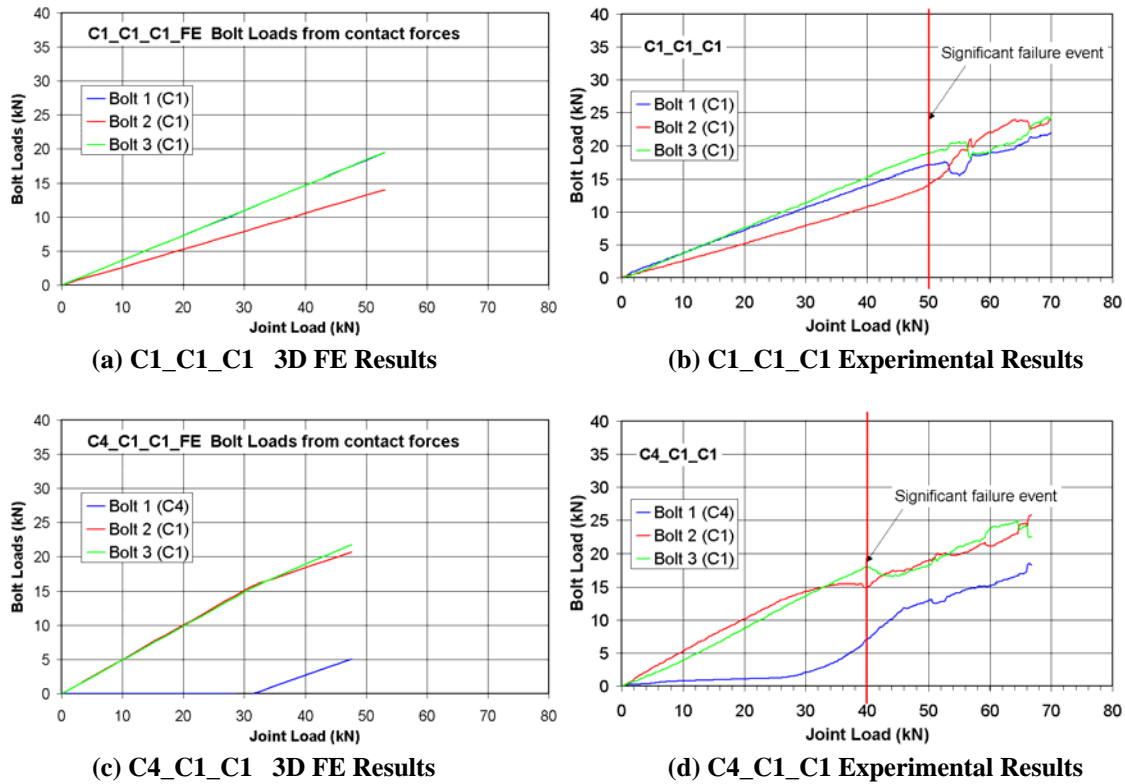


**Figure 4.4.65 Bolt load distribution for ULIM double-lap joint obtained from 3D FE and experimentally from strain gauges**

Fig. 4.4.65 shows the bolt load distribution obtained from 3D FE compared to that obtained experimentally using strain gauges (see WP 5) for two different clearance cases. The agreement is very good. The strain gauge results showed an interesting sensitivity to an initial significant failure event (well before final failure). It was determined that this event was bearing failure at the highest loaded hole. This event is of interest for limit load design of aircraft.

From personal communication with Airbus Deutschland the mean value of the bearing yield allowable for this material and lay-up is 519 MPa. Shown in Table 4.4.12, is the total joint load at which the bearing stress in one or more holes first reached 519 MPa, in the models and in the experiments. This is a measure of how accurately the models could predict *initial* joint failure (through bearing failure of one of the holes). It can be seen that the prediction is within 6% in four cases, and is only seriously in error in one case (the C3\_C3\_C1 case). The poor result in this one case may be due to a failure to centre the bolts in the holes in the experiment, which means that the conditions in the model do not match those in the experiment (i.e. not a failure of the model itself). Thus it can be said that a 3D linear model like this, without any damage analysis, can predict quite well the *initial* failure of multi-bolt joints.



Joint	Joint Load at which bearing stress in one hole reached 519 MPa (kN)		Difference
	3D FE	Experiment	
C1_C1_C1	47.5	45.5	+4.4%
C1_C3_C1	35	34.6	+1.2%
C1_C1_C4	36.3	34.5	+5.2%
C2_C1_C1	43.7	40.5	+7.9%
C4_C1_C1	36	38.2	-5.8%
C3_C3_C1	26	33	-21.2%

**Table 4.4.12 Prediction of initial joint (bearing) failure load**

Having validated the models against experiment, the models were used to gain insight into the internal load and stress/strain distributions in the joint. Firstly, on loading the C1\_C1\_C1 joint in tension and compression, it was found that the joint is stiffer when loaded in compression than when loaded in tension. The joints were not loaded experimentally in quasi-static compression, but during fatigue tests, they were loaded to an equal load level (in load control) in tension and compression (i.e.  $R = -1$ ). It was found that the initial (i.e. before damage starts) peak stroke in compression is less than in tension, so the joint is evidently stiffer in compression than in tension, which agrees with the models. Note this result was repeated in all tests and all models. Free body diagrams and stress distribution plots at several sections in the joint (presented in D4.4-1) explained the reasons for this effect.

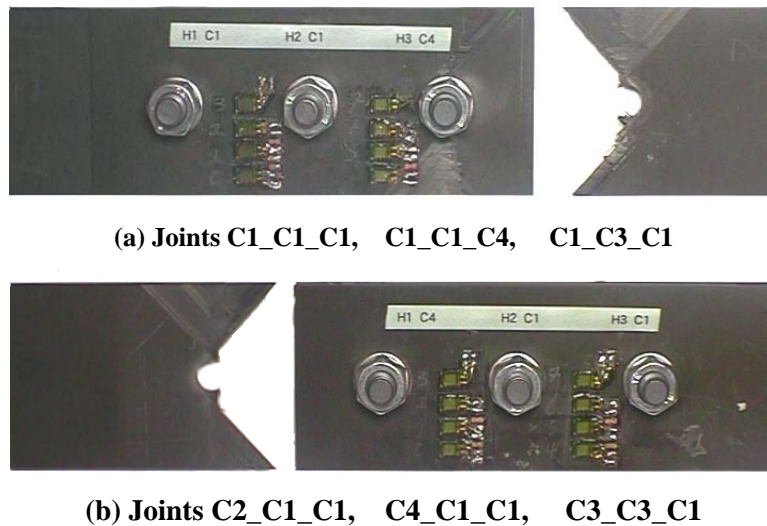
It was noted in WP 5 that the *ultimate* failure mode of the double-lap joints tested quasi-statically in tension was affected by clearance. In fact, as illustrated in Fig. 4.4.66, the joints fell into two groups:

1. Group A: Joints with a neat fit in Hole 1 failed by net section failure of the splice (outer) plates at Hole 3
2. Group B: Joints with a clearance fit in Hole 1 failed by net section failure of the skin (middle) plate at Hole 1

To investigate the reasons for this, the C4\_C1\_C1 and C1\_C1\_C4 joints were examined further. Fig. 4.4.67 shows the NET section free body diagrams and stresses at Hole 1 in the skin and Hole 3 in the splice plate for the C4\_C1\_C1 joint. The load taken by the splice plate section is half that taken by the skin section, but the splice plate is half as thick as the skin, so the *average* stress is the same in both. However, the distribution in the splice plate is more severe (higher peak near the hole). This would indicate that net section failure should occur in the splice plate. But in fact, failure occurred in the skin!

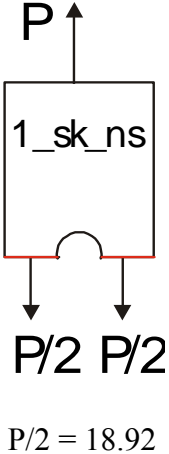
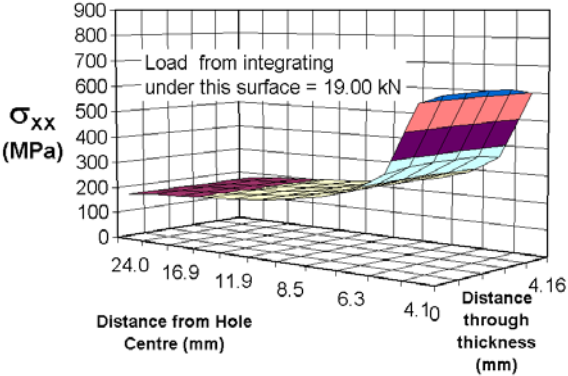
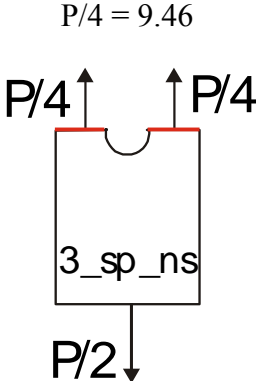
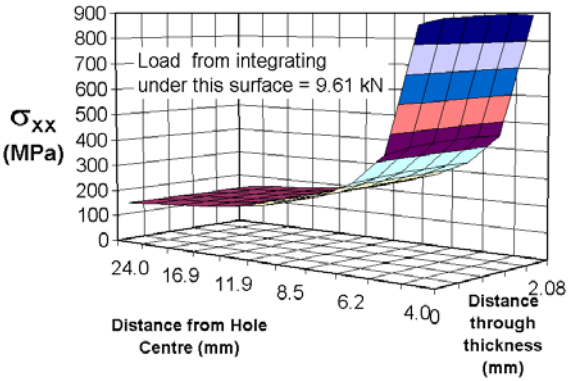
The reason for this is shown in Fig. 4.4.68, which shows the GROSS section free body diagrams and stresses for the loads and stresses *bypassing* Hole 1 in the skin and Hole 3 in the splice plate for the same C4\_C1\_C1 joint. It can be seen that, because of the very low load taken by Bolt 1 (due to the clearance in that hole), the *bypass* stress around Hole

1 in the skin is very high. In comparison, because Bolt 3 takes a much higher load than Bolt 1 in this case, the *bypass* load around Hole 3 in the splice plate is much lower. Thus the *bypass* stresses are more critical than the *net section* stresses in determining the location for net section failure. This finding that net section stresses do not by themselves determine net section failure is interesting, and illustrates that failure involves a complex interaction between bearing and bypass stresses. Note that the exact opposite to all of the above occurs in the C1\_C1\_C4 joint (not shown).



**Figure 4.4.66 Ultimate failure modes of double-lap joints with variable clearances**

Finally, returning to the differences between tensile and compressive loading, Fig. 4.4.69 illustrates that even when the total bolt loads are the same in tension and compression, the *distribution* of radial stresses around the hole is different. In compression, the contact area (particularly in Holes 1 and 2) is clearly less than in tension, and the stresses are thus distributed over a smaller area, resulting in a larger peak at the centre (bearing plane). The reason for this is most likely that in compression the holes are widened laterally, thus moving away from contact with the bolt, whereas the opposite happens in tension. From this, we would predict that bearing failure should occur at lower loads in compression than in tension. Again, we had no quasi-static, compressive data to confirm this, but Fig. 4.4.70 shows that in fatigue, failure initiated on the compressive stroke before initiating on the tensile stroke, which agrees with the modelling prediction. This result was repeated in almost all fatigue tests, the only exception being tests at the highest load (with very short fatigue life).

<p><b>FBD section loads</b> (<math>P_1 = 2.00\text{kN}</math>, <math>P_2 = 17.74\text{kN}</math>, <math>P_3 = 18.03\text{kN}</math> obtained from contact forces on hole)  (NOTE: Low load taken by Bolt 1)</p>	<p><b>Section stress distributions</b></p>
<p><b>Net section, SKIN, Hole 1</b></p>  <p><math>P/2 = 18.92</math></p>	<p><b>Net section, SKIN, Hole 1</b></p> 
<p><b>Net section, SPLICE PLATE, Hole 3</b></p> <p><math>P/4 = 9.46</math></p> 	<p><b>Net section, SPLICE PLATE, Hole 3</b></p> 

**Figure 4.4.67 Skin (middle) plate and splice plate NET section free body diagrams + stress distributions from 3D models – C4\_C1\_C1 joint loaded in TENSION with joint load = 37.83 kN**

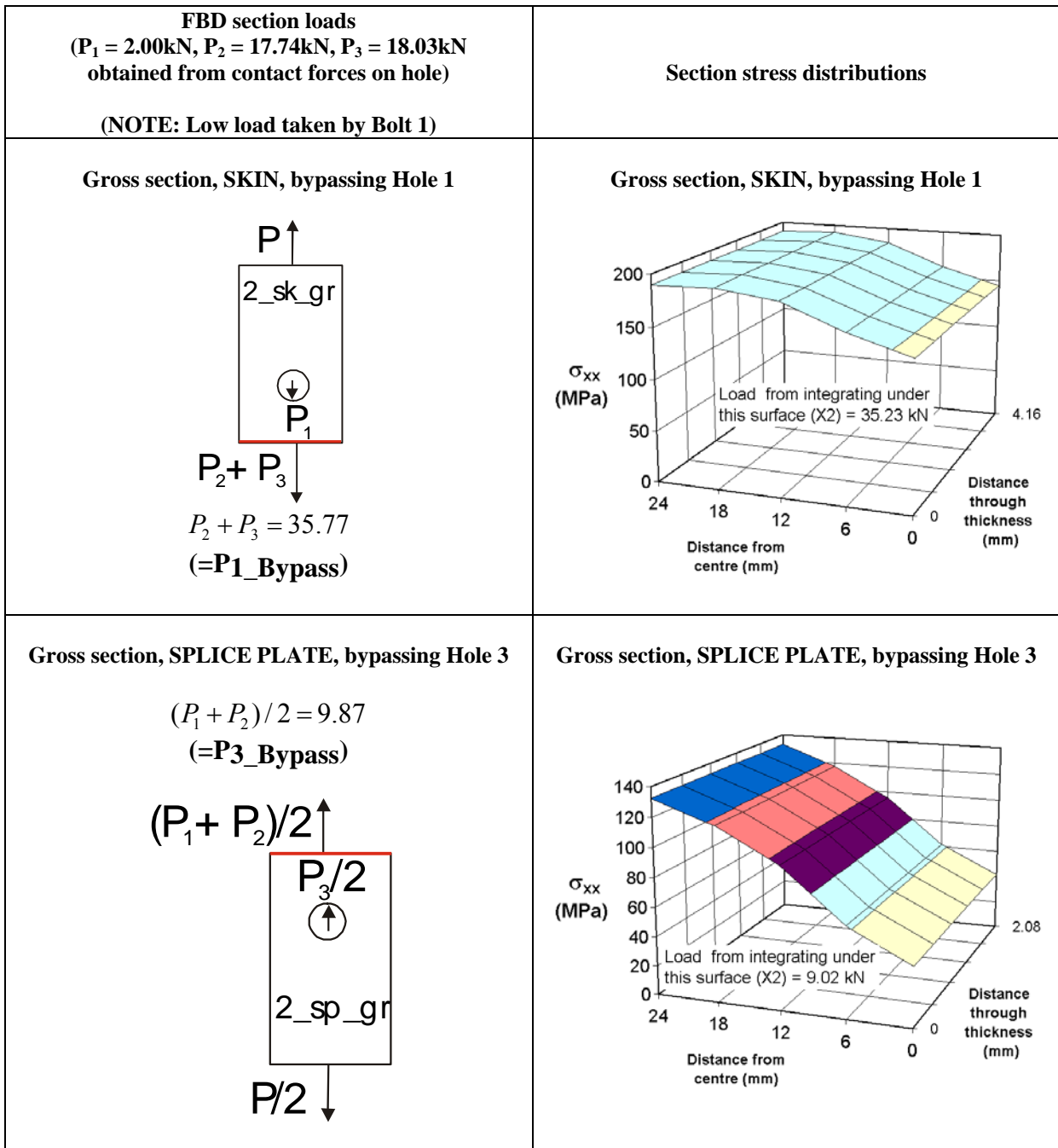


**Figure 4.4.68 Skin (middle) plate and splice plate GROSS section free body diagrams + stress distributions from 3D models – C4\_C1\_C1 joint loaded in TENSION with joint load = 37.83 kN**

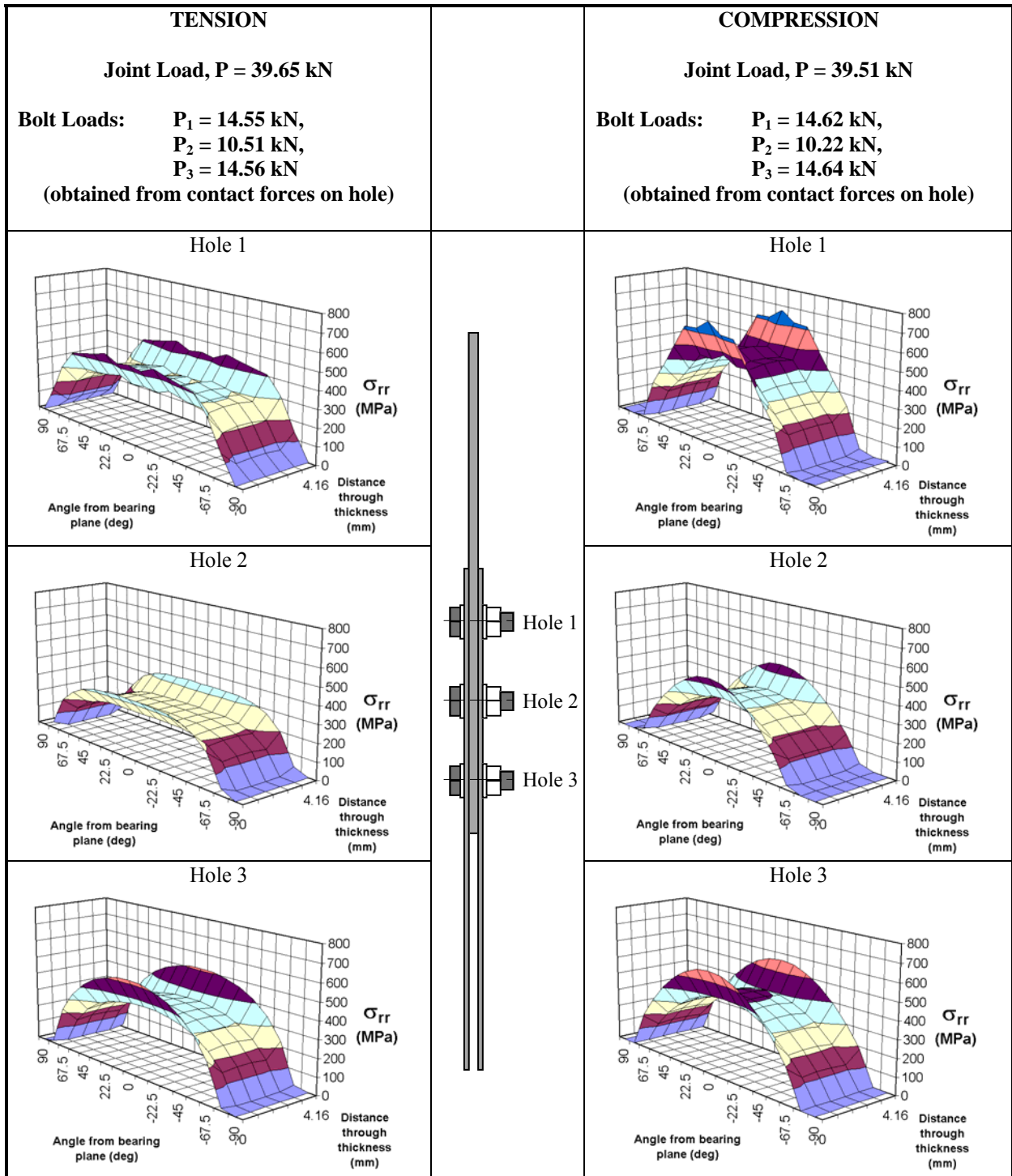


**Figure 4.4.69 C1\_C1\_C1 joint, Radial stress distributions in skin under TENSILE and COMPRESSIVE loading**

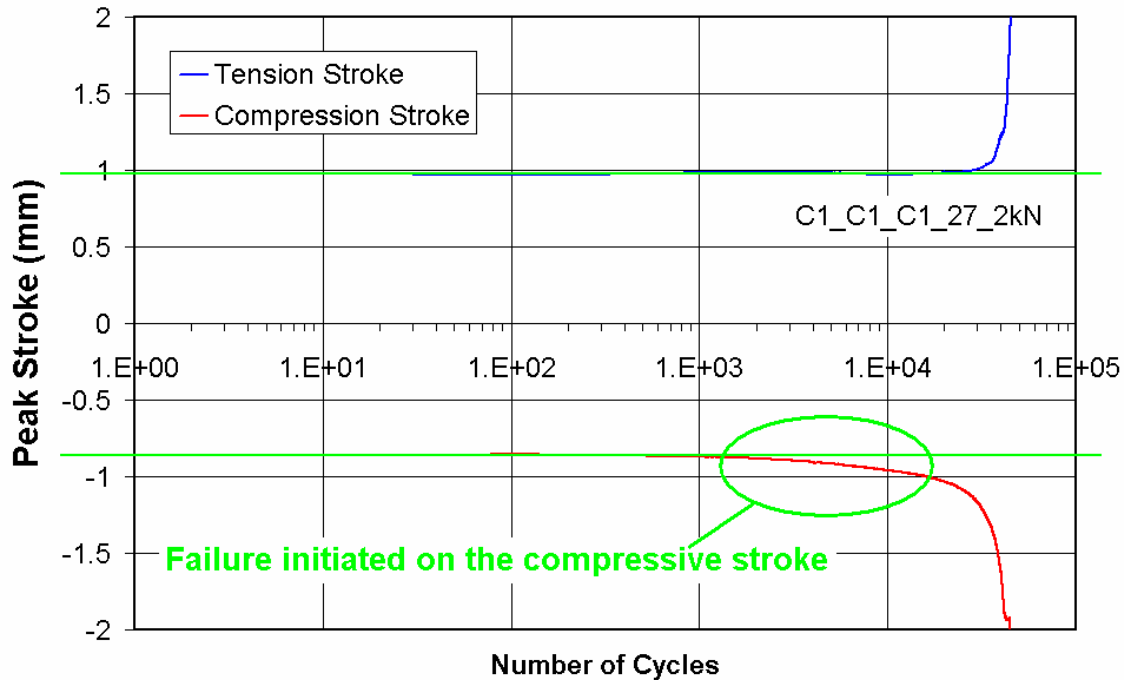
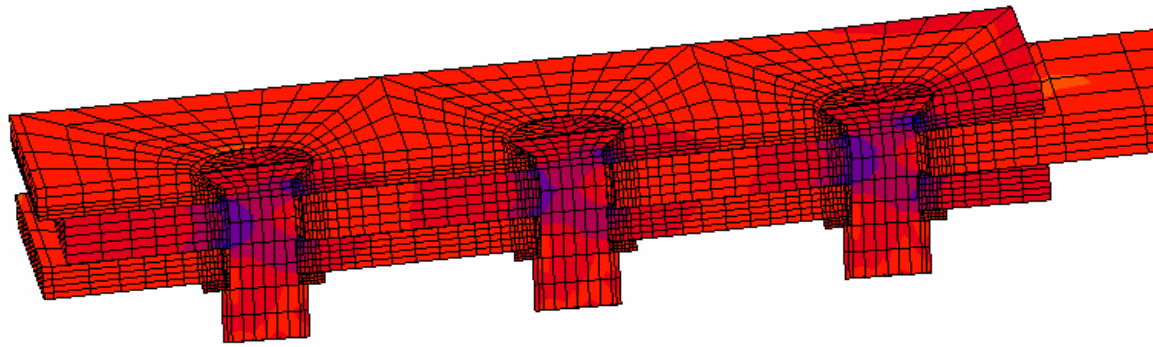


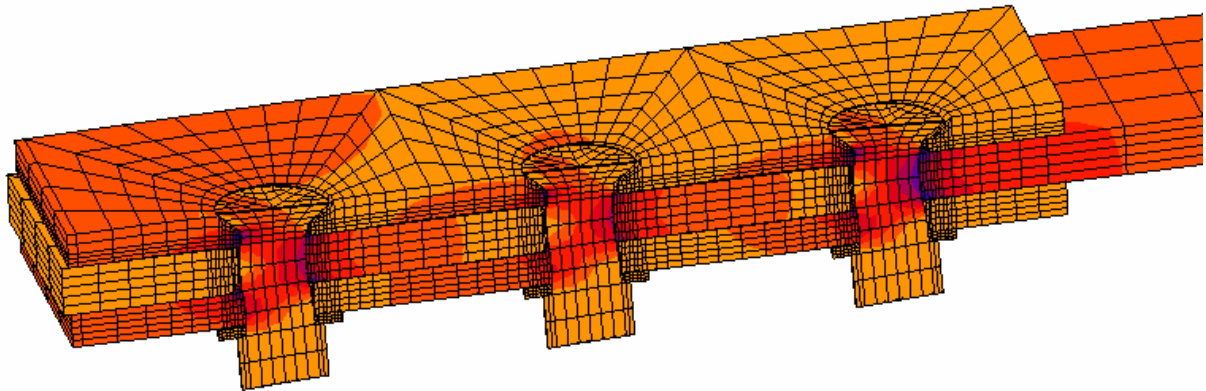
**Figure 4.4.70 Peak tensile and compressive strokes during fatigue loading at +/-27 kN (R=-1)**

ULIM's final study in Task 4.4 was on the *Multi-Bolt Benchmark* (BAE-BM-2C). Fig. 4.4.71 shows the 3D model loaded in tension and compression, from which some phenomenological differences are evident, e.g. the tendency of the splice plates to separate at the end of the joint, when loaded in tension.

The stiffness and load distribution in the joint under tensile and compressive loading were determined and were already presented, along with results from global models of other partners, in Fig. 4.2.49 above. Note that this joint was also found to be stiffer in compression than in tension, and after obtaining some extra data from AUK (not given in their deliverable) this was found to be borne out by experiment. As a further validation of the model, strains from the model were compared with strains measured experimentally by AUK (see Fig. 4.3.3 above for strain gauge positions). Fig. 4.4.72 shows the results from AUK's deliverable D3-7, and from ULIM's 3D FE model, when the joint was loaded in compression. The results for the model are only shown up to about 200 kN applied load (above which non-linear behaviour due to joint damage occurred in the experiment, which cannot be captured in this model since damage is not included). The comparison between experiment and model is very good.



(a) Tension Loading



(b) Compression Loading

Figure 4.4.71 Deformed shape and stress distributions of one end of the *Multi-Bolt Benchmark* joint, loaded in tension and compression

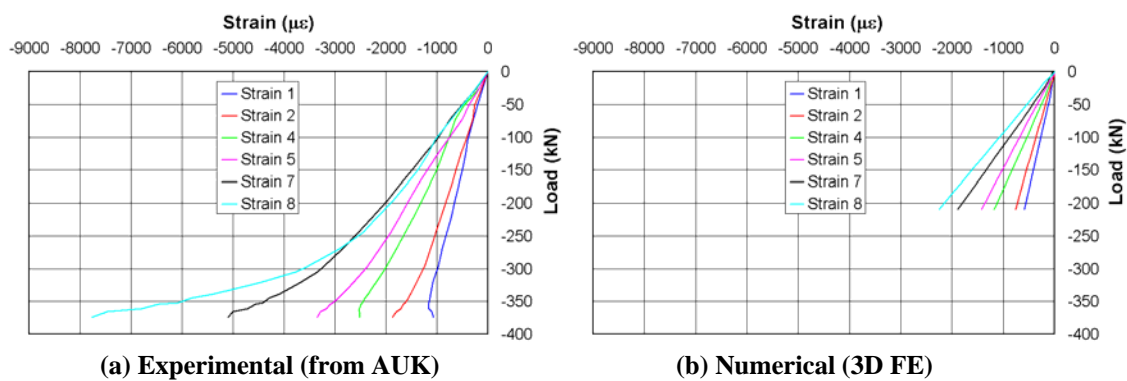


Figure 4.4.72 Strain gauge results for *Multi-Bolt Benchmark*

Finally in WP 4, ULIM made significant modifications to BOLJAT and released Version 2.0 of the software, together with a revised user's manual (given the number D4.1-7). This second release was not required in the BOJCAS Description of Work, but as part of the modelling work in Task 4.4, new features were added, so this second release was delivered to make these features available to the BOJCAS partners.

The major changes since Version 1.0 were:

- Implementation of double-lap joints (four new modules for single and three-bolt joints, with countersunk and protruding-head bolts)
- Different thicknesses and material properties allowed for each plate (all modules)
- Different bolt sizes allowed in a single joint (all modules)
- Isotropic as well as orthotropic material properties allowed for each plate (allowing e.g. composite-metal joints to be modelled)
- User selection of full or half models (using symmetry boundary conditions)
- Elimination of manual steps required after exiting BOLJAT before submitting the analysis job (except for one step, needed if “analytical” contact is to be used).

Airbus Deutschland showed particular interest in using BOLJAT, but did not have MSC.Patran running in an MS Windows environment. To facilitate compilation of the BOLJAT routines in AD's UNIX environment, a non-disclosure agreement was signed between AD and ULIM, and ULIM then provided the source code to AD. BOLJAT has now been successfully compiled on AD's system.

#### **Task 4.4 KTH**

KTH's objective in Task 4.4 was to use the developed FE-model in Task 4.1 to investigate the importance of selected parameters with respect to load transfer, out-of-plane deflection and longitudinal stiffness.

The baseline joint geometry was shown in Fig. 4.4.19. Several variations on this joint, outlined in Table 4.4.13, were tested in WP 5 and modelled here. Configuration 4 was considered to be the reference joint, and in all other configurations, one parameter has changed compared to this reference joint. The varied parameters were clamping force, free length of the plates, row spacing, thickness of the aluminium plate and fastener diameters. The most important results are summarised here, both in terms of influence of the investigated parameters and how well the FE-model agreed with the experiments.

Load distribution between the fasteners was significantly affected by the stiffness mismatch between the member plates. In the reference joint configuration, which utilised a thick aluminium plate and a thin composite plate, the load was clearly shifted towards the outer bolts i.e. bolts one and four in Fig. 4.4.19. Reducing the thickness of the aluminium plate resulted in the load being shifted to the inner bolts.



Conf. [Nr.]	Torque [Nm]	Row sp. [mm]	Length [mm]	Alu. thi. [mm]	Bolt Type	Diam [mm]	Nr. of Specs.
4	6	32	376	8	P.H.	4x6	13
5	6	32	296	8	P.H.	4x6	3
6	6	32	376	8	P.H.	4x6	3
7	6	20	376	8	P.H.	4x6	3
8	6	32	376	4	P.H.	4x6	3
9	6	32	376	8	C.S.	4x6	3
10	6/14	32	376	8	P.H.	3x6+1x8	3
11	6/14	32	376	8	P.H.	2x6+2x8	3
12	6/14	32	376	8	P.H.	1x6+3x8	3
13	6/14	32	376	8	P.H.	4x8	3

**Table 4.4.13 Varied parameters in the KTH experimental programme**

Out-of-plane deformation of the joints (illustrated in Fig. 4.4.73) was not affected by the diameters of the fasteners or by the clamping force. Reducing the length of the member plates resulted in smaller deflection. Using a thin aluminium plate increased the deflection, mainly due to increased bending of the aluminium plate. Joints with small row spacing were slightly more deformed compared to the reference joint.

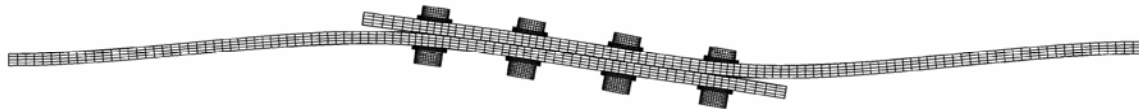


**Figure 4.4.73 Out-of-plane displacement for KTH joint configuration 8**

Longitudinal stiffness of the joints increased when the diameters of the fasteners were increased or when the lengths of the plates were reduced. Reducing the clamping force made the joint less stiff for small loads when the load transfer was dominated by friction between the plates. Once contact was established between the bolts and the plates, the stiffness was comparable to the reference joint. Using a thin aluminium plate or reducing the row spacing created a less stiff joint.

Bolt load distribution was in general not predicted accurately by the FE-model. This was due to unknown hole eccentricities present during testing which had a large impact on the results. For the cases where the hole positions in the FE model were adjusted to resemble the experiments (as described in Task 4.1 above), good agreement was achieved.

Total load transferred by the bolts and by friction between the plates were predicted accurately by the FE model. Longitudinal stiffness and out-of-plane displacements were also predicted accurately by the FE-model.

#### **Task 4.4 CIRA**

In this task the three-dimensional FE model introduced in Task 4.2 and validated for the single-lap joint, protruding-head bolt configuration in D4.2-4 was tested against different geometrical configurations in order to analyse the full range of parameter variations in the test series of WP 5. Both single-lap joints with protruding and countersunk bolts, and double-lap configurations were considered in the analyses.

For the single-lap specimens the behaviour in terms of deformed shapes was found to be in agreement with the experimental results from CIRA tests of WP5 (Fig. 4.4.74). The contact penetration distributions gave proof of the effectiveness of the penalty parameter chosen for computations as can be seen in Fig. 4.4.75. The penetration was found to be very small if compared to the maximum displacement of the joint.

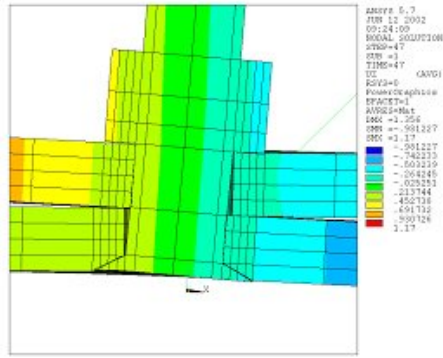
Analysing the force-deflection curves, the proposed approach was found able to simulate the behaviour of the single-lap joint from the beginning of the loading process up to the final failure. Only for the joints with composite/aluminium interface, was there a slight overestimation of the failure load due to the lack of plasticity in aluminium plates.

The progression of damage for all the configurations was predicted very well as demonstrated by the comparison with the experimental NDE results (see Fig. 4.4.76).

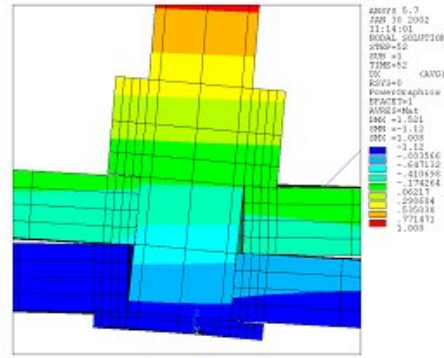
Finally the strain distributions were found in good agreement with the strain gauge readings for all the configurations.

Three double-lap configurations representative of the different failure modes (net tension, bearing and shear-out) were examined by using the developed numerical approach. The results in terms of deformed shapes, contact stress distributions, failure loads, strains and progression of damage (see Fig. 4.4.77) were found to be in excellent agreement with the experimental ones. The numerical tool was capable of simulating the net-tension, bearing and the shear-out failure mode giving realistic distributions of damage and failure loads (see Table 4.4.14).

In conclusion, the numerical tool has demonstrated itself to be fully capable of simulating the effects on the structural behaviour of joints, related to the changes in the selected parameters both for single-lap (bolt type, interface and hole diameter) and for double-lap joints (W/D and E/D).

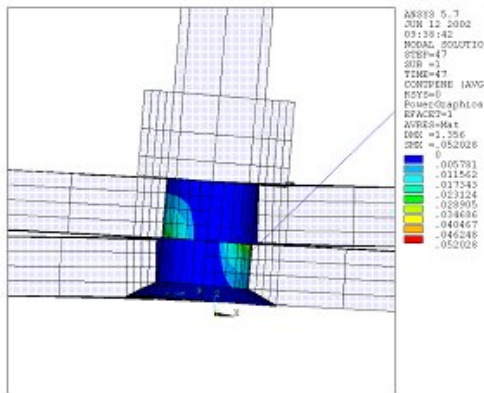


**Configuration 5**  
(Comp/comp -D=6.4 mm – countersunk)

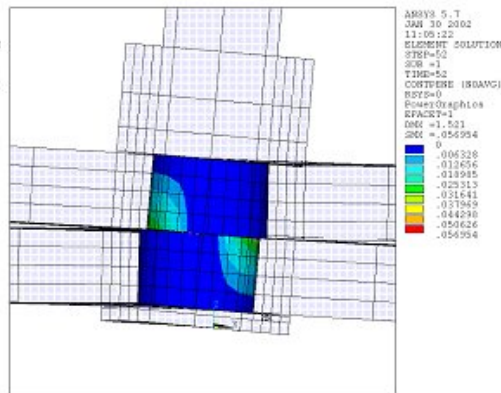


**Configuration 6**  
(Comp/comp -D=6.4 mm – protruding)

**Figure 4.4.74 Deformed shapes – (cut views) single-lap CIRA specimen Configuration 5 and 6**



**Configuration 5**  
(Comp/comp -D=6.4 mm – countersunk)



**Configuration 6**  
(Comp/comp -D=6.4 mm – protruding)

**Figure 4.4.75 Contact penetration – (cut views) single-lap CIRA specimen Configuration 5 and 6**

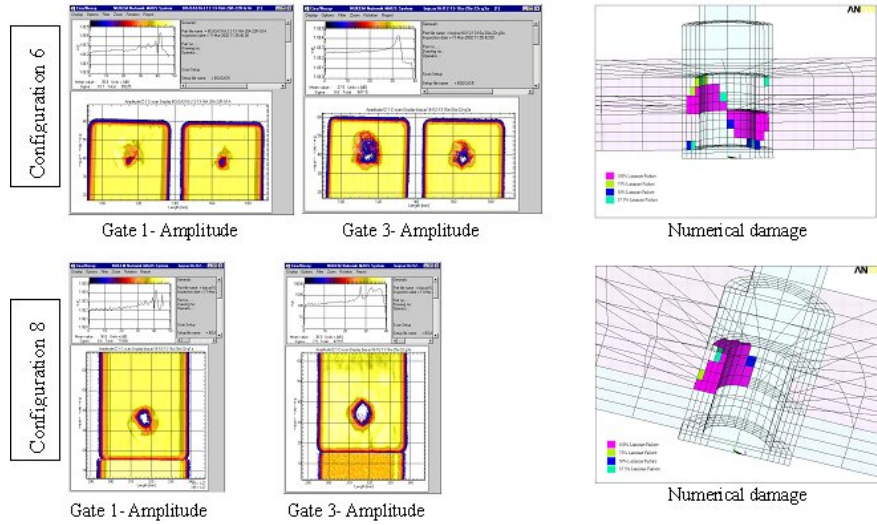


**Figure 4.4.76 Progression of damage - comparison between experimental and numerical results – Configuration 6 and 8**

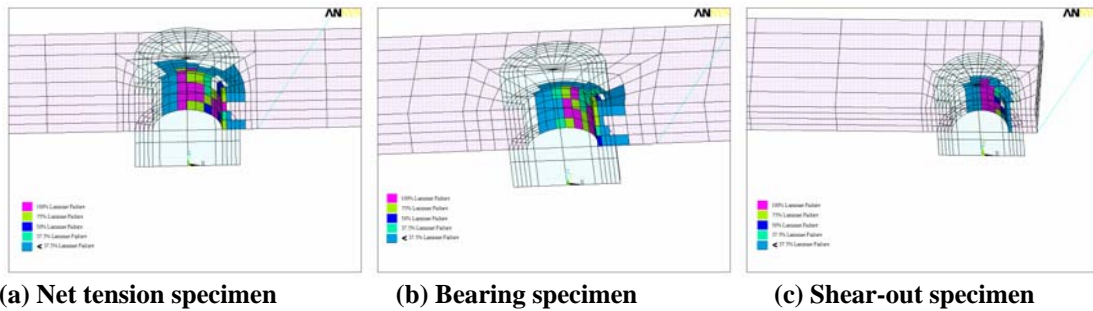


**Figure 4.4.77 CIRA double-lap specimen - Percentage of broken plies in elements at collapse – shear-out, bearing and net-tension failure mechanisms**

Specimen Number	Conf.	Numerical failure load (KN)	Last step Failure load (KN)	Real failure mode
52	8	21,761	24,09	Net-tension
53	8		24,07	Net-tension
54	8		25,02	Net-tension
25	9	23,860	26,74	bearing
26	9		24,18	bearing
27	9		26,38	bearing
28	10	13,836	14,21	Shear-out
29	10		13,98	Shear-out
30	10		13,85	Shear-out

**Table 4.4.14 Comparison between numerical and experimental failure loads for the analysed double-lap CIRA specimens**

#### Task 4.4 FOI

The main objectives of FOI's work in Task 4.4 were to:

- Perform an optimisation study of the SAAB benchmark test specimen in which the objective is to find the (minimum) number of bolts (and indirectly the corresponding optimal bolt pattern).
- Determine damage tolerance properties of the optimal design with respect to lost bolts, i.e. determine the (statistical) fatigue life and load bearing capacity due to loss of one or several bolts in randomly selected positions

Such types of analysis require very efficient analysis tools. Thus, following on from developments in Task 4.3, further novel capabilities were developed in Task 4.4.

Firstly, a meshless method for bolt modelling on the global level was developed. When numerous 3D solutions are needed, as in statistical analysis, optimisation etc., one *cannot* afford to frequently re-analyse the global problem for various bolt patterns or damage patterns. Hence, a method was needed where a single global analysis is sufficient for deriving the  $10^4$  to  $10^6$  virtually exact non-linear solutions that might be required. A kind of meshless solution algorithm (on the global analysis level) to be used together with the splitting scheme was developed (see deliverable D4.4-4A).

Secondly, a system for optimisation, statistical and damage tolerance analysis of bolted joints was developed. Fig. 4.4.78 gives an overall view of the analysis tools created. The upper left corner in the figure illustrates a very simple *global domain* (the SAAB benchmark test specimen). Note that bolts and bolt-holes are not explicitly modelled on the global level! The local domains (upper right corner) contain all geometrical details. This made it possible to determine stresses accurately and with control of the error in regions where stresses are singular. By using the meshless bolt strategy the desired complex analysis types could be performed.

Concerning bolt pattern optimisation, one main difficulty is the discrete and non-convex character of the optimisation problem. Hence, several local minima might exist which requires non-standard approaches. However, having access to a fast solver that can solve a bolted joint problem in a very short time, general optimisation methods like genetic algorithms, extensive search algorithms etc. can be afforded for simpler cases. The optimisation procedure developed used a restricted search space where bolt centres  $(x_i, y_i) \in (X, Y)$  where  $(X, Y)$  are discrete sets containing allowable bolt coordinates. The reason for limiting the search space to a fixed set of coordinates is that the computational efficiency can be increased by several orders of magnitude.

A gradient-based optimisation algorithm was used for most of the studies reported in D4.4-4B. Bolts were moved in the fixed grid of allowable bolt locations until an optimum (in most cases a local optimum) was found. Often,  $10^4$  to  $10^5$  full 3D solutions were derived in the process of finding an optimum solution. The novel developments in Task 4.4 made such optimisation studies possible on a modern SMP-computer.

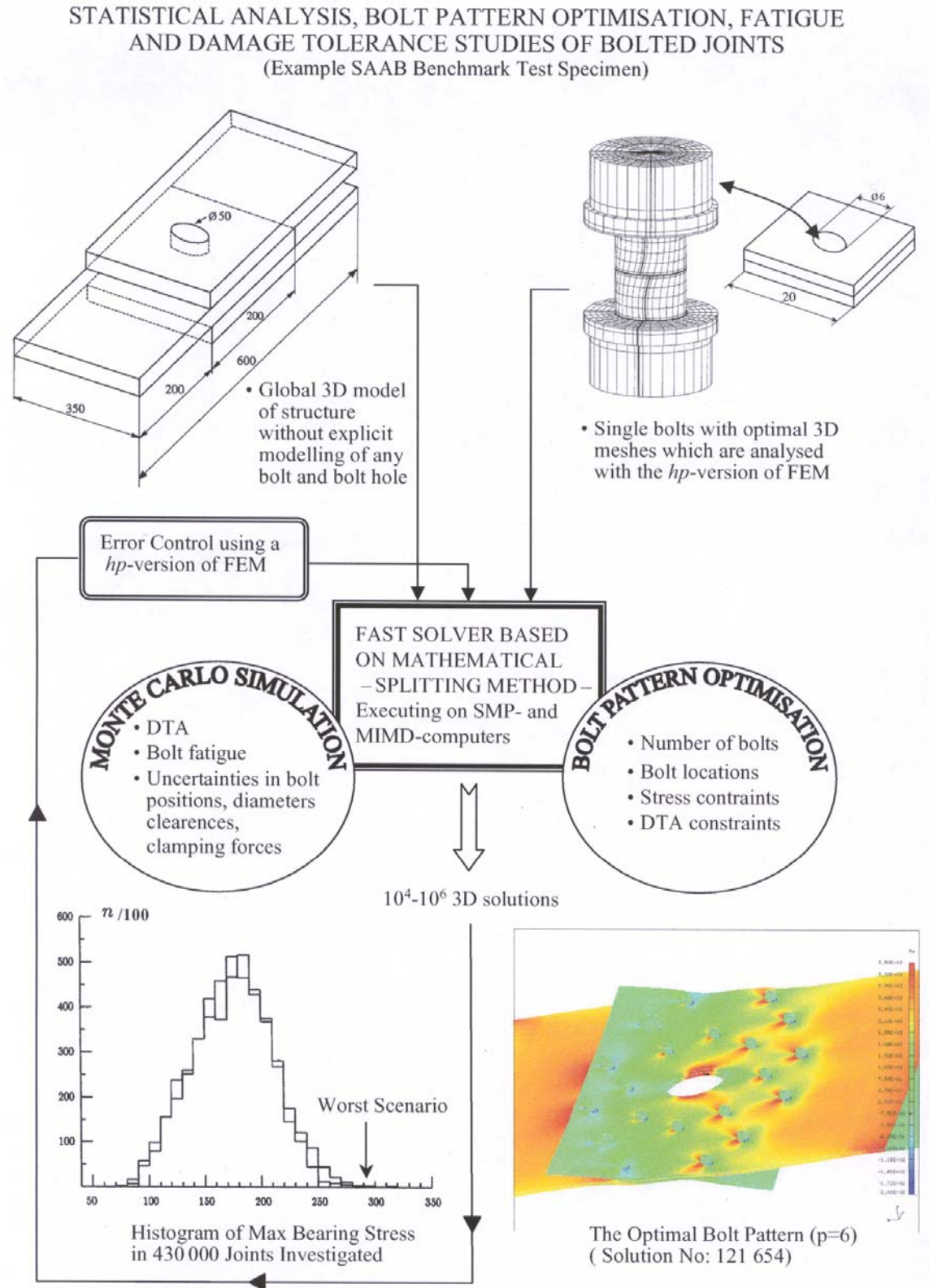


**Figure 4.4.78 Simulation system created in Task 4.4**

The SAAB Benchmark test specimen was considered in several types of optimisation studies. The following design-related questions were addressed in deliverable D4.4-4B:

- how does the number of bolts influence the optimal strength of the joint?
- how does the number of bolts influence the optimal bolt pattern?

A simpler 2.5D bolt model (no bolt head) was used in the optimisation studies. The reason for using the simpler bolt representation was that the general bolt model (see upper right corner in Fig. 4.4.78) has still not been verified for optimisation studies. The simpler 2.5D model used has characteristics that are similar to the structural elements used in the SAAB Global Design Method and the QinetiQ Global Design Method.

To compare joints with different number of bolts  $N$  an optimality index  $\eta_N$  was used:

$$\eta_N = N \cdot \sigma_{rr}^{(REF)} / 20 \cdot \max_{m,n}^{M,N} {}^m \sigma_{rr}^{(n)}$$

where  ${}^m \sigma_{rr}^{(n)}$  is the maximum bearing stress in plate  $m$  at bolt  $n$ .

The feasible bolt pattern closest to Bolt Pattern 1 in the SAAB benchmark test specimens corresponded to  $\eta_N = 0.86$ . The higher the value of  $\eta_N$  the more optimal the configuration.

Optimal bolt patterns were generated for  $N = 12-28$  bolts. Fig. 4.4.79 shows the iteration history for the case of the SAAB benchmark specimen geometry with 28 bolts. The small filled circles mark the start bolt pattern, open circles show bolt locations at each iteration, and the large filled circles the optimal positions maximising  $\eta_N$ . The optimum solution which was obtained after 7 iterations, and solution of 190681 non-linear bolted joint problems, corresponds to  $\eta = 1.10$ .

Results from bolt pattern optimisations using different start solutions (resulting in different local optima) gives a quite clear picture on how the bolt pattern depends on the number of bolts  $N$ . Two characteristic bolt patterns leading to approximately the same optimum  $\eta_N$  values can be observed for the cases with 12-28 bolts. In the first type of pattern all bolts are located in a large single “ellipse shaped” pattern. With increasing  $N$  there is a tendency for the bolts to become more clustered close to the circular hole. The second type of pattern is with the bolts on a roughly straight line parallel to the upper and lower horizontal edges (see Fig. 4.4.79).

Concerning the load carrying capacity as a function of number of bolts, the various optimisation studies reported in D4.4-4B for cases with 12-28 bolts showed that it is possible to find bolt patterns having  $\eta_N$  of order 1.10 to 1.17. The optimum  $\eta_N$  values decreased with increasing number of bolts. The main conclusion is that for the SAAB benchmark joint, the load carrying capacity increases roughly linearly with the number of bolts (if only bearing failure is considered) if optimum bolt locations are used.



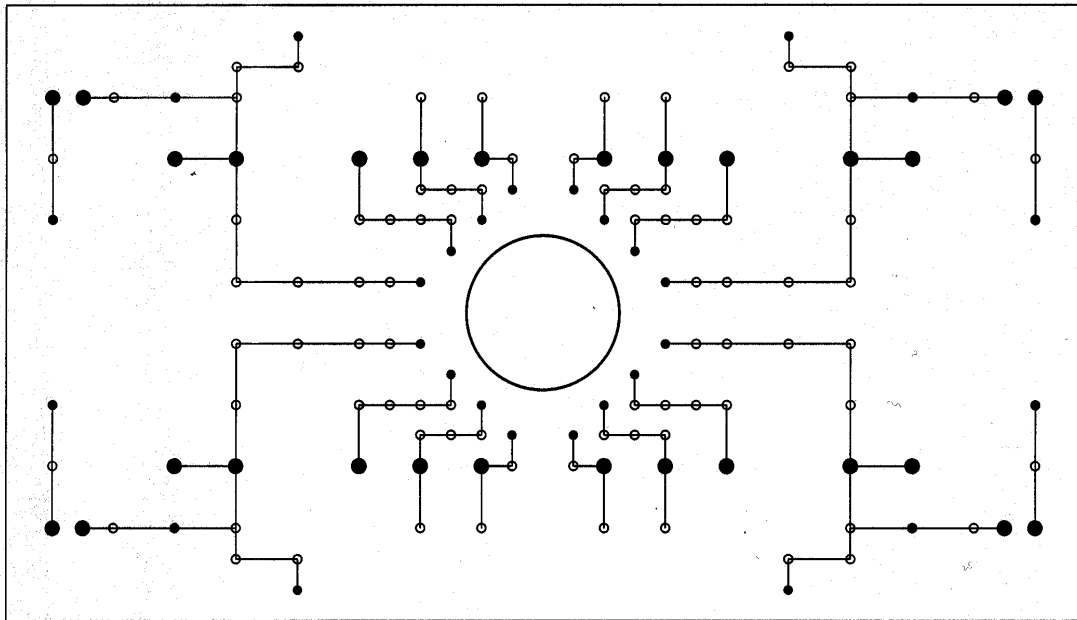


**Figure 4.4.79** Iteration history for the case  $N = 28$  bolts. The start configuration has the bolts on a circle close to the hole boundary. The local optimum found after 7 iterations has  $\eta_N = 1.10$ .

We finally note that only bearing constraints were considered in the optimisation studies. The 2.5D model used is perhaps also too simple. Future application of the computational framework (using full 3D modelling and many more types of constraints) for optimisation might lead to important insight into *design of bolted joints*.

The damage tolerance properties of bolted joints for different number of bolts were investigated in case of loss of one, two and three bolts, respectively, *at arbitrary positions* in the joint.

An extensive search strategy is economically feasible (when the splitting method is used) since  $k$  of the  $N$  bolts in the optimal joint design can be removed in only  $\binom{N}{k}$  different ways. Hence, for  $k = 1, 2, 3$  and for  $N$  bolts originally, only

$$\binom{N}{1} + \binom{N}{2} + \binom{N}{3}$$

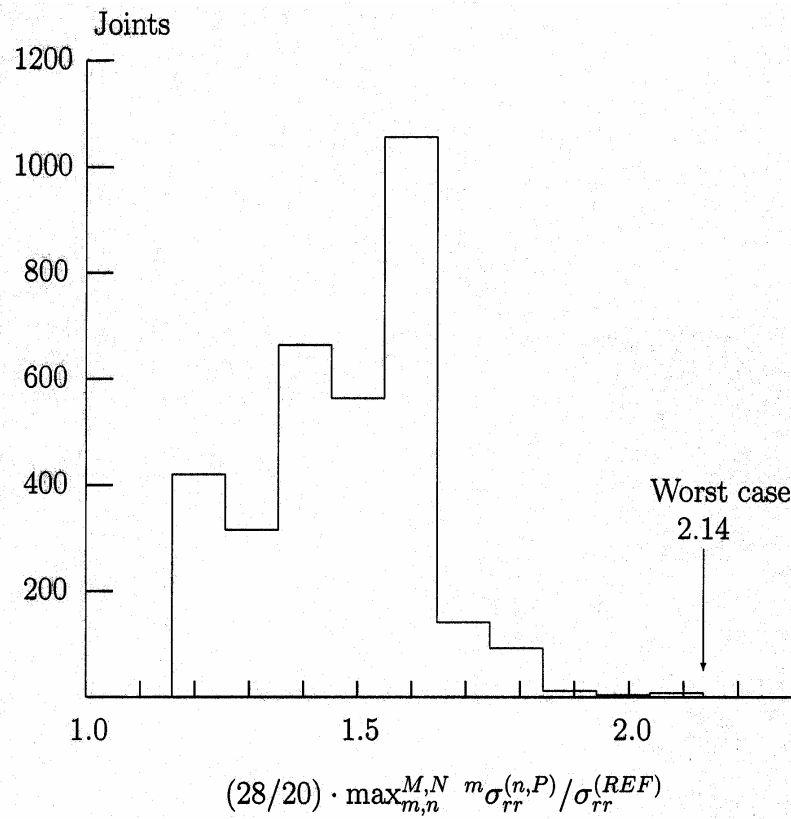
configurations need to be analysed. For  $N = 20$  there are  $20 + 190 + 1140$  cases to analyse. For  $N = 28$  there are  $28 + 378 + 3276$  cases.

Fig. 4.4.80 summarises the 3276 solutions corresponding to loss of three bolts in all possible positions. The optimum bolt pattern shown in Fig. 4.4.79 was considered. The



worst case among all possible positions of the missing bolts corresponds to a bearing stress magnification factor of 2.14. However, the figure also shows that there are very few cases (i.e. damage patterns) that exhibit such high magnification factors. If damage tolerance constraints are included in the optimisation scheme, it seems likely that damage tolerance properties can be very much improved.

As in the case of the optimisation studies, we note that the novel analysis scheme developed might provide useful answers to difficult questions related to design and aircraft safety.



**Figure 4.4.80** Histogram of maximum bearing stress in 3276 joints having  $N=28$  with  $L=3$  (i.e. *three* lost bolts). Undamaged (optimal) bolt positions are shown in Figure 4.4.79.

## 2.5 WP 5: Specimen Structural Testing

In this workpackage, NLR, CIRA, FOI, KTH and ULIM performed experimental tests on composite joint specimens, for generation of basic research data and validation of models in WP 4. SAAB manufactured the specimens for KTH. NLR manufactured the specimens for CIRA.

### WP 5 University of Limerick

ULIM examined the effects of bolt-hole clearance in single and multi-bolt joints. Table 4.4.1 above presented the four clearances that were obtained through the use of four reamers, manufactured to high precision for the project. The clearances ranged from neat-fit to somewhat larger than that permitted in the aerospace industry.

In the single-bolt test series, single-lap joints of the type shown in Fig. 4.4.1 above were tested. This series involved 78 specimens, tested quasi-statically in tension. The chief variable was clearance, but other variables included lay-up, bolt-type, load level and torque level. Some tests were performed to failure, some were performed to percentages of failure and destructively analysed, while others were fitted with strain gauges and photoelastic coatings, and loaded in the elastic range. Purpose-built jigs were built for accurate drilling and reaming of four different size holes, as well as centring of the bolts within the holes.

These tests were reported in D5-10 (Part 1). The chief findings were that clearance caused a delay in load pick-up, reduced joint stiffness (by about 10% in the largest clearance case), and increased strain to failure. The ultimate failure *strength* was not much affected, but the *initial* (first damage) strength was. Microscopy revealed that larger clearance leads to smaller contact areas and higher levels of damage in the laminate. The results have been published in three journal articles [14, 15, 16].

Some further unplanned tests were performed on these single-bolt specimens. After the 12-month progress meeting, a comprehensive study was carried out to investigate the possible causes for the differences between the computed and measured stiffness of the single-bolt, single-lap elastic benchmark. Flat, tensile test specimens, both aluminium and quasi-isotropic HTA/6376, were first strained within their elastic region. Both 50mm and 75mm grips were used, and the response was measured by the stroke transducer in the load frame, by two independent LVDT's placed against the inserts of the grips in the machine, by two extensometers attached to the specimens, and also by strain gauges on the specimens. The strain gauge and extensometer results confirmed that the tensile material properties being assumed for the composite were essentially correct. However, the stroke readings showed clearly that machine stroke cannot be used as an accurate measure of specimen stiffness. In fact the material modulus estimated from the stroke readings was only half the true modulus. Further tests were then carried out on the single-bolt benchmark joint with revised instrumentation, and revised methods of determining the true specimen stiffness were suggested. Results of this study were reported on in D5-10 (Part 1), Appendix A.

The next test series involved multi-bolt, single-lap joints loaded quasi-statically in tension. See Fig. 4.4.2 above for the baseline geometry and Table 4.4.5 for the clearance cases considered. Six joints were tested to failure, and six were tested in the elastic region, using instrumented bolts to determine bolt load distribution. Special purpose jigs were designed for drilling the holes in exactly the right position, and for joint assembly, to allow simultaneous centring of the bolts within the holes, alignment of the instrumented bolts with the loading axis of the joint, and torquing of the bolts to prescribed levels (a complex operation). The instrumented bolts had to be first calibrated using single-bolt joints with different clearances. Fig. 4.5.1 shows one of the assembly jigs and two of the instrumented bolts in position for testing.

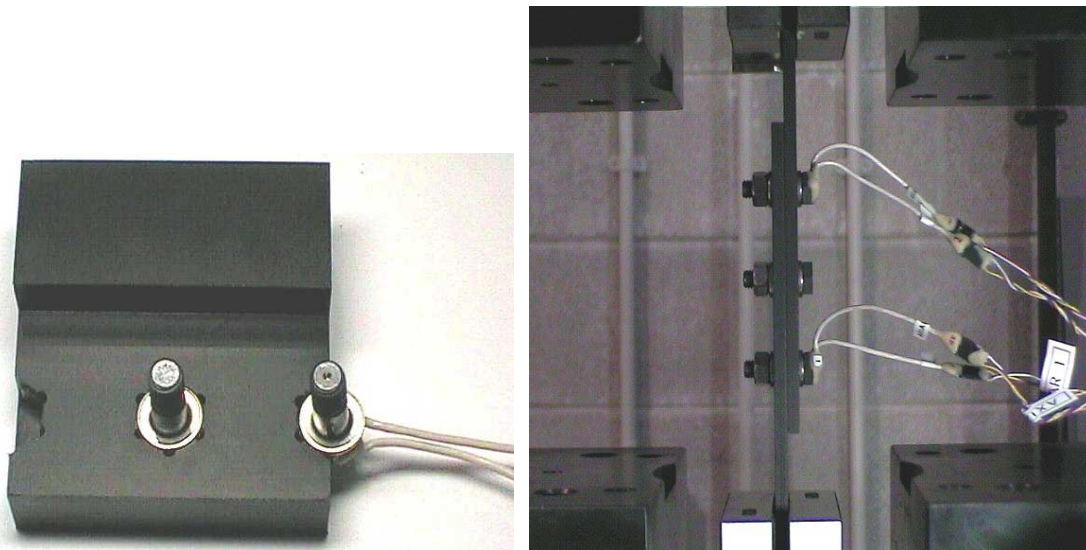


**Figure 4.5.1 ULIM Multi-bolt joint assembly jig + test setup for instrumented bolts**

These tests were also reported on in D5-10 (Part 1). As noted in Task 4.1 above, the chief finding was that clearance can have a significant influence on bolt load distribution in multi-bolt joints (see Fig. 4.4.11 above). For example, the centre bolt in a three-bolt joint is usually considered to be relatively lightly loaded and therefore not in danger of failure. But with a large clearance in one of the outer bolts, the middle bolt picks up additional load. In one joint tested to failure the middle bolt failed (see Fig. 4.5.2).

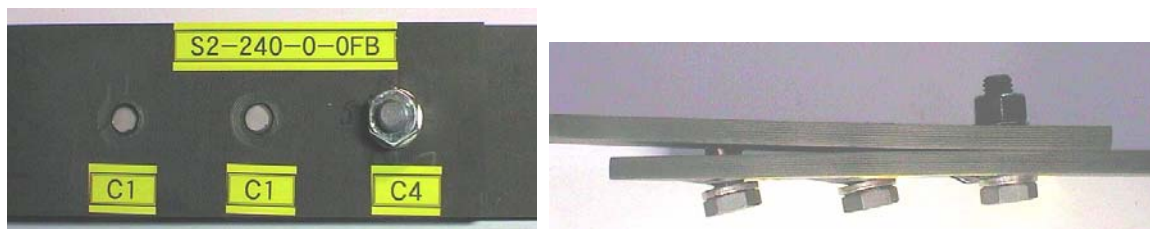


**Figure 4.5.2 C1\_C1\_C4 joint which failed by simultaneous failure of bolts 1 and 2**

Even more interesting though, was the excellent agreement between the instrumented bolt results and the finite element simulations in Task 4.1, which was a validation of both the models and the use of instrumented bolts. Provided great care is taken when using them, instrumented bolts can evidently give excellent information about bolt load distribution. Note that the strain gauge method frequently used with double-lap joints (see next test series) is less valid for use with single-lap joints, since the stress distribution is not constant through the thickness. Instrumented bolts have no difficulty with single-lap configurations. The main *disadvantages* of instrumented bolts are their high cost, the specificity to a single joint configuration (e.g. any change to the joint thickness, requires a new instrumented bolt), and the need to keep the load levels below that which would damage the bolts (cannot test to failure). The results from this study were published in two journal articles [17, 18].

The next series involved six multi-bolt, *double-lap* joints tested under quasi-static loading (reported in D5-10, Part 2). See Fig. 4.5.3 for the baseline geometry and strain gauge locations (for load distribution measurement). Each joint had a different configuration of bolt-hole clearances (Table 4.5.1). Several tests were performed in the elastic range, and then the joints were tested to failure. Fig. 4.5.4 shows a typical distribution of strain across the width, as measured by the strain gauges – the strain is assumed to be symmetric about the hole centre. Clearly the distribution is not constant across the width, and the variation across the width depends on the joint, the position in the joint, and the applied load. This is the reason why the method used by AUK in WP 3 (Fig. 4.3.3) did not work very well. The strain distribution in Fig. 4.5.4 can be integrated across the width to give the average strain at the section, and from this, the load crossing this section can be determined. From this, the bolt loads can be deduced.

As was noted in Task 4.4, the load distributions varied considerably among the six different clearance cases, and the results compared very favourably with 3D FE analysis. Thus, for *double-lap* joints, the strain gauge method used here works very well. Compared to instrumented bolts, the strain gauge method is cheaper and (consequently) can be used in tests to failure. It is also more flexible for application to joints of different thicknesses etc.

Also noted in Task 4.4 was the fact that, with regards to ultimate failure *mode*, the joints split into two groups of three, one group having a neat-fit in Hole 1, the other not. The reasons for this were discussed in Task 4.4. The ultimate failure *load* was found to be very little affected by clearance. However, from the strain gauges it was also possible to get a good indication of when the *initial* failure due to bearing failure at the highest loaded hole occurred (see Fig. 4.4.65 above). Table 4.5.2 shows the load at which this initial failure occurred for all six joints. From this, clearance is seen to have a much more substantial effect on load at initial failure, than it does on ultimate failure load. In the C3\_C3\_C1 case, where Bolt 3 takes most of the load by itself, we get a **first major failure event at a 25% lower load than in the neat-fit joint**, which is quite substantial. From a design point of view, it appears that clearance is a factor of considerable importance in calculating limit load, but has less effect on ultimate load.

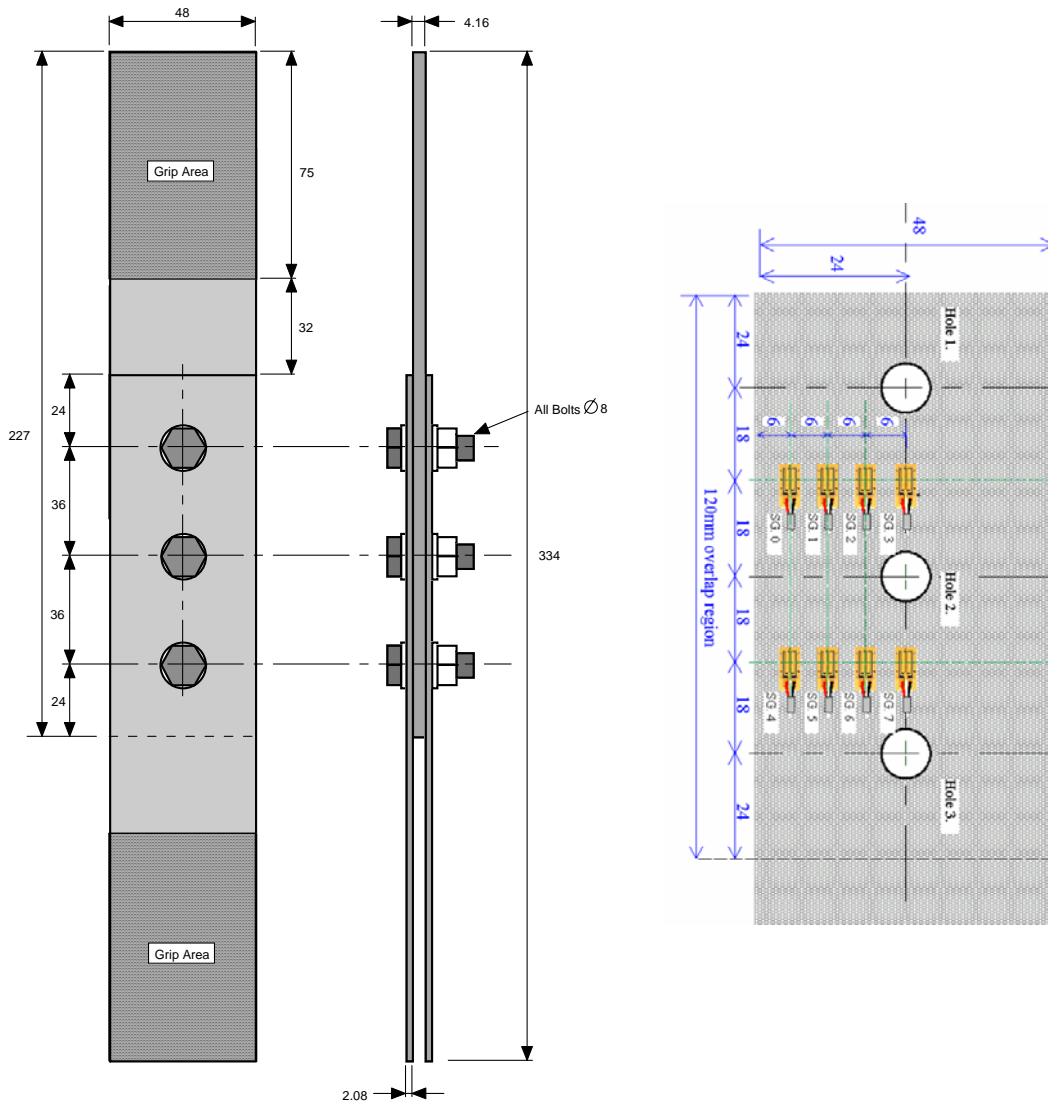


**Figure 4.5.3 ULIM multi-bolt, double-lap joint with strain-gauge locations**

Code	Nominal Clearance ( $\mu\text{m}$ )		
	Hole 1	Hole 2	Hole 3
C1 C1 C1	0	0	0
C1 C3 C1	0	160	0
C1 C1 C4	0	0	240
C2 C1 C1	80	0	0
C4 C1 C1	240	0	0
C3 C3 C1	160	160	0

**Table 4.5.1 Clearance cases for quasi-static, multi-bolt, double-lap joint tests**

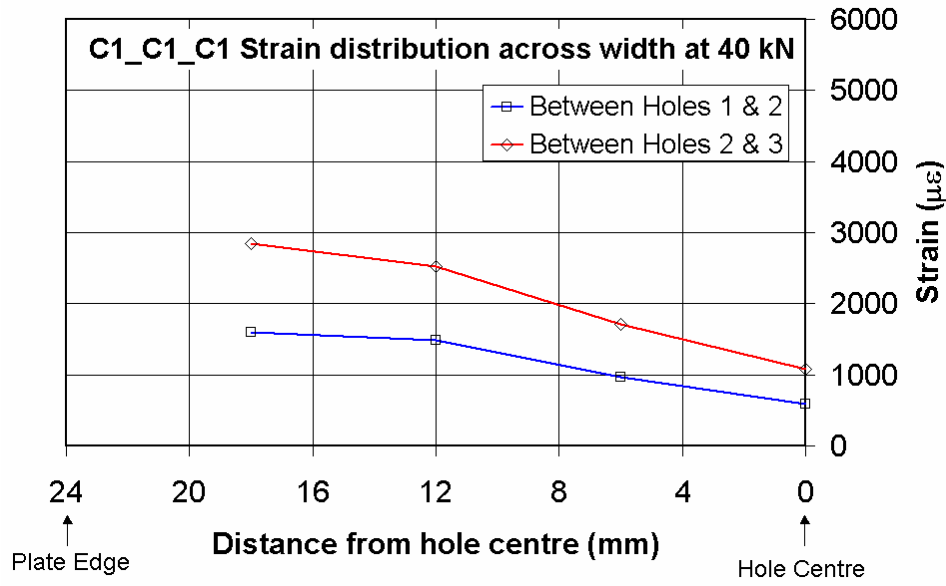
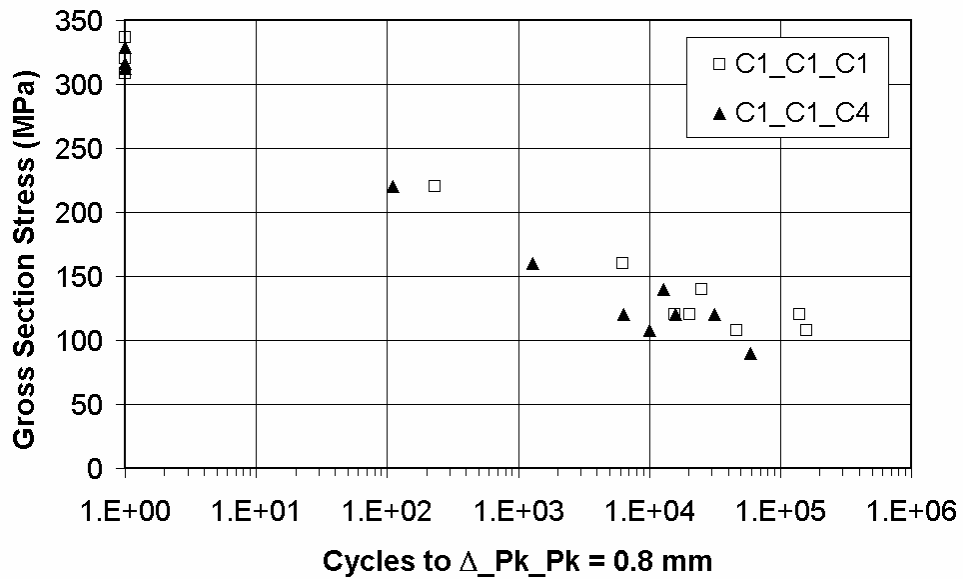


Figure 4.5.4 Typical measured strain distributions in C1\_C1\_C1 joint

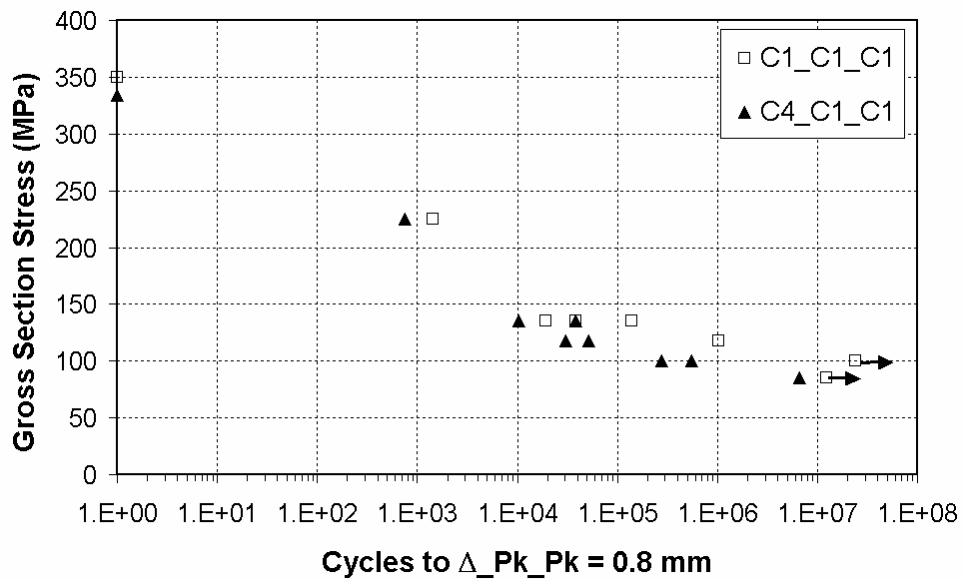
Code	Load at first major failure event (kN)	Percentage Difference from C1_C1_C1
C1_C1_C1	50	0%
C1_C3_C1	44	12%
C1_C1_C4	44.3	11.4%
C2_C1_C1	43.2	13.6%
C4_C1_C1	40	20%
C3_C3_C1	37.2	25.6%

Table 4.5.2 Loads at first major failure event (obtained from strain gauges) – quasi-static loading, double-lap joints

The final test series involved fatigue loading of 16 multi-bolt, *single-lap* joints (geometry as in Fig. 4.4.2), and 16 multi-bolt, *double-lap* joints (geometry in Fig. 4.5.3). Loading was constant amplitude, sine-wave,  $R = -1$ . In each case, two different clearance cases were examined: joints with all-neat-fit holes, and joints with one loose bolt. Results were reported in D5-10, Part 2. Anti-buckling guides and a cooling system using compressed air applied to each bolt were designed and implemented. Various different criteria for definition of fatigue life were used. The single-lap joints eventually failed catastrophically, in net-tension at high loads (70% of quasi-static strength) and bolt failure at lower loads, so one criterion for these joints was ultimate failure. The double-lap joints did not fail catastrophically – instead extreme but gradual hole elongation occurred. A hole elongation failure criterion suggested by FOI was used for all joints, defined as an increase in peak-to-peak displacement of 0.8 mm.



(a) Single-lap joints



(b) Double-lap joints

Figure 4.5.5 Cycles to “Hole Elongation failure”, i.e. increase in peak-to-peak displacement of 0.8 mm. NOTE: Arrows indicate RUN-OUT, i.e. 0.8mm peak-to-peak increase was not reached

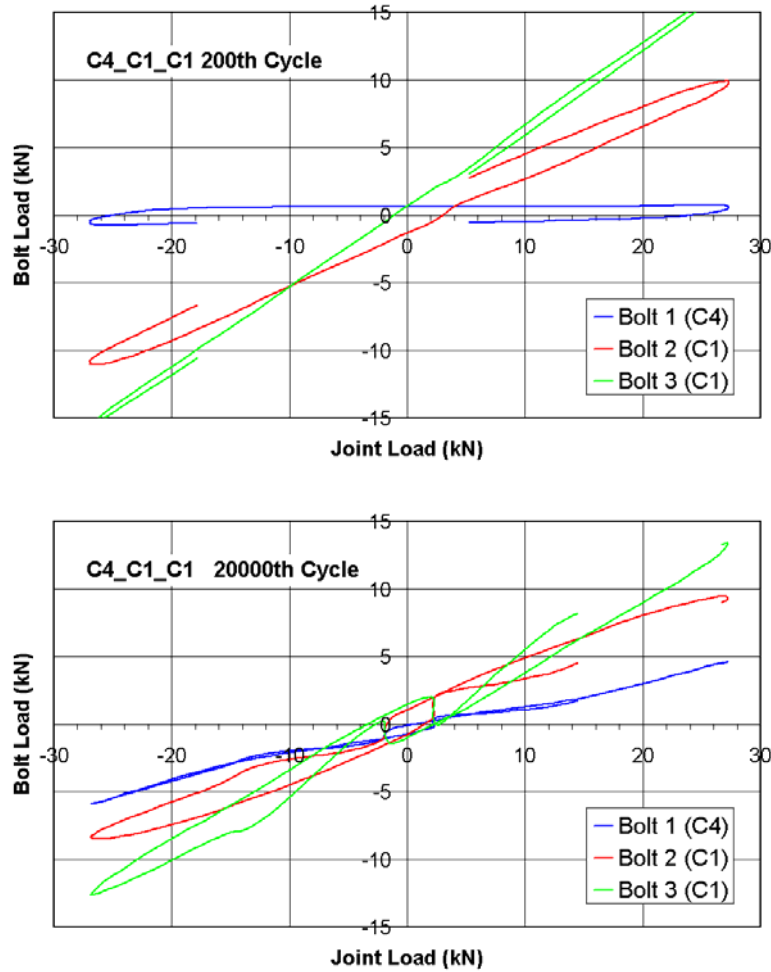


**Figure 4.5.6 Bolt Load distribution at the 200<sup>th</sup> and 20000<sup>th</sup> cycles (calculated from strain gauges) - double-lap, three-bolt C4\_C1\_C1 joint with applied load of +/-27 kN**

Results are shown in Fig. 4.5.5. It can be seen that there is a tendency for the joints with one loose-fit bolt to have shorter fatigue lives than those with all neat-fit bolts, but the trend is not definitive (given the typical level of scatter in fatigue testing), as not enough tests could be performed in the timeframe of the project. As can be seen two tests were stopped without reaching the criterion (after 23 million cycles in one case).

It was noticed from the peak-to-peak curves, that the loose-fit joints had a tendency to start damaging earlier than the all-neat-fit joints. Thus a plot of life to 0.2 mm increase in peak-to-peak displacement was also performed. This showed a clearer difference between the two clearance cases, which indicates that clearance may have its greatest effect in failure initiation and is less influential as failure progresses. The reason for this is that the hole clearances in the joint with one loose-fit bolt even out as the test progresses and hole wear occurs, making the bolt load distribution more even. Evidence was obtained for this using strain gauges in two fatigue tests. Fig. 4.4.6 confirms that the load distribution is more even in the C4\_C1\_C1 joint after 20000 cycles than it was after 200 cycles.



Finally, in the course of analysing the single-bolt joint data, a new *Initial Damage Criterion* for joint strength was suggested by ULIM. Standards such as the ASTM standard [19], MIL-HDBK-17 [20] as well as internal Airbus standards refer to offset criteria such as 2% offset strain or 4% hole deformation. ULIM pointed out some problems with such criteria. Firstly, a lot of damage was found to exist at such load levels, so they are not appropriate for use in limit load design. Secondly offset criteria are not directly associated with any physical principle, so may not correlate well with the amount of damage in the joint. Finally, some variability can occur from one user to another in applying the criteria (involves drawing a best fit slope through the “linear” portion of the load-deflection curve - in fact the load-deflection curve is often not linear at all).

The alternative criterion suggested by ULIM for defining the *Initial Damage Strength* of the joint was the strength at a certain percentage loss in joint stiffness. The method is illustrated in Fig. 4.5.6. The black line is the bearing stress vs. bearing strain curve (see y-axis on left). The red curve is the slope of this line, giving the bearing stiffness (see y-axis on the right). The stress (and load) at which the stiffness has dropped by a certain percentage (e.g. 30%) from its maximum value can then be calculated. This strength is likely to be closely related to the amount of damage in the joint, and does not vary from user to user (provided some standards are agreed upon for data acquisition and filtering). The percentage loss to use can be tuned to the industry’s needs for what is acceptable for limit load. The suggested criterion was published in a journal article [14].

Discussions with Airbus indicated that such issues were also being considered in the TANGO project and the suggested criterion has been passed on to the TANGO project. Additionally a number of partners in the BOJCAS project applied the criterion to their own data and some initial results were presented at the 36-month progress meeting.

ULIM applied the criterion to its double-lap, *multi-bolt* specimens in D5-10, Part 2 and found a remarkably good correlation between the load at 30% loss in stiffness, and the load at first significant failure indicated by the interruption of the strain gauge pattern. Thus the criterion shows promise for identifying the initial damage load in multi-bolt joints without the use of strain gauges.

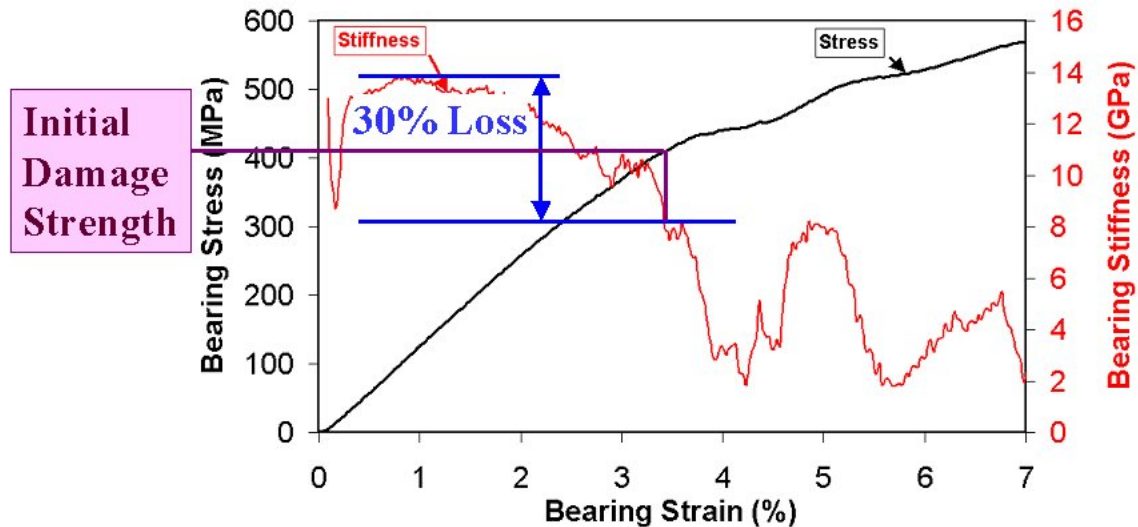


**Figure 4.5.6 Illustration of ULIM's *Initial Damage Criterion* (based here on 30% stiffness loss)**

#### **WP 5 CIRA**

Within WP 5, CIRA performed tests to validate the numerical FE methodologies developed at the local level in WP 4. The single-bolt coupons used in the tests were manufactured by NLR. In the report D5-1 the test matrix was presented while in the report D5-6 all the performed tests were comprehensively described.

Eight single-bolt, single-lap joint configurations (with at least three repeats of each) were loaded quasi-statically in tension in order to investigate the effects of different fastener type (countersunk and protruding head), different plate configurations (composite-composite and composite-aluminium), and different geometry (diameter and width) on damage on-set and progression near the fastener hole. The secondary bending phenomenon was examined in detail.

It was found that clamping force had a large effect on the initial slope of the load-deflection curve, but not much effect on final failure load. The joints with countersunk bolts were less stiff and capable of sustaining less load than the joints with protruding-head bolts. Plastic deformations in the aluminium plates at the bolt-hole interface and due to secondary bending were found to strongly influence the force-deflection curves of the composite-aluminium joints. Larger bolt diameters led to increased maximum loads.

Twelve single-bolt, *double-lap* configurations were loaded quasi-statically in tension. The objective was to investigate the variation of failure modes (net-tension, shear-out and bearing) due to the change of geometrical parameters.

The failure modes of the double-lap specimens were as expected, although in specimens with  $w/d = 3$ , the failure mode was net tension. This is not that surprising, since this  $w/d$  ratio is generally considered on the borderline for bearing and net tension failure. The load-deflection curves for the bearing specimens were non-linear, but were almost linear for the tension and shear-out specimens.

For both sets of specimens, ultrasonic C-scan inspections were performed at different load steps to evaluate the progression of damage. Fig. 4.5.8 shows C-scan results for the various double-lap specimens. It is easy to pick out the specimens that failed in net-tension and shear-out. In addition, the variable degree of damage around the hole in the various different bearing configurations can be seen.

Finally, microscopic investigations on some samples were carried out in order to investigate the failure mechanisms inside the joint and their interactions (Fig. 4.5.9). In all the investigated specimens, delaminations and shear matrix cracks were found in the bearing plane and in the plane perpendicular to loading direction.

The results can be considered as a useful experimental database for the validation of damage progression numerical activities in BOJCAS and in the future.



**Figure 4.5.7 Extensometer used for single-lap specimens**

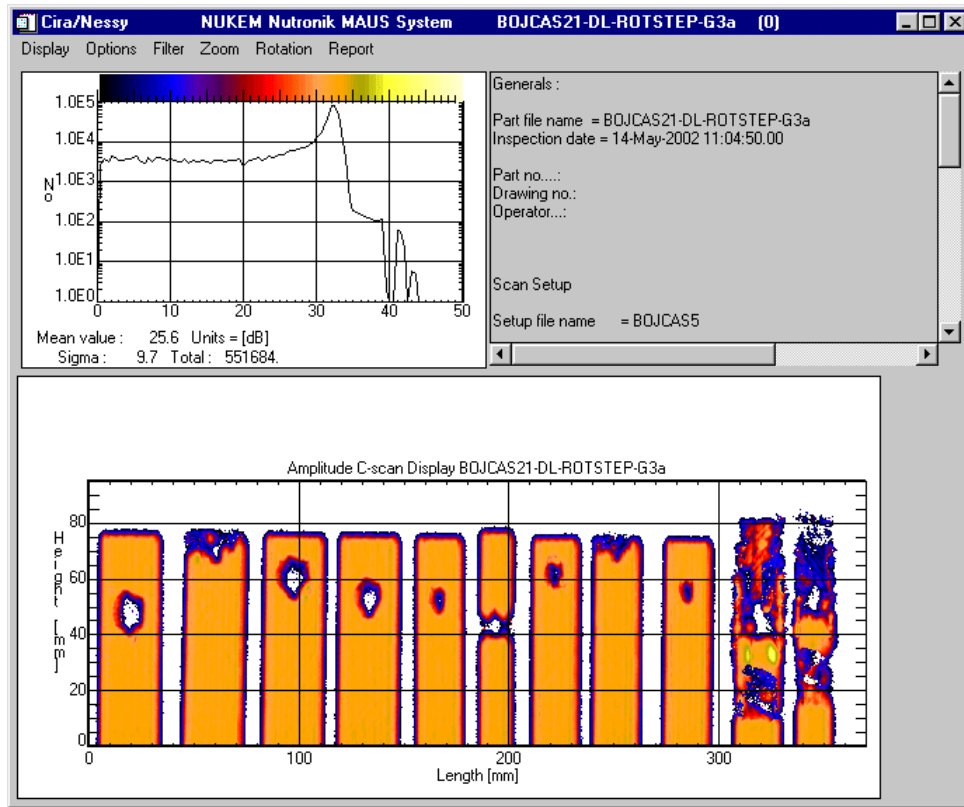


Figure 4.5.8 Double-lap joints inspected with C-scan – gate 3, amplitude

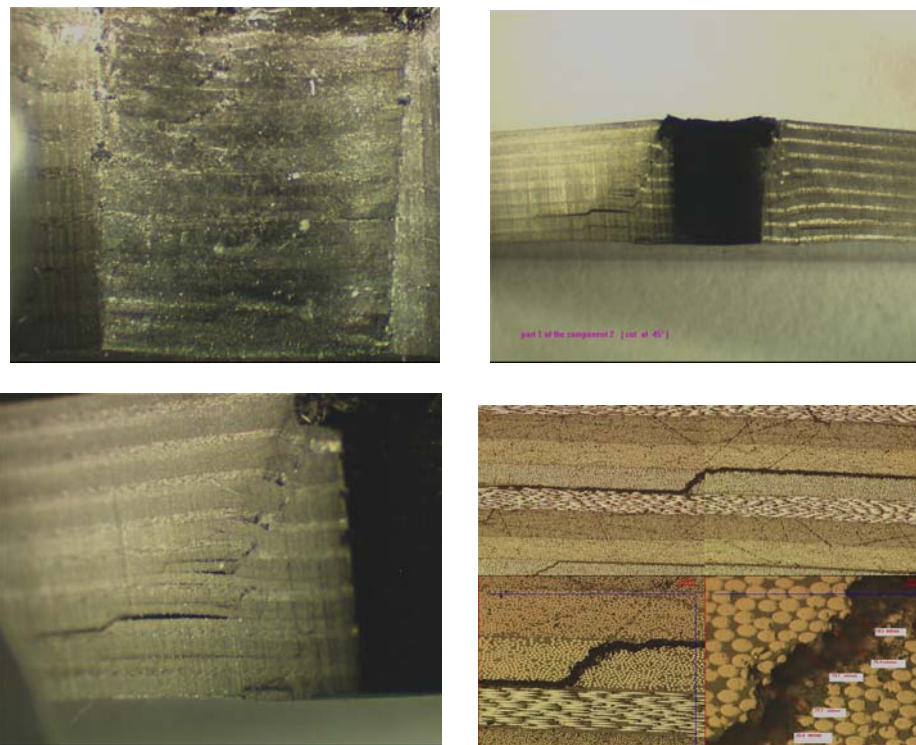


Figure 4.5.9 Microscopic inspection of failure modes in CIRA joints

## WP 5 KTH

The comprehensive test programme conducted by KTH in WP 5 was initiated to generate basic research information about composite-to-metal, multi-fastener, single-lap joints. The goal was to generate an improved understanding of the mechanisms and parameters that are important for this class of joints, and to support the development of detailed FE models in WP 4. The study was restricted to the behaviour of the joints under quasi-static tensile loading in room temperature using dry laminates.

The baseline joint geometry was given in Fig. 4.4.19 above. The main parameters considered were bolt type, clamping force, row spacing, length, bolt diameters and thickness of the metal plate. The tested configurations are given in Table 4.5.3. Configuration 4 was regarded as the reference configuration and is denoted “c4” in the following sections. Length refers to the free length of the joint, i.e. the length between the test machine grips. P.H. and C.S. denote protruding head fastener and countersunk fastener respectively. Configuration 10 had one 8 mm bolt in position one according to Fig. 4.4.19. Configurations 11 and 12 had two and three 8 mm bolts in positions 1-2 and 1-3 respectively.

Conf. [Nr.]	Torque [Nm]	Row sp. [mm]	Length [mm]	Alu. thi. [mm]	Bolt Type	Diam [mm]	Nr. of Specs.
4	6	32	376	8	P.H.	4x6	13
5	6	32	296	8	P.H.	4x6	3
6	6	32	376	8	P.H.	4x6	3
7	6	20	376	8	P.H.	4x6	3
8	6	32	376	4	P.H.	4x6	3
9	6	32	376	8	C.S.	4x6	3
10	6/14	32	376	8	P.H.	3x6+1x8	3
11	6/14	32	376	8	P.H.	2x6+2x8	3
12	6/14	32	376	8	P.H.	1x6+3x8	3
13	6/14	32	376	8	P.H.	4x8	3

**Table 4.5.3 Parameters varied in KTH experimental test programme**

The distribution of load between the fasteners is an important aspect of multi-fastener joints. The intention was to clarify the importance of the varied parameters on the load distribution through measurements with instrumented bolts. However, due to hole eccentricities present in the joints, as discussed in WP 4, the results were difficult to interpret. It appears that the hole eccentricities had a comparable influence on the bolt loads as the parameters that were investigated. The main achievement instead became a validation of the instrumented bolts. The bolt load from an instrumented bolt is compared with a bolt load that was calculated from strains measured with a heavily instrumented joint (36 strain gauges) in Fig. 4.5.10. It can be seen that the instrumented bolts generated accurate results and can be used for this kind of joint. Examples of the type of information that can be obtained from their use are illustrated in Figs. 4.5.11 and 4.5.12. In Fig. 4.5.11 the influence of friction and clamping force on the bolt load is shown and in Fig. 4.5.12 the total amount of load transferred by the bolts and by friction is plotted.

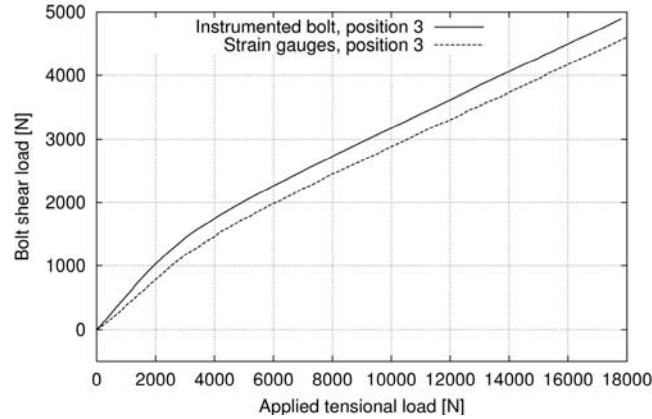


**Figure 4.5.10 Comparison of bolt load from instrumented bolt and bolt load calculated from strain gauges on a heavily instrumented aluminium plate**

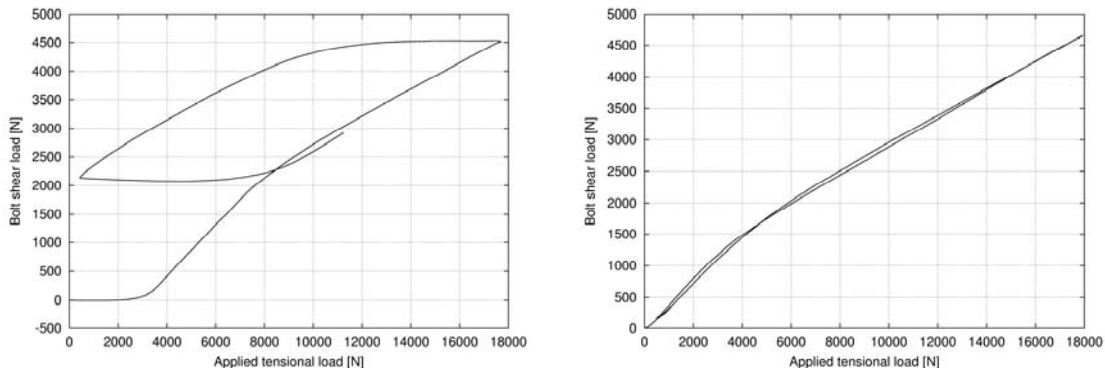


**Figure 4.5.11 Bolt load measured with instrumented bolt torqued to 6 Nm (left) and finger tightened (right)**

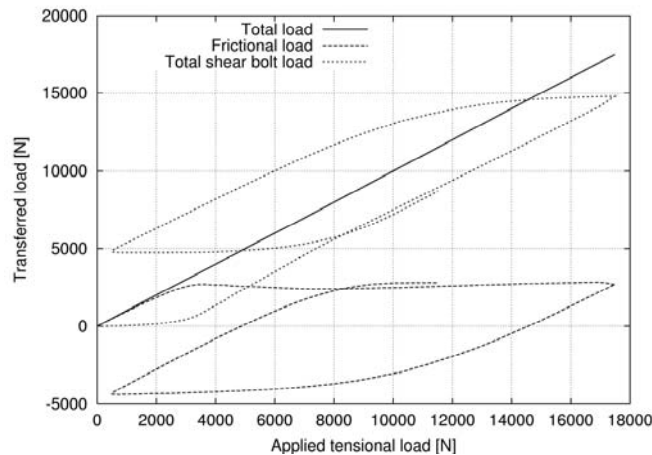


**Figure 4.5.12 Total amount of load transferred by the bolts and by friction between the plates. The loads were measured with instrumented bolts**

The optical whole field deformation measurement system “Aramis” was used to measure 3D displacements of the composite surface during loading. Out-of-plane deformations along the length of the joints are plotted in Fig. 4.5.13. It can be seen that the only parameters that significantly affected the out-of-plane deformations were the length (c5), the row spacing (c7) and the thickness of the aluminium plate (c8). All other parameters had only a minor effect.

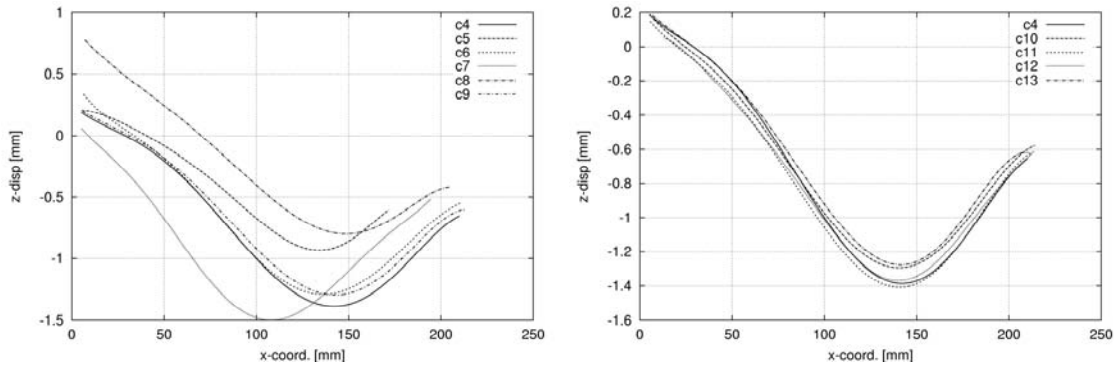


**Figure 4.5.13 Out-of-plane deformations of all joints. Deformations are plotted along the length of the joints at 18 kN tensional load**

The optical system was also used to obtain curves of load vs. longitudinal displacement. The shape of a typical load displacement curve reflects a number of stages during load-up. For small loads the slope is determined by friction due to the clamping force, which prevents relative sliding of the plates. At some point the plates start to slide and a sudden decrease in stiffness appears. The stiffness is increased as contact is established between the bolts and the plates and the curve becomes almost linear. As the load increases, the curve starts to deviate from linear behaviour due to the introduction of bearing damage in the composite plate. Load displacement curves for all joint configurations are shown in Fig. 4.5.14.

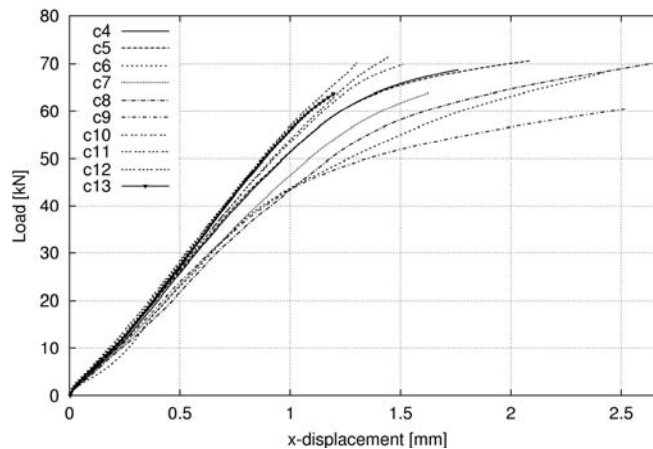


**Figure 4.5.14 Load-displacement curves for all joint configurations as measured with the Aramis system**



It can be seen that reducing the length (c5) has no effect on the stiffness at any load level. Finger tightening the fasteners (c6) creates a less stiff joint and bearing damage appears to be introduced earlier than for the reference joint (c4). Similar behaviour is shown for joints using countersunk fasteners (c9). Reduced row spacing (c7) and reduced thickness of the aluminium plate (c8) result in less stiff joints but bearing damage seems to occur at approximately the same load as for c4. Introducing 8 mm fasteners increases the stiffness and postpones bearing damage due to the increased contact area between the bolt and the hole edge.

Bearing damage was studied with an optical microscope and to some extent with acoustic sensors that recorded micro-mechanical failure events during loading. Damage was introduced first at Bolt 4 for all joints due to the strain concentration generated by the secondary bending. Countersunk fasteners reduced the bearing strength due to the reduced cylindrical length of the bolt. Finger tightened bolts reduced the bearing strength due to the fact that no load was transferred through friction between the plates.

Bolt diameter proved to have a significant effect on the bearing strength, as indicated by the load displacement curves in Fig. 4.5.14. Bearing damage at Bolt 2 in a c4 joint and a c11 joint is illustrated in Fig. 4.5.15. The c4 joint contained four 6 mm bolts, whereas the c11 joint contained two 6 mm and two 8mm bolts. Both specimens were subjected to the same load and it can be seen that the c4 joint suffered from severe bearing damage consisting of crushing, intra-laminar shear cracks and delaminations. The c11 joint is almost undamaged.

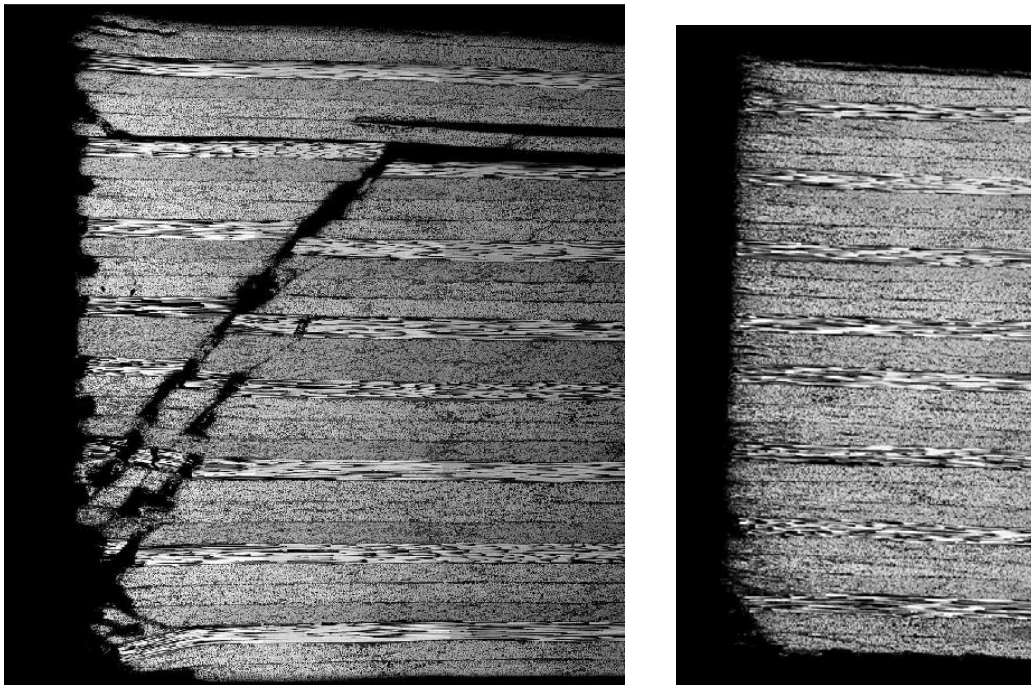


**Figure 4.5.15 Bearing damage in two different joints subjected to equal load. The left picture shows hole number 2 in a c4 joint and the right picture shows hole number 2 in a c11 joint, i.e. an 8 mm bolt was used in hole 2**



## WP 5 FOI

FOI undertook two separate test series in WP 5, one being a study of fatigue of composite bolted joints, the other being a study of coefficient of friction between composite/composite and composite/metallic plates.

In all 93 fatigue specimens were tested. The baseline geometry for the fatigue study is shown in Fig. 4.5.16. In this baseline, 6 mm titanium alloy, protruding-head bolts torqued to the recommended torque level (“fully torqued”) were used. Results for this baseline were available from a previous project [21]. In BOJCAS, the following variations on this baseline were tested:

- 4 mm bolts (fully torqued)
- 6 mm bolts, finger-tightened
- 8 mm bolts (fully torqued) - joint dimensions were scaled up to keep w/d ratios etc. constant
- 6 mm Huck-comp fasteners
- Thinner plates (4.16 mm middle plate, 2.08 mm outer plate)
- Bolts re-tightened at intervals during fatigue loading

The Huck-comp fasteners are installed with a special tool – the resulting pre-load in the bolt is unknown, but is probably larger than in the standard (torqued) protruding-head fastener. The effect of re-tightening bolts was examined because it has been observed that bolts loosen during fatigue.

The specimens were manufactured from carbon fibre/epoxy, HTA7/6376 composite (which was used by many partners in the project) with quasi-isotropic stacking sequence. Lateral supports with Teflon sheets between specimen and support (to reduce friction) were used, and frequency was adjusted to maintain the temperature of the bolts below 35°C. The constant amplitude fatigue tests were done with a load ratio  $R=-1$ , for most of the tests and with  $R=-0.2$  for two tests. Failure was defined as an increase in peak-to-peak grip displacement of 0.8 mm.

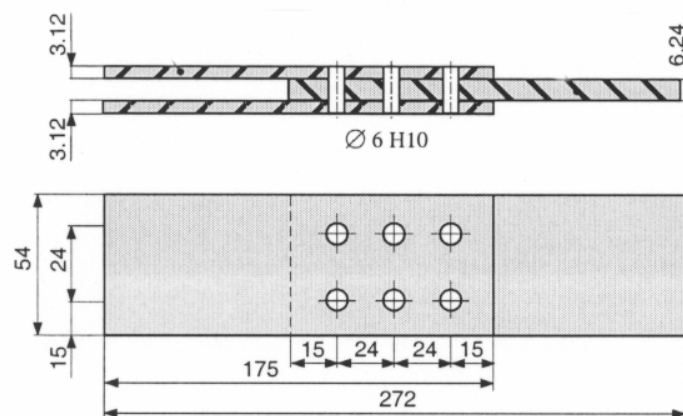


**Figure 4.5.16 Baseline geometry for FOI fatigue study**

Spectrum fatigue loading was also carried out. A load spectrum associated with the lower fitting of the wing of the JAS 39 fighter aircraft, called ovkb, was used. The spectrum is tension dominated and if the maximum peak and trough is considered the spectrum has an R-value close to  $-0.2$ . Results were also compared with literature results for a spectrum associated to the aft fitting of the vertical fin of the JAS 39 fighter aircraft called bfbk. This spectrum has an overall R-value close to  $-1$ . Load cycles were eliminated from both spectra based on the load range of the cycles. A 50% elimination means that all load cycles with a load range less than 50% of the overall peak to peak load range of the spectra were eliminated - these spectra are called bfbk50 and ovkb50.

Quasi-static tests were first carried out. For tensile loading, it was found that the pre-load in the bolts (finger-tight and fully torqued bolts, plus Huck-comp bolts) had no effect on the gross section failure stress (all joints failed in net tension). The thinner specimens had a slightly higher gross section failure stress, which may be due to a more even stress distribution in the thickness direction due to less bending of the fasteners (hence a higher “average” stress across the section). Specimens with 4 mm bolts failed in bearing instead of net tension (though the failure stress was unchanged). When loaded in compression, the failure stress increased for all specimens (compared to tensile loading). In compression contact can occur on both sides of the fastener. This creates a load path through the fastener, which causes the stress concentration at the bolt-hole to decrease. As a result the net-section failure stress increases (see also ULIM’s work in Task 4.4 for differences between tensile and compressive loading).

Fig. 4.5.17 shows the constant amplitude fatigue test results. The baseline results are from [21]. The following conclusions were made. Joints with finger tight fasteners had a slightly shorter fatigue life than joints with fasteners tightened to normal torque. Joints with Huck-comp fasteners had a higher fatigue life than joints with standard protruding head fasteners. Joints with reapplied torque had a longer fatigue life than joints with fasteners torqued only once. It was found that if a nut began to come loose during fatigue loading of a joint it continued to do so even if the torque was reapplied. The higher the fatigue load on the joint the more nuts came loose during loading. For specimens with a decreased thickness the failure mode changed from bolt failure to hole elongation and the fatigue curve was not as steep as for the baseline. For specimens with 4 mm bolts (instead of the 6 mm bolts used in the baseline) the fatigue life decreased. A joint with 4 mm fasteners fatigue loaded at 35% of quasi-static strength failed after 6300 cycles, demonstrating the importance of fatigue in some cases.

Fatigue testing, with the special spectra described above, suggested that load cycles with a 50% range of the overall range of the spectra reduce the fatigue life. But, realistic load spectra do not contain that many cycles with a 50% load range. Therefore, a 50% elimination can be used on realistic load spectra.

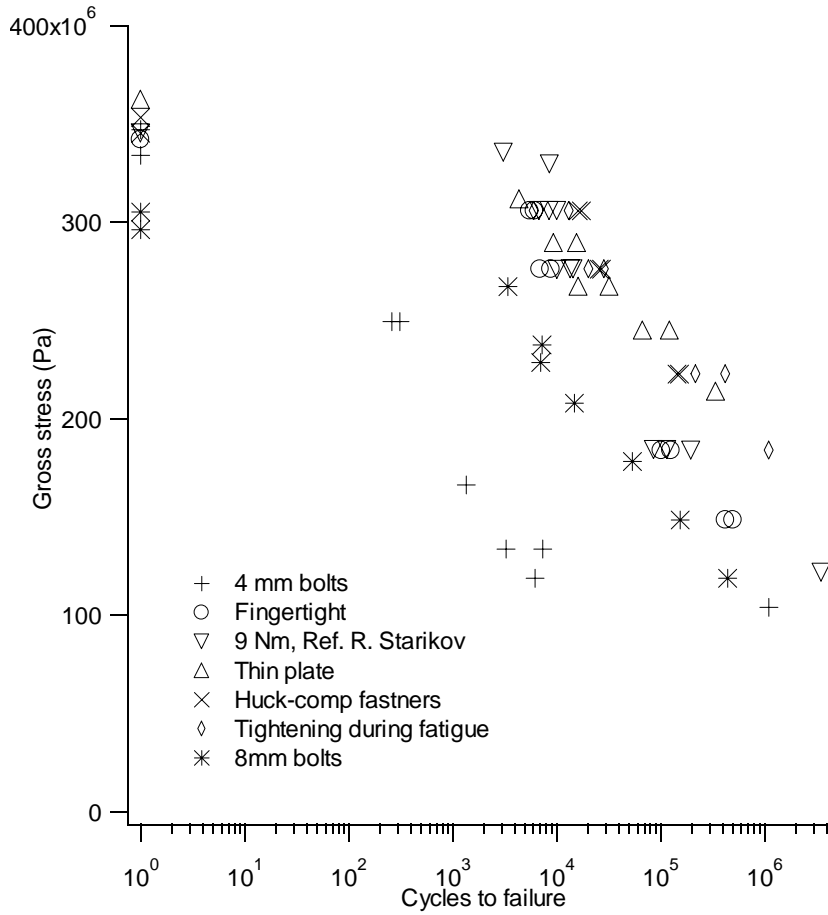


Figure 4.5.17 Fatigue results for bolted joints loaded at R=-1

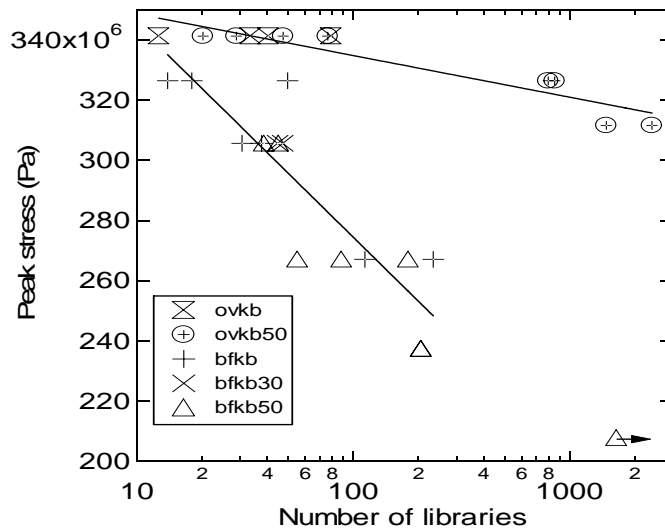


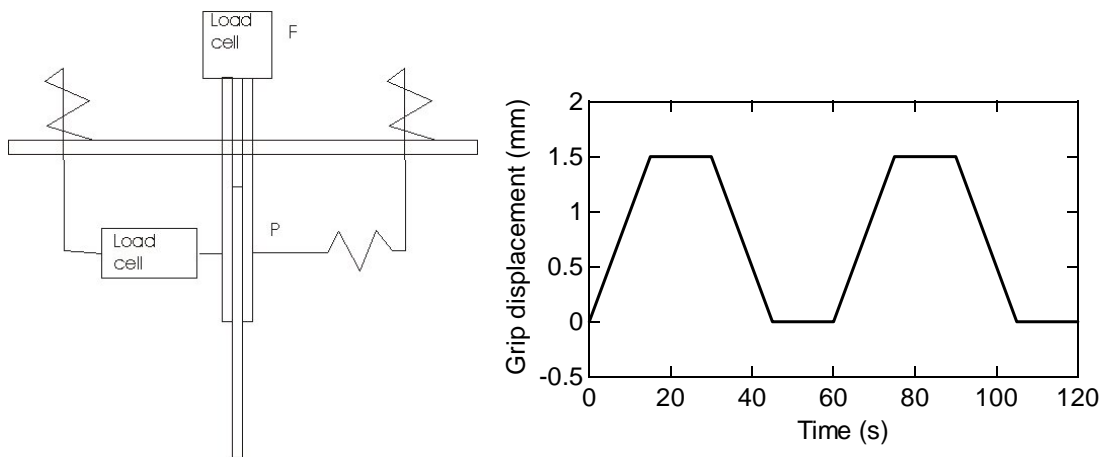
Figure 4.5.18 Fatigue life of spectrum fatigue loaded joints

The set-up for FOI’s test series on friction coefficients is shown in Fig. 4.5.19. Two material combinations were tested: composite/composite and composite/aluminium. The normal force,  $P$ , was applied on the same type of washers as was used in bolted joint testing. The specimens were inserted in a mechanical testing machine and a relative sliding motion between the specimens was applied. The friction force,  $F$ , and normal force  $P$  were measured with load cells. Since the specimens elongated and compressed during loading the system for applying the normal force had to move with the specimens. This was obtained by having the system hanging in soft springs.

The testing was done in displacement control following the displacement cycle in Fig. 4.5.19. The hold portions of the cycles were to allow for cooling of the contact surfaces. One load cycle took one minute to do, which meant that approximately 10000 cycles could be done in one week, making testing time-consuming. The coefficient of friction was calculated from:

$$\mu = \frac{F}{2P}$$

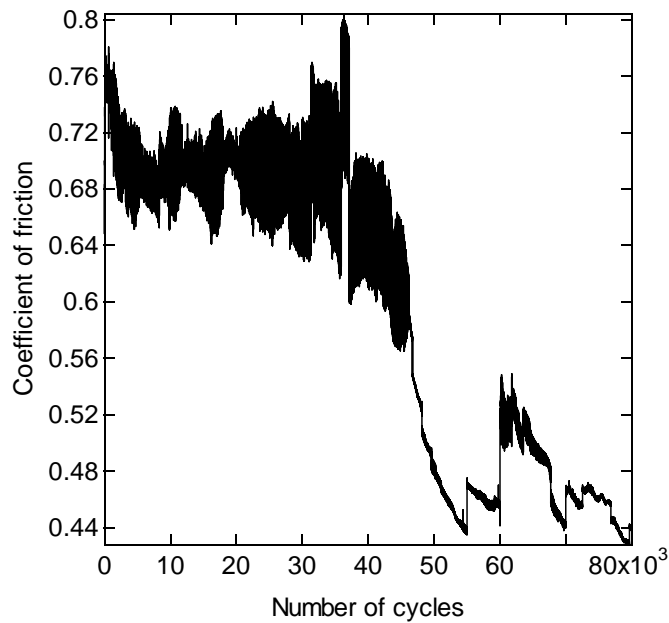
Some specimens were taken apart, ultrasonically cleaned and studied in a scanning electron microscope.



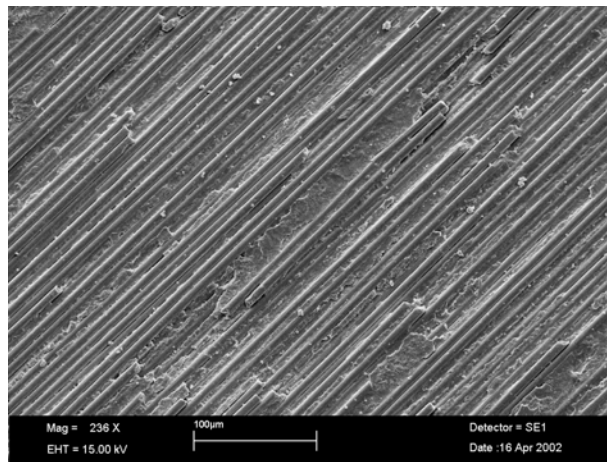
**Figure 4.5.19 Schematic set-up for measurement of coefficient of friction**

Fig. 4.5.20 shows a typical result. During the first 100 or so cycles, the coefficient of friction increased (only visible on a log scale). Then it stayed constant for several thousand cycles, before starting to drop off. Average initial and peak values for the coefficient of friction were calculated from several tests. For composite/composite contact the initial coefficient of friction was 0.65 and the peak coefficient of friction after wear-in was 0.74. For composite/aluminium contact the initial coefficient of friction was approximately 0.23 and the peak coefficient of friction after wear-in was 0.68. Since all

wear mechanisms observed in the composite/composite friction specimen were also observed in the joint specimen it is possible to transfer the measured coefficient of friction from the composite/composite friction specimens to the joints. The information generated was used by other partners in their FE models (e.g. ULIM in Task 4.4). Fig. 4.5.21 shows a sample SEM picture of the wear surface.



**Figure 4.5.20 Coefficient of friction versus number of cycles for a composite/composite friction specimen**



**Figure 4.5.21 Broken fibres on surface**

## **WP 5 NLR**

In WP 5, the NLR defined a test programme, manufactured and instrumented specimens, and performed quasi-static static tests on these specimens. The specimens represent structural features in the SAAB and DA benchmark structures. In addition, a number of basic tests were performed, namely: filled-hole tension tests, bearing tests and tensile tests. The material used was HTA/6376, which was used by several partners in the project, so the test results provided useful data for the modellers. The test results will also add to the available data from the literature, to support the development of design guidelines.

Specimens represented:

1. the permanent or temporary skin repair for the DA skin repair benchmark,
2. the permanent or temporary skin repair for the DA skin/stringer repair benchmark,
3. the permanent or temporary web repair for the DA benchmark,
4. the single shear SAAB benchmark, and
5. the double shear SAAB benchmark.

In addition, filled-hole tension, bearing and tension tests were performed on specimens from five laminates. The tests were extensively instrumented, as illustrated in Fig. 4.5.22.

The test results were reported on in D5-8. Comparison of the results for the joint specimens and results for the filled-hole tension, bearing and tension specimens showed that:

- The average strain at failure for the joint specimen types that failed in net-section tension was slightly lower than the average strain at failure for the filled-hole tension specimens.
- The average strain at failure for the joint specimen types that failed in bearing was considerably less than the average strain at failure for the filled-hole tension specimens, and was mostly slightly more than 0.3 percent.
- The bearing ultimate stress (BUS) for the specimen types with blind bolts and aluminium patches was relatively low.
- The BUS for the single-lap specimen types was comparable or slightly less than the BUS determined with the bearing specimens.
- The BUS of the double-lap specimen types was higher than or comparable to the BUS determined with the bearing specimens.
- The filled-hole tension specimens showed some relation between the percentage of 0°-plies and the average strain in the net section at failure.

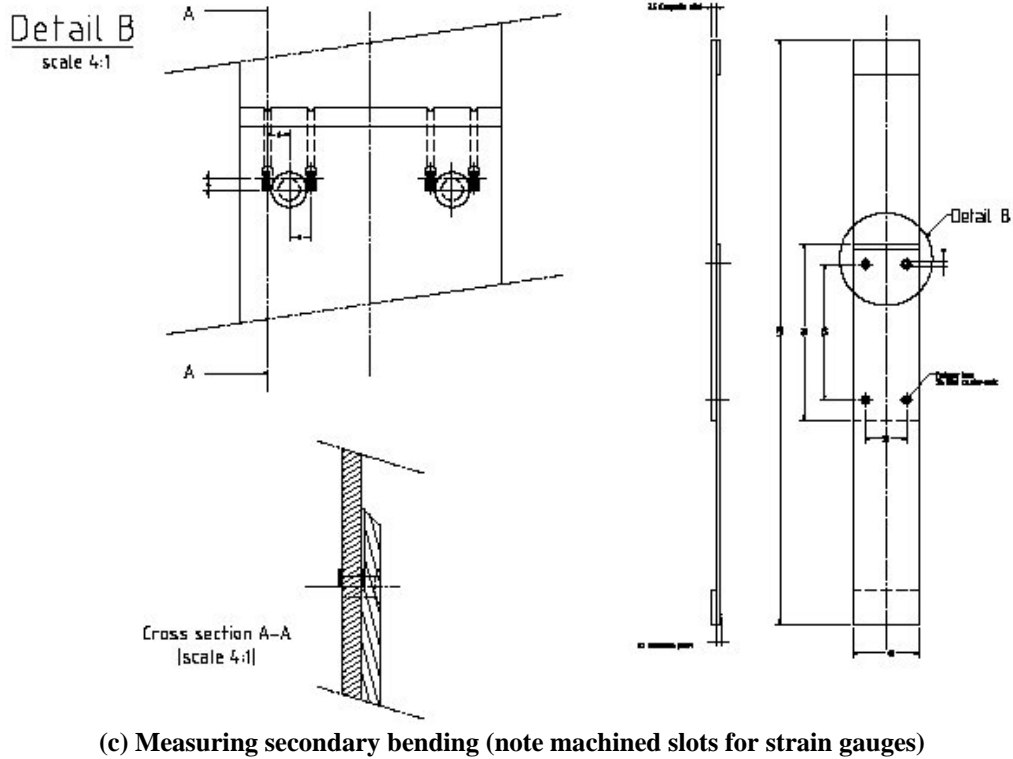
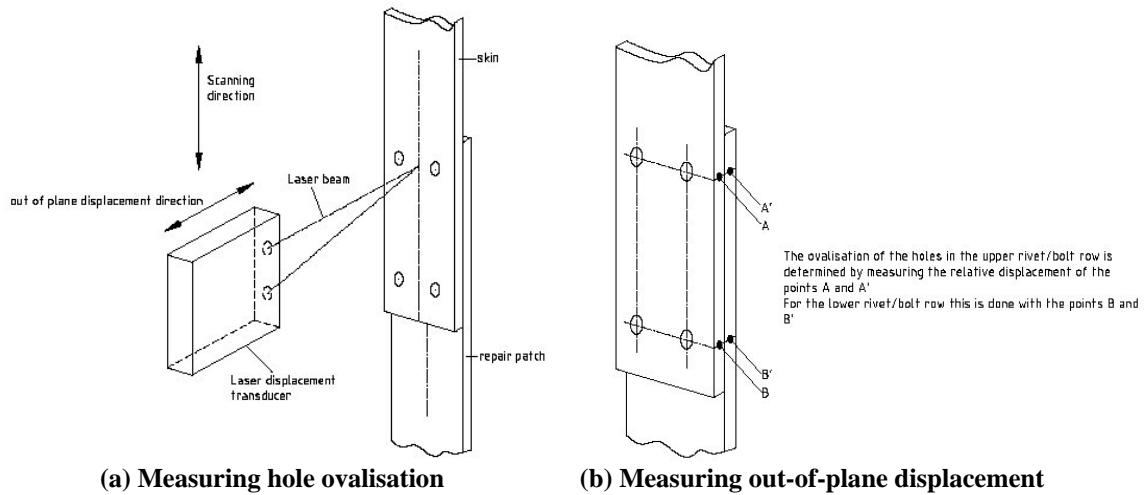


Figure 4.5.22 Some of the instrumentation used in NLR's specimen tests

## 2.6 WP 6: Design Methodology

### 2.6.1 Task 6.1 Assessment of detailed design methods

In this task, CIRA assessed the potential of detailed design tools (including the global-local approaches) developed within the project. The results were presented in D6.1-1.

Firstly, the state of the art of the detailed design methods for composite joints in aircraft structures was described. Then, starting from the modelling and test results described in the deliverables of WP 4 and WP 5, the different paths followed in developing the detailed design tools were critically assessed. The coupling between the detailed design tools and the global methods (developed in WP 2) was also critically analysed.

Finally a classification of the proposed methodologies based on the accuracy of results, user-friendliness, set-up times, run times and other relevant factors, was given. In performing such a task, the satisfaction of the BOJCAS targets of reduction of time and cost in the development phase was continuously checked. Summary tables and charts of the kind shown in Table 4.6.1 and Fig. 4.6.1 were produced.

	Discretisation type			Element type		Contact definition	Input data		Bolt representation		Generic FEM code	Boundary conditions	
	3D	3Din 2D	2D in 2D	8 nodes	20 nodes		Menu driven	Batch file	3D	Simpl.		Rigid modes Prevent	Applied force displ.
ULIM	√			√	√	√	√		√		√	√	√
KTH	√			√	√	√		√	√			√	√
SMR	√	√	√	√	√*			√					
QinetiQ		√	√	√	√*	√		√	√+	√	√*	√	√

\* to be demonstrated

+ in development

° Conventionally limited to ABAQUS but designed to be expanded to other codes

**Table 4.6.1 Pre-processor characteristics**

	prestress	Bolt type		Number of bolts		Single-lap	double-lap	composit/metal	static	fatigue	
		Protruding	contersunk	single	multi						
Layered element											CIRA
3D element											ISTRAM
Non linear FEM											KTH / ULIM
Contacts											CIRA / ISTRAM
Friction											CIRA / KTH / ULIM
Progressive damage											ALL
											CIRA / KTH
											CIRA / ULIM
											KTH / ULIM / ISTRAM

**Figure 4.6.1 Detailed local models field of coverage**



## 2.6.2 Task 6.2 Design Guidelines

QinetiQ was responsible for collating a report containing design guidelines for bolted joints in composite aircraft structures. It was not feasible to cover all topics in the field so the report focused on the guidelines that emerged from within BOJCAS. The guidelines were presented in three parts.

The first part concentrated on characterising the behaviour of single-bolt joints, because they are the building blocks from which the behaviour of more complex joints can be derived. Recommended approaches to characterising the behaviour were presented, and the relevant analysis methods and experimental results that were obtained within BOJCAS were set in the context of the overall design process.

The second part concentrated on characterising the behaviour of multi-bolt joints. It included observations on the behaviour of these joints, and various design approaches were recommended.

The third part presented flowcharts showing how the various design and analysis tools that were developed within BOJCAS could be used in the design process. Fig. 4.6.2 shows a sample flowchart developed.

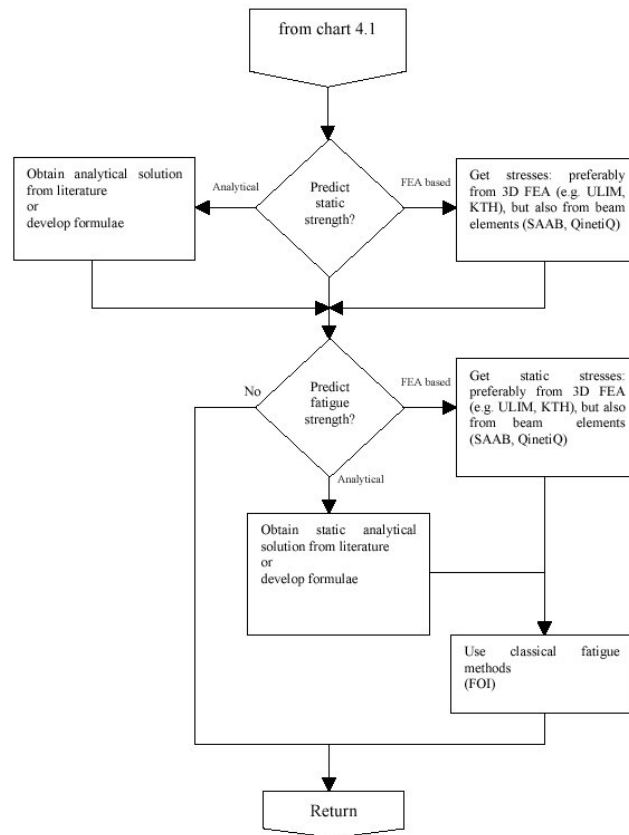


**Figure 4.6.2 Sample flow chart on use of analysis methods in design**  
**2.7 WP 7: Network Management**

### **2.7.1 Task 7.1 Management**

Management is covered in Section 7.

### **2.7.2 Task 7.2 Exploitation**

In this task, QinetiQ produced the Technology Implementation Plan (TIP), and SMR created the website, and a CD containing all the deliverables of the project.

#### **Task 7.2 QinetiQ**

In the first 12 months of the programme an Exploitation Report was produced, identifying both the potential that existed for exploiting technical results and the dissemination routes.

The TIP was then developed. The draft document was delivered at mid-term, and the final version is being submitted in parallel to the current report. The TIP identified the overall results of the programme and particular results from the partners. The TIP also listed the intentions of the partners to exploit the results, and described the use and economic impact of the results.

#### **Task 7.2 SMR**

SMR started this task by collecting the ideas of each partner about electronic reporting. Opinions about computer security varied greatly between the different partners. Finally, it was agreed to allow for different methods of electronic distribution of reports, depending on the needs and wishes of each partner, either in Portable Document Format (PDF) or Microsoft Word. Long discussions were held about the issue of computer security. Airbus Deutschland has a requirement that no attachments can be sent unencrypted. SMR set up an account for the BOJCAS partners on its server, which can be accessed using the secure shell protocol (version 2). Airbus Deutschland tested this and was able to place documents on the server, which could then be retrieved by other partners. However, due to unfamiliarity of these methods by the other partners, this possibility has rarely been used. SMR now offers the possibility of anonymous access to the server, where documents can be placed or retrieved, but not both, i.e. a user can place a document on the server, which can then not be seen or read, or a user can copy a document, but not remove it. When a document has been placed on the server, SMR can move the document, so that it can be read by other users. This functionality has been used several times when reports were too large in size to be sent out by email.

The website (<http://www.smr.ch/bojcas/>) aims at distributing information about public knowledge generated inside the BOJCAS project. In order to allow as wide as possible access to the site, SMR decided not to include non-standard features that require additional browser plug-ins. In addition, the use of “frames”, has been avoided in order to

allow the available information to be as accessible and retrievable as possible (note: on internet search engines, the information stored in the databases of the internet search engines is obtained by automatically browsing the web. Only directly accessible web-pages, i.e. those viewable directly by typing their complete URL, are stored. Therefore, the search engine cannot access information inside a framed page). The result is a fully W3C (world-wide-web consortium) compliant website, which can be viewed using any browser.

A beta version of the BOJCAS website was created in the first year of the project and made accessible to the public. The site has been announced to several search-engines (e.g. a search at [www.google.com](http://www.google.com) for “bolted composite aircraft” will show the BOJCAS website as one of the first listed references). Logs of the HTTP-server show considerable interest in the website.

The final version of the BOJCAS website has been released in Month 36. SMR will continue to maintain the BOJCAS site until well after the project.

As soon as all reports in electronic format are available at SMR, a CD-ROM will be produced by SMR containing all reports with a HTML-based index, and additional information, including the web site.

### 5. List of Deliverables

In this section, a list of deliverables in each task is given, followed by a snapshot showing the timing of each delivery.

Deliverable No.	Month Due	Description	Resp. Partner(s)	Status
D1-1	2	Definition of BAE benchmark joint configurations.	AUK	Delivered Month 3
D1-2	2	Definition of DA benchmark joint configurations.	AD	Delivered Month 3
D1-3	2	Definition of SAAB benchmark joint configurations	SAAB	Delivered On Schedule

Deliverables Status		Duration																																															
Date:	04-Mar-03	1st year												2nd year												3rd year																							
		1	2	3	4	5	6	7	8	9	10	11	12	13	14	15	16	17	18	19	20	21	22	23	24	25	26	27	28	29	30	31	32	33	34	35	36	37	38	39	40								
<b>Workpackage 1: Design Requirements</b>																																																	
Original Planned Duration		←→																																															
Actual Duration		←→																																															
Item	Description																																																
D1-1	BAe Benchmark Definition Report (AUK)		◆																																														
D1-2	DA Benchmark Definition Report (AD)		◆																																														
D1-3	SAAB Benchmark Definition Report (SAAB)		◆																																														
◆ Original Planned Delivery Date																																																	
Actual Delivery Date																																																	

TABLE 5.1: DELIVERABLES LIST AND TIMING – WP 1

<b>Deliverable No.</b>	<b>Month Due</b>	<b>Description</b>	<b>Resp. Partner(s)</b>	<b>Status</b>
D2.1-1	6	Engineering drawings of BAE benchmark joint parts, lay-ups and assembly. Predictions of load distributions, failure loads and failure modes, and description of design methods used (Written report). Drawings for four configurations by Month 4 to allow WP 3 to begin.	BAE	Delivered Month 7
D2.1-2	6	Engineering drawings of DA benchmark joint parts, lay-ups and assembly. Predictions of load distributions, failure loads and failure modes, and description of design methods used (Written report). Drawings for at least two configurations by Month 4 to allow WP 3 to begin.	DA	Delivered Month 7
D2.1-3	6	Engineering drawings of SAAB benchmark joint parts, lay-ups and assembly. Predictions of load distributions, failure loads and failure modes, and description of design methods used (Written report). Drawings for the SAAB configurations by Month 4 to allow WP 3 to begin.	SAAB	Delivered On Schedule
D2.2-1	12	Description of global methodology and predictions of load distributions between fasteners, failure loads and failure modes for the SAAB benchmark structures (Written report). Models for SAAB benchmarks.	SAAB	Delivered Month 14
D2.2-2	12	Description of global methodology and predictions of load distributions between fasteners, failure loads and failure modes for the BAE benchmark structures (Written report). Models for BAE benchmarks.	DERA	Delivered Month 20
D2.2-3	12	Description of global methodology and predictions of load distributions between fasteners, failure loads and failure modes for the DA benchmark structures (Written report). Models for DA benchmarks.	NLR	Delivered Month 25

**TABLE 5.2A: DELIVERABLES LIST - TASKS 2.1 AND 2.2**

Deliverables Status		Duration																																							
		1st year										2nd year										3rd year																			
Date:	04-Mar-03	1	2	3	4	5	6	7	8	9	10	11	12	13	14	15	16	17	18	19	20	21	22	23	24	25	26	27	28	29	30	31	32	33	34	35	36	37	38	39	40
<b>Workpackage 2: Global Design Methods</b>																																									
Original Planned Duration																																									
Actual Duration																																									
<b>Task 2.1 Design of Benchmark Structures</b>																																									
Original Planned Duration																																									
Actual Duration																																									
Item	Description																																								
D2.1-1	BAe Benchmark Report + Drawings (AUK)																																								
D2.1-2	DA Benchmark Report + Drawings (AD)																																								
D2.1-3	SAAB Benchmark Report + Drawings (SAAB)																																								
<b>Task 2.2 Benchmark Modelling w/ Existing Global Design Methods</b>																																									
Original Planned Duration																																									
Actual Duration																																									
Item	Description																																								
D2.2-1	SAAB Report of Methodology and Predictions + Models (SAAB)																																								
D2.2-2	DERA Report of Methodology and Predictions + Models (QinetiQ)																																								
D2.2-3	NLR Report of Methodology and Predictions + Models (NLR)																																								
◆ Original Planned Delivery Date		Actual Delivery Date																																							

TABLE 5.2B: DELIVERABLES TIMING - TASKS 2.1 AND 2.2

<b>Deliverable No.</b>	<b>Month Due</b>	<b>Description</b>	<b>Resp. Partner(s)</b>	<b>Status</b>
D2.3-1	21	Interim description of global methods developed, including assessment of improvements made relative to methods in Task 2.2 (Written Report).	SAAB	Delivered Month 24
D2.3-2	21	Interim description of global methods developed, including assessment of improvements made relative to methods in Task 2.2 (Written Report).	QinetiQ	Delivered Month 25
D2.3-3	21	Interim description of global methods developed, including assessment of improvements made relative to methods in Task 2.2 (Written Report).	NLR	Delivered Month 25. Combined with D2.2-3 above
D2.3-4	27	Final description of global methods developed, including assessment of improvements made relative to methods in Task 2.2 (Written Report).	SAAB	Delivered Month 30
D2.3-5	27	Final description of global methods developed, including assessment of improvements made relative to methods in Task 2.2 (Written Report).	QinetiQ	Delivered Month 34
D2.3-6	27	Final description of global methods developed, including assessment of improvements made relative to methods in Task 2.2 (Written Report).	NLR	Report consisted of a description of the translation of SMR's global-local models from B2000 to Nastran – delivered in combination with SMR's D4.3-8c in Month 32
D2.4-1	35	Assessment of global design methods developed in BOJCAS (Written Report).	SAAB (with input from BAe and DA)	Delivered Month 36

**TABLE 5.2C: DELIVERABLES LIST - TASKS 2.3 AND 2.4**

Deliverables Status		Duration																																							
		1st year												2nd year												3rd year															
Date:	04-Mar-03	1	2	3	4	5	6	7	8	9	10	11	12	13	14	15	16	17	18	19	20	21	22	23	24	25	26	27	28	29	30	31	32	33	34	35	36	37	38	39	40
<b>Workpackage 2: Global Design Methods</b>																																									
Original Planned Duration																																									
Actual Duration																																									
<b>Task 2.3 Development of Global Design Methods</b>																																									
Original Planned Duration																																									
Actual Duration																																									
Item	Description																																								
D2.3-1	SAAB Interim Report of Developed Global Methodology (SAAB)																																								
D2.3-2	DERA Interim Report of Developed Global Methodology (QinetiQ)																																								
D2.3-3	NLR Interim Report of Developed Global Methodology (NLR)																																								
D2.3-4	SAAB Final Report of Developed Global Methodology (SAAB)																																								
D2.3-5	DERA Final Report of Developed Global Methodology (QinetiQ)																																								
D2.3-6	NLR Final Report of Developed Global Methodology (NLR)																																								
<b>Task 2.4 Industrial Assessment of Global Design</b>																																									
Original Planned Duration																																									
Actual Duration																																									
Item	Description																																								
D2.4-1	Report of Assessment of the Developed Global Methods (SAAB)																																								
	Original Planned Delivery Date																																						Actual Delivery Date		

TABLE 5.2D: DELIVERABLES TIMING - TASKS 2.3 AND 2.4



Deliverable No.	Month Due	Description	Resp. Partner(s)	Status
D3-1	9	BAE Benchmark test specification summarising test specimen details, test rig details, instrumentation, environmental conditions, static and fatigue loading (Written Report).	AUK	Delivered Month 11
D3-2	9	DA Benchmark specification summarising test specimen details, test rig details, instrumentation, environmental conditions and static/fatigue loading (Written Report).	NLR	Delivered Month 15
D3-3	9	SAAB Benchmark specification summarising test specimen details, test rig details, instrumentation, environmental conditions and static/fatigue loading (Written Report).	NLR	Delivered Month 15
D3-4	15	BAe Benchmark Structural items manufactured and instrumented (30+ test specimens)	AUK	Delivered Month 18
D3-5	15	DA Benchmark Structural items manufactured and instrumented (4-8 test specimens)	NLR	Delivered Month 28
D3-6	15	SAAB Benchmark structural items manufactured and instrumented (12+ test specimens).	NLR	Delivered Month 23
D3-7	18	BAe benchmark <b>static</b> test data such as total load, displacement, fastener load distribution, stress distribution, bearing loads, by-pass loads and final failure load (Written Report).	AUK	Delivered Month 25
D3-8	18	DA benchmark <b>static</b> test data w/ similar information to above (Written Report).	NLR	Delayed to Month 33
D3-9	18	SAAB benchmark <b>static</b> test data w/ similar information to above (Written Report).	NLR	Delivered Month 32
D3-10	21	BAe benchmark <b>fatigue</b> test data such as loading cycle, amplitude, bearing loads, number of cycles to failure, failure mode (Written Report).	AUK	Delivered Month 32
D3-11	21	DA benchmark <b>fatigue</b> test data w/ similar information to above (Written Report).	NLR	Cancelled
D3-12	21	SAAB benchmark <b>fatigue</b> test data w/ similar information to above (Written Report).	NLR	Delivered Month 32

**TABLE 5.3A: DELIVERABLES LIST - WP 3**

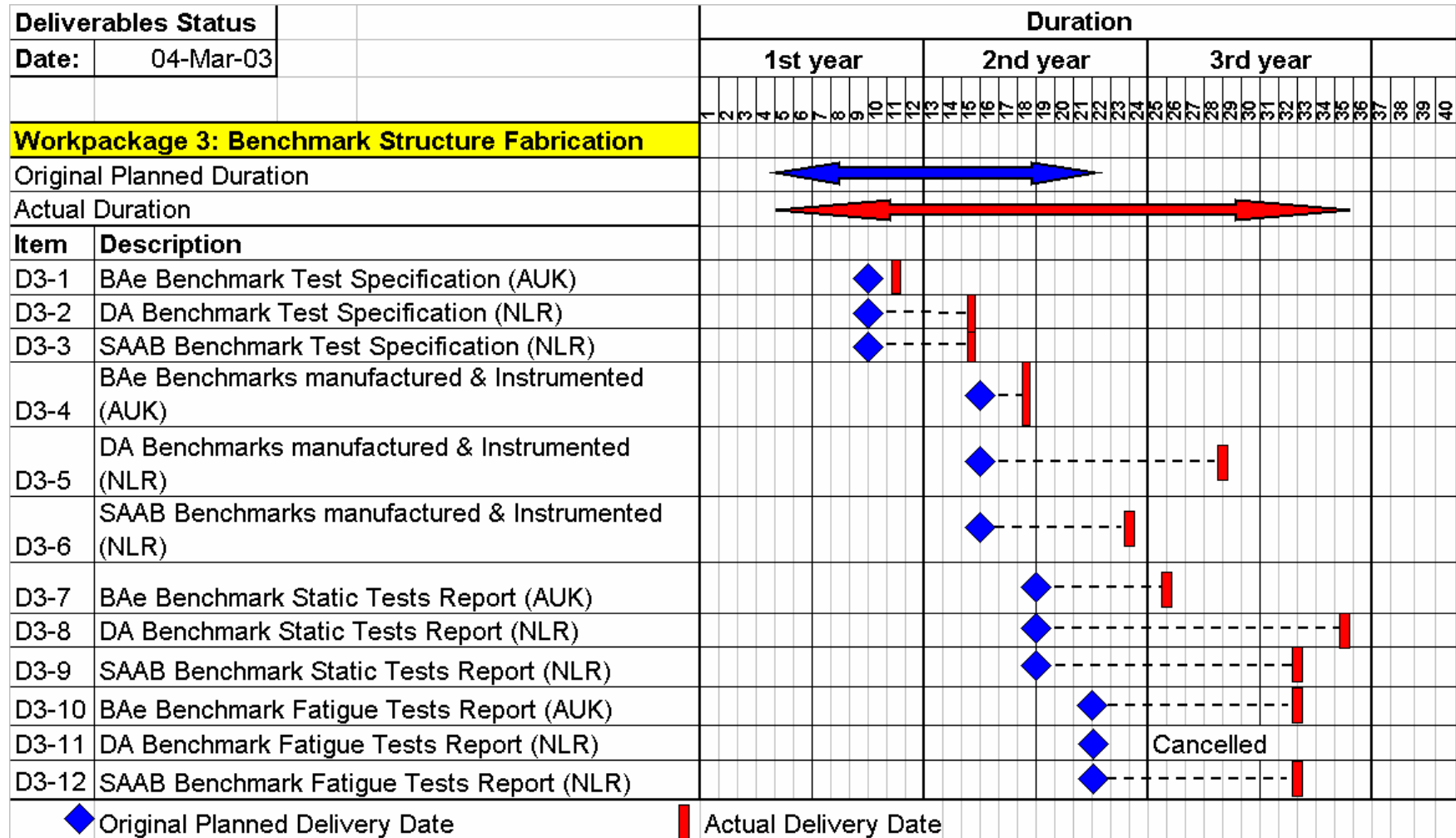


TABLE 5.3B: DELIVERABLES TIMING – WP 3

<b>Deliverable No.</b>	<b>Month Due</b>	<b>Description</b>	<b>Resp. Partner(s)</b>	<b>Status</b>
D4.1-1	12	Interim composite-to-metal 3D stress analysis including preliminary case studies (Written Report).	KTH	Delivered Month 15
D4.1-2	12	Interim 3D stress analysis of bolt-hole clearance including preliminary case studies (Written Report).	ULIM	Delivered On Schedule
D4.1-3	21	Final composite-to-metal 3D stress analysis including validated case studies (Written Report).	KTH	Delivered Month 34
D4.1-4	21	Final 3D stress analysis of bolt-hole clearance including validated case studies (Written Report).	ULIM	Delivered On Schedule
D4.1-5	21	Pre-processing software for 3D finite element composite joint models in ABAQUS including user's manual (software).	KTH	Delivered On Schedule
D4.1-6	21	Pre-processing software for 3D finite element composite joint models in PATRAN including user's manual (software).	ULIM	Delivered On Schedule

**TABLE 5.4A: DELIVERABLES LIST – TASK 4.1**

<b>Deliverable No.</b>	<b>Month Due</b>	<b>Description</b>	<b>Resp. Partner(s)</b>	<b>Status</b>
D4.2-1	12	Interim <b>static</b> progressive damage models implemented in ANSYS/B2000. Description of the finite element models and the implementation of the failure criteria and the property degradation rules. Details of linking of methods to global-local modelling in Task 4.3 (Written Report).	CIRA	Delivered Month 14
D4.2-2	12	Interim <b>fatigue</b> progressive damage models in ANSYS. Description of the finite element models and the implementation of the failure criteria and the property degradation rules (Written Report).	ISTRAM	Delivered On Schedule.
D4.2-3	12	Beta version of B2000 code with improved contact algorithm (software)	SMR	Delivered to CIRA Month 13
D4.2-4	21	Final static progressive damage models validated against CIRA's tests in WP 5 (Written Report).	CIRA	Delivered Month 25
D4.2-5	21	Final fatigue progressive damage models with verification of the methodology, together with parametric studies and investigation concerning linkage to the global analysis in WP 2 (Written Report).	ISTRAM	Delivered Month 25
D4.2-6	21	Fatigue bolt-failure criterion with results to support validity (Written Report)	FOI	Delivered Month 26
D4.2-7	21	Description of implementation of B2000 contact algorithms and damage models (Written Report)	SMR	Delivered On Schedule
D4.2-8	21	Final version of B2000 code with improved contact algorithm (software)	SMR	Delivered Month 24

**TABLE 5.4B: DELIVERABLES LIST – TASK 4.2**

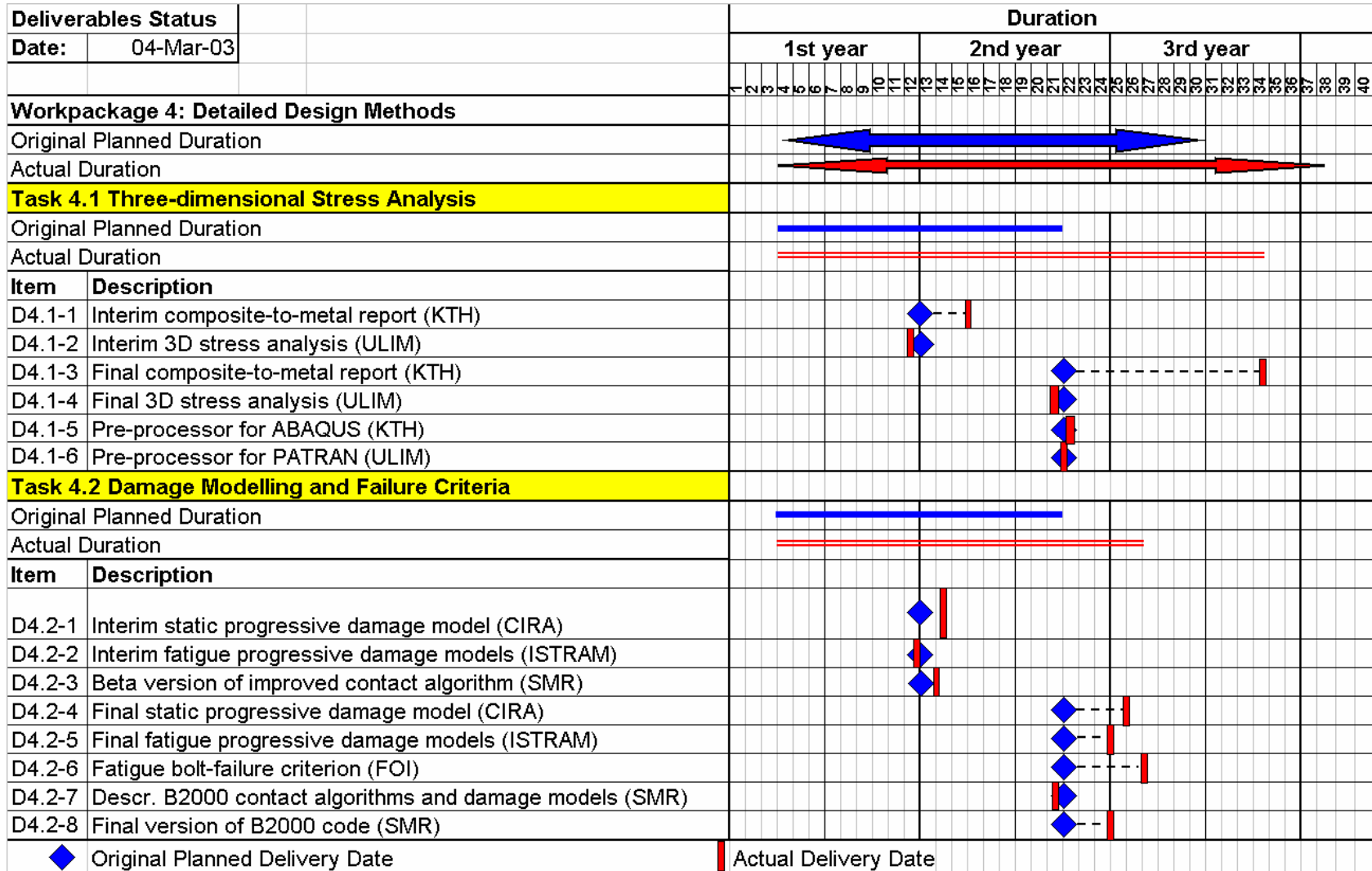


TABLE 5.4C: DELIVERABLES TIMING – TASKS 4.1 AND 4.2

Deliverable No.	Month Due	Description	Resp. Partner(s)	Status
D4.3-1	6	Review of techniques to couple global-local analyses (Written Report).	CIRA	Delivered On Schedule
D4.3-2	12	Description of progress on methods of coupling 2D and 3D models, and methods by which global models will be improved through independent local 3D modelling (Written Report).	DERA	Delivered Month 18.
D4.3.3	12	Description of progress on B2000 implementation of global-local coupling methods and initial models of DA benchmarks (Written Report).	SMR	Delivered Month 13
D4.3-4	12	Beta version of coding of global-local techniques in B2000 (Software)	SMR	Delivered to CIRA Month 13
D4.3-5	12	Splitting Method interim report including numerical algorithms and a 3D solution of two SAAB benchmark problems without friction (Written Report).	FFA	Delivered Month 14
D4.3-6	18	Validation of global-local analysis techniques developed by SMR, with local progressive damage models, and suggestions for inclusion of damage effects in global B2000 models (Written Report).	CIRA	Delivered Month 36
D4.3-7	21	Coupled 2D/3D analysis methods final report, describing algorithms and software developed, results from application to the BAe benchmark structures, comparison of method relative to the global method, and updated methods for improvement of global models (Written Report).	QinetiQ	Part A delivered Month 25 Part B delivered Month 34
D4.3-8	21	Final report on coupled 2D/3D analysis methods in B2000, describing algorithms implemented, results from application to the DA benchmark structures, and suggestions for improvement of global models in B2000 (Written Report).	SMR	Part A delivered Month 21 Part B delivered Month 25 Part C delivered Month 32
D4.3-9	21	Final version of coding of global-local techniques in B2000 (Software)	SMR	Delivered Month 28
D4.3-10	21	Splitting Method final report including mathematical proofs of existence, uniqueness and exponential convergence properties to the exact full 3D-solution and implementation aspects of the splitting scheme on multi-processor computer systems. A 3D solution of two SAAB benchmark problems with friction (Written Report).	FOI	Part A (theory) delivered Month 31 Part B (results) delivered Month 33

**TABLE 5.4D: DELIVERABLES LIST – TASK 4.3**

<b>Deliverable No.</b>	<b>Month Due</b>	<b>Description</b>	<b>Resp. Partner(s)</b>	<b>Status</b>
D4.4-1	30	Results from numerical parameter studies on the effects of bolt-hole clearance under different joint configurations, material lay-ups and loading (Written Report).	ULIM	Delivered Month 32
D4.4-2	30	Results from optimisation study on multi-row joints, including design guidelines (Written Report).	KTH	Delivered Month 34
D4.4-3	30	Results from numerical parameter studies using damage models (Written Report).	CIRA	Delivered Month 32
D4.4-4	30	Results from optimisation study, and damage tolerance study of the SAAB benchmark (Written Report).	FOI	Part A (theory) delivered Month 35 Part B (results) delivered Month 38

**TABLE 5.4E: DELIVERABLES LIST – TASK 4.4**

Deliverables Status		Duration																																					
		1st year											2nd year											3rd year															
		1	2	3	4	5	6	7	8	9	10	11	12	13	14	15	16	17	18	19	20	21	22	23	24	25	26	27	28	29	30	31	32	33	34	35	36	37	38
Date:	04-Mar-03																																						
<b>Workpackage 4: Detailed Design Methods</b>																																							
Original Planned Duration																																							
Actual Duration																																							
<b>Task 4.3 Coupled Global-Local Methods</b>																																							
Original Planned Duration																																							
Actual Duration																																							
Item	Description																																						
D4.3-1	Review of coupled global-local analysis (CIRA)																																						
D4.3-2	Description of progress on coupling 2D and 3D models (QinetiQ)																																						
D4.3-3	Progress of global-local coupling (SMR)																																						
D4.3-4	Beta version of global-local techniques (SMR)																																						
D4.3-5	Interim report on splitting method (FOI)																																						
D4.3-6	Validation of global-local analysis technique (CIRA)																																						
D4.3-7	Coupled 2D/3D analysis methods (QinetiQ)																																						
D4.3-8	Coupled 2D/3D analysis methods in B2000 (SMR)																																						
D4.3-9	Coding of global-local techniques in B2000 (SMR)																																						
D4.3-10	Splitting method final report (FOI)																																						
<b>Task 4.4 Parameter Studies</b>																																							
Original Planned Duration																																							
Actual Duration																																							
Item	Description																																						
D4.4-1	Results from numerical parameter studies (ULIM)																																						
D4.4-2	Results from optimisation study (KTH)																																						
D4.4-3	Results from numerical parameter studies (CIRA)																																						
D4.4-4	Results from optimisation study and damage tolerance (FOI)																																						
Original Planned Delivery Date		Actual Delivery Date		Part 1,2,3 (delivered)																																			

**TABLE 5.4F: DELIVERABLES TIMING – TASKS 4.3 AND 4.4**



<b>Deliverable No.</b>	<b>Month Due</b>	<b>Description</b>	<b>Resp. Partner(s)</b>	<b>Status</b>
D5-1	6	Specification report on progressive damage specimen tests summarising test matrix, instrumentation, and loading (Written Report).	CIRA	Delivered On Schedule
D5.2	6	Specification report on friction and fatigue specimen tests summarising test matrix, instrumentation, and static/fatigue loading (Written Report).	FFA	Delivered On Schedule
D5-3	6	Specification report on environment specimen tests summarising test matrix, instrumentation, environmental conditions, and static/fatigue loading (Written Report).	NLR	Delivered Month 10
D5-4	6	Specification report on composite-to-metal specimen tests summarising test matrix, instrumentation, and loading (Written Report).	KTH	Delivered Month 7
D5-5	6	Specification report on hole tolerance specimen tests summarising test matrix, instrumentation, and static/fatigue loading (Written Report).	ULIM	Delivered On Schedule
D5-6	18	Test data + analysis of results from progressive damage specimen tests (Written Report).	CIRA	Delivered Month 28
D5-7	18	Test data + analysis of results from friction and fatigue specimen tests (Written Report).	FOI	Delivered Month 28
D5-8	18	Test data + analysis of results from environment specimen tests (Written Report).	NLR	Delivered Month 32
D5-9	18	Test data + analysis of results from composite-to-metal specimen tests (Written Report).	KTH	Delivered Month 33
D5-10	18	Test data + analysis of results from bolt-hole clearance specimen tests (Written Report).	ULIM	Part 1 delivered On Schedule Part 2 delivered Month 35

**TABLE 5.5A: DELIVERABLES LIST – WP 5**

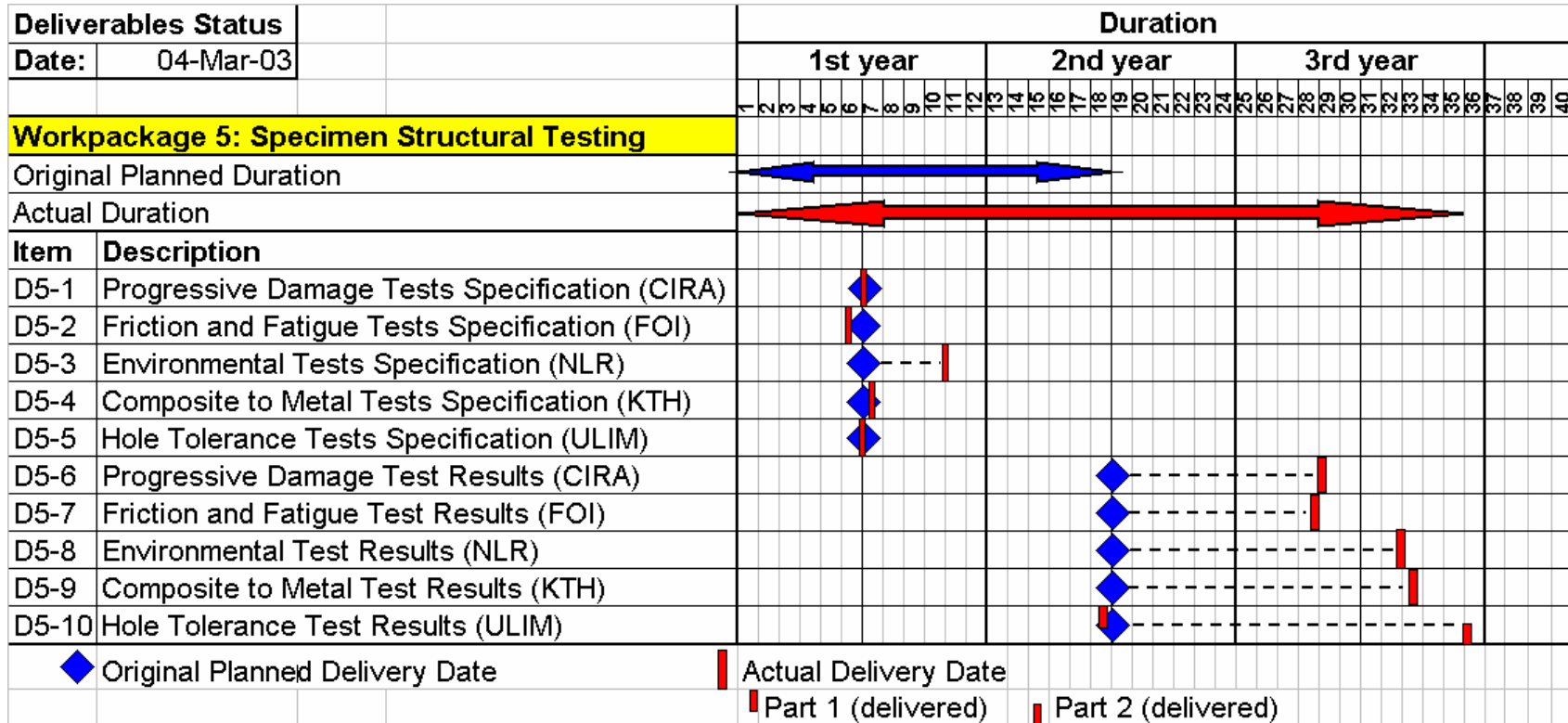


TABLE 5.5B: DELIVERABLES TIMING – WP 5

Deliverable No.	Month Due	Description	Resp. Partner(s)	Status
D6.1-1	35	Report on assessment of detailed design tools (Written Report).	CIRA	Delivered Month 37
D6.2-1	35	Report on design guidelines (Written Report).	QinetiQ	Delivered Month 38

Deliverables Status		Duration																																							
Date:	04-Mar-03	1st year											2nd year											3rd year																	
		1	2	3	4	5	6	7	8	9	10	11	12	13	14	15	16	17	18	19	20	21	22	23	24	25	26	27	28	29	30	31	32	33	34	35	36	37	38	39	40
<b>Workpackage 6: Design Methodology</b>																																									
Original Planned Duration																																									
Actual Duration																																									
<b>Task 6.1 Assessment of Detailed Design Methods</b>																																									
Original Planned Duration																																									
Actual Duration																																									
<b>Item</b>	<b>Description</b>																																								
D6.1-1	Assessment Report - Detailed Design Tools (CIRA)																																								
<b>Task 6.2 Design Guidelines</b>																																									
Original Planned Duration																																									
Actual Duration																																									
<b>Item</b>	<b>Description</b>																																								
D6.2-1	Design Guidelines Report (QinetiQ)																																								
◆ Original Planned Delivery Date																																									
Actual Delivery Date																																									

TABLE 5.6: DELIVERABLES LIST AND TIMING – WP 6

<b>Deliverable No.</b>	<b>Month Due</b>	<b>Description</b>	<b>Resp. Partner(s)</b>	<b>Status</b>
D7.1-1	8	Project 6-Month Report	ULIM	Delivered On Schedule
D7.1-2	14	Project 12-Month Report	ULIM	Delivered On Schedule
D7.1-3	21	Project Mid-term Assessment Report	ULIM	Delivered On Schedule
D7.1-4	26	Project 24-Month Report	ULIM	Delivered On Schedule
D7.1-5	32	Project 30-Month Report	ULIM	Delivered On Schedule
D7.1-6	38	Project Final Report	ULIM	To be delivered Month 42
D7.2-1	21	Draft Technology Implementation Plan	DERA	Delivered On Schedule
D7.2-2	38	Technology Implementation Plan	DERA	To be delivered Month 42
D7.2-3	6	Guidelines to partners on electronic reporting	SMR	Delivered Month 10
D7.2-4	18	Beta Version of BOJCAS Web Site	SMR	Delivered On Schedule
D7.2-5	36	CD or DVD with all project results. Final BOJCAS Web Site	SMR	Website delivered On Schedule CD to be delivered Month 38

**TABLE 5.7A: DELIVERABLES LIST – WP 7**

Deliverables Status		Duration																																							
		1st year										2nd year										3rd year																			
Date:	04-Mar-03	1	2	3	4	5	6	7	8	9	10	11	12	13	14	15	16	17	18	19	20	21	22	23	24	25	26	27	28	29	30	31	32	33	34	35	36	37	38	39	40
<b>Workpackage 7: Network Management</b>																																									
Original Planned Duration																																									
Actual Duration																																									
<b>Task 7.1 Management</b>																																									
Original Planned Duration																																									
Actual Duration																																									
Item	Description																																								
D7.1-1	Project 6-Month Report (ULIM)																																								
D7.1-2	Project 12-Month Report (ULIM)																																								
D7.1-3	Project Mid-Term Assessment Report (ULIM)																																								
D7.1-4	Project 24-Month Report (ULIM)																																								
D7.1-5	Project 30-Month Report (ULIM)																																								
D7.1-6	Project Final Report (ULIM)																																								
<b>Task 7.2 Exploitation</b>																																									
Original Planned Duration																																									
Actual Duration																																									
Item	Description																																								
D7.2-1	Draft Technology Implementation Plan (QinetiQ)																																								
D7.2-2	Technology Implementation Plan (QinetiQ)																																								
D7.2-3	Guidelines to Partners on Electronic Reporting (SMR)																																								
D7.2-4	Beta Version of BOJCAS Web Site (SMR)																																								
D7.2-5	CD or DVD with all Project Results. Final BOJCAS Website (SMR)																																								
◆	Original Planned Delivery Date																																								
■	Actual Delivery Date																																								

TABLE 5.7B: DELIVERABLES TIMING – WP 7

## 6. Planned Activities vs. Actual Work

As can be seen from the list of deliverables in the previous section, to a large extent (probably more than 95%), the work content was delivered directly in line with the Description of Work, although clearly there were some significant delays. Thus, presented here, are the main deviations from the work plan.

### NLR

NLR deviated from the work plan as follows:

- WP 3: The fatigue DA benchmark tests were cancelled (a total of two tests)
- WP 2: The development of a new global design method was curtailed. The original spring method was slightly improved by the use of beams, but no significantly new method was developed, and validation against test results did not occur.

The main reasons for this deviation were:

- A mismatch between budget and work required. Basically, the work involved in the testing was underestimated. NLR was involved in WP 2, 3, 5, and 7, i.e. modelling, benchmark testing, specimen testing, and management, which spread resources thinly.
- Elaborate instrumentation was applied which made the results much more valuable, but aggravated the budgetary problems.
- The manufacture of the specimens for WP 5 was much more complex than anticipated as a result of the effort to assess the behaviour of various benchmark details.
- NLR was involved much more in the *design* of the SAAB and particularly the DA benchmark structures, than anticipated. NLR had expected to simply receive production drawings, from which to manufacture the specimens, but this was not the case.
- The mismatch between the resources allocated and the work required would not have been solved with a different management approach. However, the magnitude of the problem only became evident in the later stages of the project, and communication on these issues should have been more timely. Moreover, the pressure to produce results and deliverables aggravated the above-mentioned mismatch.

NLR tried to be as responsive as possible in the circumstances, and spent a large amount of money and man-months from its own resources. NLR's experimental results provided a valuable contribution to the programme for the verification of the design methods. NLR's contribution to the modelling work provided an important stepping-stone for the implementation of the global-local methodology.

The major effects of this deviation on the project were:

- There was no knock-on effect of the cancelled fatigue tests, since these were not to be modelled. There was only a loss of basic research information from two fatigue tests.
- Originally, there were to be three global design methods developed within BOJCAS, each taking a different approach. The other two global design methods have been

developed successfully by SAAB and QinetiQ. Thus there were two instead of three global design methods developed in BOJCAS.

- A knock-on effect of the cancellation of NLR's modelling developments existed in Task 2.4, in which Airbus Deutschland was to implement NLR's developed method into MSC.Patran and MSC.Nastran, and evaluate the method in an industrial setting. An alternative work plan for this task was drawn up, whereby Airbus Deutschland implemented SMR's global-local method from Task 4.3 instead of NLR's global method from Task 2.3. This was written as an amendment to the contract, which was accepted by the EU in Autumn 2002.

### **Airbus Deutschland**

As noted above, AD revised its work in Task 2.4. In the very short time period available, AD implemented SMR's global-local method in ANSYS, and tested it on the DA benchmark structure. SMR provided FORTRAN source for developing parameterised models, but as AD was unable to port this to their environment in the time available, they decided to develop their own tool in the ANSYS programming language.

### **QinetiQ**

Once work within BOJCAS began, it became apparent that QinetiQ's original work descriptions for Tasks 2.3 and 4.3 were inappropriate, and that the aims of the tasks could be achieved using alternative methods. The original plan was to use modified spring-elements for the global methods and to calibrate these methods using a coupling between local 3D solid models and the shell-element and spring-element based global models. For the improved global methods the emphasis changed to the use of beam and analytical rigid surface representations of the fastener and foundation, which did not rely upon calibration from local solid models. For the global-local coupling methods the emphasis changed to the transfer of boundary conditions between separate global and local shell models.

These changes were demonstrated to be extremely effective. QinetiQ consider their method to be the most flexible of the tools developed within BOJCAS. The methods can deal with complex geometry, they are quick to solve, they can be used with a range of commercial pre-processors, and they can be easily modified to work with a range of commercial FEA codes.

### **KTH**

In May 2002, KTH requested a change to their work plan that was accepted by the EU without an amendment to the contract, since it did not affect their total effort or budget breakdown. Briefly, the details of the change were:

- KTH originally planned 26 tests in WP 5. However, the programme was greatly expanded and more than 200 tests were performed.
- As noted in Task 4.1 above, there were discrepancies between the tests and the models, which took a great deal of time to explain (eventually it turned out to be due to the non-concentric holes in the aluminium and composite plates).

- Due to the above extra efforts, the originally planned optimisation study in Task 4.4 was not possible. Instead extensive comparisons between simulations and the expanded test programme were performed.

### **Delays**

As seen in Section 5, there were a number of delays compared to the planned programme. In the end, these delays were recovered. It would be untrue however to say that the delays had no effect on the programme. The main effect was probably that in some cases, validation of developed modelling methods to the extent originally hoped for was not possible.

### **Extra work**

A number of partners performed work beyond that originally planned. A non-exhaustive list includes:

- Modelling of the *Single-Bolt Benchmark* and the *Multi-Bolt Benchmark*.
- QinetiQ modelled the DA benchmark for comparison with other methods
- ULIM produced a Version 2.0 of BOLJAT in Task 4.4, which was not planned
- KTH greatly expanded their experimental programme in WP 5
- SMR wrote a document on encryption for the consortium
- ULIM performed extra tests to try to understand the difference between the experimental and numerically measured stiffness of the *Single-Bolt Benchmark*.



## **7. Management and Co-ordination Aspects**

### **7.1 Performance of the Consortium**

In general the Consortium interacted well, and showed a high degree of dedication to the project. Several partners went over budget, and used internal funds to complete the work. Meetings generally lasted 2.5 days, which is unusually long, but this allowed for valuable technical discussions between partners. Attendance at meetings was very good. Co-operation between partners has been excellent, and results and advice were freely exchanged. Partners were flexible in taking on extra work, e.g. the modelling of the *Single* and *Multi-Bolt Benchmarks* was not in the original programme, but was a valuable exercise. Several publications have already resulted from BOJCAS (listed in the following sections) and many more are planned.

Unfortunately delays were experienced due to various reasons, such as overly ambitious targets in the first half of the project, unexpected complexities in some of the testing (particularly for the benchmark structures), performance of extra work beyond the Description of Work, and difficulties in obtaining priority for BOJCAS within partner organisations. However, deliverables have generally been of a high standard, and many valuable results have come out of the project.

Specific difficulties of partners, and deviations from the programme were covered in the previous section.

Manpower/progress and Budget Follow-up Tables are given at the end of this report (Tables 7.1 and 7.2).

## 7.2 Contacts for Follow-up

The contact details for follow-up of the project are listed in Table 7.1.

Partner	Contact Details
ULIM	Dr. Michael McCarthy Department of Mechanical and Aeronautical Engineering University of Limerick Limerick, Ireland Tel: +353-61-202-222 Email: <a href="mailto:michael.mccarthy@ul.ie">michael.mccarthy@ul.ie</a>
AUK	Mr. Eoin Simon Airbus UK Building 07C Filton Bristol BS99 7AR, UK Tel: +44 117 936 3219 Email: <a href="mailto:eoin.simon@airbus.com">eoin.simon@airbus.com</a>
AD	Dr. Dieter Hachenberg Airbus Deutschland Kreetslag 10 Hamburg 21129, Germany Tel: +49 40 74 376 897 Email: <a href="mailto:dieter.hachenberg@airbus.com">dieter.hachenberg@airbus.com</a>
SAAB	Dr. Tomas Ireman SAAB AB Saab Aerospace SE-581 88 Linköping, Sweden Tel: +46 13 182 595 Email: <a href="mailto:tomas.ireman@saab.se">tomas.ireman@saab.se</a>
CIRA	Dr. Aniello Riccio Centro Italiano Ricerche Aerospaziali S.C.p.A. (CIRA) Via Maiorise 81043 Capua, Italy Tel: +39 0823 623 508 Email: <a href="mailto:a.riccio@cira.it">a.riccio@cira.it</a>
QinetiQ	Mr. Peter Hopgood QinetiQ Ltd Future Systems Technology Division Room 2015/A7 Building Cody Technology Park Farnborough Hampshire GU14 0LX, UK Tel: +44 125 239 5148 Email: <a href="mailto:pjhopgood@qinetiq.com">pjhopgood@qinetiq.com</a>
FOI	Professor Börje Andersson Swedish Defence Research Agency (FOI) Aeronautics Division SE-17290 Stockholm, Sweden Tel: +46 8 555 04269 Email: <a href="mailto:ba@foi.se">ba@foi.se</a>

**Table 7.1 Partner contact details (continued overleaf)**

Partner	Contact Details
NLR	Mr. Joost van Rijn National Aerospace Laboratory (NLR) P.O. Box 153 8300 AD Emmeloord The Netherlands Tel: +31 527 248 603 Email: <a href="mailto:rijn@nlr.nl">rijn@nlr.nl</a>
ISTRAM	Professor Paraskevas Papanikos Institute of Structures and Advanced Materials (ISTRAM) 57, Patron-Athinon Road Patras 264 41, Greece Tel: +30 061 0426 570 Email: <a href="mailto:istram@hol.gr">istram@hol.gr</a>
KTH	Professor Dan Zenkert Kungl. Tekniska Högskolan Department of Aeronautical and Vehicle Engineering SE-100 44 Stockholm, Sweden Tel: +46 70 349 64 35 Email: <a href="mailto:danz@kth.se">danz@kth.se</a>
SMR	Dr. Pieter Volgers SMR S.A. Case postale 4014 CH-2500 Bienne 4, Switzerland Tel: +41 32 345 2123 Fax: +41 32 345 2120 Email: <a href="mailto:volgers@smr.ch">volgers@smr.ch</a>

**Table 7.1 (continued) Partner contact details**

## 7.3 Publications

### 7.3.1 Chapter in Book

The following chapter of a book is in preparation. It refers (with their permission) to the work of some of the partners in BOJCAS.

Schön, J., “Fatigue of Joints in Composite Structures”, *in*, “Fatigue in Composite Materials - A Review of the Science and Technology of the Fatigue Response of Fibre-Reinforced Plastics”, edited by Bryan Harris, University of Bath, Woodhead Publishing Ltd.

### 7.3.2 Journal Papers

The following papers have been published in journals:

	<b>Journal Paper</b>	<b>Partner</b>
1	Papanikos, P., K.I. Tserpes, Sp. Pantelakis, 2003, Modelling of fatigue damage progression and life of CFRP laminates, <i>Fatigue &amp; Fracture of Engineering Materials &amp; Structures</i> , 26, pp. 37-47.	ISTRAM
2	Padhi, G.S., M.A. McCarthy, C.T. McCarthy, 2002, BOLJAT – A tool for designing composite bolted joints using three-dimensional finite element analysis, <i>Composites, Part A</i> , 33/11, pp. 1573-1584.	ULIM
3	McCarthy, M.A., V.P. Lawlor, W.F. Stanley, C.T. McCarthy, 2002, Bolt-hole clearance effects and strength criteria in single-bolt, single-lap, composite bolted joints, <i>Composites Science and Technology</i> , Vol. 62, pp. 1415-1431.	ULIM
4	Lawlor, V.P., M.A. McCarthy, W.F. Stanley, 2002, Experimental Study on the Effects of Clearance on Single-Bolt, Single-Shear, Composite Bolted Joints, <i>Journal of Plastics, Rubber and Composites</i> , The Institute of Materials, London, UK, Vol. 31, No. 9, pp. 405-411.	ULIM
5	Stanley, W.F., M.A. McCarthy, V.P. Lawlor, 2002, Measurement of Load Distribution in Multi-Bolt, Composite Joints, in the presence of Varying Clearance, <i>Journal of Plastics, Rubber and Composites</i> , The Institute of Materials, London, UK, Vol. 31, No. 9, pp. 412-418.	ULIM
6	McCarthy, M.A., C.T. McCarthy, 2002, Finite Element Analysis of the effects of Clearance on Single-Shear, Composite Bolted Joints, <i>Journal of Plastics, Rubber and Composites</i> , The Institute of Materials, London, UK, Vol. 32, No. 2, in-press.	ULIM
7	Lawlor, V.P., W.F. Stanley, M.A. McCarthy, 2002, Characterisation of damage development in single-shear bolted composite joints, <i>Journal of Plastics, Rubber and Composites</i> , The Institute of Materials, London, UK, Vol 31, No. 3, pp. 126-133.	ULIM
8	M.A. McCarthy, 2001, BOJCAS: Bolted Joints in Composite Aircraft Structures, <i>Air and Space Europe</i> , No. 3/4, Vol. 3, pp. 139-142.	ULIM

### 7.3.3 Conference Publications

The following papers have been presented at conferences:

	<b>Conference Paper</b>	<b>Partner</b>
1	Perugini, P, A. Riccio and F. Scaramuzzino, 2001, Three-Dimensional Progressive Damage Analysis of Composite Joints, in Proceedings of the Eighth International Conference on Civil and Structural Engineering Computing, B.H.V. Topping, (Editor), Civil-Comp Press, Stirling, United Kingdom, paper 62.	CIRA
2	Riccio A and Scaramuzzino F., 2002, Influence of Damage Onset and Propagation on The Tensile Structural Behaviour of Protruding Composite Joints, presented at The 4th GRACM Congress on Computational Mechanics GRACM 2002, Patras, Greece, 27-29 June.	CIRA
3	Schön, J., 2002, Fatigue life prediction of composite bolted joints with bolt failure, FATIGUE 2002, Stockholm, June 2002, Vol. 2/5, pp. 1119-1126.	FOI
4	Tserpes, K.I., P. Papanikos, and Th. Kermanidis, 2002, Progressive fatigue damage modelling of CFRP laminates at the meso-scale level, Proceedings of the International Symposium of Multiscaling in Mechanics, Messini, 2-6 September, Greece, pp. 71-82.	ISTRAM
5	Volgers, P.T.G., 2002, Detailed 3D analysis of bolted joints in global shell structures, 4th B2000 Workshop, Ligerz, Switzerland.	SMR
6	McCarthy, C.T., M.A. McCarthy, G.S. Padhi, 2002, Automated Three-dimensional Finite Element Modelling of Composite Aircraft Bolted Joints – Modelling Issues, Worldwide Aerospace Conference and Technology Showcase, Toulouse, 8-10 April, published on CD-ROM and on <a href="http://www.mscsoftware.com/events/aero2002/">http://www.mscsoftware.com/events/aero2002/</a> .	ULIM
7	McCarthy, M.A., C.T. McCarthy, G.S. Padhi, 2002, Initial Multi-Bolt Results from BOLJAT, a Tool for Semi-Automated Three-dimensional Modelling of Composite Aircraft Bolted Joints, Worldwide Aerospace Conference and Technology Showcase, Toulouse, 8-10 April, published on CD-ROM and on <a href="http://www.mscsoftware.com/events/aero2002/">http://www.mscsoftware.com/events/aero2002/</a> .	ULIM
8	Lawlor, V.P, M.A. McCarthy, W.F. Stanley, 2002, Experimental Study on the Effects of Clearance on Single-Bolt, Single-Shear, Composite Bolted Joints, Ninth International Conference on Fibre-Reinforced Composites, University of Newcastle, 25-28 March, pp. 316-326.	ULIM
9	Stanley, W.F., M.A. McCarthy, V.P. Lawlor, 2002, Measurement of Load Distribution in Multi-Bolt, Composite Joints, in the presence of Varying Clearance, Ninth International Conference on Fibre-Reinforced Composites, University of Newcastle, 25-28 March, pp. 296-307.	ULIM

Continued overleaf →

	<b>Conference Paper</b>	<b>Partner</b>
10	McCarthy, M.A., C.T. McCarthy, 2002, Finite Element Analysis of the effects of Clearance on Single-Shear, Composite Bolted Joints, Ninth International Conference on Fibre-Reinforced Composites, University of Newcastle, 25-28 March, pp. 427-436.	ULIM
11	McCarthy, C.T., M.A. McCarthy, G.S. Padhi, 2001, Three-dimensional Modelling of Single-Bolt Composite Joints, 9th Annual Conference, Association for Computational Mechanics in Engineering, University of Birmingham, 8-10 April, pp. 111-114.	ULIM
12	McCarthy, M.A., C.T. McCarthy, G.S. Padhi, 2001, Three-dimensional Modelling of Multi-Bolt Composite Joints, 9th Annual Conference, Association for Computational Mechanics in Engineering, University of Birmingham, 8-10 April, pp. 123-126.	ULIM
13	Lawlor, V.P, W.F. Stanley, M.A. McCarthy, 2001, Characterisation of damage development in bolted composite joints, 6th International Conference on Deformation, Yield and Fracture of Composites, UMIST Manchester, 4-5 April, pp. 377-386.	ULIM
14	McCarthy, M. A., G. S.Padhi, W. Stanley, C. McCarthy and V. Lawlor. 2000, Three-dimensional Stress Analysis of Composite Bolted Joints. Tenth National Seminar on Aerospace Structures, Indian Institute of Technology, Kanpur, India, December 8-9, pp. 153-167.	ULIM
15	Padhi, G.S., M.A. McCarthy, 2002, Bolted Joint Analysis Tool (BOLJAT), abstract only, Irish Society for Scientific and Engineering Computation Annual Symposium, 24-25 May, p.9.	ULIM
16	McCarthy, C.T., M.A. McCarthy, 2002, Strength prediction and damage initiation of composite aircraft bolted joints, abstract only, Irish Society for Scientific and Engineering Computation Annual Symposium, 24-25 May, p.7.	ULIM
17	McCarthy, M.A., 2001, BOJCAS: Bolted Joints in Composite Aircraft Structures, abstract only, Fourth EU Community Aeronautical Days, Hamburg, Germany, 29-31 January, p. 167.	ULIM
18	McCarthy, C.T., M.A. McCarthy, G.S. Padhi, 2001, Finite Element Modelling of Single-Bolt Composite Joints, abstract only, Irish Society for Scientific and Engineering Computation Annual Symposium, 18-19 May, p.12.	ULIM
19	McCarthy, M.A., C.T. McCarthy, G.S. Padhi, 2001, Finite Element Modelling of Multi-Bolt Composite Joints, abstract only, Irish Society for Scientific and Engineering Computation Annual Symposium, 18-19 May, p.20.	ULIM
20	McCarthy, M.A., G.S. Padhi, W.Stanley, C. McCarthy, V. Lawlor, 2000, Bolted Joints in Composite Aircraft Structures, abstract only, Irish Society for Scientific and Engineering Computation Annual Symposium, 19-20 May, p.7.	ULIM

### **7.3.4 Other Publications**

QinetiQ and AUK gave a joint presentation at an Institute of Materials Seminar in the UK in April 2002.

QinetiQ presented the Aerodays presentation (courtesy of ULIM) and a summary of QinetiQ's work to the Imperial College/QinetiQ one-day industrial workshop on 'Joining and Assembly of Composite Components' at Imperial College on 26th April 2001.

An article on ULIM's activities in BOJCAS appeared in the *Irish Times*, June 14<sup>th</sup>, 2001.

## 8. Results and Conclusions

The principal tools/methodologies resulting from BOJCAS are:

- The SAAB global analysis method
- The QinetiQ global analysis method
- The SMR global-local coupling method
- The FOI splitting method, developed for optimisation and damage tolerance studies of bolted joints
- The QinetiQ global-local analysis method
- BOLJAT – ULIM's tool for creation of 3D bolted joint models
- The KTH tool for creation of 3D bolted joint models
- The CIRA quasi-static progressive damage methodology for composites (implemented as a new element in SMR's code, B2000)
- The ISTRAM fatigue progressive damage methodology for composites
- The ULIM Initial Damage Criterion

In addition a great deal of basic research information has been generated. Among the more interesting findings are:

- Traditional global joint modelling methods, whereby the fastener load is introduced at a point into a shell mesh result in excessively uneven load distributions. They also suffer from mesh sensitivity and difficulties with calibration by experiment.
- The developed global methods showed good agreement with experimental and 3D modelling results concerning load distributions and (for SAAB's method) strains 4 mm from holes in complex joints. Results for single-lap joints were not as good as for double-lap joints. Both developed methods are convenient to use and possess fast execution times.
- Series and parallel global-local coupling methods have been implemented. Parallel methods are probably preferable for accuracy. Parallel coupling of linear shell and solid elements has been performed, and at least in the initial post-buckled state, the presence of the local model did not appreciably disturb the global displacement shapes and stress levels. The use of the new progressive damage element in B2000 within a global-local model has been demonstrated.
- With a very efficient computational method such as the splitting method, implemented on modern SMP computers, optimisation of complex real-life, bolted joints is feasible. Optimisation on the basis of multiple constraints, covering all modes of failure has not yet been demonstrated though.
- Instrumented bolts have been shown (by comparison with 3D FE) to give accurate results for the load distribution in in-line, multi-bolt joints, provided they are used with great care. The method works with single-lap and double-lap geometries. The disadvantages of instrumented bolts are high cost, specificity to a single joint configuration (e.g. any change to the joint thickness, requires a new instrumented bolt), and the need to keep the load levels below that which would damage the bolts (cannot test to failure).



- Strain gauge measurement of bolt load distribution has been shown (again by comparison with 3D FE) to give an accurate estimate of load distribution in in-line, *double-lap* joints. KTH also showed that by machining slots to allow placing of gauges in the shear plane, they can also be used for determining load distribution in *single-lap* joints (see D5-9). This can only be done if one of the joined parts is metallic. The advantages of the strain gauge method are relative low cost, relative ease-of-use, and (due to lower cost) ability to be used in tests to failure. It is also more flexible for application to joints of different thicknesses etc.
- Predictions for compressive BAe benchmark joints were found to be quite conservative, indicating the possibility for optimisation of bolted CFC compression joints.
- Measurement techniques for out-of-plane displacement (laser displacement transducers used by NLR, optical whole field measurement by KTH) showed good tie-up with models, indicating their validity.
- Measurement of joint longitudinal deflection for comparison with FE cannot be done using machine stroke. Some kind of measurement on the specimen is needed (extensometers, LVDTs, optical whole field measurement etc).
- Provided great care is taken to accurately model the geometric and material properties of the joint, 3D finite element analysis has been shown to provide very accurate predictions of joint behaviour, capable of capturing 3D stress distributions, and sensitive to small changes in parameters. Indeed, provided contact and friction are modelled correctly, the agreement with techniques such as instrumented bolts was so good, that 3D FE can be confidently used to predict load and strain/stress distributions in bolted joints.
- The main exception to the above statement is in the region of singularities arising from point or line contact between parts, and discontinuous fibre directions in material layers (causing singularities at the hole edge). The domain governed by the singularities is typically 2-3 ply thicknesses in size. Stresses in such regions are infinite.
- One difference between the 3D models and the experiments, found by several partners, was that the simulations tended to give a slightly (10-12%) higher stiffness than the experiments. This was true of even the most refined models. The consistency of the difference though means that parameter studies should be valid.
- A major benefit from 3D models is the insight they give into the complex interactions (e.g. bearing-bypass interactions) within multi-bolt joints.
- The amount of information generated by 3D models is very large, and it has not yet been determined how best to use all the information that becomes available. Post-processing is a time-consuming process at present.
- Pre-processing tools like ULIM and KTH tools can dramatically reduce the time needed to create 3D models. Post-processing capabilities should be implemented in such tools in the future.
- Bolt-hole clearance has been found by ULIM to have an important effect on the load distribution, and initial failure strength of composite bolted joints. Interestingly, though KTH did not initially set out to investigate clearance, they found that only by accurately modelling the actual clearances in their tests, could they achieve a match

between simulations and experiments. ULIM also found that clearance could affect the initial failure strength of double-lap, multi-bolt joints by as much as 25%.

- Comparing joint configurations solely by their *ultimate* strength may mask effects of joint variables. Comparison of “initial damage” strength is likely to be more sensitive to joint parameters.
- ULIM’s *Initial Damage Criterion* may be more closely related to joint damage than traditional offset methods, and may be less sensitive to operator variations.
- Progressive damage modelling methods appear to be able to model the non-linear behaviour in composite joints quite well. Results were however better for some configurations than others, some tuning is required, and the models do not always run to the “end” of the experiment. Developing a fatigue progressive damage modelling methodology, that does not require enormous quantities of test data as input, is an on-going research problem.
- For joints that fail due to fatigue failure of bolts, their failure can be predicted from fatigue curves of the metal they are made from.
- Fatigue failure of joints is affected by torque. However maintaining torque over the lifetime of the joint is a problem.
- Fatigue can be a serious consideration in some composite bolted joint configurations.
- Simple failure criteria have not been addressed in BOJCAS. Future work might involve developing simple criteria usable in 3D models.

Overall, the state-of-the-art in terms of modelling techniques and know-how for bolted composite joints has been significantly advanced in BOJCAS. It is believed that as the new knowledge is assimilated into the European aircraft industry, improved composite bolted joint design will be possible. It can thus be said that the BOJCAS project objectives have been achieved.

## **9. Acknowledgements**

The BOJCAS consortium wishes to gratefully acknowledge the financial support of the EU for the work, and particularly the helpful advice and assistance received from the EU Officer, Mr. Hans von den Driesch.

## 10. References

1. Nelson, W.D., Bunin, B.L., Hart-Smith, L.J., “Critical Joints in Large Composite Aircraft Structure”, NASA Contractor Report 3710, 1983.
2. Barrois W., ”Stresses and displacements due to load transfer by fasteners in structural assemblies”, Engineering Fracture Mechanics, Vol. 10, No. 1, 1978.
3. Whitney J. M. and Nuismer R. J., “Uniaxial failure of composite laminates containing stress concentrations”, Journal of composite materials, Vol. 8, 1974, pp 253-265.
4. Grumman Aerospace Corporation, Viggen Composite Vertical Stabilizer, First Quarterly Progress Report, pp.3-15, 1977.
5. Padhi, G.S., M.A. McCarthy, C.T. McCarthy, 2002, “BOLJAT – A tool for designing composite bolted joints using three-dimensional finite element analysis”, Composites, Part A, 33/11, pp. 1573-1584.
6. M. Doreille. Athapascan-1: vers une modèle de programmation parallèle adapté au calcul scientifique. (in French) PhD thesis. INPC University of Grenoble, Grenoble, France. 1999
7. P.T.G. Volgers. Lagrange-like contact in ETA. MSc thesis, Delft University of Technology, Delft, the Netherlands. 1997
8. T. Ireman Three-dimensional stress analysis of bolted single-lap composite joint. Composite Structures. 43, pp. 195-216, 1998.
9. M.M. Shokrieh, L.B. Lessard, Progressive fatigue damage modelling of composite materials. Part I: Modelling. J. Composite Materials. 34, pp. 1056-1080, 2001.
10. M.M. Shokrieh, L.B. Lessard Progressive fatigue damage modeling of composite materials. Part II: Material characterization and model verification. J. Composite Materials. 34, pp. 1081-1116, 2001.
11. ASTM D953. Standard Test Method for Bearing Strength of Plastics.
12. K.I. Tserpes, P. Papanikos, Th. Kermanidis. A three-dimensional progressive damage model for bolted joints in composite laminates subjected to tensile loading. Fatigue Fract Engng Mater Struct, 24(10), pp.663-675, 2001.
13. Hyer, M.W., Klang, E.C., and Cooper, D.E., “The Effects of Pin Elasticity, Clearance, and Friction on the Stresses in a Pin-Loaded Orthotropic Plate” Journal of Composite Materials, Vol.21, March 1987.
14. McCarthy, M.A., V.P. Lawlor, W.F. Stanley, C.T. McCarthy, 2002, Bolt-hole clearance effects and strength criteria in single-bolt, single-lap, composite bolted joints, Composites Science and Technology, Vol. 62, pp. 1415-1431.
15. Lawlor, V.P, M.A. McCarthy, W.F. Stanley, 2002, Experimental Study on the Effects of Clearance on Single-Bolt, Single-Shear, Composite Bolted Joints, Journal of Plastics, Rubber and Composites, The Institute of Materials, London, UK, Vol. 31, No. 9, pp. 405-411.
16. Lawlor, V.P, W.F. Stanley, M.A. McCarthy, 2002, Characterisation of damage development in single-shear bolted composite joints, Journal of Plastics, Rubber and Composites, The Institute of Materials, London, UK, Vol 31, No. 3, pp. 126-133.
17. Stanley, W.F., M.A. McCarthy, V.P. Lawlor, 2002, Measurement of Load Distribution in Multi-Bolt, Composite Joints, in the presence of Varying Clearance, Journal of Plastics, Rubber and Composites, The Institute of Materials, London, UK, Vol. 31, No. 9, pp. 412-418.

18. McCarthy, M.A., C.T. McCarthy, 2002, Finite Element Analysis of the effects of Clearance on Single-Shear, Composite Bolted Joints, Journal of Plastics, Rubber and Composites, The Institute of Materials, London, UK, Vol. 32, No. 2, in-press.
19. ASTM standard D 5961 / D 5961M - 96, Standard test method for bearing response of polymer matrix composite laminates, 1996.
20. DODSSP, Polymer Matrix Composites, MIL-HDBK-17, DODSSP, Naval Publications and Forms Center, Standardization Documents Order Desk, Building 4D, 700 Robbins Ave., Philadelphia, PA 19111-5094.
21. Starikov, R. and Schön, J., Experimental study on fatigue resistance of composite joints with protruding-head bolts, Comp. Struct., Vol. 55 (2001), pp. 1-11.

WP/Task (N°/title)	Partner (Name/ abbrev.)	----- Man-Month -----								----- Technical Progress % -----			Comments on major deviations and/or modifications of planned efforts.	
		Planned efforts - at start of period				Actual effort (MM)				Devia- tion (MM)	Planned (%)	Assessed* (%)		Devia- tion (%)
		Year 1	Year 2	Year 3	Total	Year 1	Year 2	Years 3&4	Total	Totals	Years 1-4	Years 1-4		Now
		a	b	c	d	a1	b1	c1	d1	d1-d				
1. Design Requirements														
	AUK	1			1	1			1		100%	100%		
	AD	1			1	1			1		100%	100%		
	SAAB	1			1	1			1		100%	100%		
	<b>Total</b>	<b>3</b>			<b>3</b>	<b>3</b>			<b>3</b>		<b>100%</b>	<b>100%</b>		

\*) Please note that the actual technical progress percentage and the updated remaining efforts must reflect the physically assessed status of the work.

**TABLE 7.1 FINAL MANPOWER AND PROGRESS FOLLOW-UP TABLE (WORKPACKAGE 1)**

WP/Task (N°/title)	Partner (Name/ abbrev.)	----- Man-Month -----								----- Technical Progress % -----			Comments on major deviations and/or modifications of planned efforts.	
		Planned efforts - at start of period				Actual effort (MM)				Devia- tion (MM)	Planned (%)	Assessed* (%)		Devia- tion (%)
		Year 1	Year 2	Year 3	Total	Year 1	Year 2	Years 3&4	Total	Totals	Years 1-4	Years 1-4		Now
		a	b	c	d	a1	b1	c1	d1	d1-d				
2.1 Design of Benchmark Structures														
	AUK	2			2	2			2		100%	100%		
	AD	2			2	2			2		100%	100%		
	SAAB	1			1	1			1		100%	100%		
	<b>Total</b>	<b>5</b>			<b>5</b>	<b>5</b>			<b>5</b>		<b>100%</b>	<b>100%</b>		
2.2 Benchmark Modelling with Existing Global Design Methods														
	SAAB	1.5			1.5	1	0.5		1.5		100%	100%		
	QinetiQ	3.3			3.3	3.3			3.3		100%	100%		
	NLR	1			1		2		2	1	100%	100%		
	AUK	0.5			0.5	0.5			0.5		100%	100%		
	AD	0.5			0.5	0.5			0.5		100%	100%		
	<b>Total</b>	<b>6.8</b>			<b>6.8</b>	<b>5.3</b>	<b>2.5</b>		<b>7.8</b>	<b>1</b>	<b>100%</b>	<b>100%</b>		

\*) Please note that the actual technical progress percentage and the updated remaining efforts must reflect the physically assessed status of the work.

**TABLE 7.1 (CONTINUED) FINAL MANPOWER AND PROGRESS FOLLOW-UP TABLE (TASKS 2.1 AND 2.2)**

WP/Task (N°/title)	Partner (Name/ abbrev.)	----- Man-Month -----								----- Technical Progress % -----			Comments on major deviations and/or modifications of planned efforts.	
		Planned efforts - at start of period				Actual effort (MM)				Devia- tion (MM)	Planned (%)	Assessed* (%)		Devia- tion (%)
		Year 1	Year 2	Year 3	Total	Year 1	Year 2	Years 3&4	Total	Totals	Years 1-4	Years 1-4		Now
		a	b	c	d	a1	b1	c1	d1	d1-d				
2.3 Development of Global Design Methods														
	SAAB		3.6	0.9	4.5		3.1	0.9	4	-0.5	100%	100%		0.5 mm to WP 5
	QinetiQ		4.3	1.6	5.9		4.3	2.6	6.9	1	100%	100%		
	NLR		2.6	0.4	3		1	2	3		100%	10%	-90%	See Section 6
	AUK		0.5		0.5		0.25	0.25	0.5		100%	100%		
	AD		0.5		0.5		0.5		0.5		100%	100%		
<b>Total</b>		<b>11.5</b>	<b>2.9</b>	<b>14.4</b>		<b>9.15</b>	<b>5.75</b>	<b>14.9</b>	<b>0.5</b>	<b>100%</b>	<b>82%</b>	<b>-18%</b>		
2.4 Industrial Assessment of Global Design Methods														
	AUK			3	3			3	3		100%	100%		
	AD			3	3			3	3		100%	100%		
	SAAB			1	1			1	1		100%	100%		
	<b>Total</b>			<b>7</b>	<b>7</b>			<b>7</b>	<b>7</b>		<b>100%</b>	<b>100%</b>		

\*) Please note that the actual technical progress percentage and the updated remaining efforts must reflect the physically assessed status of the work.

**TABLE 7.1 (CONTINUED) FINAL MANPOWER AND PROGRESS FOLLOW-UP TABLE (TASKS 2.3 AND 2.4)**



WP/Task (N°/title)	Partner (Name/ abbrev.)	----- Man-Month -----								----- Technical Progress % -----			Comments on major deviations and/or modifications of planned efforts.	
		Planned efforts - at start of period				Actual effort (MM)				Devia- tion (MM)	Planned (%)	Assessed* (%)		Devia- tion (%)
		Year 1	Year 2	Year 3	Total	Year 1	Year 2	Years 3&4	Total	Totals	Years 1-4	Years 1-4		Now
		a	b	c	d	a1	b1	c1	d1	d1-d				
3. Benchmark Structural Testing														
	AUK	7	7		14	6.6	10.25		16.85	2.85	100%	100%		
	NLR	3.8	5.6		9.4	2.2	8.8	3	14	4.6	100%	100%		
	<b>Total</b>	<b>10.8</b>	<b>12.6</b>		<b>23.4</b>	<b>8.8</b>	<b>19.05</b>	<b>3</b>	<b>30.85</b>	<b>7.45</b>	<b>100%</b>	<b>100%</b>		

\*) Please note that the actual technical progress percentage and the updated remaining efforts must reflect the physically assessed status of the work.

**TABLE 7.1 (CONTINUED) FINAL MANPOWER AND PROGRESS FOLLOW-UP TABLE (WORKPACKAGE 3)**

WP/Task (N°/title)	Partner (Name/ abbrev.)	----- Man-Month -----								----- Technical Progress % -----			Comments on major deviations and/or modifications of planned efforts.	
		Planned efforts - at start of period				Actual effort (MM)				Devia- tion (MM)	Planned (%)	Assessed* (%)		Devia- tion (%)
		Year 1	Year 2	Year 3	Total	Year 1	Year 2	Years 3&4	Total	Totals	Years 1-4	Years 1-4		Now
		a	b	c	d	a1	b1	c1	d1	d1-d				
4.1 Three-dimensional Stress Analysis														
	KTH	8	8		16	8	7	1	16		100%	100%		
	ULIM	9.3	9		18.3	9.3	9		18.3		100%	100%		
	<b>Total</b>	<b>17.3</b>	<b>17</b>		<b>34.3</b>	<b>17.3</b>	<b>16</b>	<b>1</b>	<b>34.3</b>		<b>100%</b>	<b>100%</b>		
4.2 Damage Modelling and Failure Criteria														
	CIRA	3.9	2.1		6	3.9	1.5	0.6	6		100%	100%		
	SMR	2	1	1	4	2	2	1	5	1	100%	100%		
	ISTRAM	7	4		11	5	5.5	1.5	12	1	100%	100%		
	FOI		1.5		1.5		1	1.5	2.5	1	100%	100%		
<b>Total</b>	<b>12.9</b>	<b>8.6</b>	<b>1</b>	<b>22.5</b>	<b>10.9</b>	<b>10</b>	<b>4.6</b>	<b>25.5</b>	<b>3</b>		<b>100%</b>	<b>100%</b>		

\*) Please note that the actual technical progress percentage and the updated remaining efforts must reflect the physically assessed status of the work.

**TABLE 7.1 (CONTINUED) FINAL MANPOWER AND PROGRESS FOLLOW-UP TABLE (TASKS 4.1 AND 4.2)**

WP/Task (N°/title)	Partner (Name/ abbrev.)	----- Man-Month -----								----- Technical Progress % -----			Comments on major deviations and/or modifications of planned efforts.	
		Planned efforts - at start of period				Actual effort (MM)				Devia- tion (MM)	Planned (%)	Assessed* (%)		Devia- tion (%)
		Year 1	Year 2	Year 3	Total	Year 1	Year 2	Years 3&4	Total	Totals	Years 1-4	Years 1-4		Now
		a	b	c	d	a1	b1	c1	d1	d1-d				
4.3 Coupled Global-Local Methods														
	QinetiQ	2.3	4.1		6.4	2.1	4.3		6.4		100%	100%		
	FOI	2	2.5		4.5	1.5	4	1	6.5	2	100%	100%		
	SMR	1	2	1	4	0.5	2.5	1	4		100%	100%		
	CIRA	1	1		2	1	1	1	3	1	100%	100%		
	<b>Total</b>	<b>6.3</b>	<b>9.6</b>	<b>1</b>	<b>16.9</b>	<b>5.1</b>	<b>11.8</b>	<b>3</b>	<b>19.9</b>	<b>3</b>	<b>100%</b>	<b>100%</b>		
4.4 Parameter Studies														
	ULIM		3	7	10		3	7	10		100%	100%		
	KTH		2	6	8			8	8		100%	100%		
	CIRA		0.5	1.5	2		0.5	1.5	2		100%	100%		
	FOI		0.5	1.5	2		0.5	2.75	3.25	1.25	100%	100%		
	<b>Total</b>		<b>6</b>	<b>16</b>	<b>22</b>		<b>4</b>	<b>19.25</b>	<b>23.25</b>	<b>1.25</b>	<b>100%</b>	<b>100%</b>		

\*) Please note that the actual technical progress percentage and the updated remaining efforts must reflect the physically assessed status of the work.

**TABLE 7.1 (CONTINUED) FINAL MANPOWER AND PROGRESS FOLLOW-UP TABLE (TASKS 4.3 AND 4.4)**

WP/Task (N°/title)	Partner (Name/ abbrev.)	----- Man-Month -----								----- Technical Progress % -----			Comments on major deviations and/or modifications of planned efforts.	
		Planned efforts - at start of period				Actual effort (MM)				Devi- ation (MM)	Planned (%)	Assessed* (%)		Devi- ation (%)
		Year 1	Year 2	Year 3	Total	Year 1	Year 2	Years 3&4	Total	Totals	Years 1-4	Years 1-4		Now
		a	b	c	d	a1	b1	c1	d1	d1-d				
5. Specimen Structural Testing														
	SAAB	1			1	1	0.5		1.5	0.5	100%	100%		0.5 MM from WP 2
	CIRA	1.3	1.7		3	0.25	1.75	2	4	1	100%	100%		
	FOI	5	3.5		8.5	5	1.7	0.5	7.2	-1.3	100%	100%		
	NLR	3.5	1.5		5	3.1	10.6		13.7	8.7	100%	100%		
	KTH	4	4		8	4	3	1	8		100%	100%		
	ULIM	13	7		20	13	8	2	23	3	100%	100%		
<b>Total</b>	<b>27.8</b>	<b>17.7</b>		<b>45.5</b>	<b>26.35</b>	<b>25.55</b>	<b>5.5</b>	<b>57.4</b>	<b>11.9</b>	100%	100%			

**TABLE 7.1 (CONTINUED) FINAL MANPOWER AND PROGRESS FOLLOW-UP TABLE (WORKPACKAGE 5)**

WP/Task (N°/title)	Partner (Name/ abbrev.)	----- Man-Month -----								----- Technical Progress % -----			Comments on major deviations and/or modifications of planned efforts.	
		Planned efforts - at start of period				Actual effort (MM)				Devia- tion (MM)	Planned (%)	Assessed* (%)		Devia- tion (%)
		Year 1	Year 2	Year 3	Total	Year 1	Year 2	Years 3&4	Total	Totals	Years 1-4	Years 1-4		Now
		a	b	c	d	a1	b1	c1	d1	d1-d				
6.1 Assessment of Detailed Design Methods														
	CIRA			2	2			2	2		100%	100%		
	<b>Total</b>			<b>2</b>	<b>2</b>			<b>2</b>	<b>2</b>		<b>100%</b>	<b>100%</b>		
6.2 Design Guidelines														
	QinetiQ			1.1	1.1			1.1	1.1		100%	100%		
	<b>Total</b>			<b>1.1</b>	<b>1.1</b>			<b>1.1</b>	<b>1.1</b>		<b>100%</b>	<b>100%</b>		

\*) Please note that the actual technical progress percentage and the updated remaining efforts must reflect the physically assessed status of the work.

**TABLE 7.1 (CONTINUED) FINAL MANPOWER AND PROGRESS FOLLOW-UP TABLE (WORKPACKAGE 6)**

WP/Task (N°/title)	Partner (Name/ abbrev.)	----- Man-Month -----								----- Technical Progress % -----			Comments on major deviations and/or modifications of planned efforts.	
		Planned efforts - at start of period				Actual effort (MM)				Devia- tion (MM)	Planned (%)	Assessed* (%)		Devia- tion (%)
		Year 1	Year 2	Year 3	Total	Year 1	Year 2	Years 3&4	Total	Totals	Years 1-4	Years 1-4		Now
		a	b	c	d	a1	b1	c1	d1	d1-d				
7.1 Management														
	ULIM	5.3	4.4	4.3	14	5.3	4.4	5.3	15	1	100%	100%		
	AD	1			1	1			1		100%	100%		
	SAAB	0.4	0.3	0.3	1	0.4	0.3	0.3	1		100%	100%		
	AUK	0.5	0.5		1	0.5	0.5		1		100%	100%		
	FOI	0.25	0.4	0.35	1	0.25	0.4	0.35	1		100%	100%		
	NLR	0.4	0.4	0.2	1	0.4	0.4		0.8	-0.2	100%	100%		
	CIRA			1	1			1.5	1.5	0.5	100%	100%		
<b>Total</b>	<b>7.85</b>	<b>6</b>	<b>6.15</b>	<b>20</b>	<b>7.85</b>	<b>6</b>	<b>7.45</b>	<b>21.3</b>	<b>1.3</b>	<b>100%</b>	<b>100%</b>			
7.2 Exploitation														
	QinetiQ	0.5	0.5	1.1	2.1	0.5	0.5	1.1	2.1		100%	100%		
	SMR	1	2	2	5	1.5	1.5	2	5		100%	100%		
<b>Total</b>	<b>1.5</b>	<b>2.5</b>	<b>3.1</b>	<b>7.1</b>	<b>2</b>	<b>2</b>	<b>3.1</b>	<b>7.1</b>		<b>100%</b>	<b>100%</b>			

\*) Please note that the actual technical progress percentage and the updated remaining efforts must reflect the physically assessed status of the work.

**TABLE 7.1 (CONTINUED) FINAL MANPOWER AND PROGRESS FOLLOW-UP TABLE (WORKPACKAGE 7)**

WP/Task (N°/title)	Partner (Name/ abbrev.)	----- Man-Month -----								----- Technical Progress % -----			Comments on major deviations and/or modifications of planned efforts.	
		Planned efforts - at start of period				Actual effort (MM)				Devia- tion (MM)	Planned (%)	Assessed* (%)		Devia- tion (%)
		Year 1	Year 2	Year 3	Total	Year 1	Year 2	Years 3&4	Total	Totals	Years 1-4	Years 1-4		Now
		a	b	c	d	a1	b1	c1	d1	d1-d				
TOTALS	ULIM	27.6	23.4	11.3	62.3	27.6	24.4	14.3	66.3	4	100%	100%		
	AUK	11	8	3	22.0	10.6	11	3.25	24.9	2.85	100%	100%		
	AD	4.5	0.5	3	8.0	4.3	0.5	3.2	8.0		100%	100%		
	SAAB	4.5	4.3	2.2	11.0	4.5	4.3	2.2	11.0		100%	100%		
	CIRA	6.2	5.7	4.1	16.0	5.15	4.75	8.6	18.5	2.5	100%	100%		
	QinetiQ	6.1	8.9	3.8	18.8	5.9	9.1	4.8	19.8	1	100%	100%		
	FOI	7	8.5	2	17.5	6.75	7.6	6.1	20.5	2.95	100%	100%		
	NLR	8.7	10	0.7	19.4	5.7	22.8	5	33.5	14.1	100%	95%	-5%	
	ISTRAM	7	4		11.0	5	5.5	1.5	12.0	1	100%	100%		
	KTH	12	14	6	32.0	12	10	10	32.0		100%	100%		
	SMR	4	5	4	13.0	4	6	4	14.0	1	100%	100%		
	<b>Total</b>		<b>98.6</b>	<b>92.3</b>	<b>40.1</b>	<b>231</b>	<b>91.5</b>	<b>105.95</b>	<b>62.95</b>	<b>260.4</b>	<b>29.4</b>	<b>100%</b>	<b>100%</b>	<b>0%</b>

\*) Please note that the actual technical progress percentage and the updated remaining efforts must reflect the physically assessed status of the work.

\* ULIM’s planned effort revised at start of project in agreement with EU Officer due to hiring of staff at lower rates than in CPF

**TABLE 7.1 (CONTINUED) FINAL MANPOWER AND PROGRESS FOLLOW-UP TABLE (TOTALS)**

PARTNER	Cost Category	BUDGET (EUR)	ACTUAL COSTS (EUR)					Total Pct. Spent (%)				Remaining Budget (EUR)	Comments on major deviations from budget.
			Year 1	Year 2	Years 3&4		Total	Year 1	Year 2	Years 3&4			
			e	a1	b1	c1		e1	a1/e	a1+b1/e	a1+b1+c1/e		
1. ULIM	Labour	181,790	73,169	67,264	39,029		179,462	40%	77%	99%		2,328	
	Overheads	42,680	19,551	16,168	7,351		43,070	46%	84%	101%		-390	
	<b>Labour +Overheads</b>	<b>224,470</b>	<b>92,720</b>	<b>83,432</b>	<b>46,380</b>		<b>222,532</b>	<b>41%</b>	<b>78%</b>	<b>99%</b>		<b>1,938</b>	Move balance to consumables
	Travel	21,000	5,243	9,470	5,826		20,539	25%	70%	98%		461	Move balance to consumables
	Durable Eqmt.	15,000	14,983	0	0		14,983	100%	100%	100%		17	Move balance to consumables
	Consumables	23,500	11,005	14,476	588		26,069	47%	108%	111%		-2,569	Consumables overspend was due to purchase of instrumented bolts (agreed with EU Officer)
	Computing	0	0	0	0		0	#DIV/0!	#DIV/0!	#DIV/0!		0	
	Subcontracting	0	0	0	0		0	#DIV/0!	#DIV/0!	#DIV/0!		0	
	Other	0	0	0	0		0	#DIV/0!	#DIV/0!	#DIV/0!		0	
	<b>Total</b>	<b>283,970</b>	<b>123,951</b>	<b>107,379</b>	<b>52,793</b>	<b>0</b>	<b>284,123</b>	<b>44%</b>	<b>81%</b>	<b>100%</b>		<b>-153</b>	

**TABLE 7.2 FINAL BUDGET SUMMARY TABLE (PARTNER 1)**



PARTNER	Cost Category	BUDGET (EUR)	ACTUAL COSTS (EUR)					Total Pct. Spent (%)				Remaining Budget (EUR)	Comments on major deviations from budget.
			Year 1	Year 2	Years 3&4		Total	Year 1	Year 2	Years 3&4			
			e	a1	b1	c1		e1	a1/e	a1+b1/e	a1+b1+c1/e		
2. AUK	Labour	112,962	38,584	49,373	24,490		112,448	34%	78%	100%		514	Initial costing underestimated the work involved in testing and manufacturing test specimens  Initial costing underestimated the work involved in testing and manufacturing test specimens
	Overheads	124,653	68,211	96,452	12,505		177,168	55%	132%	142%		-52,515	
	<b>Labour +Overheads</b>	<b>237,615</b>	<b>106,795</b>	<b>145,826</b>	<b>36,995</b>		<b>289,616</b>	<b>45%</b>	<b>106%</b>	<b>122%</b>		<b>-52,001</b>	
	Travel	12,000	1,560	4,696	5,886		12,141	13%	52%	101%		-141	
	Durable Eqmt.	0		0	0		0	#DIV/0!	#DIV/0!	#DIV/0!		0	
	Consumables	29,812	7,691	0	0		7,691	26%	26%	26%		22,121	
	Computing	0		0	0		0	#DIV/0!	#DIV/0!	#DIV/0!		0	
	Subcontracting	18,128	10,821	22,474	37,448		70,743	60%	184%	390%		-52,615	
	Other	0		0	0		0	#DIV/0!	#DIV/0!	#DIV/0!		0	
	<b>Total</b>	<b>297,555</b>	<b>126,866</b>	<b>172,996</b>	<b>80,329</b>		<b>380,191</b>	<b>43%</b>	<b>101%</b>	<b>128%</b>		<b>-82,636</b>	

**TABLE 7.2 (CONTINUED) FINAL BUDGET SUMMARY TABLE (PARTNER 2)**

PARTNER	Cost Category	BUDGET (EUR)	ACTUAL COSTS (EUR)					Total Pct. Spent (%)				Remaining Budget (EUR)	Comments on major deviations from budget.
			Year 1	Year 2	Year 3	Year 4	Total	Year 1	Year 2	Year 3	Year 4		
			e	a1	b1	c1	d1	e1	a1/e	a1+b1/e	a1+b1+c1/e		
3. DA	Labour	90,220	37,089	7,828	36,710		81,627	41%	50%	90%	0%	8,593	
	Overheads	10,590	1,718	633	2,474		4,825	16%	22%	46%	0%	5,765	
	<b>Labour +Overheads</b>	<b>100,810</b>	<b>38,807</b>	<b>8,461</b>	<b>39,183</b>	<b>0</b>	<b>86,452</b>	<b>38%</b>	<b>47%</b>	<b>86%</b>	<b>0%</b>	<b>14,358</b>	
	Travel	13,130	1,508	3,445	4,247		9,200	11%	38%	70%	0%	3,930	
	Durable Eqmt.	0	0	0	0		0	#DIV/0!	#DIV/0!	#DIV/0!	0%	0	
	Consumables	3,060	471	15	0		486	15%	16%	16%	0%	2,574	
	Computing	0	0	0	0		0	#DIV/0!	#DIV/0!	#DIV/0!	0%	0	
	Subcontracting	0	0	0	0		0	#DIV/0!	#DIV/0!	#DIV/0!	0%	0	
	Other	0	288	0	0		288	#DIV/0!	#DIV/0!	#DIV/0!	0%	-288	
	Adjustments	0	0	0	850		850	#DIV/0!	#DIV/0!	#DIV/0!	0%	-850	
	<b>Total</b>	<b>117,000</b>	<b>41,074</b>	<b>11,921</b>	<b>44,280</b>	<b>0</b>	<b>97,276</b>	<b>35%</b>	<b>45%</b>	<b>83%</b>	<b>0%</b>	<b>19,724</b>	

**TABLE 7.2 (CONTINUED) FINAL BUDGET SUMMARY TABLE (PARTNER 3)**

PARTNER	Cost Category	BUDGET (EUR)	ACTUAL COSTS (EUR)					Total Pct. Spent (%)				Remaining Budget (EUR)	Comments on major deviations from budget.
			Year 1	Year 2	Years 3&4		Total	Year 1	Year 2	Years 3&4			
			e	a1	b1	c1		e1	a1/e	a1+b1/e	a1+b1+c1/e		
4. SAAB	Labour	71,626	21,469	28,028	21,320		70,817	30%	69%	99%		809	Use balance to cover overspend in other categories
	Overheads	72,613	25,286	34,455	17,302		77,043	35%	82%	106%		-4,430	
	<b>Labour +Overheads</b>	<b>144,239</b>	<b>46,755</b>	<b>62,483</b>	<b>38,622</b>		<b>147,861</b>	<b>32%</b>	<b>76%</b>	<b>103%</b>		<b>-3,622</b>	
	Travel	19,800	2,679	4,642	5,595		12,916	14%	37%	65%		6,884	
	Durable Eqmt.	0					0	#DIV/0!	#DIV/0!	#DIV/0!		0	
	Consumables	5,200	4,418	242	983		5,643	85%	90%	109%		-443	
	Computing	0					0	#DIV/0!	#DIV/0!	#DIV/0!		0	
	Subcontracting	0					0	#DIV/0!	#DIV/0!	#DIV/0!		0	
	Other	0					0	#DIV/0!	#DIV/0!	#DIV/0!		0	
	<b>Total</b>	<b>169,239</b>	<b>53,852</b>	<b>67,367</b>	<b>45,200</b>		<b>166,420</b>	<b>32%</b>	<b>72%</b>	<b>98%</b>		<b>2,819</b>	

**TABLE 7.2 (CONTINUED) FINAL BUDGET SUMMARY TABLE (PARTNER 4)**

PARTNER	Cost Category	BUDGET (EUR)	ACTUAL COSTS (EUR)					Total Pct. Spent (%)				Remaining Budget (EUR)	Comments on major deviations from budget.
			Year 1	Year 2	Years 3&4		Total	Year 1	Year 2	Years 3&4			
			e	a1	b1	c1		e1	a1/e	a1+b1/e	a1+b1+c1/e		
5. CIRA	Labour	81,605	25,954	24,400	44,567		94,921	32%	62%	116%		-13,316	Move balance to labour
	Overheads	79,456	25,272	23,756	43,396		92,423	32%	62%	116%		-12,967	
	<b>Labour +Overheads</b>	<b>161,061</b>	<b>51,226</b>	<b>48,156</b>	<b>87,963</b>		<b>187,344</b>	<b>32%</b>	<b>62%</b>	<b>116%</b>		<b>-26,283</b>	
	Travel	10,000	1,947	3,870	4,411		10,227	19%	58%	102%		-227	
	Durable Eqmt.	0					0	#DIV/0!	#DIV/0!	#DIV/0!		0	
	Consumables	6,000		862	4,000		4,862	0%	14%	81%		1,138	
	Computing	0					0	#DIV/0!	#DIV/0!	#DIV/0!		0	
	Subcontracting	0					0	#DIV/0!	#DIV/0!	#DIV/0!		0	
	Other	0					0	#DIV/0!	#DIV/0!	#DIV/0!		0	
	<b>Total</b>	<b>177,061</b>	<b>53,173</b>	<b>52,888</b>	<b>96,373</b>		<b>202,434</b>	<b>30%</b>	<b>60%</b>	<b>114%</b>		<b>-25,373</b>	

**TABLE 7.2 (CONTINUED) FINAL BUDGET SUMMARY TABLE (PARTNER 5)**

PARTNER	Cost Category	BUDGET (EUR)	ACTUAL COSTS (EUR)					Total Pct. Spent (%)				Remaining Budget (EUR)	Comments on major deviations from budget.
			Year 1	Year 2	Years 3&4		Total	Year 1	Year 2	Years 3&4			
			e	a1	b1	c1		e1	a1/e	a1+b1/e	a1+b1+c1/e		
6. QINETIQ	Labour	72,727	20,880	28,859	13,727		63,466	29%	68%	87%		9,261	
	Overheads	127,273	57,692	82,255	14,865		154,813	45%	110%	122%		-27,540	
	<b>Labour +Overheads</b>	<b>200,000</b>	<b>78,572</b>	<b>111,114</b>	<b>28,592</b>		<b>218,279</b>	<b>39%</b>	<b>95%</b>	<b>109%</b>		<b>-18,279</b>	
	Travel	15,000	2,316	5,483	4,054		11,854	15%	52%	79%		3,146	
	Durable Eqmt.	0	0	0	0		0	#DIV/0!	#DIV/0!	#DIV/0!		0	
	Consumables	2,000	0	47	0		47	0%	2%	2%		1,953	
	Computing	0	0	0	0		0	#DIV/0!	#DIV/0!	#DIV/0!		0	
	Subcontracting	0	0	0	0		0	#DIV/0!	#DIV/0!	#DIV/0!		0	
	Other	0	859	283			1,142	#DIV/0!	#DIV/0!	#DIV/0!		-1,142	
	Adjustment	0			-612.85*		-613	#DIV/0!	#DIV/0!	#VALUE!		613	
	<b>Total</b>	<b>217,000</b>	<b>81,748</b>	<b>116,928</b>	<b>32,647</b>		<b>230,709</b>	<b>38%</b>	<b>92%</b>	<b>107%</b>		<b>-13,709</b>	

\* The "adjustment" in Years 3 and 4 represents an adjustment to costs previously reported (see explanation provided with final cost statement)

**TABLE 7.2 (CONTINUED) FINAL BUDGET SUMMARY TABLE (PARTNER 6)**

PARTNER	Cost Category	BUDGET (EUR)	ACTUAL COSTS (EUR)					Total Pct. Spent (%)				Remaining Budget (EUR)	Comments on major deviations from budget.
			Year 1	Year 2	Years 3&4		Total	Year 1	Year 2	Years 3&4			
			e	a1	b1	c1		e1	a1/e	a1+b1/e	a1+b1+c1/e		
7. FOI	Labour	146,565	53,846	56,802	52,279		162,927	37%	75%	111%		-16,362	
	Overheads	49,398	19,365	38,491	46,267		104,122	39%	117%	211%		-54,724	
	<b>Labour +Overheads</b>	<b>195,963</b>	<b>73,211</b>	<b>95,293</b>	<b>98,546</b>		<b>267,050</b>	<b>37%</b>	<b>86%</b>	<b>136%</b>		<b>-71,087</b>	
	Travel	15,000	3,802	2,603	4,269		10,674	25%	43%	71%		4,326	Move balance to labour
	Durable Eqmt.	0	0				0	#DIV/0!	#DIV/0!	#DIV/0!		0	
	Consumables	6,120	4,954	397	753		6,104	81%	87%	100%		16	Move balance to labour
	Computing	0	0				0	#DIV/0!	#DIV/0!	#DIV/0!		0	
	Subcontracting	0	0				0	#DIV/0!	#DIV/0!	#DIV/0!		0	
	Other	0	0				0	#DIV/0!	#DIV/0!	#DIV/0!		0	
	<b>Total</b>	<b>217,083</b>	<b>81,967</b>	<b>98,293</b>	<b>103,568</b>		<b>283,827</b>	<b>38%</b>	<b>83%</b>	<b>131%</b>		<b>-66,744</b>	

**TABLE 7.2 (CONTINUED) FINAL BUDGET SUMMARY TABLE (PARTNER 7)**

PARTNER	Cost Category	BUDGET (EUR)	ACTUAL COSTS (EUR)					Total Pct. Spent (%)				Remaining Budget (EUR)	Comments on major deviations from budget.
			Year 1	Year 2	Years 3&4		Total	Year 1	Year 2	Years 3&4			
			e	a1	b1	c1		e1	a1/e	a1+b1/e	a1+b1+c1/e		
8. NLR	Labour	68,178	21,039	84,276	24,306		129,622	31%	154%	190%		-61,444	
	Overheads	115,904	38,098	152,539	39,134		229,770	33%	164%	198%		-113,866	
	<b>Labour +Overheads</b>	<b>184,082</b>	<b>59,137</b>	<b>236,815</b>	<b>63,440</b>		<b>359,392</b>	<b>32%</b>	<b>161%</b>	<b>195%</b>		<b>-175,310</b>	
	Travel	10,000	1,705	2,351	1,252		5,308	17%	41%	53%		4,692	
	Durable Eqmt.	0	0	0	0		0	0%	0%	0%		0	
	Consumables	9,400	7,528	7,615	1,660		16,804	80%	161%	179%		-7,404	
	Computing	0	0	0			0	0%	0%	0%		0	
	Subcontracting	4,000	0	11,990	1,292		13,282	0%	300%	332%		-9,282	
	Other	19,500	449	10,696	2,072		13,217	2%	57%	68%		6,283	
	<b>Total</b>	<b>226,982</b>	<b>68,819</b>	<b>269,468</b>	<b>69,715</b>		<b>408,002</b>	<b>30%</b>	<b>149%</b>	<b>180%</b>		<b>-181,020</b>	

**TABLE 7.2 (CONTINUED) FINAL BUDGET SUMMARY TABLE (PARTNER 8)**

PARTNER	Cost Category	BUDGET (EUR)	ACTUAL COSTS (EUR)					Total Pct. Spent (%)				Remaining Budget (EUR)	Comments on major deviations from budget.
			Year 1	Year 2	Years 3&4		Total	Year 1	Year 2	Years 3&4			
			e	a1	b1	c1		e1	a1/e	a1+b1/e	a1+b1+c1/e		
9. ISTRAM	Labour	51,975	18,354	29,700	10,044		58,098	35%	92%	112%		-6,123	
	Overheads	13,329	4,365	6,800	2,214		13,379	33%	84%	100%		-50	
	<b>Labour +Overheads</b>	<b>65,304</b>	<b>22,719</b>	<b>36,500</b>	<b>12,258</b>		<b>71,476</b>	<b>35%</b>	<b>91%</b>	<b>109%</b>		<b>-6,172</b>	
	Travel	12,400	2,567	3,320	1,025		6,911	21%	47%	56%		5,489	Move balance to labour
	Durable Eqmt.	1,800	587	979	0		1,566	33%	87%	87%		234	Move balance to labour
	Consumables	470	320	0	0		320	68%	68%	68%		151	Move balance to labour
	Computing	0	0	0	0		0	#DIV/0!	#DIV/0!	#DIV/0!		0	
	Subcontracting	0	0	0	0		0	#DIV/0!	#DIV/0!	#DIV/0!		0	
	Other	0	0	0	0		0	#DIV/0!	#DIV/0!	#DIV/0!		0	
	<b>Total</b>	<b>79,974</b>	<b>26,192</b>	<b>40,798</b>	<b>13,282</b>		<b>80,272</b>	<b>33%</b>	<b>84%</b>	<b>100%</b>		<b>-298</b>	

**TABLE 7.2 (CONTINUED) FINAL BUDGET SUMMARY TABLE (PARTNER 9)**



PARTNER	Cost Category	BUDGET (EUR)	ACTUAL COSTS (EUR)					Total Pct. Spent (%)				Remaining Budget (EUR)	Comments on major deviations from budget.
			Year 1	Year 2	Years 3&4		Total	Year 1	Year 2	Years 3&4			
			e	a1	b1	c1		e1	a1/e	a1+b1/e	a1+b1+c1/e		
10.KTH	Labour	133,868	47,355	48,363	37,703		133,421	35%	72%	100%		447	
	Overheads	29,501	10,891	10,209	7,997		29,097	37%	72%	99%		404	
	<b>Labour +Overheads</b>	<b>163,369</b>	<b>58,246</b>	<b>58,572</b>	<b>45,699</b>		<b>162,517</b>	<b>36%</b>	<b>72%</b>	<b>99%</b>		<b>852</b>	
	Travel	9,000	3,101	2,203	2,280		7,584	34%	59%	84%		1,416	
	Durable Eqmt.	0					0			#DIV/0!		0	
	Consumables	4,639	4,000	482			4,482	86%	97%	97%		157	
	Computing	0					0			#DIV/0!		0	
	Subcontracting	0					0			#DIV/0!		0	
	Other	0					0			#DIV/0!		0	
	<b>Total</b>	<b>177,008</b>	<b>65,347</b>	<b>61,257</b>	<b>47,979</b>		<b>174,583</b>	<b>37%</b>	<b>72%</b>	<b>99%</b>		<b>2,425</b>	

**TABLE 7.2 (CONTINUED) FINAL BUDGET SUMMARY TABLE (PARTNER 10)**

PARTNER	Cost Category	BUDGET (EUR)	ACTUAL COSTS (EUR)				Total	Total Pct. Spent (%)			Remaining Budget (EUR)	Comments on major deviations from budget.	
			Year 1	Year 2	Years 3&4			Year 1	Year 2	Years 3&4			
			a1	b1	c1			a1/e	a1+b1/e	a1+b1+c1/e			
		e				e1						e-e1	
11. SMR	Labour	147,290	45,970	67,861	43,799	157,630	31%	77%	107%		-10,340		
	Overheads	0	0	0	0	0	#DIV/0!	#DIV/0!	#DIV/0!		0		
	<b>Labour +Overheads</b>	147,290	45,970	67,861	43,799	157,630	31%	77%	107%		-10,340		
	Travel	14,140	4,210	2,825	2,739	9,774	30%	50%	69%		4,366	Move balance to labour	
	Durable Eqmt.	5,237	0	0		0	0%	0%	0%		5,237	Move balance to labour	
	Consumables	0	0	0		0	#DIV/0!	#DIV/0!	#DIV/0!		0		
	Computing	0	0	0		0	#DIV/0!	#DIV/0!	#DIV/0!		0		
	Subcontracting	0	0	0		0	#DIV/0!	#DIV/0!	#DIV/0!		0		
	Other	0	0	0		0	#DIV/0!	#DIV/0!	#DIV/0!		0		
	<b>Total</b>	166,667	50,180	70,686	46,538	167,404	30%	73%	100%		-737		

**TABLE 7.2 (CONTINUED) FINAL BUDGET SUMMARY TABLE (PARTNER 11)**